THE EARTHQUAKE RESISTANCE OF REINFORCED CONCRETE STRUCTURAL WALLS OF LIMITED DUCTILITY

A thesis presented for
the degree of
Master of Engineering
at the
University of Canterbury,
Christchurch, New Zealand

by

J.M. MESTYANEK

September 1986

ABSTRACT

This thesis presents the results of an experimental study of three 1/3 to 1/2 scale model walls failing in shear under reversed cyclic loading. The main test parameter was the wall aspect ratio (height over length). The following characteristics of response were considered: strength, displacement ductility, energy dissipation, and damageability. Recommendations are made for the design of future walls of limited ductility and the assessment of the likely seismic performance of existing walls that may respond primarily in a shear rather than flexural mode.

ACKNOWLEDGEMENTS

The first and most important acknowledgement is given to God, the Father of our Lord Jesus Christ, for the opportunity to learn something more about His creation. Also, without His steadfast enabling, guidance, and protection in the project, nothing would have been accomplished. "Unless the Lord build the house, they labour in vain who build it." (Psalm 127:1)

The work described in this thesis was carried out in the Department of Civil Engineering at the University of Canterbury under the overall supervision of its Head, Professor R. Park. Financial assistance was provided by the Ministry of Works and Development.

I thank Professor T. Paulay for his insight and his enthusiastic and energetic guidance in the project. However, more importantly, I thank him for his true care and concern regarding all aspects of my life. He has been much more than a technical supervisor. In truth, he has looked after me as his very son.

I also thank the technical staff in the department, particularly Messrs. P.G. Mitchell, P.F. Coursey, and N.J. Hickey for their meticulous construction of the test units. I thank Mr. P.F. Coursey for his willingness to teach me some of the skills of his trade, and I thank Mr. N.J. Hickey for his precision and competence in testing.

I thank Mr. Ray Brown, Mrs. V.J. Grey, and Mr. Gwyn Clark for their invaluable help with the draughting work and also Mrs. D. Ball for her help with the typing.

Also, I thank my parents and family in California for the whole-hearted support which they have shown me during my entire life, and particularly in my decision to study in New Zealand.

Finally, many women nobly support and encourage their husbands in their work, but, to be sure, my lovely wife-to-be, Katrina, excels them all.

TABLE OF CONTENTS

		Page
ABSTRACT		I
ACKNOWLEDGEMENTS		II
TABLE OF CONTENTS		III
NOTATION		VIII
1	INTRODUCTION	1
2	A REVIEW OF THE PROBLEM	2
2.1	Current New Zealand Requirements for Earthquake Resistance	2
2.2	Walls as Earthquake-resisting Elements	4
2.3	Types of Structural Walls	4
2.4	Design Approaches	6
2.5	Capacity Design	8
2.6	Structural Walls of Limited Ductility	9
2.7	Uniform Rectangular Walls of Limited Ductility	10
2.8	Uniform Flanged Walls of Limited Ductility	12
3	MECHANISMS OF LATERAL LOAD RESISTANCE IN CANTILEVER WALLS	14
3.1	General Comments	14
3.2	Flexural Failure (Failure in Beam Action)	22
3.3	Base Sliding Failure	22
3.4	Construction Joint Failure	22
3.5	Shear Failure (Failure of Arch Action or Equilibrium Truss)	24
3.6	Postulated Behaviour of Present Test Units	25
4	LITERATURE SURVEY	27
4.1	Barda (17,18)	27
4.2	Synge (7,8)	40
4.3	Robinson (19)	41
4.4	Glogau (20)	41
4.5	Hutchison and Van Geldermalsen (21)	43
5	SCOPE OF THE PROJECT AND EXPERIMENTAL PROGRAMME	45
5.1	Definitions	45
5.2	Main Test Objectives	46

5.3 Main Test Parameter 46
5.4 Constant Length vs. Constant Height 47
5.5 Web Bars 47
5.6 Axial Load 49
5.7 Design Calculations 49

6 DETAILS OF THE TEST PROGRAMME 53
6.1 Test Rig 53
6.2 Construction of Wall Units 56
6.2.1 Construction Programme 56
6.2.2 Formwork 57
6.2.3 Strain Gauging 59
6.2.4 Tying of Reinforcement 59
6.2.5 Concreting 60
6.3 Material Properties 63
6.3.1 Reinforcement 63
6.3.2 Concrete 65
6.4 Instrumentation 65
6.4.1 General Objectives 65
6.4.2 Load Cell 66
6.4.3 Strain Gauges 66
6.4.4 Linear Displacement Potentiometers (LDPs) 66
6.4.5 Automatic Datalogger 69
6.4.6 Dial Gauges 69
6.4.7 DEMEC Points 70
6.4.8 Crack Width Microscope 70
6.5 Testing Programme - General Comments 70
6.5.1 Test Setup 70
6.5.2 Initial Load Level 71
6.5.3 Cyclic Loading 71
6.5.4 Recording of Data 73

7 UNIT 1.0 - LOADING HISTORY, GENERAL BEHAVIOUR, AND TEST RESULTS 75
7.1 Presentation of Results 75
7.2 Loading History 75
7.3 Description of Observed Behaviour 78
7.4 Failure Mechanism 84
7.5 Test Results 89
7.5.1 Elastic Cycles 89

7.5.2 Lateral Load vs. Total Top Displacement 90
7.5.3 Cumulative Displacement Ductility and Strength Reduction 94
7.5.4 Dissipation of Energy 96
7.5.5 Lateral Load vs. Top Displacement Due to Shear Deformations 100
7.5.6 Components of Top Deflection 101
7.5.7 Strains in Horizontal Web Bars 106
7.5.8 Strains in Vertical Boundary Element Bars 108
7.5.9 Strains in Vertical Web Bars 110
7.5.10 Location of the Vertical Compression Resultant 112
7.5.11 Strains in Vertical Bars Below Base Level 115
7.5.12 Axial Extension of the Wall 122
7.5.13 Base Beam Behaviour 122
7.5.14 Top Beam Behaviour 122
7.5.15 Sliding Along Horizontal Construction Joints 123
7.5.16 Displacements at Diagonal Cracks 123

8 UNIT 1.5 - LOADING HISTORY, GENERAL BEHAVIOUR, AND TEST RESULTS 124
8.1 Loading History 124
8.2 Description of Observed Behaviour 124
8.3 Failure Mechanism 132
8.4 Test Results 137
8.4.1 Elastic Cycles 137
8.4.2 Lateral Load vs. Total Top Displacement 137
8.4.3 Cumulative Displacement Ductility and Strength Reduction 143
8.4.4 Dissipation of Energy 143
8.4.5 Lateral Load vs. Top Displacement Due to Shear Deformations 146
8.4.6 Components of Top Deflection 146
8.4.7 Strains in Horizontal Web Bars 149
8.4.8 Strains in Vertical Boundary Element Bars 151
8.4.9 Strains in Vertical Web Bars 151
8.4.10 Location of the Vertical Compression 154

Resultant
8.4.11 Strains in Vertical Bars Below Base Level 154
8.4.12 Axial Extension of the Wall 158
8.4.13 Base Beam Behaviour 158
8.4.14 Top Beam Behaviour 159
8.4.15 Sliding Along Horizontal Construction Joints 159
8.4.16 Displacements at Diagonal Cracks 159

9 UNIT 2.0 - LOADING HISTORY, GENERAL BEHAVIOUR, AND TEST RESULTS 161
9.1 Loading History 161
9.2 Description of Observed Behaviour 163
9.3 Failure Mechanism 172
9.4 Test Results 174
9.4.1 Elastic Cycles 174
9.4.2 Lateral Load vs. Total Top Displacement 175
9.4.3 Cumulative Displacement Ductility and Strength Reduction 179
9.4.4 Dissipation of Energy 170
9.4.5 Lateral Load vs. Top Displacement Due to Shear Deformations 183
9.4.6 Components of Top Deflection 183
9.4.7 Strains in Horizontal Web Bars 186
9.4.8 Strains in Vertical Boundary Element Bars 186
9.4.9 Strains in Vertical Web Bars 190
9.4.10 Location of the Vertical Compression Resultant 190
9.4.11 Strains in Vertical Bars Below Base Level 194
9.4.12 Axial Extension of the Wall 196
9.4.13 Base Beam Behaviour 196
9.4.14 Top Beam Behaviour 196
9.4.15 Sliding Along Horizontal Construction Joints 196
9.4.16 Displacements at Diagonal Cracks 196

10 DISCUSSION OF TEST RESULTS 198
10.1 Major Features of Test Unit Behaviour 198

10.2 Lateral Load Resistance Mechanisms 199
10.3 Failure Mechanisms 201
10.4 Stiffness in the Elastic, Fully Cracked State 202
10.5 Effect of Reduced Stiffness in the Elastic Range on Ductility Demand in the Inelastic Range 206
10.6 Effect of Larger Number of Cycles at Lower Displacement Levels on Ductility Demand 209
10.7 Effect of Reduced Stiffness on Damage Control During Minor Earthquakes 211
10.8 Total Displacement Hysteretic Behaviour 212
10.9 Strength 216
10.10 Energy Dissipation 219
10.11 Components of Wall Deflections 221
10.12 Strains in Vertical Bars Below the Base Level 221
10.13 Hysteretic Damping and Shift in Structural Period 222

11 SUMMARY OF PERFORMANCE AND RECOMMENDATIONS 225
11.1 Summary of Performance of Test Units 225
11.1.1 Strength 225
11.1.2 Energy Dissipation 226
11.1.3 Displacement Ductility Capacity 226
11.1.4 Damageability 227
11.1.5 Main Finding of the Tests 227
11.2 Design Recommendations for Cantilever Walls of Limited Ductility 228
11.2.1 New Walls 228
11.2.2 Existing Walls 233
11.3 Recommendations for Further Research 235

REFERENCES 237

APPENDIX A STRENGTH CALCULATIONS 4pp.

APPENDIX B STIFFNESS CALCULATIONS 3pp.

APPENDIX C POTENTIAL FOR CONSTRUCTION JOINT FAILURE 1pp.

NOTATION

a = calculated lateral displacement at mid-height on the left-hand side of wall due to shear deformations alone, mm

A_b = cross-sectional area of an individual bar, mm^2

A_{bh} = cross-sectional area of an individual horizontal web bar, mm^2

A_{bv} = cross-sectional area of an individual vertical web bar, mm^2

A_c = total cross-sectional area of columns at one level in a building, mm^2

A_f = total area of floors and roof above the storey considered, mm^2

A_g = gross area of wall section, mm^2

A_w = total cross-sectional area of walls at one level in a building (ref. 20), mm^2,

= also, effective cross-sectional area of wall, mm^2, used in the calculation of shear deflection of a homogeneous, elastic cantilever

b = calculated lateral displacement at mid-height on the right-hand side of wall due to shear deformations alone, mm

b_w = web width, mm

B = $(\mu_\Delta - 1)2\Delta_y$ = parameter used in evaluating the hysteretic area of an idealized elasto-plastic system

c = neutral axis depth measured from extreme compression fibre, or

= parameter used in evaluating the code-required development length of a reinforcing bar (ref. 3, section 5)

C = compressive force resultant on a cross section, kN also, basic seismic coefficient (ref. 1, Eq. 28)

d = distance from extreme compression fibre to centroid of tension reinforcement, assumed $0.8x\ell_w$ for walls, mm

d_b = nominal diameter of bar, the diameter of a bar of equivalent area, mm

$d_4 - d_7$ = lengths in the deformed state of diagonals instrumented with LDPs for the calculation of shear deformations, mm

e = calculated lateral displacement at an elevation of 2250mm above the base of the wall due to shear deformations alone, mm

E = energy dissipated in one cycle, kNm

E_o = initial elastic stiffness of Ramberg-Osgood model for stress-strain response of a reinforcing bar, MPa

E_i = energy dissipated by the ideal or assumed structure, kNm

E_c = modulus of elasticity of concrete, MPa
$4700\sqrt{f'_c}$

E_r = energy dissipated by the real structure, kNm

E_s = modulus of elasticity of steel, MPa

f = form factor for a given cross section, used in calculating the shear deflection of a homogeneous, elastic beam

= 1.2 for rectangular cross sections

f'_c = compressive strength of concrete, MPa

$(f'_c)_{28}$ = compressive strength of concrete measured at 28 days, MPa

f_c^* = effective compressive strength of concrete, MPa, $< f'_c$

f_r = modulus of rupture of concrete, MPa

f_{sn} = equivalent normal stress on inclined crack plane due to tension in web reinforcement = $T_n/b_w s'$

f_t = tensile strength of concrete obtained from a split cylinder tensile test, MPa

f_{ult} = stress in reinforcing bar at fracture, MPa

f_y = yield strength of reinforcement, MPa

f_{yh} = yield strength of horizontal web reinforcement, MPa

f_{yv} = yield strength of vertical web reinforcement, MPa

F = $30I_e/h_w^2\, b_w\, \ell_w$ = factor applied to I_e to account for the combined effects of flexural, shear, and anchorage pullout deformations (ref. 6)

F' = $90I_e/h_w^2\, b_w\, \ell_w$ = factor applied to I_e to account for the combined effects of flexural, shear, and anchorage pullout deformations in walls responding predominantly in shear

g = vertical distance between the ends of the lower

diagonal potentiometer rods used in measuring shear deformations, mm

G_c = shear modulus for concrete = 0.4 E_c, MPa

h = vertical distance between the ends of the upper diagonal potentiometer rods used in measuring shear deformations, mm

h_j = vertical distance between the loading point and the jth horizontal cross section in the wall height of wall unit from top of base beam to level of lateral load application = 2500mm for all units

h_w/ℓ_w = aspect ratio

I_{cr} = moment of inertia of cracked, transformed section, mm^4

I_e = effective moment of inertia accounting for the effects of cracking, mm^4

I_g = moment of inertia of gross concrete section about the centroidal axis, neglecting reinforcement, mm^4

I_w = effective wall moment of inertia accounting for the effects of cracking and flexural, shear, and anchorage pullout deformations, used in the calculation of deflections, mm^4

jd = internal lever arm between the compression and tension resultants on a cross section, mm

k = stiffness ratio = K_r / K_i

k_{tr} = an index of the transverse reinforcement provided along an anchored bar (ref. 3, clause 5.3.7.3(d)), mm

K = stiffness of wall, kN/mm

K_{dc} = stiffness of wall just after the onset of diagonal cracking, kN/mm

K_e = stiffness of wall in the elastic state just prior to the onset of diagonal cracking, kN/mm

K_i = assumed stiffness of the ideal structure

K_r = actual stiffness of the real structure

ℓ = horizontal distance between the ends of the diagonal potentiometer rods used in measuring shear deformations, mm

ℓ_d = development length, mm

ℓ_{db} = basic development length of a straight bar, mm

ℓ_w = length of wall unit from outside of LHBE to outside of RHBE

LDP = linear displacement potentiometer

LH = left-hand

LHBE = left-hand boundary element

m_1 = modification factor for development length taking account of high strength steel (ref.3, clause 5.3.7.3(a))

m_2 = modification factor for development length taking account of the effects of transverse reinforcement (ref. 3, clause 5.3.7.3(d))

M = bending moment

= also, structural material factor (ref. 1, Eq. 28)

M_a = external bending moment applied to a cross section

M_{cr} = cracking moment

$(M_i)_{flex}$ = ideal flexural moment strength of a cross section

M_u = factored bending moment applied to a section, Nmm

N = axial load on wall

P_e = design axial load on wall due to gravity and seismic loading

P_u = factored axial load on wall section, N

Q = cumulative dissipated energy, kNm

Q_{ep} = cumulative energy dissipated by the idealized elasto-plastic system, kNm

$(Q_{ep})_{flex}$ = cumulative energy dissipated by the idealized elasto-plastic system with strength, $(V_i)_{ep} = (V_i)_{flex}$, kNm

$(Q_{ep})_{shear}$ = cumulative energy dissipated by the idealized elasto-plastic system with strength, $(V_i)_{ep} = (V_i)_{shear}$, kNm

r = Ramberg-Osgood factor affecting hysteretic loop shape (See ref. 25.)

R = lateral load resistance, kN

= also, risk factor (ref. 1, Eq. 28)

R_e = lateral load resistance of an element responding elastically, kN

R_{fd} = maximum lateral load resistance of a fully ductile element, kN

R_i = lateral load resistance of an element responding inelastically, kN

R_{ideal} = ideal lateral load resistance of a structural element, kN

R_{max} = maximum probable lateral load demand imposed on an element by the design earthquake, kN

RH = right-hand

RHBE = right-hand boundary element

s_h = vertical spacing between horizontal web bars, mm

s_v = horizontal spacing between vertical web bars, mm

s' = spacing between web bars along an inclined web crack, mm

T = tensile force resultant on a cross section, kN, or = also, fundamental period of vibration, seconds

T_e = fundamental period of vibration in the elastic state, seconds

T_i = tensile force in the i^{th} reinforcing bar crossing a horizontal cross section in the wall, kN

T_h = tensile force in horizontal web bar, kN

T_n = resultant normal tensile force due to vertical and horizontal web reinforcement crossing the inclined crack, kN

T_v = tensile force in vertical bar, kN

u = bond stress acting along the surface of an embedded bar, MPa

v_c = ideal shear stress provided by concrete, MPa

v_i = total ideal shear stress, MPa

v_s = ideal shear stress provided by reinforcement, MPa

v_u = factored shear stress, MPa

V = applied lateral load, kN

V_c = ideal shear force provided by concrete, kN

V_i = ideal lateral load strength of the wall unit, kN

$(V_i)_{flex}$ = ideal flexural strength of the wall unit, kN

$(V_i)_{shear}$ = ideal shear strength of the wall unit, kN

$(V_i)_{ep}$ = ideal strength assigned to the idealized elasto-plastic system, kN

$(V_{max})_{pos}$ = maximum lateral load applied in the positive (<--) loading direction, kN

$(V_{max})_{neg}$ = maximum lateral load applied in the negative (-->) loading direction, kN

$(V_{max})_{test}$ = maximum lateral load applied during the test = the = larger of $(V_{max})_{pos}$ and $(V_{max})_{neg}$, kN

V_n = lateral load applied at increment n, kN

V_s = ideal shear force provided by reinforcement, kN

V_u = factored shear force on cross section, kN

W = gravity load of building, N

W_t = total reduced gravity load (reactive weight) above the level of imposed lateral ground rstraint (ref. 1, Eq. 27)

x_i = horizontal distance from the extreme compression fibre to the i^{th} bar crossing the horizontal cross section of the wall, mm

Δ = lateral in-plane deflection of the wall unit measured at the level of the applied lateral load (h_w), mm

Δ/h_w = lateral drift

Δ_c = sum of the individually calculated components of top displacement of the wall unit, mm,
$= \Delta v + \Delta f + \Delta fe + \Delta s$

Δ_{dc} = top displacement of the wall unit just after the onset of diagonal cracking, mm

Δ'_{dc} = value of Δ_{dc} predicted by method outlined in ref. 6, Appendix I, mm

Δ''_{dc} = value of Δ_{dc} predicted by methods of Section 10.4, mm

Δ_e = top displacement of the wall unit in the elastic state just prior to the onset of diagonal cracking, mm

Δ'_e = value of Δ_e predicted by method outlined in ref. 6, Appendix I, mm

Δf = top displacement of the wall unit due to flexural deformations alone, mm

Δfe = top displacement of the wall unit due to the straining of vertical bars below the base level, mm

Δ_i = top displacement of the wall unit during inelastic response, mm

Δm = measured top displacement of the wall unit, mm

Δ_n = top displacement of the wall unit at increment n, mm

Δs = top displacement of the wall unit due to sliding at the base of the wall, mm

Δ_{ui} = ultimate displacement of the ideal structure, mm

Δ_{ur} = ultimate displacement of the real structure, mm

Δv = top displacement of the wall unit due to shear deformations alone, mm

$\Delta^{+}_{0.75}$ = top displacement of the wall unit measured at the application of V = $0.75V_i$ in the positive (<--) loading direction, mm

$\Delta^{-}_{0.75}$ = top displacement of the wall unit measured at the application of V = $o.75V_i$ in the negative (-->) loading direction, mm

Δ^{+}_{y} = extrapolated top displacement of the wall unit at yield in the positive (<--) loading direction, mm,
= $(4/3)\Delta^{+}_{0.75}$

Δ^{-}_{y} = extrapolated top displacement of the wall unit at yield in the negative (-->) loading direction, mm,
= $(4/3)\Delta^{-}_{0.75}$

Δ_y = experimental yield displacement of the wall unit,mm
= $0.5(\Delta^{+}_{y} + \Delta^{-}_{y})$

$(\Delta_y)_{fd}$ = yield displacement when R = R_{fd}, mm

Δ_{yi} = yield displacement of the ideal structure, mm

Δ_{yr} = yield displacement of the real structure, mm

ε_{SH} = strain in reinforcement at the onset of strain hardening

ε_{ult} = strain in reinforcement at fracture

ε_y = yield strain of reinforcement

μ_Δ = displacement ductility factor = Δ/Δ_y

$(\mu_\Delta)_{fd}$ = displacement ductility demand corresponding to fully ductile behaviour

$\mu_{\Delta i}$ = displacement ductility factor implied by the relevant loading code = Δ_{ui}/Δ_{yi}

$\mu_{\Delta r}$ = expected displacement ductility factor for the real structure subjected to the design earthquake

$\sum\mu_\Delta$ = cumulative displacement ductility

ρ_h = ratio of horizontal shear reinforcement area to gross concrete area of vertical section

ρ_n = ratio of vertical reinforcement area in wall section to gross area of horizontal section of the web alone

ρ_w = $A_{bv}/b_w d$, where $d \cong 0.8\ell_w$ for walls

θ = angle of inclination of diagonal compression strut, degrees

SECTION 1

INTRODUCTION

This thesis describes an experimental study carried out on reinforced concrete structural walls of limited ductility. The study was motivated by the need to better understand the basic behaviour of such walls. First, it is hoped that such an understanding will help engineers to better evaluate the earthquake response of existing low-rise structural wall buildings designed before capacity design procedures were introduced. Second, it is hoped that such an understanding of basic behaviour will aid engineers in effectively and economically designing new buildings that do not readily lend themselves to the use of capacity design principles.

SECTION 2

A REVIEW OF THE PROBLEM

2.1 CURRENT NEW ZEALAND REQUIREMENTS FOR EARTHQUAKE RESISTANCE

The New Zealand Loadings Code (1) defines the goodness of a structure in terms of three parameters: strength, ductility, and energy dissipation. In clause C3.2, it states that a structure must be capable of sustaining the equivalent of 4 complete cycles to an overall displacement ductility of 4 (cumulative ductility = 32) while retaining 80 percent of its original strength. (See Fig. 2.1.) (Ductility is defined as the ratio of the instantaneous top horizontal deflection to the top horizontal deflection at first yield. Yield deflection is defined in Section 2.4.) Although the code does not quantify the necessary energy dissipation capacity, it states in clauses 3.3.2.1 and 3.3.2.2 that the above ductility and strength requirements are meant to lead to satisfactory energy dissipation. So then, the requirements for the three separate parameters (strength, ductility, and energy dissipation) must be fulfilled simulataneously for satisfactory seismic performance.

It is important to note that a structure possessing adequate ductility may not necessarily exhibit adequate energy dissipation. The energy dissipated by a system is directly proportional to the area enclosed within the force-displacement hysteretic loop. Refer to Fig. 2.2. All of the responses, 1, 2, and 3 in Fig. 2.2, exhibit the same ductility but radically different energy dissipation. Response 2 is typical of flexural behaviour and shows good energy dissipation. Response 3 is typical of shear behaviour and shows poor energy dissipation. The shaded area shows the lack of energy dissipation due to shear pinching. So then, in assessing the adequacy of any structure, energy dissipation, as well as ductility and strength, must be quantified. Perhaps the most convenient means of quantifying the goodness of response is to compare the energy dissipation of the system to that of an ideal elasto-plastic (ie. the area under curve 1 in Fig. 2.2). This will be done later in this thesis.

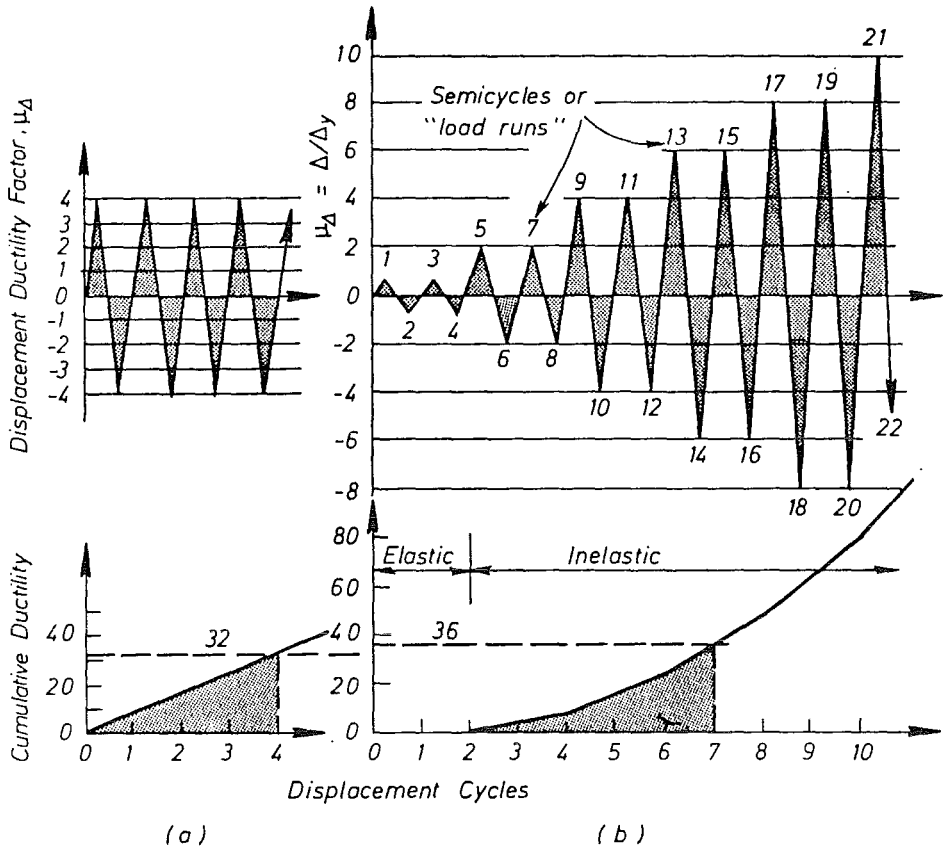

Fig. 2.1 - Load histories and cumulative ductilities used for performance tests (26)

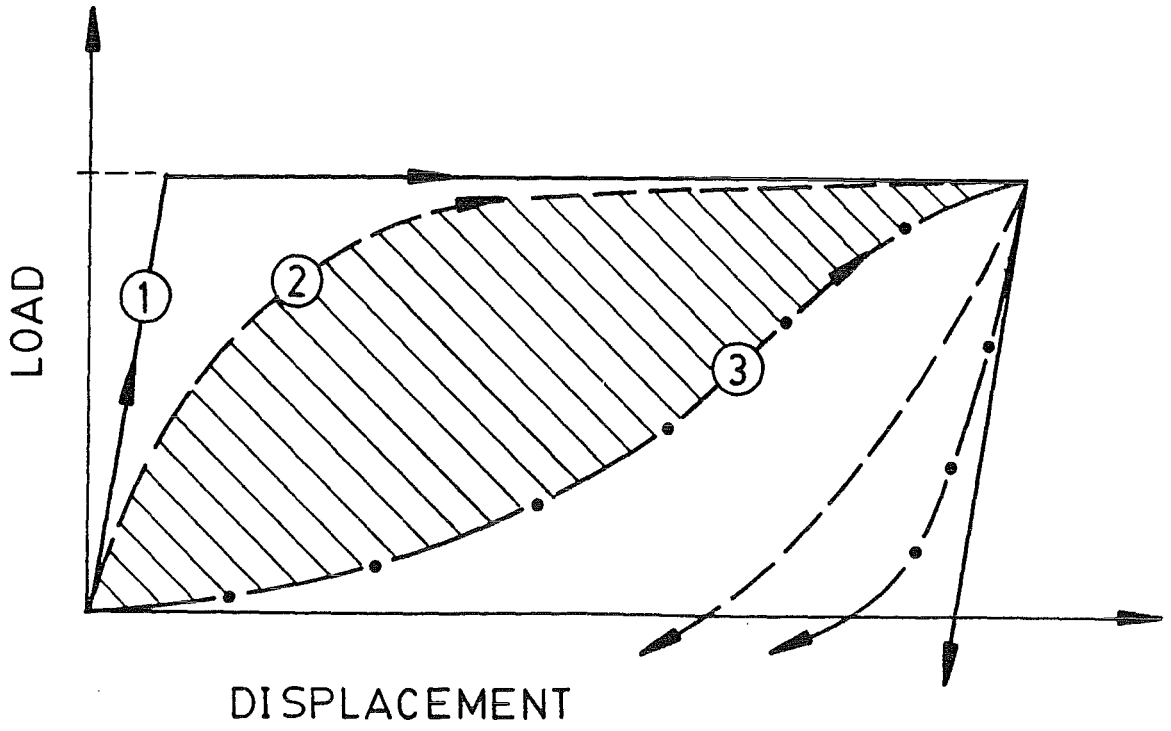

Fig. 2.2 - A comparison of load - displacement relationships (26)

In the remainder of this thesis, the terminology used in current New Zealand structural engineering practice will be used. A "fully ductile" structure refers to one which satisfies not only the ductility requirement stated above, but also the strength and energy dissipation requirements. A structure of "limited ductility" refers to a structure that in some way falls short of the code requirement for ductility. Section 14 of the current New Zealand standard NZS 3101 (3) deals with structures of limited ductility. Limited ductility structures must still meet the strength requirement. In fact, Section 14 of NZS 3101, combined with NZS 4203 (1), requires an increased strength for structures of limited ductility. Regarding energy dissipation, Section 14 specifies very little. In any case, it is important to note that each of the three quantities, strength, ductility, and energy dissipation, can and should be evaluated separately in assessing a structure's response to earthquake displacements.

2.2 WALLS AS EARTHQUAKE-RESISTING ELEMENTS

In reinforced concrete buildings, one type of structural system that resists earthquake forces is composed of structural walls, walls specially designed to resist in-plane horizontal loads in addition to vertical gravity loads. Some engineers have argued that structural walls are more efficient than frames in multistorey buildings because they are inherently stiffer. Walls deflect less laterally and thus protect nonstructural elements better against damage caused by interstorey displacements. There are, however, some doubts as to the ductility of some structural walls, especially as demonstrated by the brittle failures of some low-rise walls highly reinforced for flexure.

2.3 TYPES OF STRUCTURAL WALLS

There are two main categories of structural walls (Table 2.1): cantilever structural walls, which behave individually as cantilevers, although they may be connected to frames or other walls in parallel by means of floor slabs, and coupled structural walls, which are two or more structural walls connected in series by coupling beams. When

TABLE 2.1 - CLASSIFICATION OF STRUCTURAL WALLS

	CANTILEVER WALLS		COUPLED WALLS
Cross section	Uniform	With irregular openings	With regular openings
rectangular - existing	X	X	X
rectangular - new	-	X	-
flanged - existing	X	X	X
flanged - new	-	X	-
barbell-shaped - existing	X	X	X
barbell-shaped - new	-	X	-

X - potentially a wall of limited ductility

Note: The degree of ductility potential is largely dependent on the detailing adopted.

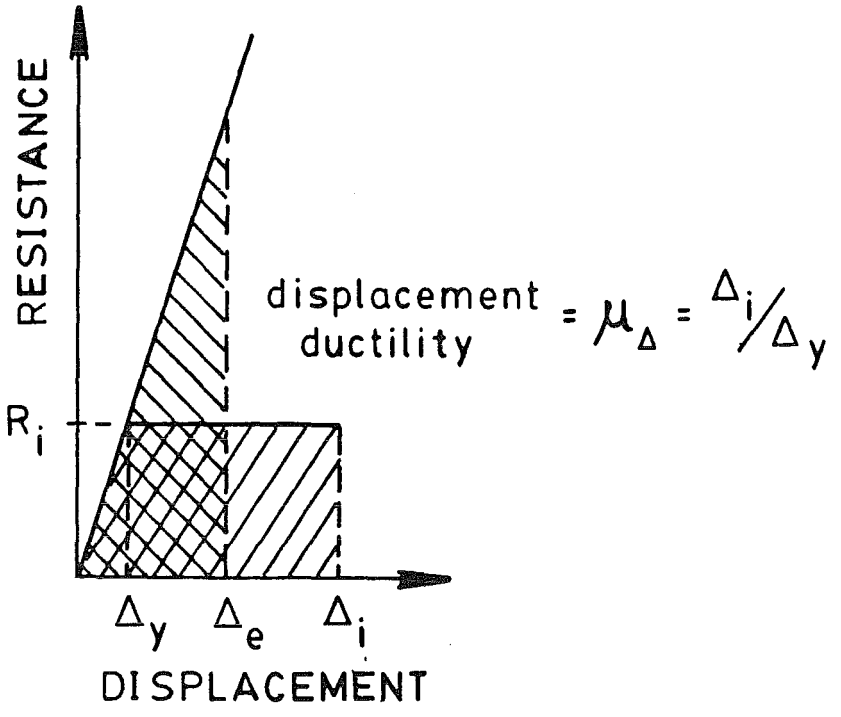

Fig. 2.3 - Idealized elastic and inelastic ductile response

made to be ductile, the coupling beams are capable of dissipating a significant amount of seismic energy. In the following, only cantilever structural walls will be considered.

2.4 DESIGN APPROACHES

There are several approaches to designing a structural wall. It can, perhaps most simply, be designed to behave elastically. The wall is designed to be so strong that it is never expected to be stressed beyond yield during its lifetime. Elastically responding walls are often used when this high strength is supplied unavoidably as a result of requirements not related to strength demand, such as requirements for minimum reinforcement or architectural considerations. This situation may occur when the cross-sectional dimensions of the wall are relatively large (eg. a fire wall) or when the inertial loads are small due to few storeys and small building mass.

In normal design situations, however, great strength is rarely necessary. A reinforced concrete structure can behave adequately even though parts of it may be forced into the inelastic range. By taking advantage of reinforced concrete's post-elastic strength and deformation characteristics, according to the now well-accepted principles of strength design, one can construct more economical and perfectly adequate walls. However, with a reduced strength, a wall must possess ductility, the ability to deform inelastically and still retain sufficient strength. In effect, the designer trades off strength for ductility. (See Fig. 2.3.) Ductility here is defined in terms of displacement at the top of the structure. Displacement ductility, μ_Δ, at any instant in the loading history is the ratio of the displacement at that instant, Δ_i, to the yield displacement, Δ_y. Since the behaviour of reinforced concrete structural walls is highly nonlinear and not perfectly elasto-plastic, as shown in Fig. 2.3, Δ_y is usually not readily identified. It is, therefore, convenient to arbitrarily define Δ_y as in Fig. 2.4. (See also ref. 26, section 4.1.)

Two questions arise: by how much can the strength be reduced, and how much ductility is required as a result of

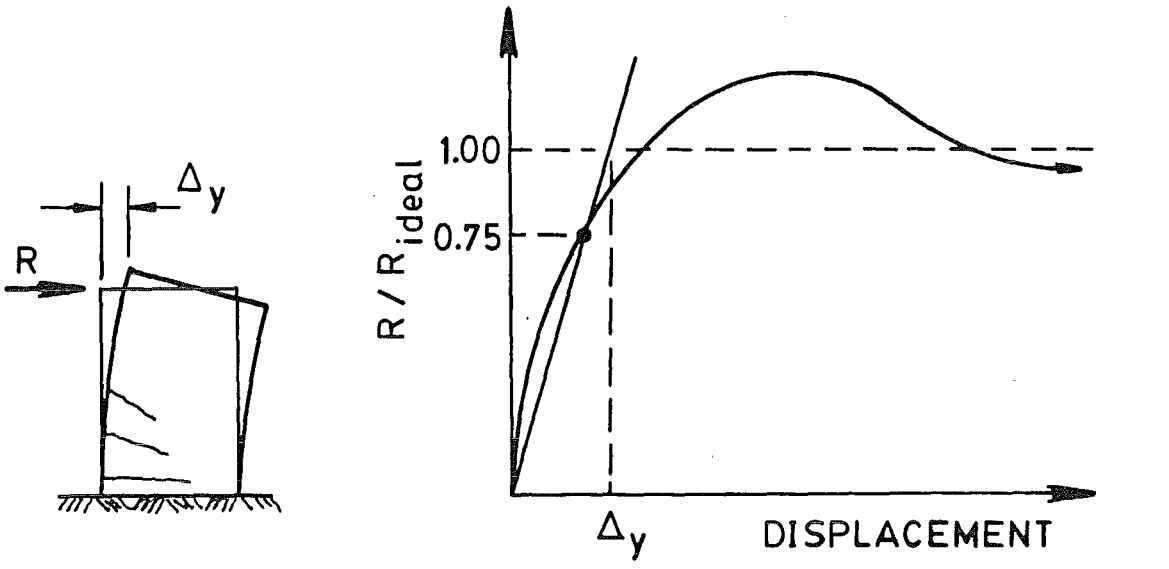

Fig. 2.4 - Definition of yield displacement

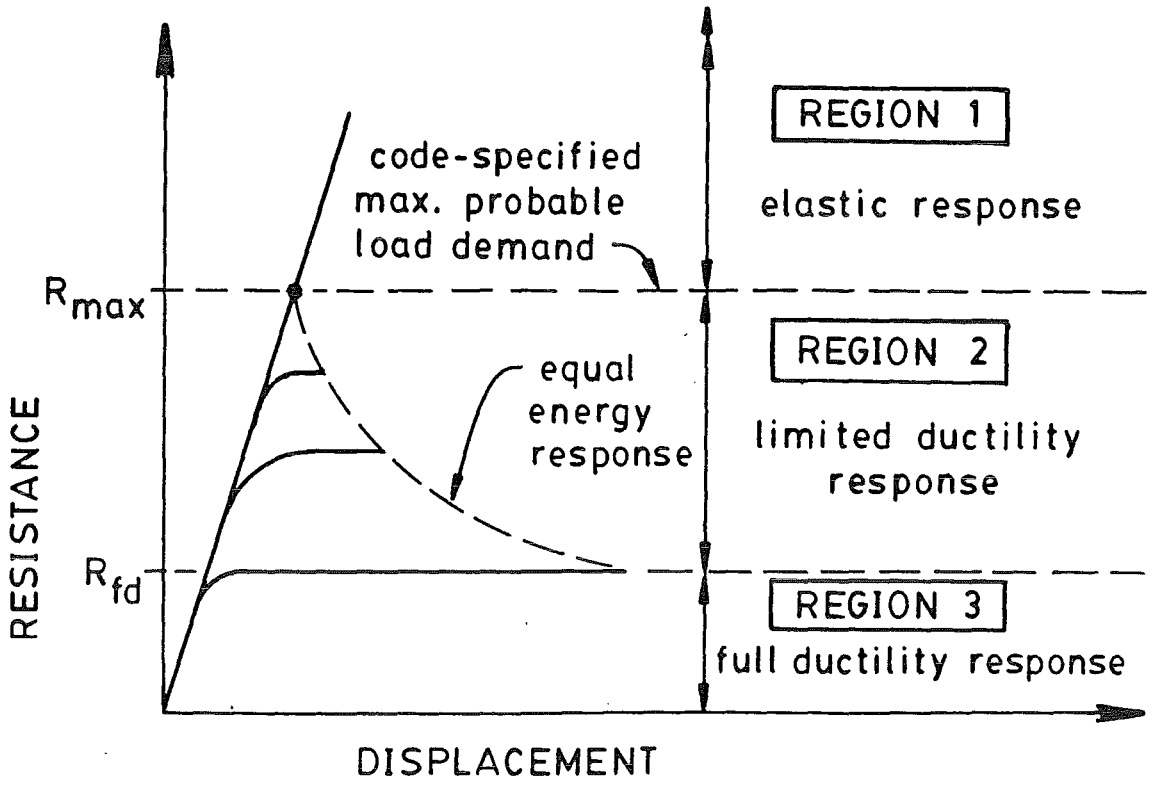

Fig. 2.5 - Elastic response, limited ductility response, and full ductility response - Resistance vs. maximum displacement imposed by a design earthquake

the reduced strength? To ensure some uniformity in the interpretation of ductility requirements, in New Zealand (1), a fully ductile structure is defined as one that can sustain eight load reversals during which the top of the structure is displaced to four times its yield displacement in each direction while the structure retains at least 80 percent of its original strength (ref. 1, clause C3.2). See Fig. 2.1.

2.5 CAPACITY DESIGN

The most rational way to achieve a fully ductile structure is by means of capacity design, a deterministic design procedure that ensures that when the structure is displaced beyond its elastic limit, only ductile flexural deformations occur and then only in predetermined areas of the structure. These areas, normally called plastic hinges, are then carefully detailed to provide ductility usually in excess of the design ductility level required by the code. As a result, then, even if an unexpectedly large earthquake occurs, the structure will yield in the preferred ductile mode dissipating energy while retaining sufficient resistance with respect to gravity and lateral loads.

In standard seismic design, an equivalent static lateral load is applied to the structure, and a reasonably accurate linear elastic analysis is carried out. It is not necessary to preserve a high degree of accuracy. First, the real load imposed by the earthquake will differ from the equivalent static load. Second, the distribution of member forces will change because of dynamic demands. Third, the distribution of member forces will change as soon as the structure enters the inelastic range. In the analysis, the aim is simply to find a solution that satisfies equilibrium and leads to a reasonable strength distribution throughout the structure. Non-ductile modes of failure are suppressed by providing resistance in these modes which is in excess of the maximum possible resistance demand controlled by flexure.

In strength design, member moments, axial forces, and shear forces resulting from the analysis are used in proportioning members. However, in capacity design, only the moments are used initially. From the moment demand predicted by the analysis, the sizes and numbers of flexural reinforcing bars are derived. The flexural overstrength of a

selected member is then calculated using the actual reinforcement layout specified. In the calculation of flexural overstrength, account is also taken of the actual yield strength of steel being larger than nominally specified and also strain hardening and the contribution of slab reinforcement to flexural tension. A possible increase in local load demand in columms and walls is also considered due to the effects of higher modes of vibration of the structure. (See ref. 5.) The shear demand on the member is then calculated from considering equilibrium at the development of flexural overstrength. Thus, the possibility of shear and other non-ductile failure modes is virtually eliminated.

2.6 STRUCTURAL WALLS OF LIMITED DUCTILITY

Figure 2.5 shows lateral load resistance, R, versus the maximum displacement imposed by the design earthquake. R_{max} represents the maximum probable lateral load demand imposed by the design earthquake. For a structure with resistance $R = R_{max}$, no ductility is required. The structure is expected to behave elastically. On the other hand, for a structure with resistance $R = R_{fd}$, the design earthquake can be expected to push the structure well into the inelastice range. Detailing for full ductility is required. For structures with resistance $R_{fd} < R < R_{max}$, only limited ductility demands are expected.

Although capacity design is generally preferred because it deterministically results in a fully ductile and usually economical structural wall, to carry out capacity design fully may, in some cases, be impractical. For example, some shorter walls may contain so much vertical reinforcement for reasons of geometric configuration or minimum code requirements that the flexural strength may be far in excess of that required by even elastic design (region 1, Fig. 2.5). In some of these cases, imposing rigidly all the requirements of capacity design may be uncalled for because the wall may be so strong that it is never expected to yield during its lifetime. For example, instead of requiring the shear strength to be greater than this excessive flexural strength, simple strength design of the shear reinforcement, using the maximum probable load demand, (R_{max}, Fig. 2.5) may suffice. In addition, because the wall

is expected to remain elastic, some of the special detailing requirements for ductility may be waived.

In the same way, for walls in the intermediate range (region 2, Fig. 2.5), with flexural strength less than that corresponding to fully elastic behaviour but still greater than that for fully ductile behaviour, it may not be necessary to ensure full ductility. It may be possible to accept a non-flexural mechanism, that is, a mechanism of limited ductility, such as shear. However, it is necessary to ensure that dramatic loss of resistance does not occur during the limited inelastic response. Because the level of resistance is not as high as the demand by elastic response, a certain amount of ductility must be available.

An important question, then, for the design engineer dealing with these intermediate walls of limited ductility is: for a given level of strength above that corresponding to fully ductile behaviour, how much ductility and energy dissipation capacity is required for a non-flexural mechanism to be considered acceptable? This question will be addressed later. There is a more fundamental question, however. How does a wall obtain such high strength in the first place? In other words, how does a wall with limited ductility ever come to exist? If capacity design is always preferred because it deterministically produces a fully ductile wall, then why does not the designer, in every case, use capacity design to purposely provide appropriate strength and ductility and avoid all mechanisms that limit ductility? These questions will be answered next by considering practical situations that lead to excessive flexural strength and limited ductility in walls.

2.7 UNIFORM RECTANGULAR WALLS OF LIMITED DUCTILITY

First, consider the simplest case: uniform rectangular walls (Fig. 2.6(a)). For new walls yet to be designed, avoiding ductility-limiting mechanisms should not be difficult. Synge (7) showed that even relatively squat walls can be designed to be ductile. In existing walls that were designed before capacity design procedures were introduced, however, the shear strength may well be less than the flexural strength. This is not to say that these walls are hazardous. Such a wall may well have been designed using

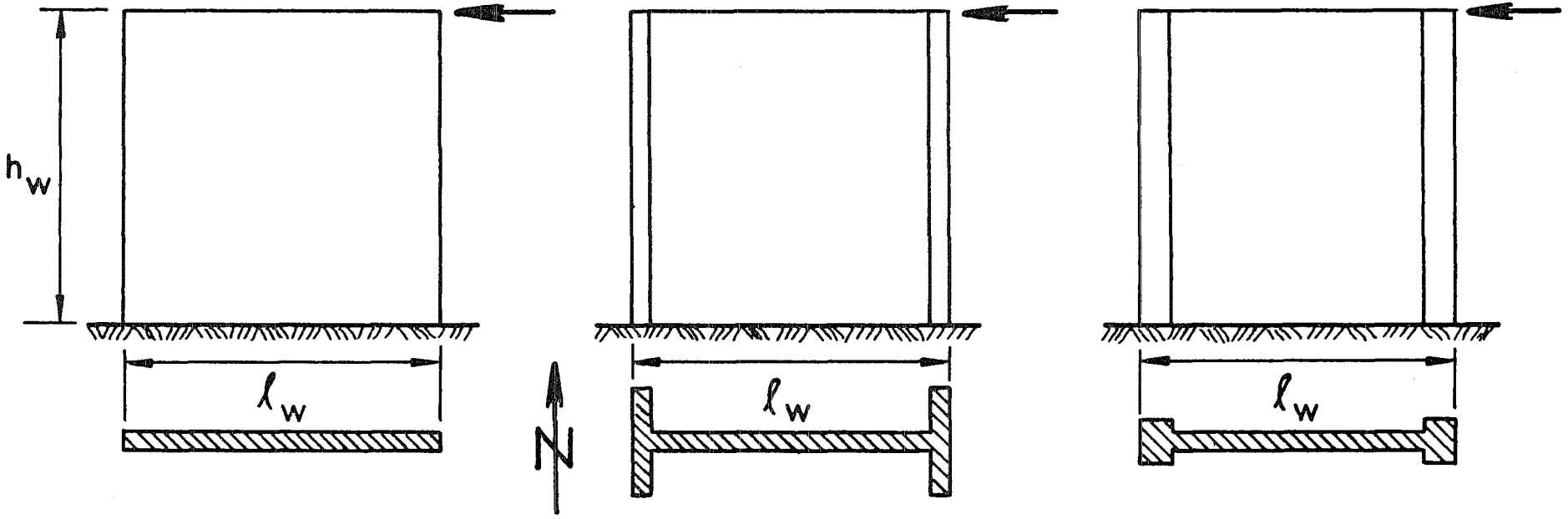

(a) Rectangular section (b) Flanged section (c) Barbell-shaped section

Fig. 2.6 - Low-rise cantilever walls

an equivalent static lateral load greater than that required today, and it may possess strength greater than that required for a fully ductile wall today (region 2, Fig. 2.5). However, if its strength is governed by shear, then it could possibly be inadequate in terms of energy dissipation. See Section 2.1, Fig. 2.2. Existing structural walls, particularly the shorter walls ($h_w / \ell_w \leq 3$), may well fall into the category of structural walls of limited ductility. (See Table 2.1.) For such walls then, it is important to identify the failure mechanism, its strength, its ductility capacity, and its energy dissipation capacity when displaced beyond its elastic limit.

2.8 UNIFORM FLANGED WALLS OF LIMITED DUCTILITY

Next, consider uniform flanged walls (Fig. 2.6(b)). Designing for temperature and shrinkage will usually result in a uniform distribution of vertical reinforcement in the web and in the middle regions of the flanges. Designing for a north-south earthquake will result in perhaps additional reinforcement in the flange tips. So before the designer even considers attack in the east-west direction, a quantity of vertical reinforcement is already specified. The same reasoning may be applied to barbell-shaped walls (Fig. 2.6(c)), where the amount of reinforcement in the columns may be governed by frame action perpendicular to the wall. The flange reinforcement in the wall of Fig. 2.6(b) needed to resist a north-south earthquake, when combined with the temperature and shrinkage reinforcement provided in the web, may well lead to excess flexural strength in the east-west direction. That is, the flexural strength may be greater than that required by the relevant loading code for a fully ductile wall (region 1 or 2, Fig. 2.5). Short walls are particularly suspect here because the code-specified lateral loads may be small because of the small masses present. The flexural strength may even be greater than that required to keep the wall elastic (region 1, Fig. 2.5). In the second case, the wall may be designed to have shear strength corresponding to elastic seismic response (R_{max}), and the requirements for ductility may be waived. In the first case, however, when the strength lies within region 2, the design method is not so clear. It may not be necessary to provide

shear resistance higher than the flexural resistance. It may well be acceptable to provide shear resistance lower than the flexural overstrength, as long as the shear resistance is kept relatively high (greater than R_{fd} in Fig. 2.5) and as long as the shear mechanism demonstrates some ductility. Also, the shear mechanism must not significantly impair the wall's ability to dissipate seismic energy.

Thus, before capacity design principles are compromised (ie. providing shear strength lower than flexural overstrength), it is necessary to evaluate the ductility and energy dissipation characteristics associated with shear mechanisms. Also, it is important to assess the adequacy of specific combinations of shear strength, ductility, and energy dissipation. First, however, a description of flexural and non-flexural failure mechanisms in cantilever structural walls is called for.

SECTION 3

MECHANISMS OF LATERAL LOAD RESISTANCE IN CANTILEVER WALLS

3.1 GENERAL COMMENTS

The mechanisms of resistance of transverse loads in beams is understood reasonably well. Two mechanisms, beam action and arch action, are generally well-accepted and are described in detail in reference 9, section 7.3. Beam action is dominant in slender beams, while arch action is dominant in deep beams. The same two mechanisms are found in cantilever walls, since walls can be thought of as deep beams oriented in the vertical direction. For simplicity, consider an isolated wall with a single lateral load at the top (Fig. 3.1). The external moment is resisted by the internal couple formed by the resultant concrete compressive force, C, and the resultant reinforcement tensile force, T, separated by the lever arm, jd.

$$M = T\ jd \qquad \text{(Eq. 3-1)}$$

The well-known equation relating shear to the rate of change of bending moment yields

$$V = \frac{dM}{dx} = \frac{d(Tjd)}{dx} = jd\ \frac{dT}{dx} + T\ \frac{d(jd)}{dx} \qquad \text{(Eq. 3-2)}$$

The first term describes beam action, while the second term describes arch action. The total shear resistance is provided by a combination of the two mechanisms.

In beam action, the internal lever arm, jd, remains constant throughout the height while the coupling force, T=C, decreases with height (dT/dx) in order to match the decrease in external moment (Fig. 3.2). The rate of change in tensile force in the reinforcement (dT/dx) implies bond forces acting along the bar. Therefore, integrity of concrete-to-steel bond and the transfer of shear stresses in the concrete are essential for beam action.

In arch action, the coupling force (T=C) remains constant while the internal lever arm shortens with height (d(jd)/dx) in order to match the decrease in external moment

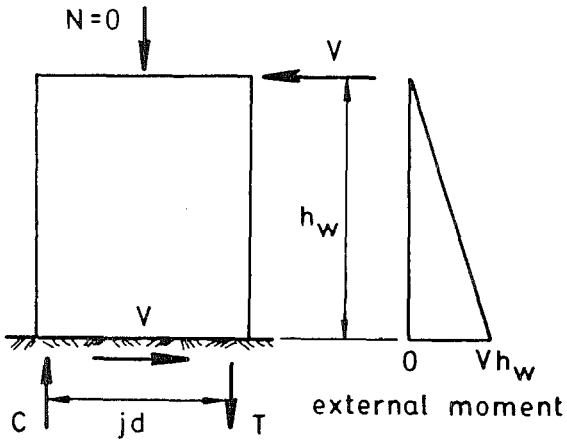

Fig. 3.1 - Forces on a cantilever wall

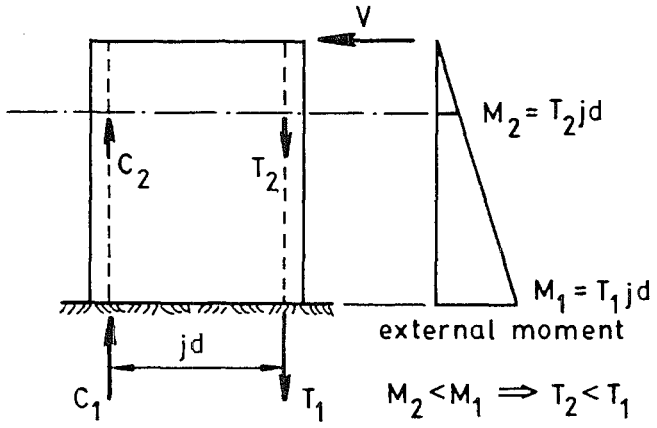

Fig. 3.2 - Beam action in a cantilever wall

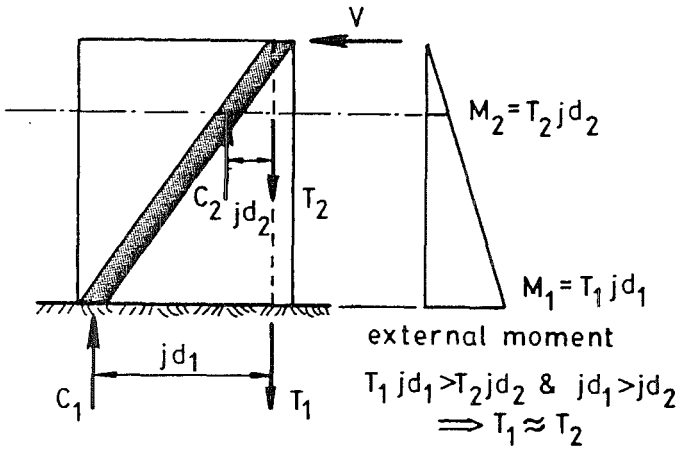

Fig. 3.3 - Arch action in a cantilever wall

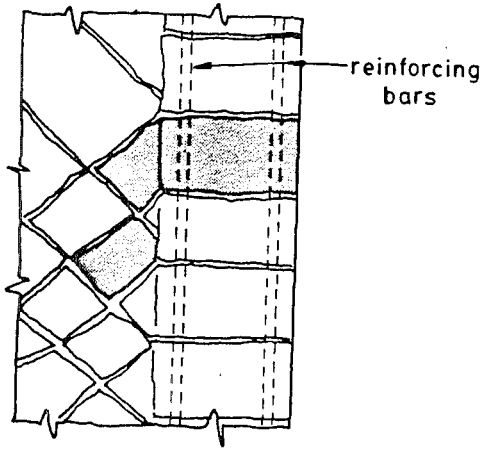

Fig. 3.4 - Diagonal cracking minimizing bond and shear transfer, which promotes arch action

(Fig. 3.3). In pure arch action, constant force in the reinforcement implies zero bond stresses acting along the bar. In real walls, the condition of zero bond stress (pure arch action) is rare, if not impossible. However, it is not so much the condition of zero bond along the bar that dictates arch action as the lack of transfer of bar force into the surrounding body of concrete. Under reversed cyclic loading, diagonal cracks separate the concrete into triangular or diamond-shaped pieces (Fig. 3.4). It is the inability of shear forces to be transferred from one block bounded by cracks to another, shown shaded in Fig. 3.4, that coincides with arch action.

As mentioned above, the lateral load on a wall is rarely resisted purely by beam action or purely by arch action. Usually a combination of the two is in effect, each mechanism resisting lateral load in proportion to its stiffness. For very slender members, the arch is quite flat and, therefore, rather ineffective. Beam action, therefore, is predominant in slender members. For squatter members, the arch can be quite effective and can therefore attract a larger portion of the lateral load. Consequently, arch action tends to predominate in low-rise walls. The relative influence of the two mechanisms can be deduced even during the elastic stages of loading by measuring the change in bar force along the height. The more the bar force changes with height, the more influencial is beam action.

In reference 9, Park and Paulay describe arch action in simply supported beams (Section 7.3.3, ref. 9). In the simplest case, arch action involves one diagonal compression strut and one steel tie (Figs. 3.5 and 3.6). However, in some members with distributed shear reinforcement, arch action may take the form of several diagonal compression struts and several tension ties. Such a system of struts appearing in a squat wall is described in ref. 9, Section 12.2.2. Several researchers have extended simple arch action to include series of parallel struts (diagonal compression fields), series of struts inclined at increasing or decreasing angles (compression fans), combined arches, struts, and fans, and specific nodal regions (10,12,13,14). MacGregor refers to such systems as equilibrium truss models, and in ref. 12 he gives an excellent summary of the

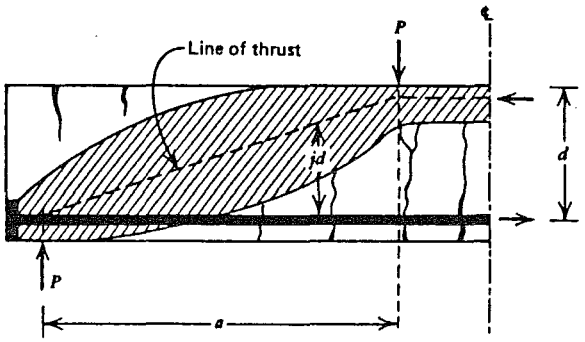

Fig. 3.5 - Arch action in an idealized beam (9)

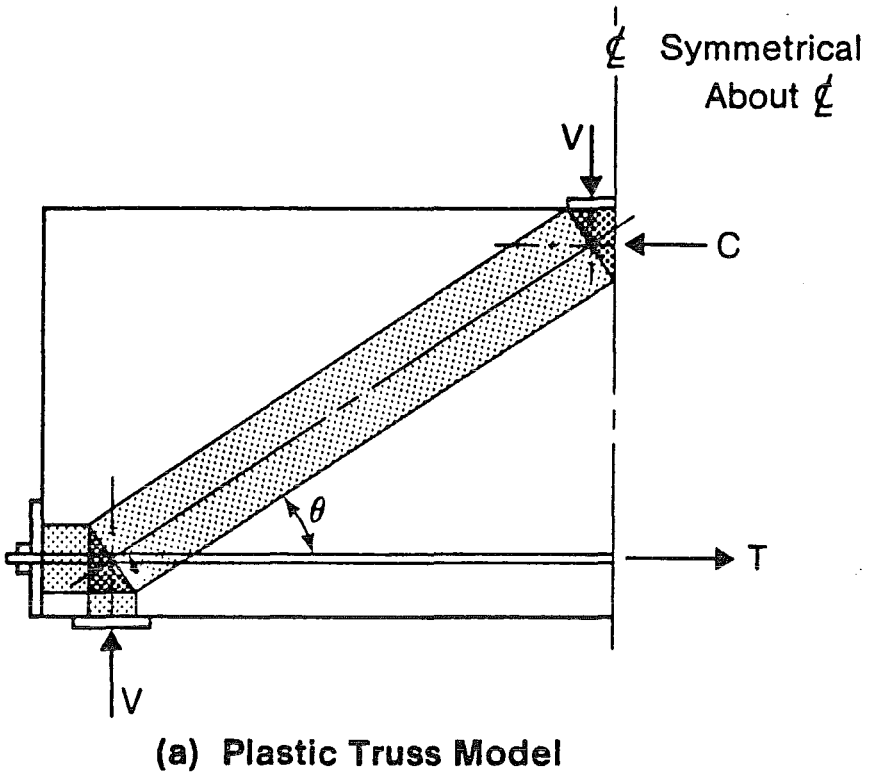

Fig. 3.6 - Plastic truss model for a beam without web reinforcement (10)

research. For an example, see Fig. 3.7. Equilibrium truss models require that:

1) Equilibrium must be satisfied.
2) The concrete resists only compression and has an effective compressive strength, f_c^*, usually less than f'_c. Marti (13) suggests that $f_c^* = 0.60f'_c$ for design purposes. Rogowski and MacGregor (11) suggest that $f_c^* = 0.67x0.85f'_c = 0.57f'_c$ for design purposes. Collins (15) suggests that f_c^* and the strut angle, θ, are interdependent.
3) Reinforcement is required to resist all tensile forces.
4) The centroidal axes of truss members and the lines of action of all externally applied loads at a joint must be concurrent.
5) Failure of the model truss occurs when a concrete compression member crushes or when a sufficient number of steel tension members reach yield to produce a mechanism.

Certain limits apply to the allowable angle of inclination of the compression struts, θ. Struts inclined at angles outside these limits are ineffective.

Marti (13) suggests	$31° < \theta < 59°$.
Schlaich (14) suggests	$30° < \theta < 60°$.
Thurlimann (16) suggests	$26.6° < \theta < 63.4°$.
MacGregor (12) suggests	$25° < \theta < 65°$.

In many of the deep beams that Rogowski and MacGregor tested, the equilibrium truss model predicted the longitudinal reinforcement stresses quite accurately, as seen in Fig. 3.7. The beam theory prediction was clearly inapplicable. The approximately constant bar stresses indicate arch action.

For the squat wall illustrated in Fig. 3.8, three regions can be identified. In region 2, a diagonal compression field (parallel struts) predominates. Here, the lateral load introduced at the top of the wall is resisted by the horizontal component of the diagonal compression, which, in turn, enters the foundation by means of direct shear at the base of the wall. Tension in the vertical bars equilibrates the vertical component of the diagonal

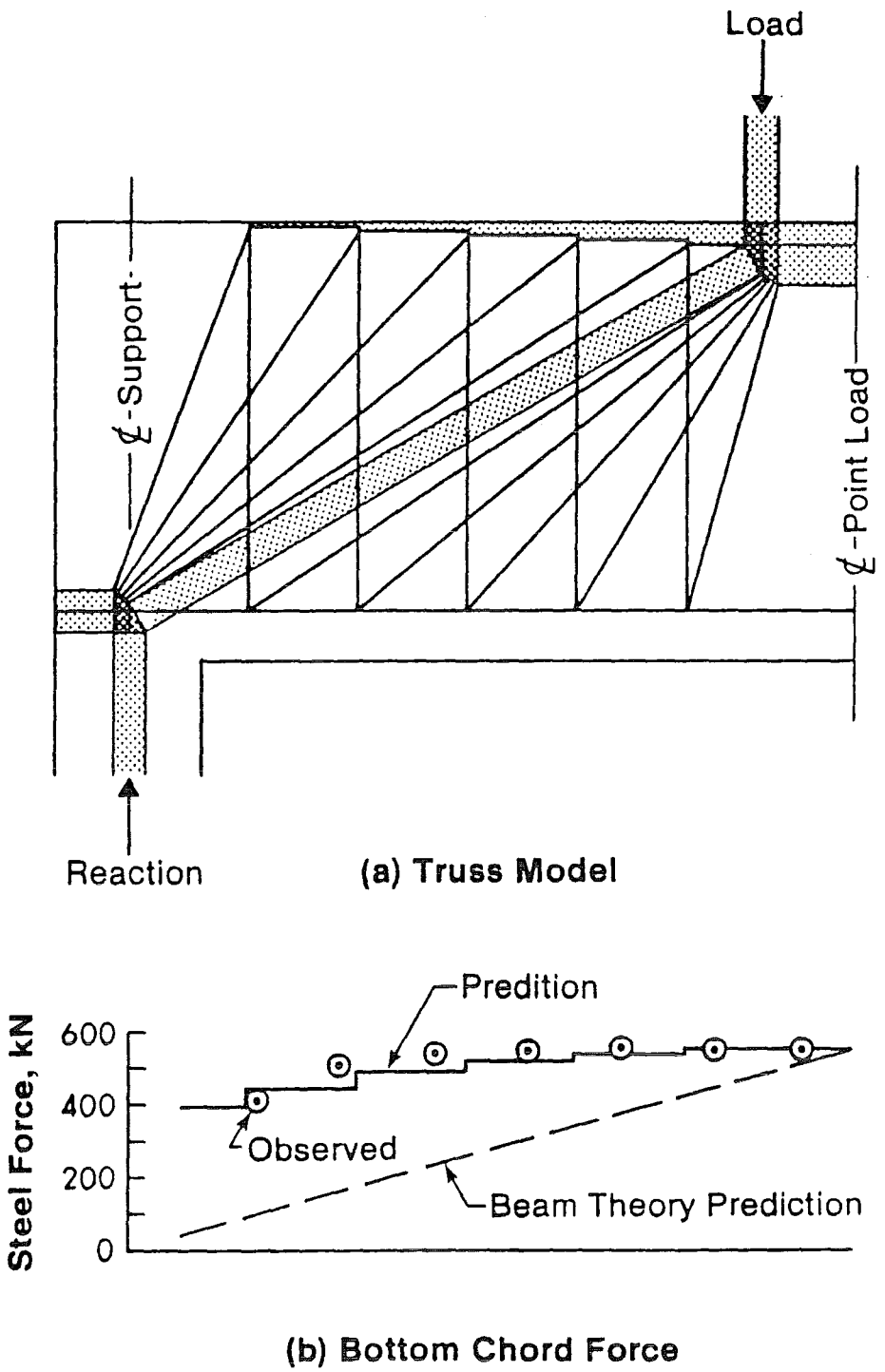

Fig. 3.7 - Plastic truss for Rowgowski and MacGregor's test beam 1/1.5N (10)

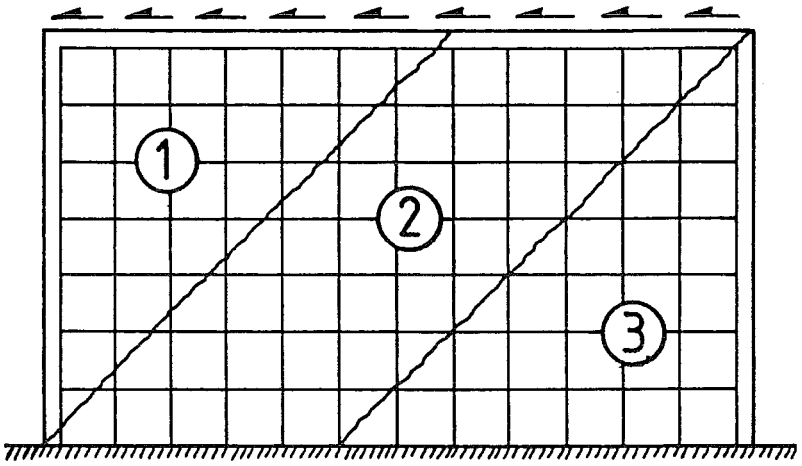

(a)

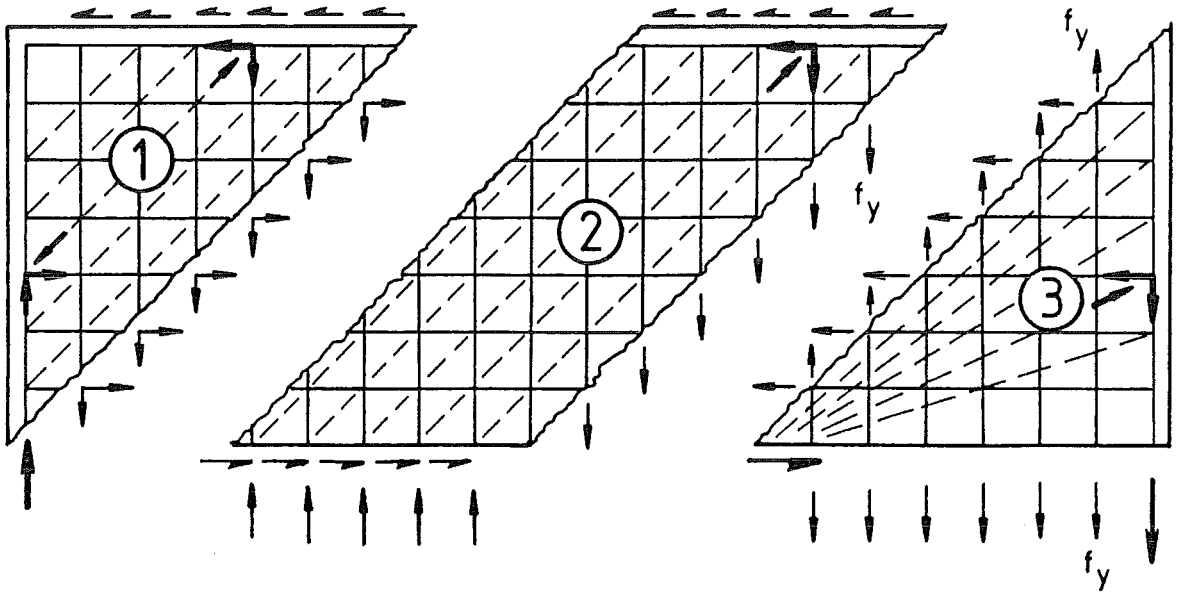

Diagonal Compression Fields Compression Fan

(b)

Fig. 3.8 - Mechanism of lateral load resistance in a low-rise wall

compression. Horizontal reinforcement is generally ineffective in region 2 and therefore is stressed approximately equally across region 2.

In region 1, a diagonal compression field exists, but horizontal bars are required to balance the horizontal component of the diagonal compression. The vertical bars are stressed as well, since they equilibrate the vertical component.

In region 3, a compression fan exists. The forces generated in the horizontal bars of region 1 are transferred with little change across region 2 to region 3. On the right-hand boundary, fanning diagonal compression struts balance these horizontal forces. The horizontal components of these fanning struts enter the foundation by aggregate interlock and dowel action at the base of region 3. Tension in the vertical boundary element bars balances the vertical components of these diagonal compression struts. Little change in vertical bar force occurs through the height of region 3 (except in the vertical boundary element).

It should be noted that the boundaries between the three regions cannot be defined with great precision. Also, in general, the deformations of the three regions of Fig. 3.8 are incompatible if a uniform shear flow along the top edge is assumed. For example, mechanisms 1 and 2 result in strains of opposite sense at the base section (refer Fig. 3.8(b)). Mechanism 1 implies tensile vertical strains, while mechanism 2 implies compressive vertical strains. This incompatibility of strains implies that the shear input at the top is not uniform. Because the forces in region 2 are compatible with observed deformations, it is likely that more shear enters region 2 than region 1. The relative effectiveness of the three regions can also be deduced by considering stiffness. For example, region 2, which involves direct compression, is stiffer than region 1, which involves tensile straining of horizontal bars. Therefore, on this basis, region 2 will attract more lateral load. It is likely that the majority of the shear is introduced into region 2 and that only a small percentage enters region 1. Indeed, for his walls, Synge (7) found that only approximately 30 percent of the top shear entered region 1.

3.2 FLEXURAL FAILURE (FAILURE IN BEAM ACTION)

When beam action dominates behaviour in a cantilever wall, flexural failure occurs. Providing that the wall is underreinforced, that the concrete is well-confined, and that the compression edge is braced laterally against out-of-plane buckling, failure occurs with the yielding and eventual fracture of vertical tension bars (Fig. 3.9(b)). After yield, the wall can normally sustain additional load due to the development of strain hardening in the vertical bars. The flexural failure mode is preferred because such a wall can often sustain very high displacement ductilities with minimal loss of strength. It also has good energy dissipation characteristics, shown in reasonably full-bodied hysteretic loops.

3.3 BASE SLIDING FAILURE

Base sliding failure generally occurs as a result of flexural yielding under reversed cyclic loading. It begins with the interconnection of horizontal flexural cracks at the base section. Grinding and pure shear between the two crack surfaces result in the loss of aggregate interlock and the mobilization of dowel action (Fig. 3.9(d)). The energy dissipation characteristics of this failure mode are poor. The hysteretic loops exhibit significant pinching.

3.4 CONSTRUCTION JOINT FAILURE

Construction joint failure is similar to base sliding failure. It initiates under load reversals with the interconnection of horizontal flexural cracks along a horizontal construction joint somewhere above the base section (Fig. 3.9(c)). Although every construction joint presents a potential plane of weakness, construction joint failure can usually be prevented by careful preparation of the joint during concreting. When the joint is not prepared properly, construction joint failure may result.

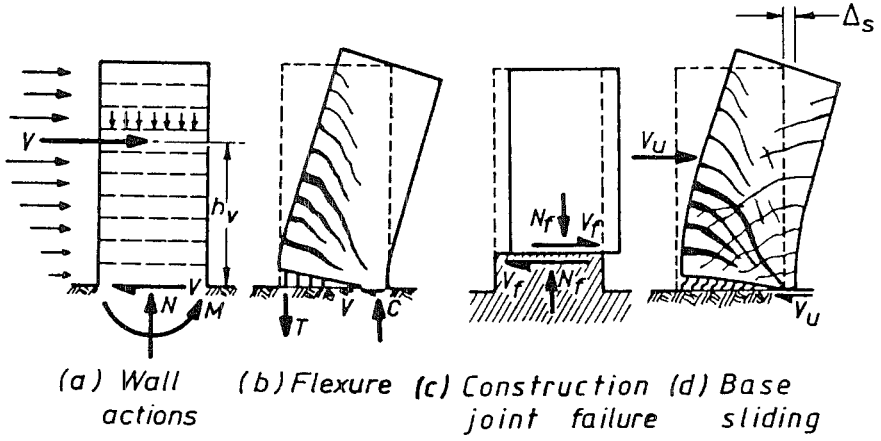

Fig. 3.9 - Failure mechanisms (5)

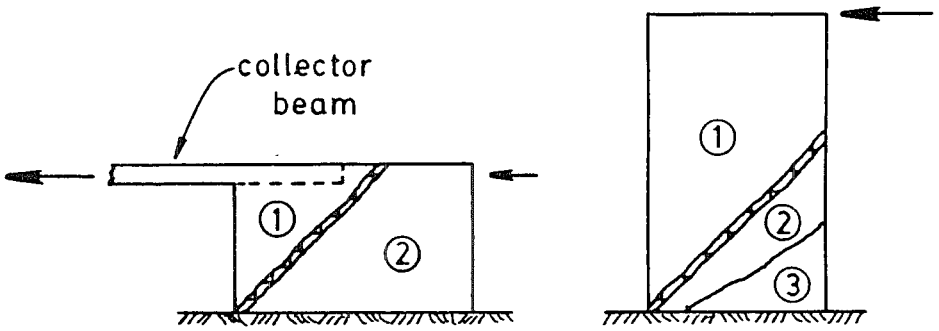

Fig. 3.12 - Yielding of web bars between regions 1 and 2

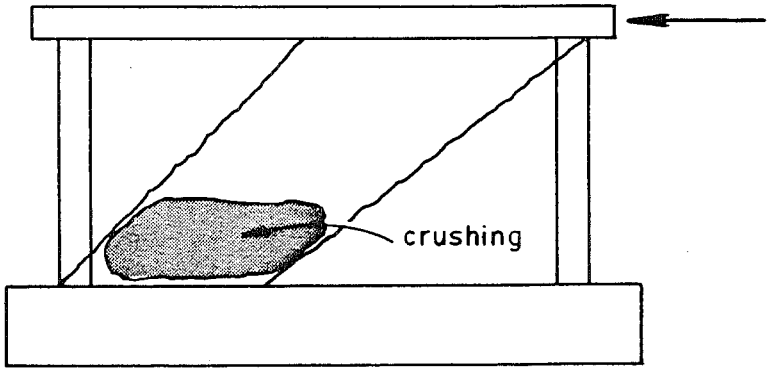

Fig. 3.10 - Diagonal compression failure

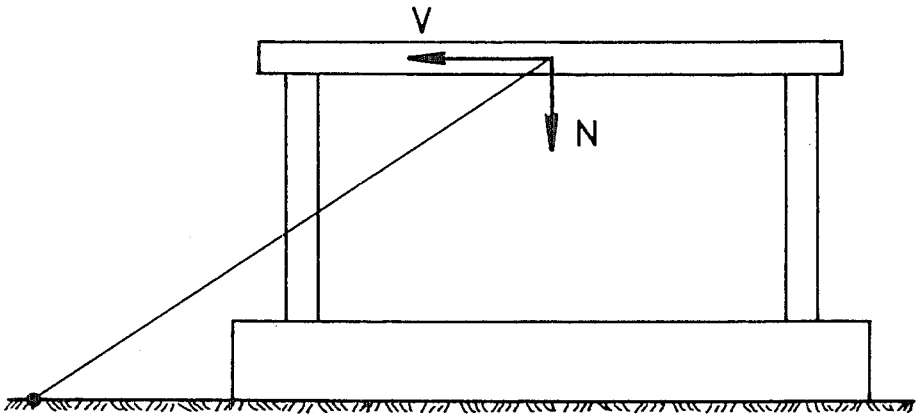

Fig. 3.11 - Force resultant on a low-rise wall

3.5 SHEAR FAILURE (FAILURE OF ARCH ACTION/EQUILIBRIUM TRUSS)

Although the following mechanisms rarely involve direct shear, as found in base sliding, they can be referred to as shear failure mechanisms because they occur when large inclined shear cracks dominate behaviour (arch action or equilibrium truss action).

One possibility is diagonal compression failure. This failure occurs when there exists so much vertical and horizontal reinforcement that the concrete crushes in the diagonal compression strut before the web reinforcement yields (Fig. 3.10). Although possible, this failure mechanism is rare in practice due to the nature of foundations in low-rise buildings. The axial load on a low-rise structural wall may be so small compared with the lateral load that would cause crushing that the resultant force may lie well beyond the foundation of the wall. Thus, the wall would generally tip before the concrete in the diagonal strut would crush (Fig. 3.11).

The second possibility of failure, when arch action predominates in a wall, is the yielding of the vertical bars that tie down the main diagonal compression strut (region 2 in Fig. 3.8). As noted earlier, the vertical bars will be stessed nearly uniformly throughout the height of the wall. Therefore, vertical bar forces are reasonably constant through the height of region 3 (Fig. 3.8(b)). In this mechanism, the wall can carry loads beyond that causing yield by mobilizing strain hardening in the vertical bars. Indeed, the ideal flexural strength may be attained in this mode of failure if the majority of the vertical bars in regions 2 and 3 in Fig. 3.8 yield. The ductility capacity of this mechanism is good. However, due to the widening and slipping that tends to occur along the inclined shear cracks, energy dissipation with reversed loading is not as good as that for a flexural mechanism. The hysteretic loops for this mechanism display significant shear pinching.

The third possibility of failure is the yielding of horizontal bars at the interface of regions 1 and 2 in Fig. 3.8. If, because of the loading system or because of a high aspect ratio (Fig. 3.12), a large portion of the lateral

load enters region 1, yielding in the horizontal web bars may occur before yielding of the vertical bars in regions 2 and 3.

Finally, the above-mentioned shear mechanisms may not necessarily be mutually exclusive. For example, depending on aspect ratio and the percentages of horizontal and vertical reinforcement, failure may involve a combination of the above-mentioned mechanisms.

3.6 POSTULATED BEHAVIOUR OF PRESENT TEST UNITS

For the present test units, it is postulated that arch action, rather than beam action was predominant, especially in the squatter walls and near the base in the more slender walls. As slenderness increased, the influence of beam action increased, especially in the upper regions of the wall away from the fixed base. The first major cracks that occurred were due to shear. These extended virtually corner-to-corner across the web. It is postulated that these diagonal cracks defined the direction of diagonal compression struts, which, in turn, governed the behaviour of the test units. In general, cracks developed at various angles. Apparently, both compression fans and diagonal compression fields were effective. It is postulated that, before attaining maximum load, the mechanism involved mainly straining of vertical boundary element bars and neighbouring web bars that tied down the main diagonal struts (region 2, Fig. 3.8). The vertical bars were strained approximately uniformly with height, indicating arch action. Horizontal bars were also strained severely along the unit's main diagonals. The ideal flexural strength of each unit was attained and exceeded as the vertical bars yielded. However, after maximum load, the yielding of horizontal bars began to dominate behaviour. The failure mechanism involved primarily a horizontal displacement of the upper region of the wall with respect to the lower region (Fig. 3.13(b)) and a loss of the flexural compression area at the base. Excessive straining and, in some cases, even fracture of horizontal web bars occurred. In addition to horizontal displacement, rotational displacement occurred (Fig. 3.13(c)), along with uniform yielding of vertical bars tying down the upper region.

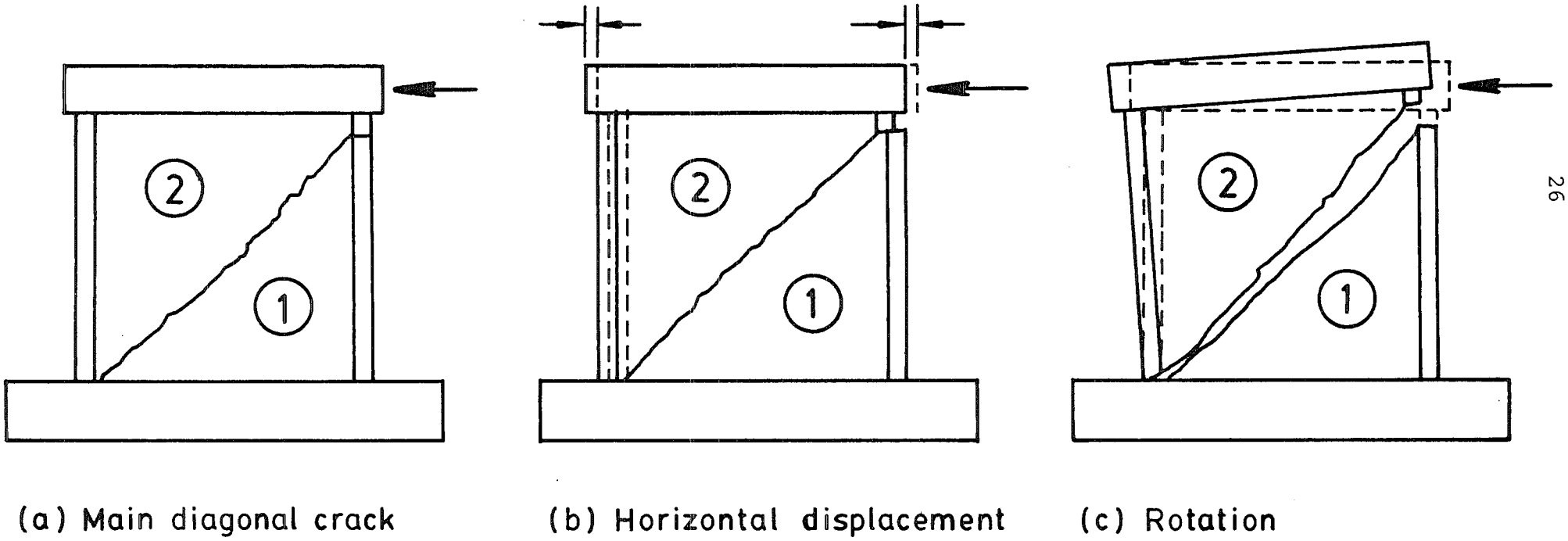

Fig. 3.13 - Proposed failure mechanism for present test units

SECTION 4

LITERATURE SURVEY

Several experimental and theoretical studies performed previously have bearing on the problems of structural walls of limited ductility.

4.1 BARDA (17,18)

At the Portland Cement Association Laboratories (17,18), a series of tests were carried out by Barda on low-rise, cast-in-place structural walls with boundary elements. The main aim of the tests was to investigate the effect of horizontal and vertical web reinforcement on the shear strength of the walls. For each test unit, Barda sought to identify the failure mechanism and evaluate its shear strength. Eight units were tested, six with $h_w/\ell_w=0.50$, one with $h_w/\ell_w=0.25$, and one with $h_w/\ell_w=1.00$. The vertical boundary elements were heavily reinforced. Thus, flexural failure was avoided. A typical test unit is shown in Fig. 4.1.

In an attempt to model earthquake loading, static, reversed cyclic loading was imposed on most of the test units. Two full cycles were imposed at each load level in increments of $2\sqrt{f'}$ (psi) average shear stress up to the attainment of maximum load. Thereafter, deflection increments, rather than load increments, were imposed, two full cycles being imposed at each displacement level. (See Fig. 4.2.) Information regarding reduction in strength and stiffness upon repeated cycling was obtained. Barda made the following observations.

BARDA'S OBSERVATIONS

Barda's observations and conclusions, relevant to this project, are summarized in this section. Subsequently, comments of this author on Barda's work are presented.

1) For all eight units, the major part of the applied lateral load was carried to the foundation by

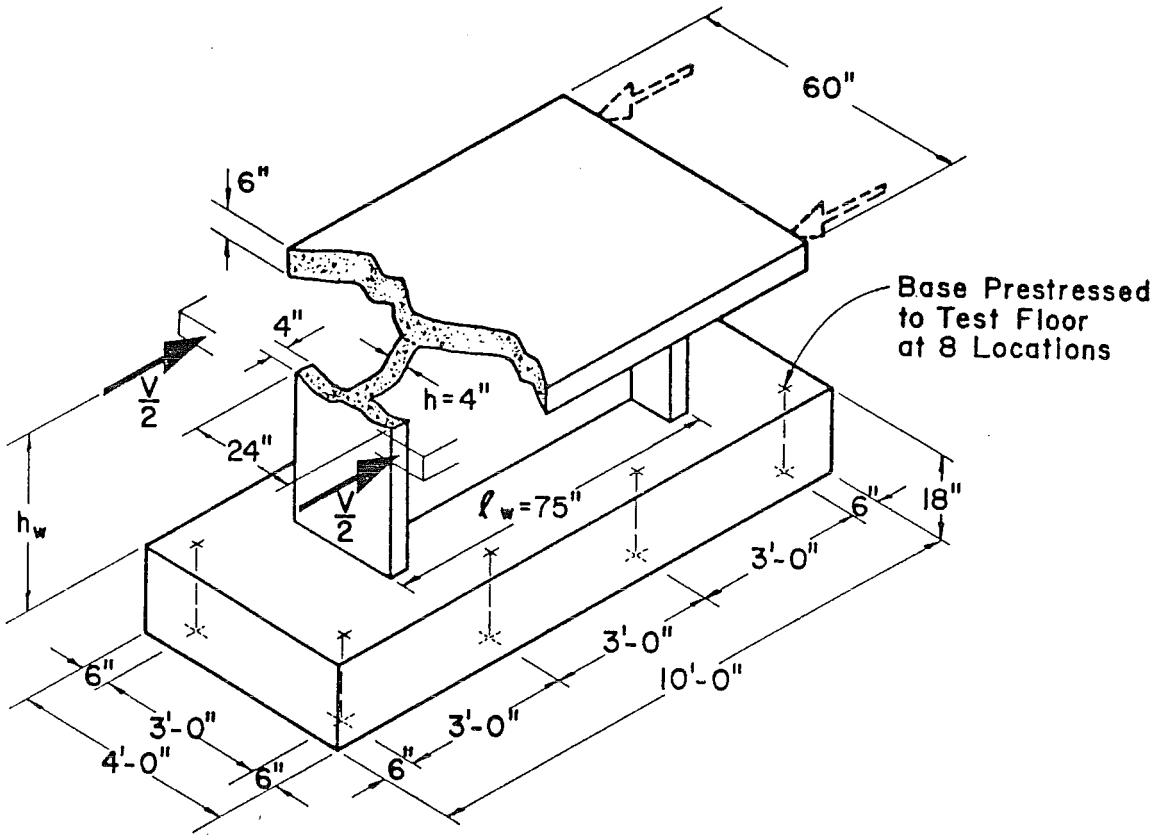

Fig. 4.1 - Typical test unit of Barda (17)

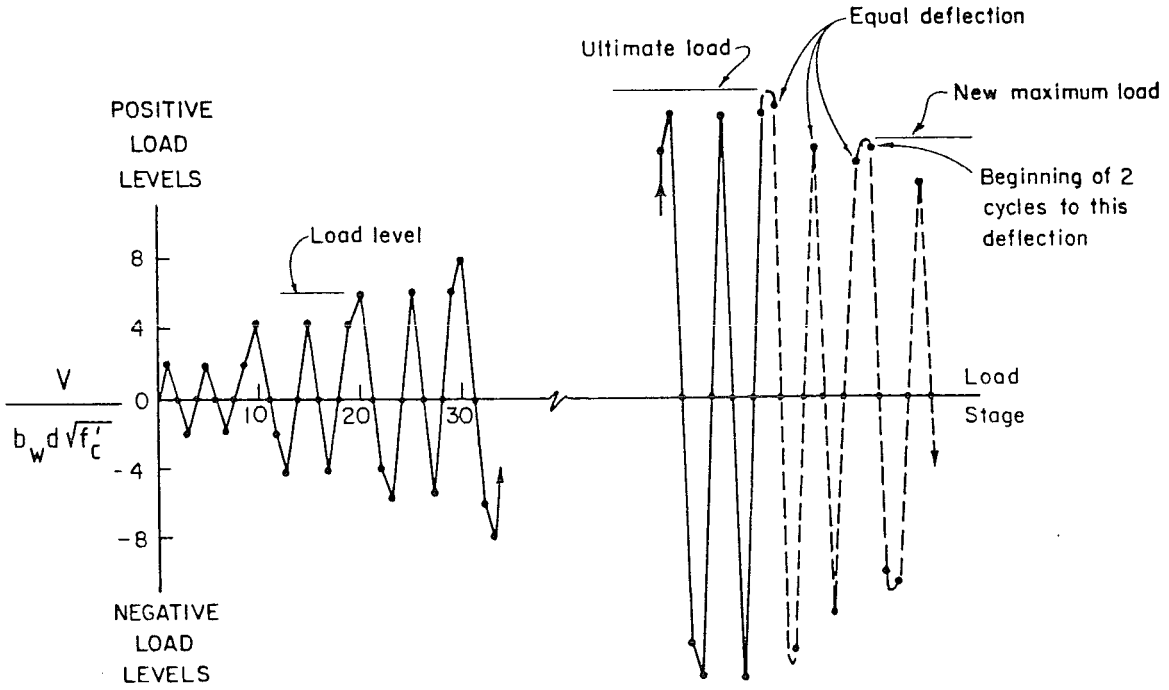

Fig. 4.2 - Loading method used in Barda's tests (17)

means of a concrete compression strut inclined at an angle of approximately 38 degrees. A slightly steeper angle was recorded for the wall with h_w/ℓ_w=1.00 (40-43 degrees). Arch action was clearly in effect. Vertical web bars effectively acted as tension ties, equilibrating the vertical component of the diagonal compression.

2) At the attainment of maximum load, the load-carrying mechanism generally involved yielding of vertical web bars only. Strains in vertical boundary element bars and horizontal web bars were small. After the attainment of maximum load, the load-carrying capacity, as well as the stiffness, degraded rapidly. Final collapse occurred due to crushing of concrete in the compression strut.

3) For walls with $h_w/\ell_w \leq 0.50$, the percentage of horizontal web reinforcement did not affect the shear strength of the wall, although it affected the distribution and widths of cracks.

4) For the wall with h_w/ℓ_w=1.00, the horizontal web bars were found to be more severely strained than the vertical web bars.

5) The percentage of vertical web reinforcement influenced the distribution and widths of cracks. It also greatly influenced the shear strength of the wall. The higher the percentage of vertical reinforcement, the greater was the lateral load resistance. Also, the participation of the vertical reinforcement in the mechanism of lateral load transfer increased as squatness increased.

6) When monotonic and reversed cyclic loading were compared, no significant difference in strength was recorded (only 10 percent difference). For reversed cyclic loading, two relatively independent diagonal compression strut systems

were utilized.

7) Shear strength was not affected by differences in the amount of flexural reinforcement in the boundary elements.

8) The shear strength of units with h_w/ℓ_w=0.25 and 0.50 were roughly the same.

9) The shear strength of the unit with h_w/ℓ_w=1.00 was 20 percent lower than the shear strength of the more squat walls.

10) Slippage and distress at construction joints occurred in three of the eight units. It occurred at approximately maximum load under both monotonic and reversed cyclic load. This may have decreased the shear strength of the walls by preempting the attainment of the full strength of the strut and tie mechanism.

11) Barda postulated that the shear strength of low-rise walls with aspect ratio $h_w/\ell_w \leq 0.50$ can be evaluated in terms of separate contributions due to concrete and reinforcement:

$$v_u = v_c + v_s = 0.70\sqrt{f'_c} + 0.95\rho_n f_y \text{ (MPa)} \qquad \text{(Eq. 4-1)}$$

12) The flexibility of the top slab greatly affected the behaviour of the walls in that it provided little restraint against the extension of vertical web bars. It was found that as the compression strut tended to rotate about its lower end, the vertical web reinforcement yielded, and the top slab hogged. Barda postulated that shear strength may have been different had a stiffer capping element been used.

13) Barda found that energy absorption, defined as the area under the envelope of the lateral load vs.

top deflection hysteresis loops, was proportional to shear strength. Therefore, he claimed that the same factors affected both energy absorption and shear strength.

14) The reductions in strength and stiffness in consecutive cycles to a given level were measured and are shown in Table 4.1. A typical set of hystertic loops is shown in Fig. 4.3.

COMMENTS ON BARDA'S OBSERVATIONS

Although Barda's loading scheme produced reasonably realistic displacements prior to maximum load, after the maximum load, the units were pushed rapidly to displacements well beyond realistic limits. (See Table 4.1.) For ductile frames, the maximum feasible displacement is considered to be Δ/h_w = 1/50 to 1/33. Beyond this, P-delta effects involving lateral instabilities come into effect. For ductile walls with no shear failure, it has been shown (29) that drifts of up to Δ/h_w = 1/33 can be attained. However, for low-rise walls failing in shear, a maximum value of Δ/h_w = 1/100 is considered realistic. Barda pushed his units to displacements as high as Δ/h_w=1/6. The behaviour of the units after Δ/h_w=1/100 (after maximum load) is of little practical use.

Regarding point 11 above, Barda developed equations for v_c and v_s using the observed truss mechanism. His equation for ultimate shear strength, v_u, was developed for walls with aspect ratio, $h_w/\ell_w \leq 0.50$, failing in shear. Barda obtained good agreement between the theoretical prediction and the test results. Barda's equation for v_u may well apply in general to squat walls subjected to earthquake-induced displacements. However, further verification of the equation may be desirable, especially for walls that are not so heavily reinforced in the boundary elements. For more slender walls ($h_w/\ell_w \geq 1.0$), Barda proposed an equation that would conservatively estimate the shear strength for design purposes:

TABLE 4.1 - STRENGTH AND STIFFNESS REDUCTION FOR THREE OF BARDA'S UNITS

Unit	Cycle No.	Approx. drift imposed Δ/h_w	Strength reduction[1] (%)		Stiffness reduction[1] (%)		
			2nd loading	3rd loading	2nd loading	3rd loading	
B3-2	1,2,3	1/660	8	16	15	15	(2)
$h_w/\ell_w = 1/2$	3,4,5	1/360	7	14	14	14	
	5,6,7	1/250	15	28	14	19	
	7,8,9	data missing		-	-	-	
	9,10,11	1/90	36.5	51	56	61	(3)
	11,12,13	1/50	36	48	57	57	
	13,14,15	1/25	26	44	44	48	
	15,16,17	1/16	15	24	52	52	
B7-5	1,2,3	-	25	29	16	21	(2)
$h_w/\ell_w = 1/4$	3,4,5	1/990	13	18	32	32	
	5,6,7	1/610	7	15	11	11	
	7,8,9	1/380	6	14	13	13	
	9,10,11	1/260	13	26	15	20	
	11,12,13	1/50	23	76	82	88	(3)
	13,14,15	1/15	70	88	82	86	
B8-5	1,2,3	1/2340	7	17	31	33	(2)
$h_w/\ell_w = 1.0$	3,4,5	1/790	4	7	40	40	
	5,6,7	1/460	7	7	21	21	
	7,8,9	1/310	12	20	14	14	
	9,10,11	1/185	23	43	29	59	
	11,12,13	1/60	61	84	71	86	(3)
	13,14,15	1/30	23	26	50	50	

(1) Reductions are reported as percent of the value observed on the first cycle to the given imposed drift level.

(2) Load-controlled cycles.

(3) Displacement-controlled cycles.

(4) Maximum load occurred during cycles 7,9, and 9 for Units B3-2, B7-5, and B8-5, respectively.

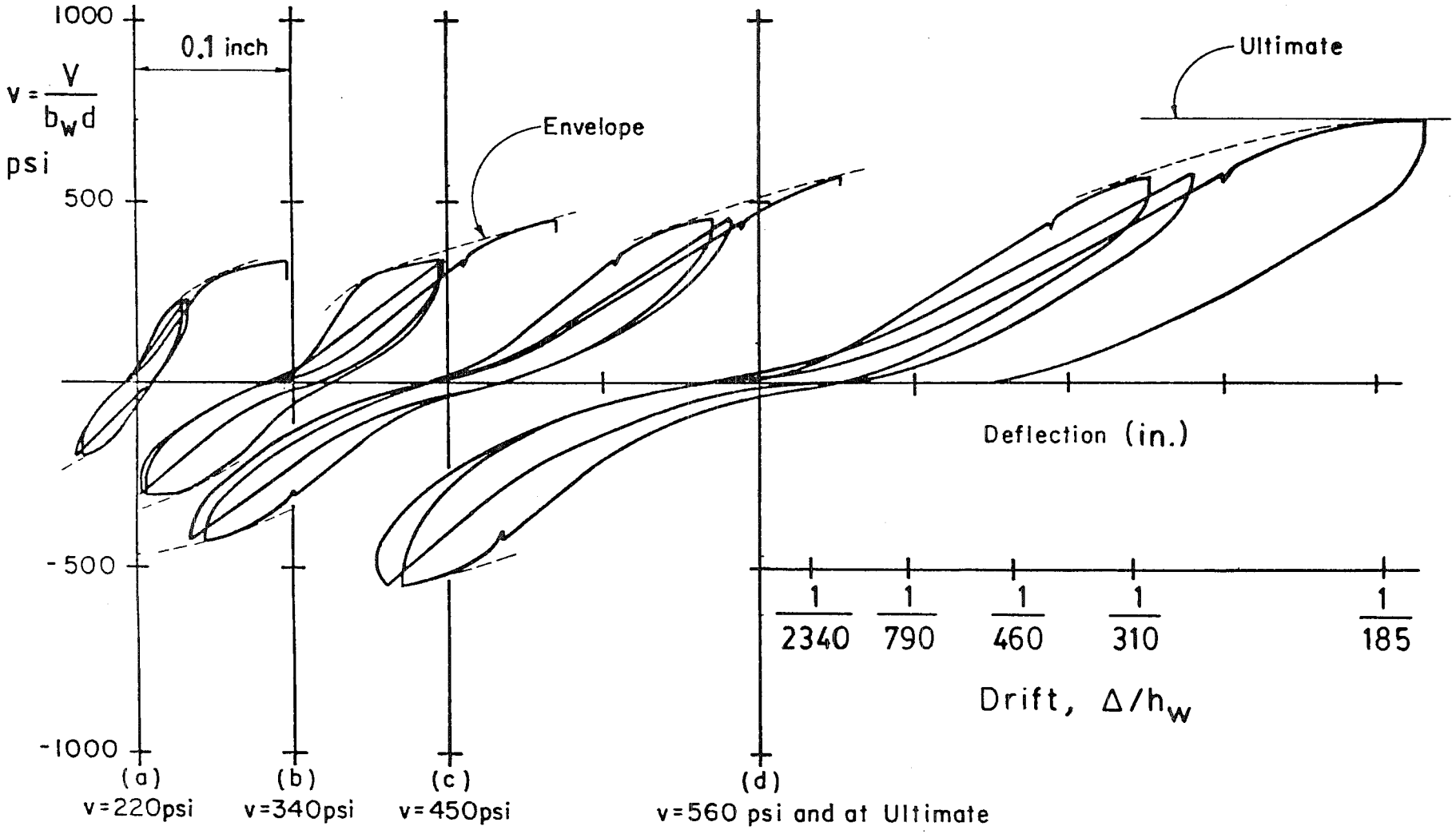

Fig. 4.3 - Hysteretic loops for Barda's Unit B8-5 prior to ultimate load (17)

$$v_u = v_c + v_s = 0.50\sqrt{f'_c} + 1.00\rho_n f_y \quad \text{(MPa)} \qquad \text{(Eq. 4-2)}$$

One drawback of the equation is that it does not allow for the influence of horizontal web reinforcement, which participates more and more in the lateral load transfer as slenderness increases. However, the applicability of this equation may be checked by means of the present tests.

Regarding point 12 above, hogging was observed in the top slab. There were three reasons for this hogging. First, the flanges were very heavily reinforced. Therefore, under lateral load, the flange bars were stressed only lightly while the vertical web bars, constituting a relatively low reinforcement ratio, were stressed highly.

The second reason for hogging of the top slab and yielding of vertical web bars while the flange bars remained elastic concerns the method of load introduction. (See Fig. 4.4.) The lateral load was introduced as two point loads on the end face of the top slab. Following 45 degree load paths, in plan and in elevation, to the top of the wall, the lateral loads would enter the web of the wall at a point 17 inches (432mm) from the tension face. Between this point and the tension face, only a small percentage of the lateral load entered the wall. Thus, the majority of the lateral load entered the diagonal strut beginning at point A. This point A coincides with the calculated position of the compression resultant at the top of the wall (Fig. 4.4(c)). Noting the requirement, as stated in Section 3.1, that all forces at a node must coincide, the resultant of the steel tensile tie force must act at or near point A, as well. Thus, vertical flange bars, being so far removed from point A, were relatively ineffective in contributing to the steel tensile force at point A. Vertical web bars in the vicinity of point A were most effective in supplying the tie force. Therefore, they yielded, while the flange bars remained elastic.

The third reason for hogging in the top slab and yielding of vertical web bars was the flexibility of the top slab. Had the capping element been stiffer (as in a massive top beam), the downward vertical force required to equilibrate the vertical component of the diagonal compression would have been supplied externally by the top beam rather than internally by the web bars. A very stiff

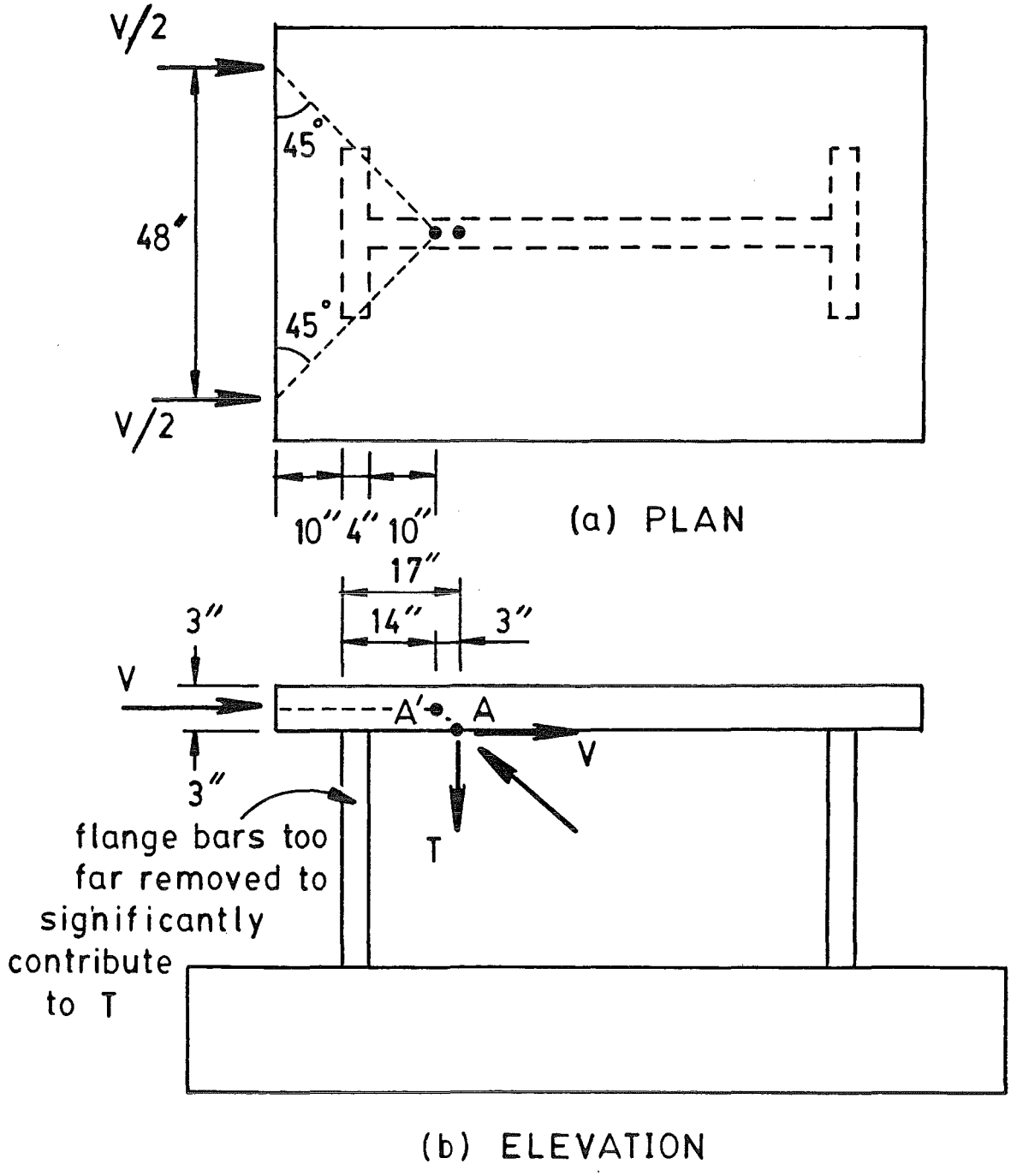

Fig. 4.4 - Loading system for Barda's units

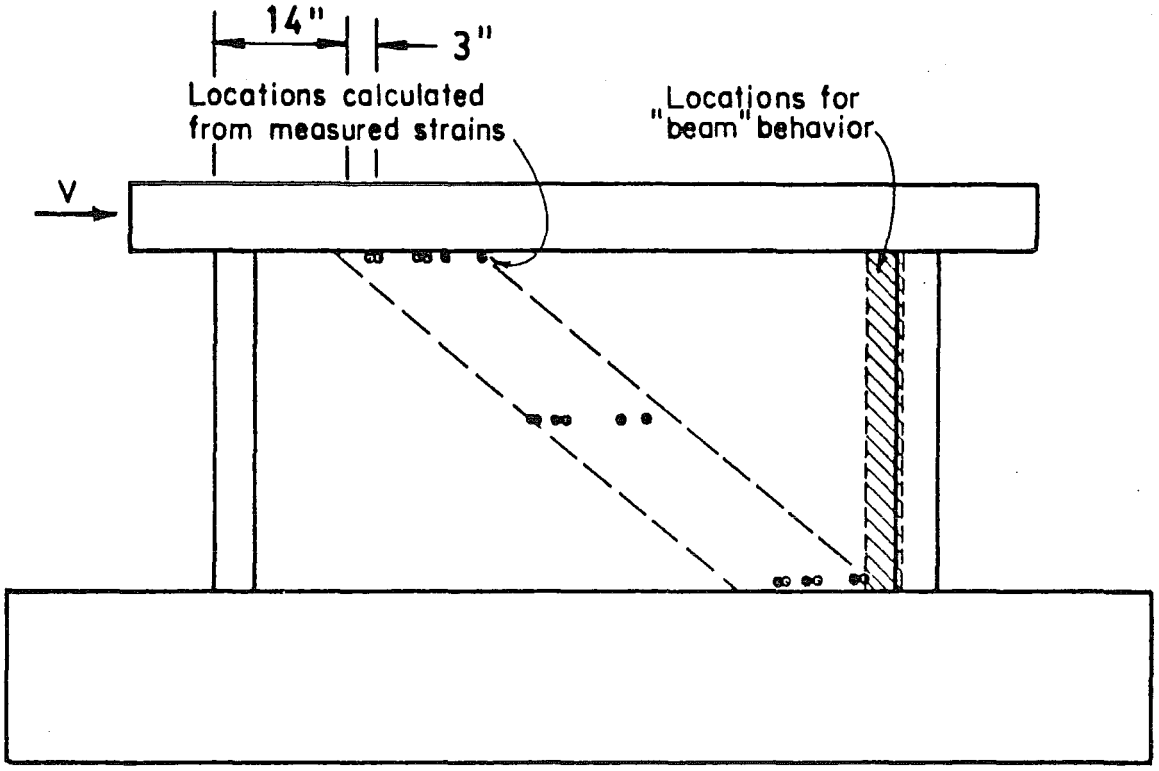

Fig. 4.4(c) - Location of vertical compression resultant for Barda's units (17)

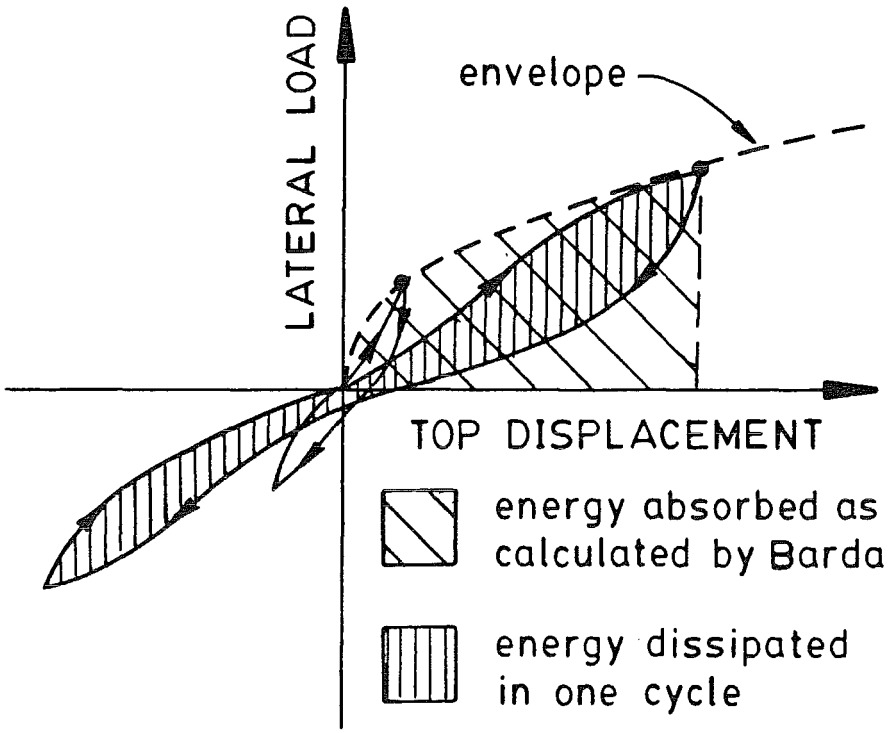

Fig. 4.5 - Energy absorbed vs. energy dissipated

capping element would have had the effect of spreading the vertical restraining force out to the heavily reinforced flanges. As it was, the top slab was relatively flexible, and the vertical web bars alone were mobilized in tying down the diagonal strut.

Regarding point 13, Barda reports results of energy absorption, defined as the area under the envelope curve of lateral load vs. top deflection. However, in seismic situations, the actual energy dissipated in a given cycle is the crucial quantity in evaluating the performance of walls. Energy dissipation per cycle can be obtained by measuring the area within one complete hysteretic loop. (See Fig. 4.5.) Energy dissipation was scaled approximately from the hysteretic loops for Barda's Unit B8-5 (h_w/ℓ_w=1.0) (Fig. 4.3).

The performance of Unit B8-5 was compared to New Zealand design practice (see Section 2.1) and the performance of the test units reported later in this thesis as follows. First, using the material properties reported for Unit B8-5, the ideal shear strength was estimated in the same way that it was for the present test units. The contribution of the reinforcement, V_s, was estimated assuming yielding of all horizontal bars crossing a 45 degree crack. The contribution of concrete, V_c, was taken as the least value resulting from Eqs. 7-31, 7-32, and 7-33 in NZS 3101. The ideal shear strength, V_i, was set equal to $V_c + V_s$. Next, from this value of V_i, the experimental yield displacement was scaled from the hysteretic loops in Fig. 4.3 using the University of Canterbury convention described in Section 6.5.3. From this value of experimental yield displacement, the experimental ductility was back-calculated given the displacement recorded for each cycle of loading. The loading history and cumulative ductility are plotted in Fig. 4.6. It is seen that at maximum load, the cumulative ductility was 13. By the time the resistance had dropped to 80 percent of the maximum, the cumulative ductility was 27, slightly less than the New Zealand standard of 32 for fully ductile structures. Also, the practical limit on the drift, Δ/h_w=1/100, is shown by cross-hatching. Next, the energy dissipation characteristics of Unit B8-5 were compared with those of an ideal elasto-plastic system. The ideal

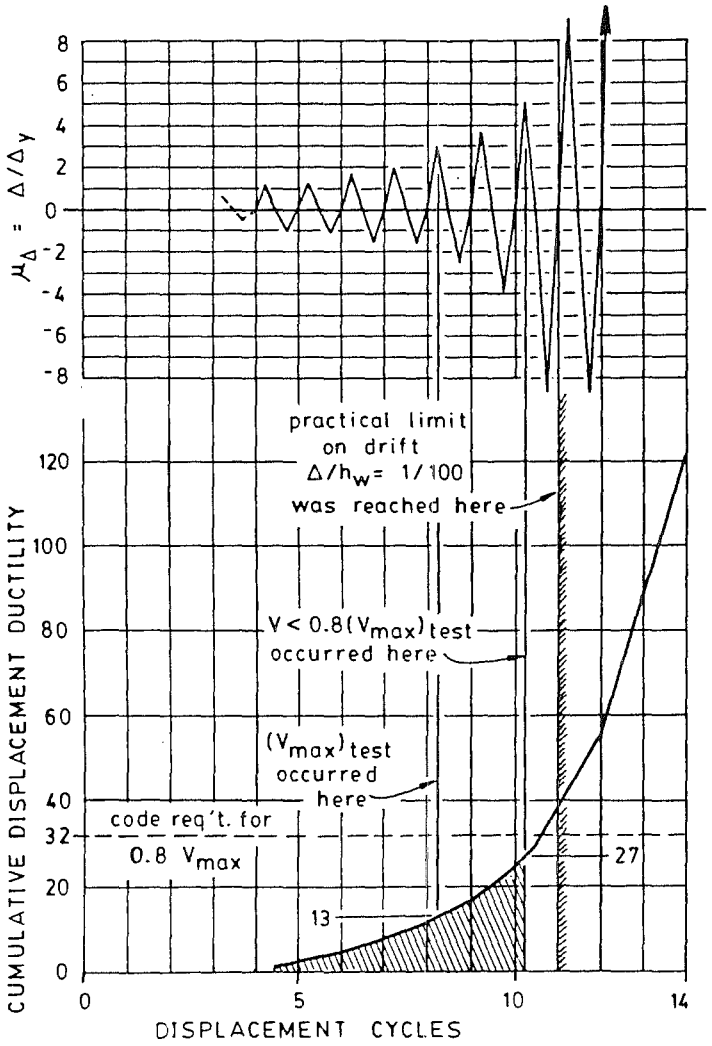

Fig. 4.6 - Barda's Unit B8-5
Cumulative displacement ductility vs. displacement cycles

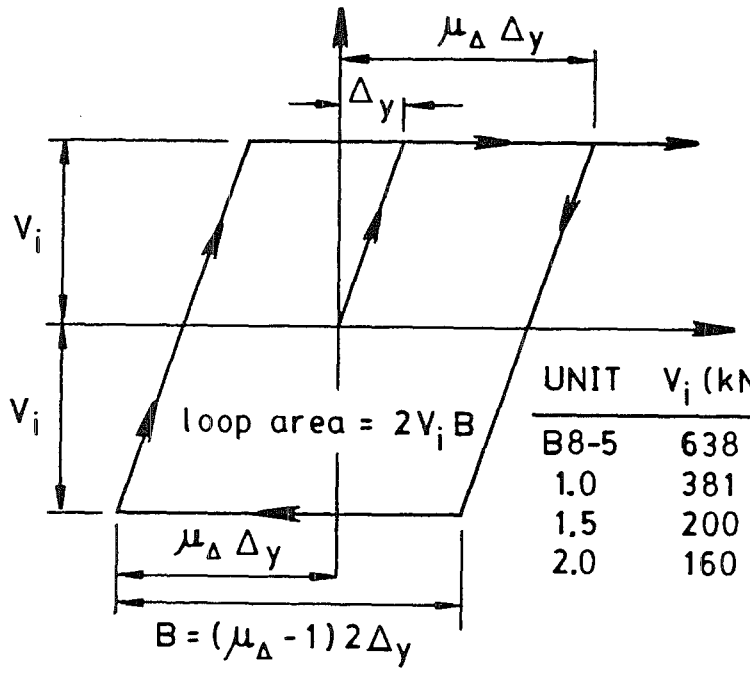

UNIT	V_i (kN)	Δ_y(mm)
B8-5	638	3.81
1.0	381	7.60
1.5	200	6.28
2.0	160	7.94

Fig. 4.7 - Idealized elasto-plastic system

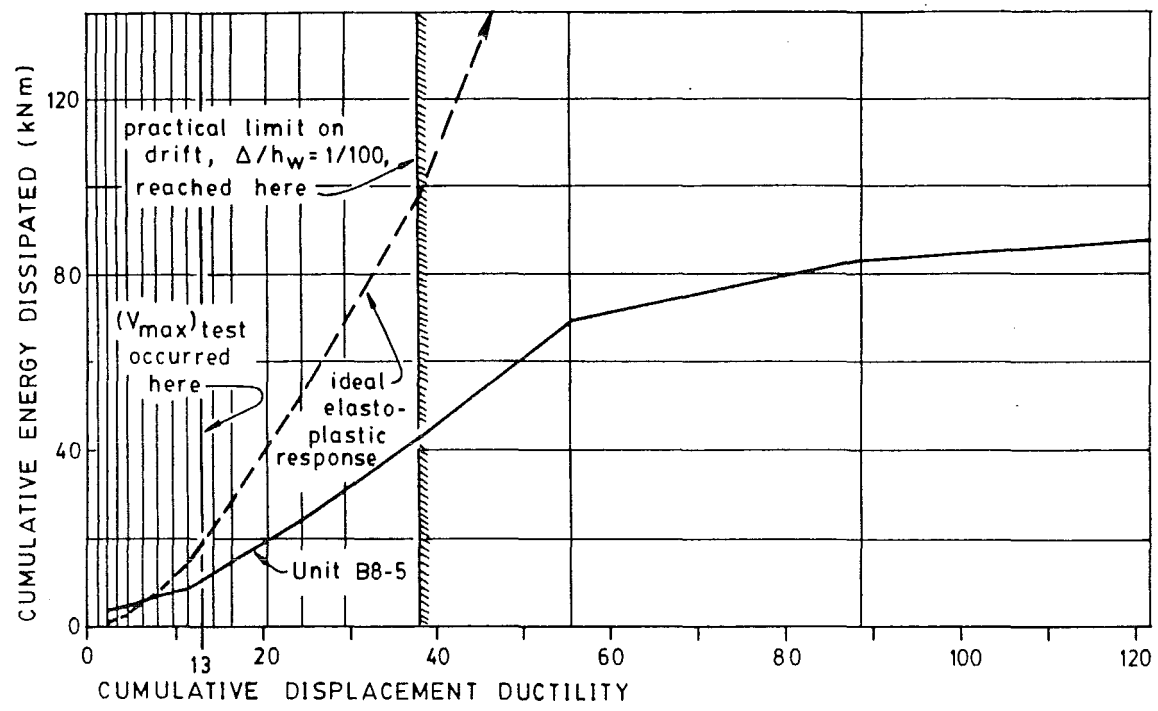

(a) Cumulative energy dissipated

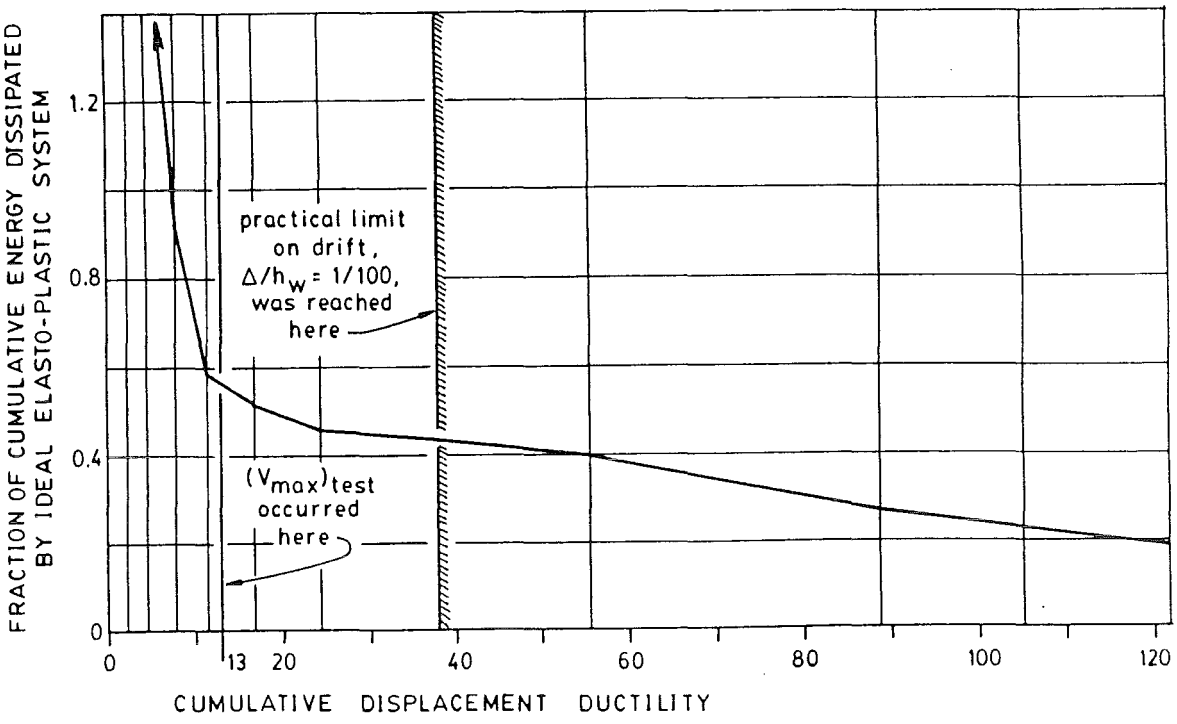

(b) Fraction of idealized response

Fig. 4.8 - Barda's Unit B8-5 - Cumulative energy dissipated vs. cumulative displacement ductility

elasto-plastic system was given the same ideal strength and yield displacement as Unit B8-5, and it was assumed to be subjected to the same displacement history. The ideal elasto-plastic system is shown in Fig. 4.7. The results of the comparison are shown in Fig. 4.8. At maximum load, the energy dissipated by Unit B8-5 was 56 percent of that dissipated by the ideal elasto-plastic system. At the practical drift limit of Δ/h_w=1/100, this ratio had dropped to 44 percent, which may be considered still reasonably good. Overall, Unit B8-5 behaved well, according to New Zealand standard.

Barda's more squat units (B3-2 with h_w/ℓ_w=0.50 and B7-5 with h_w/ℓ_w=0.25) were not analysed because it was felt that the method used for calculating ideal shear strength, V_i, was not appropriate for such squat walls.

4.2 SYNGE (7,8)

Synge (7,8) conducted tests on four squat reinforced concrete structural walls with h_w/ℓ_w=0.50. He studied their potential for fully ductile behaviour. Of his four test units, two were rectangular in cross section (one reinforced with a normal, orthogonal grid of bars and one containing additional diagonal reinforcement), and two were I-shaped in cross section (again, one without and one with diagonal reinforcement).

Synge's test units had the same aspect ratio as the majority of Barda's units (h_w/ℓ_w=0.50). However, shear failure in the web was not expected in Synge's units, as it was in Barda's units. Synge designed his units to fail in flexure. In the walls without diagonal reinforcement, failure occurred, however, by sliding along the base. This failure began under load reversals with the interconnection of horizontal flexural cracks at the base. Sliding along the base, therefore, was a consequence of flexural yielding. The addition of diagonal bars limited the sliding and allowed the full development of flexural strength. Synge found that it is possible to design even squat walls to be ductile by using diagonal reinforcement. In both Barda's and Synge's units, a diagonal compression strut was in effect. Barda observed a strut angle of 38 degrees while Synge observed a strut angle

of 35 degrees.

4.3 ROBINSON (19)

The main analytical work performed in New Zealand on structural walls of limited ductility has been centred on Section 14 in the current New Zealand code of practice for the design of concrete structures (3). Reference 19 describes in detail the background and explanation of the Section 14 provisions. Section 14 embodies a simplified, semi-empirical method for the design and detailing of structures of limited ductility. It is a response to the need, expressed by the structural engineering profession, for a simplified design procedure for buildings in the lower budget, low-rise range. The design procedure addresses structural type factors, dimensional limitations, design for flexural and axial load, confinement of concrete, design for shear, design of web reinforcement, and detailing requirements.

Since the NZS 3101 Section 14 requirements are semi-empirical, it was decided for the present tests that, rather than attempting to verify the Section 14 provisions, it would prove more useful to investigate walls of limited ductility from the point of view of trying to understand their basic behaviour.

4.4 GLOGAU (20)

In reference 20, Glogau attempts to justify the NZS 3101 Section 14 provisions for shear design. He used the results of a statistical study carried out in Japan on failures of actual low-rise buildings. The Japanese study identified the most important factor influencing the failure load of buildings to be:

$$\text{wall area ratio} = A_w/A_f = \frac{\text{area of all walls}}{\text{total floor and roof areas above the storey considered}}$$

The Japanese study found that, in general, buildings remained

undamaged when:

1) $A_w/A_f > 0.003$
2) $W/A_c < 1.2$ MPa
3) average nominal ultimate shear stress < 3.3 MPa

where W = gravity load of the building
= 0.0098MPa x A_f
A_w = total area of walls in each direction
A_f = total area of floors and roof above the storey considered
A_c = total area of columns

The Japanese used these results to formulate a criterion for assessing the risk of damage of existing buildings. The evaluation procedure was checked against more recent damages and seemed to predict damage adequately.

Glogau used the Japanese evaluation procedure to check the NZS 3101 Section 14 proposals. He stepped through the hypothetical design of a New Zealand wall and concluded that the shear demand imposed by Section 14 was conservative compared to that indicated by the Japanese evaluation procedure. Although Glogau acknowledged the shortcomings of drawing too much information from the Japanese evaluation procedure, he concluded that the NZS 3101 Section 14 provisions are conservative for design purposes.

There are, however, three important reservations to applying the results obtained from Japanese buildings to New Zealand conditions. First, the reinforcement content in the structural wall was neglected in the Japanese statistical study. Reinforcement content alone can affect the failure mode and the ductility of the wall. Indeed, reinforcement content alone could make the difference between a fully ductile wall and a wall of limited ductility. Changes in detailing also can alter behaviour. Detailing was not taken into account in the Japanese study. Second, the Japanese study did not take stiffness into account. A series of 25 walls with areas of $1m^2$ each is not equivalent to 2 walls with areas of $12.5m^2$ each. However, the evaluation procedure would assign the same risk to each building. Third, the Japanese buildings studied were designed for working stresses. Working stress design procedures are not used in

New Zealand when earthquake resistance is considered. It appears that the Japanese recommendations for these types of structures envisage fully elastic response during earthquakes.

4.5 HUTCHISON AND VAN GELDERMALSEN (21)

Reference 21 outlines a theoretical study in which the design procedures of Section 14 of NZS 3101 were compared with capacity design procedures. The authors designed four types of reinforced concrete structural walls:

A) a uniform cantilever wall with ℓ_w =10m (ductile)
B) a uniform cantilever wall with ℓ_w =10m (limited ductility, using Section 14 provisions)
C) twin cantilever walls with abutting ends (ℓ_w =5m each wall) (ductile)
D) a coupled structural wall with ℓ_w =10m overall (ductile)

In each category, a 4 storey and an 8 storey wall were designed. It was found that, although a significant difference in cost was observed for the different wall designs, the difference was not great when cost was expressed as a proportion of the cost of the entire structure. Thus, based on cost, no significant advantage was observed for a particular design method. However, as regards design effort, the limited ductility design approach proved best. See Table 4.2. The authors concluded that, for walls with aspect ratios $h_w / \ell_w \leq 3.0$, the designer would do well to choose the NZS 3101 Section 14 approach in order to take advantage of the reduced design effort.

In this author's opinion, there remains the need to understand the basic behaviour of structural walls failing in shear and, thereafter, to either verify the existing Section 14 procedures or develop new ones. The experimental programme reported in this thesis was carried out with a view to contributing to this understanding of basic behvaiour.

TABLE 4.2 - RELATIVE DESIGN EFFORT FOR EIGHT-STOREY WALLS
(from ref. 21)

EIGHT-STOREY WALL	DESIGN EFFORT
10 m Ductile	1.0
10 m Limited Ductility	0.5 (0.67)
2 x 5 m Ductile	1.0
Coupled	1.33

SECTION 5

SCOPE OF THE PROJECT AND THE EXPERIMENTAL PROGRAMME

5.1 DEFINITIONS

In this thesis, the following terminology is used. (See Fig. 5.1.)

wall unit = the entire test unit including base beam, top beam, vertical boundary elements, and web

wall = the region between the top beam and the base beam, composed of two vertical boundary elements and the web

vertical boundary elements = the two vertical column-shaped elements formed on the ends of the web

web = the portion of the test unit lying between the two vertical boundary elements and between the top and base beams, rectangular in plan and 100mm thick

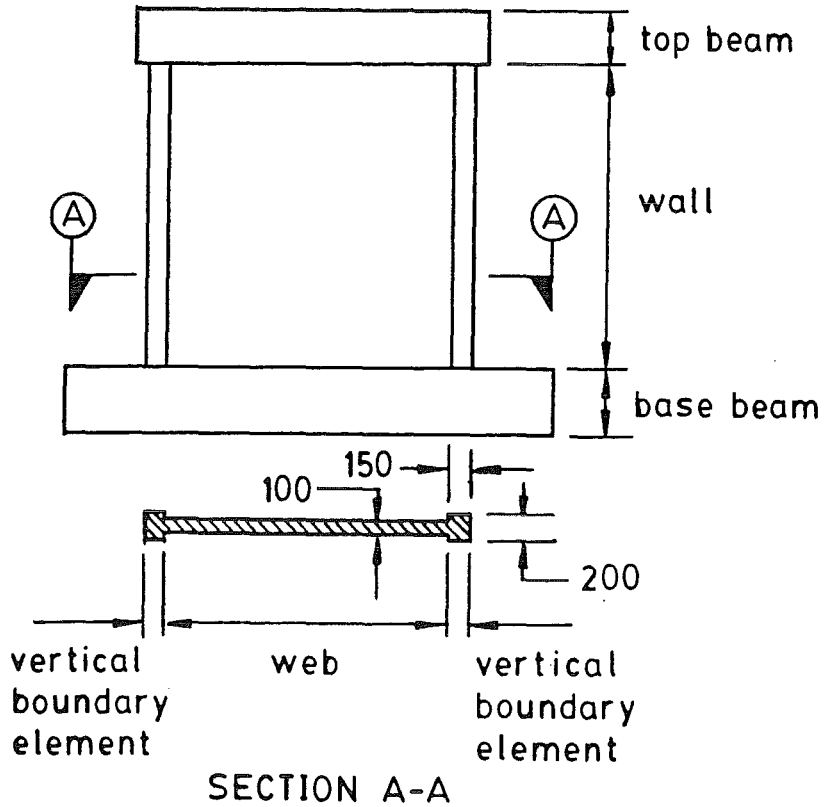

Fig. 5.1 - Definition of terminology for wall units

5.2 MAIN TEST OBJECTIVE

It was decided that the first area of research should be the investigation of shear strength, ductility, and energy dissipation characteristics of prototype walls that were designed before capacity design procedures were introduced in New Zealand. Such walls may be stronger in flexure than in shear, when subjected to lateral loading. They are considered to possess only limited ductility because of the predominant shear behaviour. Therefore, the main objective in the design of the test units was to produce walls weaker in shear than in flexure. The aim was to measure, for each test wall, the shear strength, the ductility, and the energy dissipation capacity under static, reversed cyclic loading and thus obtain an estimate of the likely performance of corresponding real walls during earthquakes.

Because such existing "pre-capacity design" walls may turn out to be stronger in flexure than in shear (for reasons of extensive effective flexural reinforcement located in flanges or cross walls and only nominal temperature and shrinkage reinforcement within the web), the test walls were proportioned using an "inverse capacity design" procedure to ensure an eventual shear rather than flexural failure. The design started with the choice of minimal reinforcement in the web. Then a quantity of vertical reinforcement, chosen in addition to the web reinforcement to provide flexural strength greater than the shear strength, was proportioned to be located in vertical boundary elements. Since the critical action during testing was expected to occur in the web of the wall, the choice of vertical boundary element (cross wall or column) was considered to be of little consequence. Rectangular column elements were chosen only because of simplicity in construction. The test walls were therefore barbell-shaped in plan.

5.3 MAIN TEST PARAMETER, h_w/ℓ_w

The main test parameter was the height-to-horizontal-length ratio, h_w/ℓ_w. Walls with $0.25 \leq h_w/\ell_w \leq 1.00$ were tested by Barda (17) and Synge (7). In the present case, therefore, it was decided to test

low-rise walls starting at h_w/ℓ_w=1.00. In squat walls, the behaviour of the wall is influenced greatly by the method of load introduction (ie. by means of a top beam, top slab, or other system). It was thought that as slenderness increased, the method of load introduction would influence less and less the behaviour of the critical region of the wall. A series of test walls with h_w/ℓ_w=1.00,1.50,2.00 was chosen. Constraints such as flexural capacity of the strong floor, load capacity of the hydraulic jack, maximum crane height, and availability of loading frame materials dictated a maximum height of the test units of 3.0m and a web width of 100mm (Fig. 5.2).

5.4 CONSTANT LENGTH VS. CONSTANT HEIGHT

In order to obtain aspect ratios of h_w/ℓ_w=1.00,1.50,2.00, two alternatives were considered: 1) maintaining constant ℓ_w while varying h_w and 2) maintaining constant h_w while varying ℓ_w. Each scheme had its good and bad points., However, scheme 2 was chosen because of the following advantages. First, a constant wall height allowed a single jacking height for all three wall units. This single jacking height meant that the same loading frame could be used for all wall units. Second, with the maximum height constraint of 3.0m, alternative 2 resulted in more realistic scale models (1/3-2/3 scale). Alternative 1 would have resulted unfavourably in smaller scale models.

5.5 WEB BARS

One of the main aims in planning the wall units was to simulate as closely as possible a realistic proportioning and layout of reinforcement in the web of the wall. The two most important details were a minimum percentage of web reinforcement and a realistic bar spacing. It was originally proposed to use two curtains of plain 5mm diameter bars (f_y=380MPa) at a spacing of 200mm. However, a quantity of high strength 6mm diameter deformed bars was obtained. This reinforcement was unsuitable as supplied because the yield strength was excessive and the stress-strain curve showed no yield plateau. (See Section 6.3.1.) Heat treatment produced

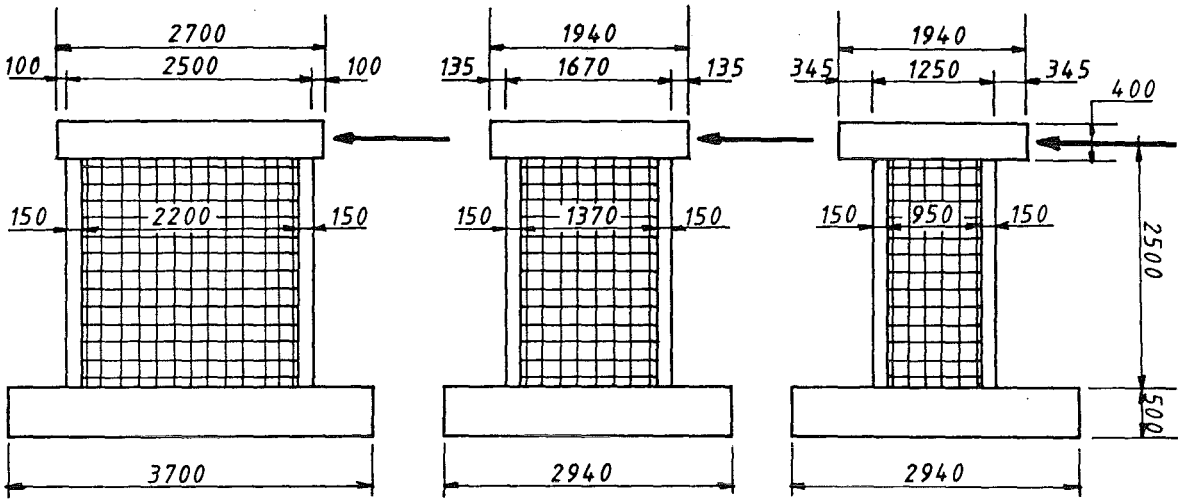

UNIT 1.0 | UNIT 1.5 | UNIT 2.0

$h_w / l_w = 1.0$ ~ 2/3 scale | $h_w / l_w = 1.5$ ~ 1/2 scale | $h_w / l_w = 2.0$ ~ 1/3 scale

web reinforcement : HD 6 - 180 e.w. $\rho_n = \rho_h = 0.0016$

(a) OVERALL DIMENSIONS

scale : 500 mm

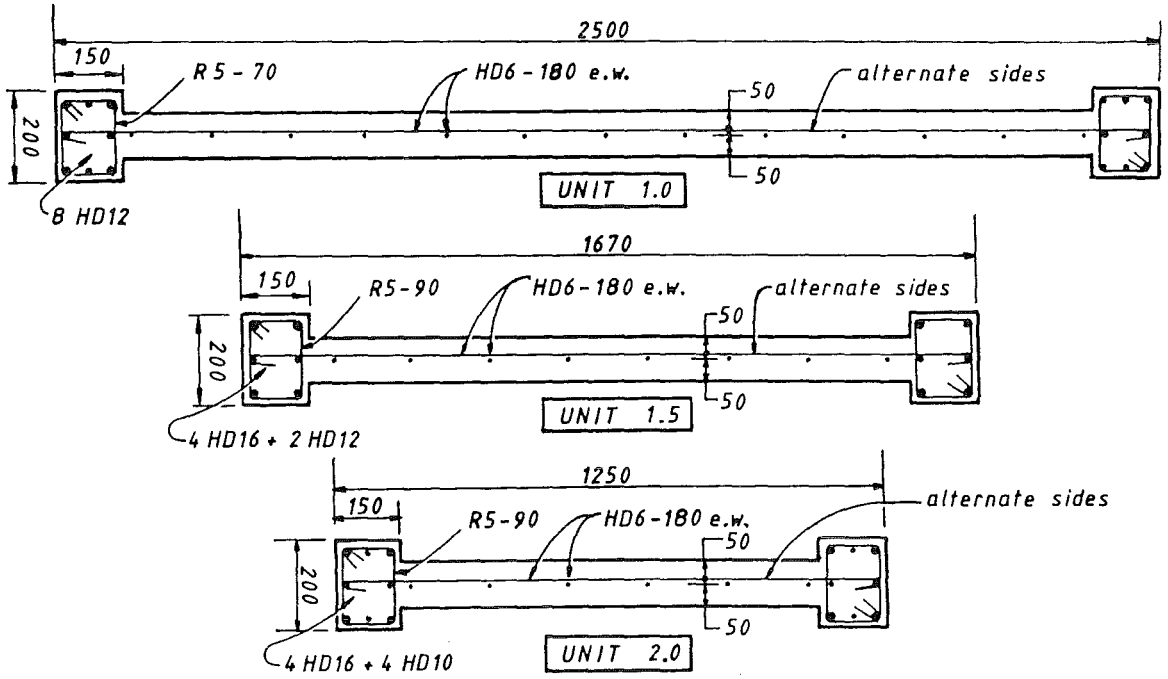

(b) WALL SECTIONS

scale : 100 mm

Fig. 5.2 - Details of test units

slightly more realistic properties. The resulting yield strength was still higher than that found in the larger diameter mild steel bars used in practice. However, since it was not possible to obtain small diameter deformed bars in mild steel, it was deemed better to accept higher strength steel than to forfeit a representative concrete-to-steel bond by using plain bars. Finally, in order to obtain a percentage of reinforcement near the minimum required for temperature and shrinkage using such high strength bars, it was necessary to use only one curtain of reinforcement in the web. A bar spacing of 180mm was chosen (Fig. 5.2(b)).

5.6 AXIAL LOAD

The axial load that would be present due to the weight of upper storeys was omitted in the tests for the sake of simplicity in testing. First, the axial load normally present in low-rise walls is small. Second, the presence of any axial load on the test units would only have enhanced the strength. Therefore, the results of tests without the use of axial load are expected to be conservative. Prototype walls may behave better. However, it is suspected that an axial load ratio of $P/f'_c A_g$ = 0.02-0.05, as may be found in low-rise walls, would probably have had little effect on the test results.

5.7 DESIGN CALCULATIONS

Typical strength calculations for one of the test units are presented in Appendix A. A summary of calculated ideal strengths is shown in Table 5.1. ACI-318 clause 11.4.1 applies in general to elements subjected to shear and moment.

$$v_c = 0.17\sqrt{f'_c} \quad \text{(MPa)} \qquad \text{(Eq. 5-1)}$$

ACI Eq. 11-4 applies to elements subjected to shear and moment but represents a more precise calculation.

$$v_c = 0.16\sqrt{f'_c} + 17.2\rho_w \frac{V_u d}{M_u} < 0.29\sqrt{f'_c} \quad \text{(MPa)} \qquad \text{(Eq. 5-2)}$$

ACI 318 Eq. 11-6 applies to elements with axial compression and reduces to the first equation for the present walls.

$$v_c = 0.17 \left(1 + 0.0005\frac{P_u}{A_g}\right) \sqrt{f'_c} \quad \text{(MPa)} \qquad \text{(Eq. 5-3)}$$

NZS 3101 Eq. 7-3 is a general equation for all cases except for slabs and deep flexural members. It is not applicable to low-rise structural walls, since they tend to be rather deep vertical cantilevers.

$$0.08\sqrt{f'_c} \leq \left[v_c = v_b = (0.07 + 10\rho_w)\sqrt{f'_c}\right] \leq 0.2\sqrt{f'_c} \quad \text{(MPa)} \qquad \text{(Eq. 5-4)}$$

NZS 3101 Eq. 7-24 applies to deep beams. It may have relevance to low-rise walls.

$$v_c = \left(2\frac{d}{a}\right) v_b \quad \text{(above)} \quad \text{(MPa)} \qquad \text{(Eq. 5-5)}$$

NZS 3101 Eq. 7-31 is a general equation for the shear strength of concrete in walls not necessarily subjected to earthquake displacements.

$$v_c = \begin{cases} 0.2\left(\sqrt{f'_c} + \dfrac{P_u}{A_g}\right) & \text{(tension)} \quad \text{(MPa)} \\ 0.2\sqrt{f'_c} & \text{(compression)} \quad \text{(MPa)} \end{cases} \qquad \text{(Eq. 5-6)}$$

NZS 3101 Eqs. 7-32 and 7-33 are more detailed calculations of the shear strength of concrete in walls in general conditions.

$$v_c = 0.27\sqrt{f'_c} + \frac{1}{4}\frac{P_u}{A_g} \quad \text{(MPa)} \qquad \text{(Eq. 5-7)}$$

$$v_c = 0.05\sqrt{f'_c} + \frac{\ell_w\left(0.1\sqrt{f'_c} + 0.2\dfrac{P_u}{A_g}\right)}{\dfrac{M_u}{V_u} - \dfrac{\ell_w}{2}} \quad \text{(MPa)} \qquad \text{(Eq. 5-8)}$$

NZS 3101 Eq. 7-43 applies to the shear strength of concrete in plastic hinge regions resulting from seismic loading. It is not applicable in the present tests because extensive flexural yielding (as found in a plastic hinge region) was

not expected.

$$v_c \leq 0.6\sqrt{\frac{P_e}{A_g}} \quad \text{(MPa)} \qquad \text{(Eq. 5-9)}$$

The ideal flexural strength, $(V_i)_{flex}$, was obtained from standard flexural strength calculations.

As seen in Table 5.1, there exists a large number of empirical equations for the contribution of concrete to shear strength, V_c, each with its own range of applicability. None of the equations apply specifically to the present case, low-rise walls failing in shear under seismic loading. Thus, the calculation of the ideal shear strength for the present test units was somewhat undefined.

For lack of any better method, the choice of ideal shear strength, V_i, as a basis for setting the loading history for the test units was carried out somewhat arbitrarily as follows. Of all the equations for V_c listed in Table 5.1, NZS 3101 Eqs. 7-31, 7-32, and 7-33 were considered most applicable. Next, it was considered important to avoid loading the test unit too severely on the initial cycles. Therefore, a value approximately equal to the least value resulting from Eqs. 5-5, 5-6, and 5-7 above was chosen as V_c, the contribution of concrete. The contribution of reinforcement, V_s, was calculated assuming yielding of all horizontal bars crossing a 45 degree web crack. The ideal shear strength was calculated as $V_i = V_c + V_s$.

For Unit 1.0, the value of V_i=410kN was obtained before the exact concrete strength was known. However, this value was retained as a basis for setting the loading. For Units 1.5 and 2.0, measured material strengths were used. For a description of the loading scheme, see Section 6.5.

TABLE 5.1 - SUMMARY OF CALCULATED IDEAL STRENGTHS

	Method		Unit 1.0			Unit 1.5			Unit 2.0			Barda's Unit B8-5		
			V_c	V_s	V_i	V_c	V_s	V_i	V_c	V_s	V_i	V_c	V_s	V_i
Shear Strength	ACI 318-71	11.4.1	177	173	350	95	123	218	88	92	180	-	-	-
	ACI 318-71	Eq.11-4	171	173	344	161	123	284	83	92	175	-	-	-
	ACI 318-71	Eq.11-6	177	173	350	95	123	218	88	92	180	-	-	-
	NZS 3101	Eq. 7-3	89	173	262	47	123	170	44	92	136	-	-	-
	NZS 3101	Eq. 7-24	142	173	315	51	123	174	35	92	127	-	-	-
	NZS 3101	Eq. 7-31	208	173	381	112	123	235	103	92	195	176	462	638
	NZS 3101	Eq. 7-32	285	173	458	154	123	277	142	92	234	238	462	700
		Eq. 7-33	267	173	440	86	123	209	61	92	153	221	462	683
	NZS 3101	Eq. 7-43	36	173	209	24	123	147	19	92	111	-	-	-
Flexural Strength	$(V_i)_{flex}$		-	-	488	-	-	332	-	-	256	-	-	-
	V_i chosen as basis for loading history		-	-	410(1)	-	-	200	-	-	160	-	-	638

NOTE: All values in kN.

(1) Obtained using approximate f'_c .

SECTION 6

DETAILS OF TEST PROGRAMME

6.1 TEST RIG

The test rig, shown in Fig. 6.1, consisted of three independent systems: an in-plane loading system, and in-plane base beam reaction system, and an out-of-plane bracing system.

The wall units were subjected to in-plane, reversed cyclic loading from a hydraulic jack applied at the level of the top beam. The jack was a double-acting (compression and tension), displacement-controlled Victor Hydraulics brand hydraulic jack with a capacity of 1100kN in compression and 840kN in tension. The ram travel was ±200mm. The jack was attached to the wall unit in such a way that, for either direction of loading, the load was introduced as compression on the end face of the top beam (Fig. 6.2). An existing structural steel frame, modified to increase its strength, was used to brace the jack in the plane of the wall.

In the past, researchers have attempted various methods of introducing shear into the test region of a unit. Although in prototype walls, lateral loads are usually introduced by means of floor or roof slabs acting as diaphragms, in the present tests, a massive top beam was considered more appropriate than a top loading slab because of its axial and flexural stiffness. The large stiffness of a massive top beam ensured that the significant deformations occurred in the region of interest of the wall and not in the top beam or other part of the loading system.

In Barda's test, a significant amount of deformation and cracking occurred in the top slab. Thus, a certain proportion of the lateral load was used in deforming the top slab. In the present tests, a massive top beam was used in order to minimize deformation in the loading member and to direct all deformations into the test region of the wall. Thus, the relationship between lateral load and wall deflection was thought to be less affected by variable boundary conditions at the top edge, although this was obtained at the expense of the less realistic simulation of

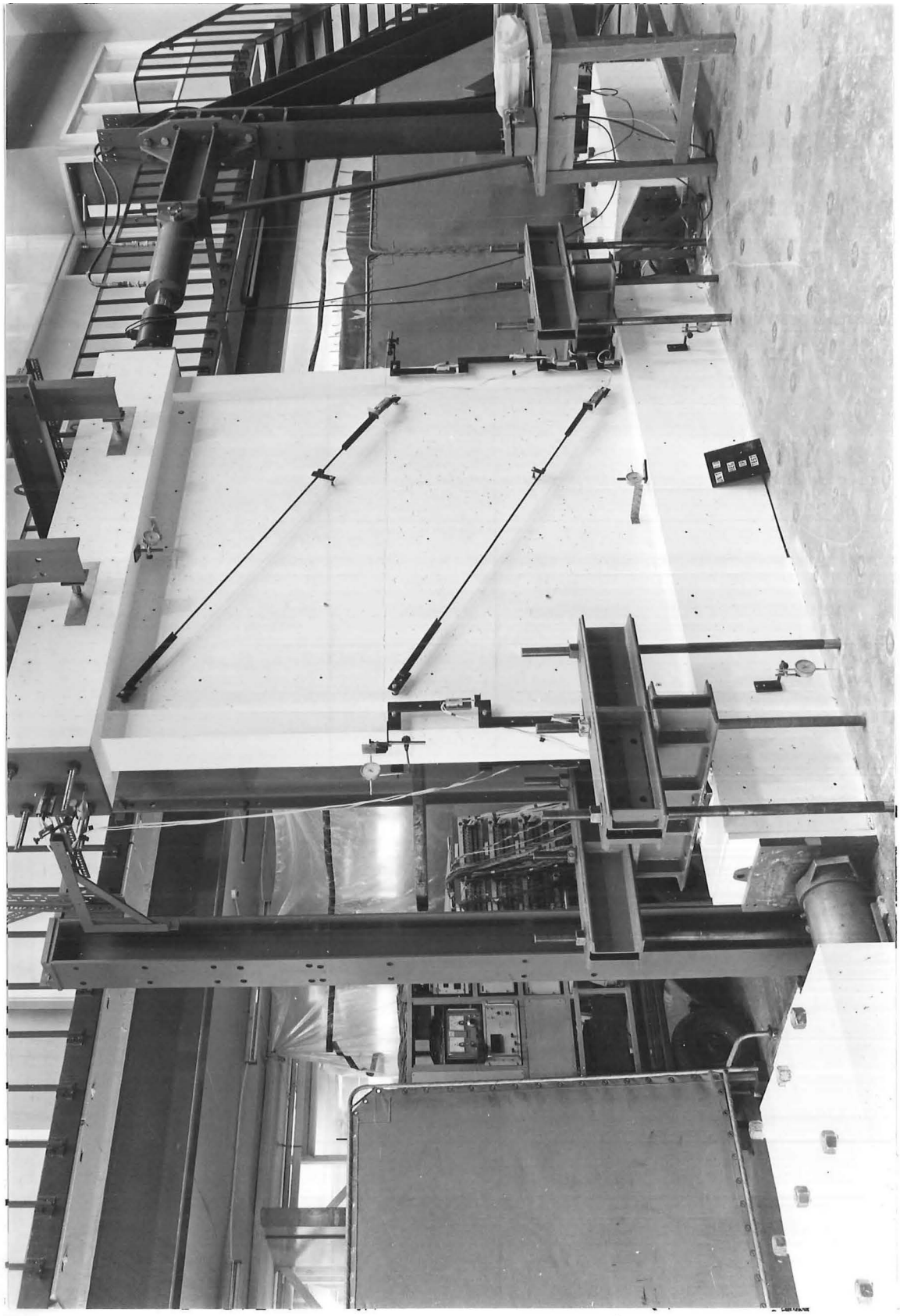

Fig. 6.1 - Test setup

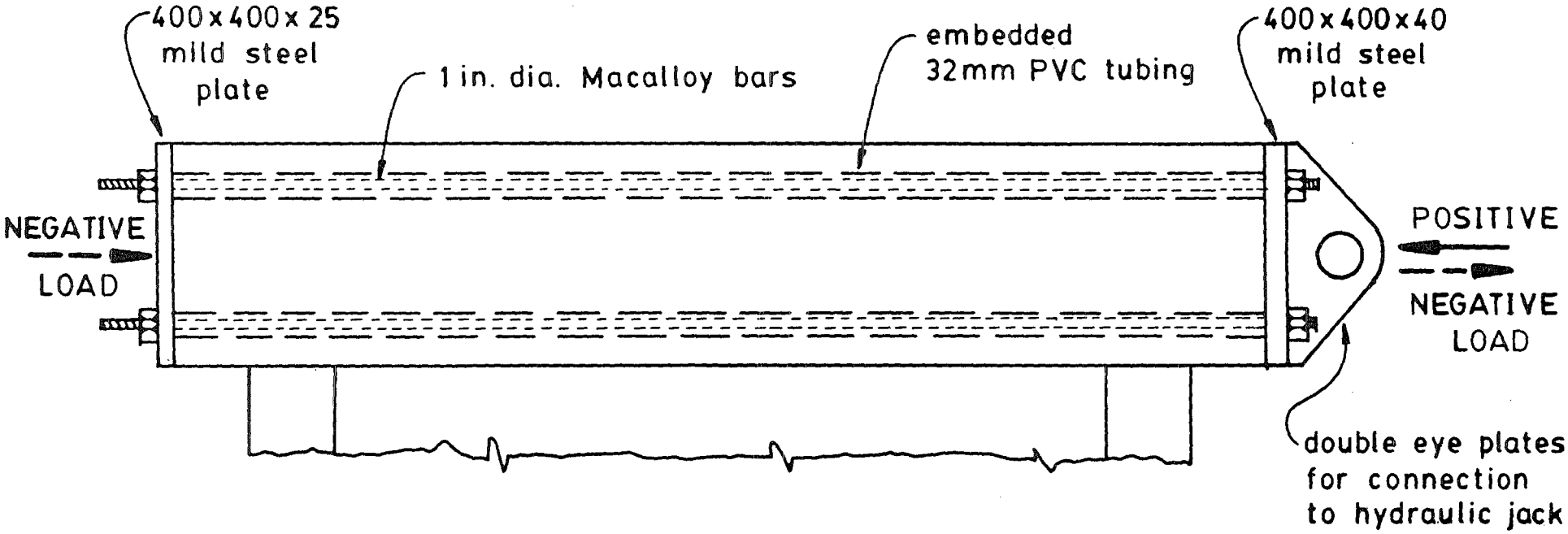

Fig. 6.2 - Introduction of lateral load to test unit

practical situations. For the present tests, deformations in the the top beam were, indeed, small.

The base beam reaction system also was designed so that the test region of the wall unit itself would experience, as near as possible, foundation forces that a prototype wall would experience. The reaction system was chosen so as to allow maximum flexibility in positioning the wall unit on the laboratory floor.

Resistance to horizontal sliding of the wall unit along the floor was provided by two concrete anchor blocks bolted to the strong floor at each end of the base beam. Large capacity, displacement-controlled hydraulic jacks were placed on the floor between each end of the base beam and the adjacent anchor block (Fig. 6.1). The hydraulic jacks were used both as convenient instruments for packing the base beam and as instruments for compressing the base beam. Before testing began, the base beam was compressed by these base jacks to a force higher than the expected maximum test load. During testing, the proper hydraulic pressure in the base jacks, and, thus, the pre-selected axial force in the base beam, was maintained with the aid of a simple oil pressure gauge and a manual oil pump. Thus, during load reversals, the base beam remained always in compression, effectively eliminating sliding of the wall unit along the floor.

The overturning of the wall unit was resisted by a series of structural steel hold-down beams placed across each end of the base beam and bolted, via six 1-1/2 inch diameter mild steel bolts at each end, to the strong floor, as seen in Fig. 6.1.

In order to model the bracing effect of a floor or roof slab in a real structure, a structural steel frame independent of the loading and reaction systems braced the top beam against out-of-plane movement. Four adjustable ball bearings (two on each side of the beam, one at each end) contacted the top beam at mid-height to constrain it to in-plane motion only.

6.2 CONSTRUCTION OF WALL UNITS

6.2.1 Construction Programme

The three wall units were constructed in the civil

engineering laboratory at the University of Canterbury over a period of eight months (January-August 1985). The units were cast vertically in four lifts: base beam, lower half of the wall, upper half of the wall, and top beam. Only Unit 2.0 contained a full-height lift in the wall region, resulting in a total of only three lifts. The units were built in a series beginning with the largest, Unit 1.0. For example, while the grid of reinforcement for the wall itself was being positioned for Unit 1.0, the formwork for the base beam of Unit 1.5 was being assembled. All three units were completed before testing commenced.

6.2.2 Formwork

The formwork was constructed initially for Unit 1.0 and was subsequently shortened in length along the floor and reused for Units 1.5 and 2.0. The formwork was designed using the New Zealand Ministry of Works and Development Basic Formwork Design Charts for the Waitaki Power Development. The forms were constructed of Pinus radiata, and all surfaces were painted with spirit-based wood primer, undercoat, and topcoat in order to facilitate reuse. The formwork consisted of 17mm plywood backed by 100mmx50mm horizontal walers spaced vertically at 250mm, which were, in turn, backed by a series of 2 - 100mmx50mm vertical strongbacks. Removable 10mm diameter threaded rods (through-bolts), passing through the wall within lengths of 16mm diameter pipe, acted to clamp the two facing sides of the formwork together. Each length of pipe, eventually cast into the unit, acted both as a sheath for a through-bolt and as a form spreader (Fig. 6.3). The formwork was plumbed and then rigidly attached to a structural steel frame in order to fix it in position for concreting. Joints in the plywood were taped on the inside of the forms to prevent leakage. Silicon caulking was also used to seal joins in the formwork. Just prior to concreting, the forms were coated with a chemical release agent, FEBSTRIKE, in order to facilitate stripping. The base beam for each unit was cast on a plywood sheet, which was removed when the forms were stripped. A bed of gypsum dental plaster, applied just prior to testing, ensured uniform bearing of the unit on the laboratory floor.

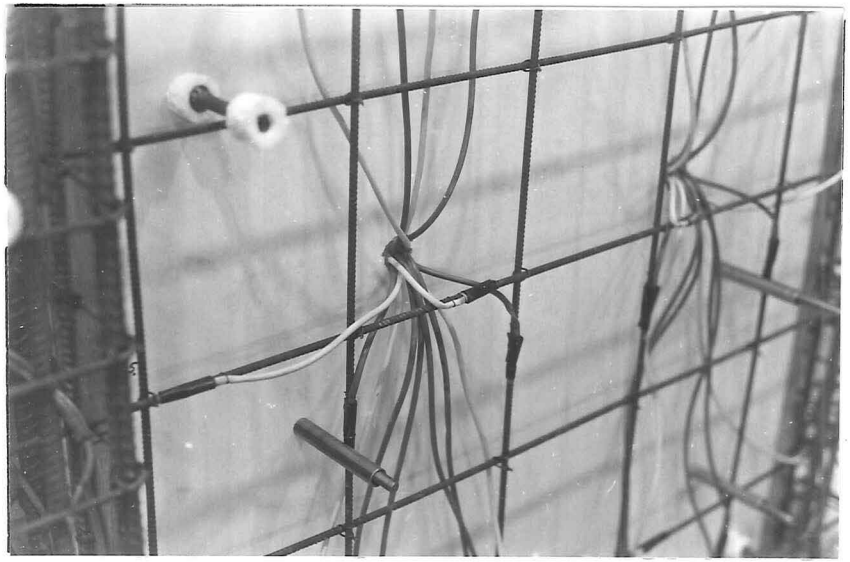

Fig. 6.3 - Web reinforcement, strain gauge leads, form spacers through-bolts, and potentiometer rod

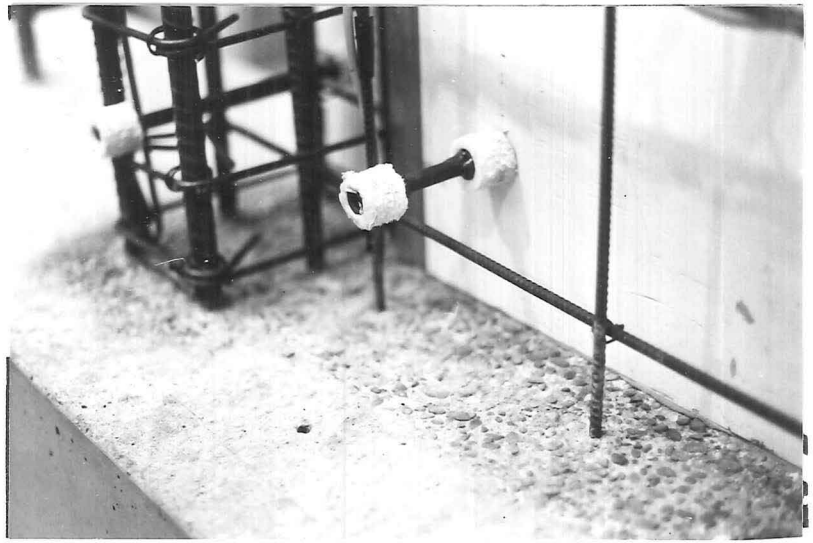

Fig. 6.5 - Dry construction joint

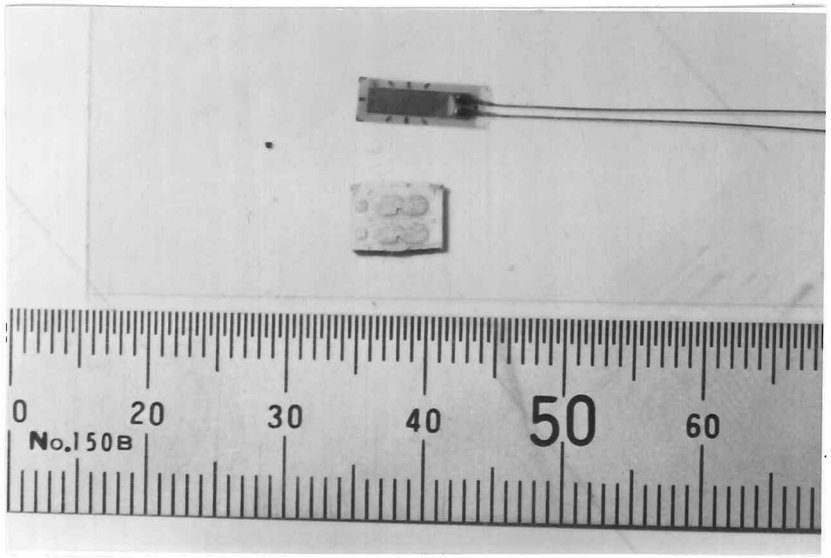

(a) Strain gauge and terminal

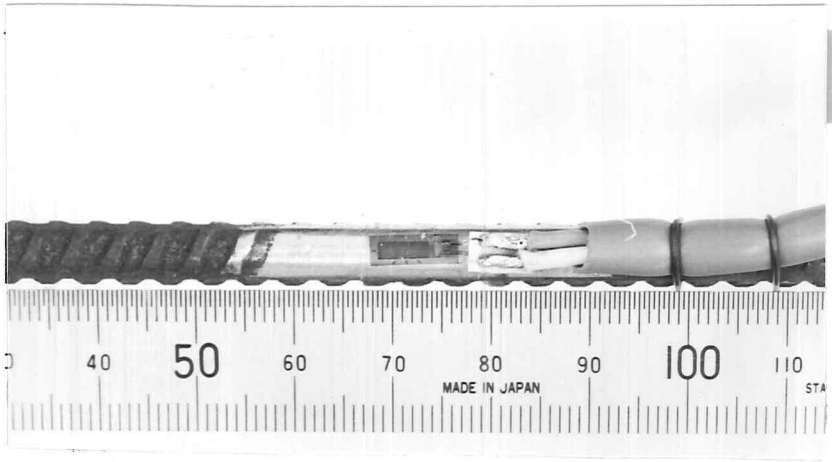

(b) Strain gauge and terminal mounted on bar

Fig. 6.4 - Electronic strain gauge

6.2.3 Strain Gauging

In order to measure strains in the main reinforcing bars during testing, approximately 100 internal electrical resistance foil strain gauges (for specification, see Section 6.4.3) were attached to selected reinforcing bars in each wall unit. The gauges were attached to the bars in the following manner before the cage was assembled. At the selected position, the surface of the bar was prepared by carefully filing off the ribs, buffing the surface with emery cloth, and then wiping the surface with methylethylketone. Care was taken to file off only the ribs on the bar so that there was minimal reduction in cross-sectional area of the bar at the gauged position. The gauge was then glued to the bar surface using cyanoacrylate adhesive. Terminals for the attachment of the two strain gauge leads were then attached to the bar alongside the gauge on a self-adhesive foam pad. Two external lead wires were then soldered to the terminals and fed through 5mm diameter hollow plastic tubing, which was led out of the concrete to the automatic datalogger. The tubing enclosing the two external lead wires ensured that the wires were free to slide within the concrete when deformations and cracking of the concrete occurred during testing. The tubing was anchored by means of soft floral wire to the reinforcing bar directly adjoining the terminals. The assembly was next coated with at least four layers of SN/4 strain gauge coating cement and a layer of vinyl/mastic tape to complete the waterproofing and provision of shock resistance. The strain gauge assembly is shown in Fig. 6.4.

6.2.4 Tying of Reinforcement

The reinforcement cages were tied using 1.5mm soft steel tying wire. The main wall grid of 6mm diameter bars was tied with single ties, and the construction tolerance on bar spacing was approximately ±2.5mm. The vertical boundary elements and the top and base beams were tied with double ties. The tolerance on the vertical spacing of hoops in the boundary elements was ±5mm. The tolerance on spacing of longitudinal bars and stirrups in the top and base beams was approximately ±10mm. All vertical wall bars were fixed into position at the base by means of welding to a length of 6mm thick steel flat laid in the bottom of the base beam mould.

Where the bars protruded out from a construction joint, they were fixed to their correct transverse position in the wall section within a tolerance of ± 2.5mm. Rods for the mounting of potentiometers (see Section 6.4.4) were tied to the reinforcement cage at the correct positions and doubled as form spreaders during concreting (Fig. 6.5). Lifting lugs, consisting of bent lengths of either 16mm or 20mm diameter deformed bar, were also tied to the reinforcement cage in appropriate positions.

6.2.5 Concreting

The concrete for all three units was obtained from local ready-mix contractors. The specifications for the various batches are shown in Table 6.1. The units were cast vertically inside the laboratory using a combination of hopper, wheelbarrow, shovels, and spades. The concrete was compacted primarily by means of a standard, immersion-type internal vibrator, but an external vibrator mounted on the outside of the formwork was activated momentarily at the finish of each pour. For Unit 2.0, in an attempt to ensure a uniform strength throughout the entire height of the test region of the wall, it was decided that only one lift of concrete would be poured for the wall proper. To effect this single, full-height lift, the formwork was strengthed at the base of the wall. The formwork for the bottom half of the wall was erected and filled, and the concrete was compacted. Then the formwork for the top half of the wall was erected. The concrete for the top half was then poured from the same truckload. A wet construction joint was formed at half height by vibrating down approximately 300mm into the lower lift of concrete.

Dry construction joints were formed between the base beam and the bottom of the wall, at mid-height of the wall (Units 1.0 and 1.5 only), and between the top beam and the top of the wall. After the concrete for the lower lift had been poured, vibrated, and levelled off with a wooden float, it was left to stand for 3-4 hours. Then a liquid concrete retarding agent, FEBOL, was sprayed on the construction joint area. Approximately 24 hours after pouring, the loose cement and sand was removed with a wire brush, exposing the aggregate. The depth of the resulting depressions in the

TABLE 6.1- CONCRETE PROPERTIES

Batch		Fresh concrete				Hardened concrete						
		Target f'_c (MPa)	MSA[1] (mm)	Slump (mm) Ordered/ received	Supplier	Date tested	Age at test (days)	f'_c (MPa) Lab cured[2]	f'_c (MPa) Fog cured	f_t (MPa) Fog cured	E_c[3] (MPa) Lab cured	$(f'_c)_{28}$ (MPa) Fog cured
UNIT 1.0	Base beam	30	13	100/75	Ashby	30/9	198	33.2	38.9	-	27 081	-
	Wall pour 1	25	13	100/75	"	"	146	25.7	28.0	3.1	23 827	26.2
	Wall pour 2	25	13	100/75	"	"	144	28.3	30.8	3.2	25 003	24.8
	Top beam	30	13	100/100	"	"	109	27.7	31.9	3.3	24 736	29.5
UNIT 1.5	Base beam	30	13	100/100	"	"	109	27.7	31.9	3.3	24 736	29.5
	Wall pour 1	25	13	100/175	"	28/10	112	17.6	19.1	2.1	19 718	11.3[4]
	Wall pour 2	25	13	100/165	"	"	110	24.4	27.3	2.8	23 216	17.3[4]
	Top beam	30	13	100/85	Firth	"	94	32.8	32.1	-	26 918	32.7
UNIT 2.0	Base beam	25	13	100/115	"	7/11	108	23.9	26.7	2.8	22 977	22.6
	Wall	25	14	100/120	"	"	92	26.5	32.5	3.3	24 195	28.1
	Top beam	30	14	100/120	"	"	76	29.4	32.7	3.2	25 484	28.8

(1) MSA = maximum size aggregate

(2) Used for theoretical strength and stiffness calculations

(3) Used for theoretical stiffness calculations

(4) Tested at 7 days

roughened surface was 3-8mm (Fig. 6.5). The construction joint area was then cured in same way as the surrounding concrete. Just before the top lift of concrete was poured, the hardened concrete and the reinforcing bars in the construction joint area were brushed again to remove any loose particles and latent retardant. The lower concrete surface was moistened, and the fresh concrete was poured.

For Unit 1.5, an unexpectedly poor batch of concrete was obtained for the lower half of the wall. (See the concrete strengths in Table 6.1.) Normal vibration procedures caused excessive segregation and the excessive accumulation of water at the top of this lower lift. As a result, when the construction joint at mid-height was prepared 24 hours after the pour, very poor quality concrete was discovered. No coarse aggregate particles were visible on the top surface. It was necessary to roughen the joint surface using a hammer and chisel. Because of the low strength of this concrete, the quality of the construction joint was suspect. Cracking and slippage along this mid-height construction joint was expected during the testing of Unit 1.5. In order to avoid such a poor construction joint for Unit 2.0, a full height pour with a wet construction joint at mid-height was carried out, as described above.

Immediately after compaction, the fresh concrete was levelled off with wooden floats. Approximately 4 hours after pouring, the concrete was trowelled off to give a smooth finish, and the concrete was covered with damp hessian sacking, which was, in turn, covered with polyurethane sheets to prevent evaporation. Approximately 24 hours after pouring, the forms were loosened but not removed. Free water was maintained on the concrete surface by periodic dampening of the hessian sacking. The concrete remained in its forms, covered as described above, for 7 days, after which the covers were removed, the forms were stripped, and the unit was allowed to stand exposed to the laboratory environment until just before testing, when it was painted with one coat of water-based white paint.

For each batch of concrete, twelve 100mmx200mm test cylinders were cast in accordance with New Zealand standard (23). The cylinders were cast in the upright position in

steel moulds without top caps, although the top surface of the concrete cylinder was trowelled off to create a smooth surface. The cylinders stood in their moulds covered with damp hessian sacking and polyurethane sheets near the wall unit itself for 24 hours. Subsequently the cylinders were taken out of their moulds and placed immediately into a 20 degree C, 100 percent humidity room. In general, nine of the twelve cylinders remained in the 100 percent humidity room until they were tested. The three remaining cylinders were removed from the 100 percent humidity room after 7 days, when the forms on the wall unit were stripped. They were placed alongside the wall unit in the laboratory to be cured under the same conditions as the wall unit itself until the testing date, at which time they were tested in compression. Of the first nine, fog-cured cylinders, three were tested in compression after 28 days, three were tested in compression at the time of test of the wall unit, and three were tested in a split cylinder test at the time of test. The testing of the cylinders and the observed strengths are reported in Section 6.3.2.

6.3 MATERIAL PROPERTIES

6.3.1 Reinforcement

The tensile testing of reinforcement was carried out on Avery universal testing machines: a 100kN capacity, type 7109DCJ, grade A machine for 6mm diameter bars and a 1000kN capacity, type 7104DCJ, grade A machine for 10mm, 12mm, and 16mm diameter bars. Force in the bar was read directly from the machine while bar extension was measured over a 2 inch gauge length using a Baty extensiometer with a resolution of 1/20000 inch. Stress was taken as bar force divided by the nominal cross-sectional area of the bar (for a 6mm diameter bar, A=36mm2). The resulting stress strain curves are plotted in Fig. 6.6. Steel properties of the bars are summarized in Table 6.2.

The longitudinal bars in the vertical boundary elements were 10mm, 12mm, and 16mm diameter high strength deformed bars routinely stocked by local suppliers. The steel properties were as expected.

For the main grid of reinforcement in the web,

TABLE 6.2 - STEEL PROPERTIES

Bar designation	f_y (MPa)	f_{ult} (MPa)	ε_y	ε_{SH}	elongation at fracture	E_s (MPa)
HD 6 (1)	515(3)	760	-	-	0.1333	-
HD 6 (2)	472	658	0.00248	0.01420	0.2000	190 000
HD10	443	576	0.00233	0.01770	0.3100	190 000
HD12	451	608	0.00234	0.01840	0.2900	193 000
HD16	465	638	0.00235	0.01620	0.2600	198 000

(1) Before heat treatment

(2) After heat treatment

(3) At 0.2% offset

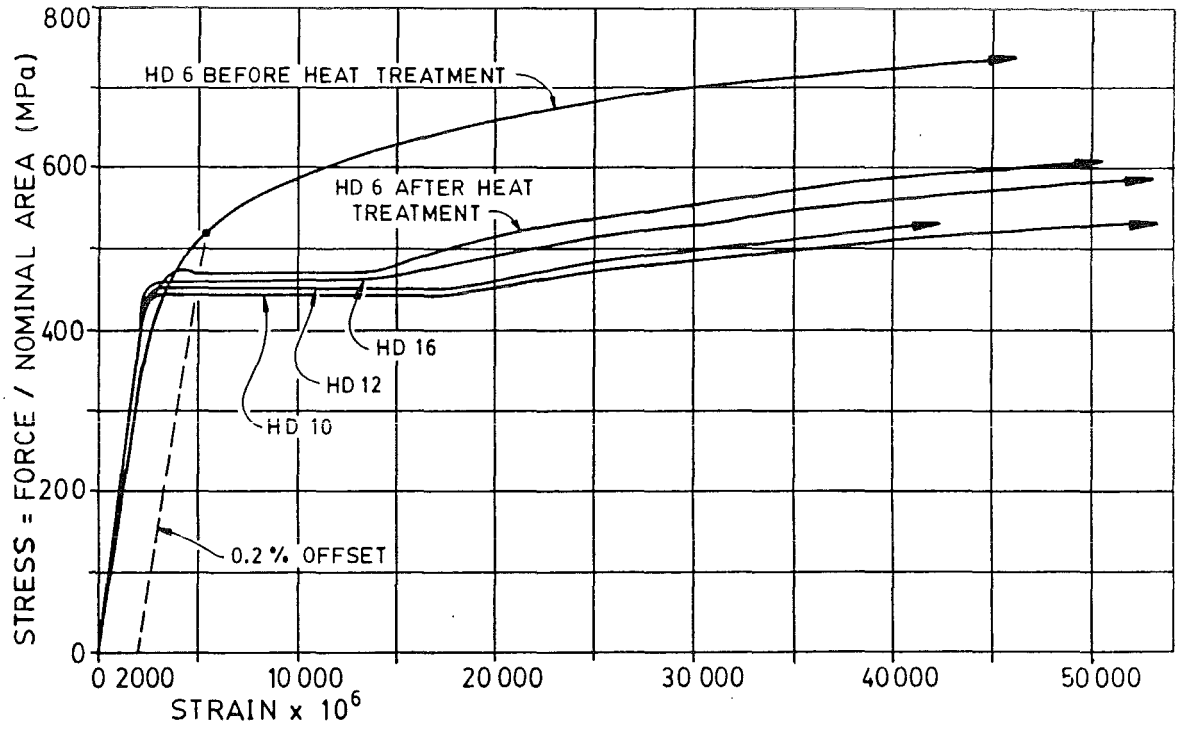

Fig. 6.6 - Stress-strain properties of reinforcement

however, there were some difficulties in obtaining small diameter deformed bars with suitable material properties. A number of 6mm diameter high strength deformed bars, manufactured in Auckland, were obtained. The nominal yield strength was 410MPa. As supplied, however, there existed no yield plateau, and the yield strength at 0.2 percent offset was approximately 515MPa. In an attempt to obtain more realistic steel properties, nearer those encountered in the larger diameter, mild steel bars normally used in practice, the 6mm diameter bars were heat treated at 600 degrees C for a period of approximately 2 hours. The resulting material properties of the bars, as used in the test units, are shown in Fig. 6.6 and summarized in Table 6.2.

The hoops for the vertical boundary elements were, by virtue of the design process, merely nominal and were expected to be very lightly stressed. Therefore, no material tests were conducted on them. The same applied for all longitudinal bars and stirrups in the top and base beams.

6.3.2 Concrete

The casting and curing of concrete cylinders for the purpose of testing concrete strength has been described in Section 6.2.5. All testing of concrete cylinders was carried out on an Avery concrete block testing machine (2500kN capacity, type 7112CCG, grade A) according to New Zealand standard (23). The results are shown in Table 6.2. The fog-cured cylinders were tested approximately one hour after removal from the 100 percent humidity room. The strengths reported in Table 6.1 are the averages of three similarly cured cylinders. (Note - Split cylinder strengths usually range from 50 to 75 percent of the modulus of rupture. See ref. 9.)

6.4 INSTRUMENTATION

6.4.1 General Objectives

The objectives in instrumenting the wall units were to observe the following.

1) lateral force imposed by the hydraulic jack at the top of the wall

2) total top lateral deflection of the wall
3) flexural deformations in the wall unit
4) shear deformations in the wall unit
5) horizontal sliding along construction joints
6) horizontal sliding of the wall unit along the laboratory floor
7) uplift of the ends of the base beam off the laboratory floor
8) overall axial (vertical) extension of the wall unit
9) out-of-plane (twisting) movement of the wall unit
10) strains in selected reinforcing bars
11) extent of yielding of vertical bars within the base beam
12) axial compression in the top beam along its length
13) hogging in the top beam

6.4.2 Load Cell

For the purposes of measuring the applied lateral load, a double-acting (compression and tension) load cell (Fig. 6.1) was fabricated in the civil engineering workshop. Its capacity was 1000kN. Used in conjunction with a Budd strain bridge, the load cell possessed a precision of approximately ± 2kN.

6.4.3 Strain Gauges

Each wall unit was instrumented with approximately 100 electrical resistance strain gauges, as described in Section 6.2.3. Positions of the strain gauges in the wall units are shown in Fig. 6.7. The strain gauges were Showa type N11-FA-5-120-11 unidirectional gauges with 5mm gauge length and 120ohm resistance. Voltages across strain gauges were recorded by an automatic datalogger to a resolution of 1 microvolt, which implies a strain of ± 1 microstrain. Less than 1 percent of the strain gauges in each wall unit was lost during construction. During testing, a strain gauge was deemed no longer reliable when the strain exceeded 0.02.

6.4.4 Linear Displacement Potentiometers (LDPs)

For measurement of top deflection, flexural deformations, and shear deformations, series of Sakae linear

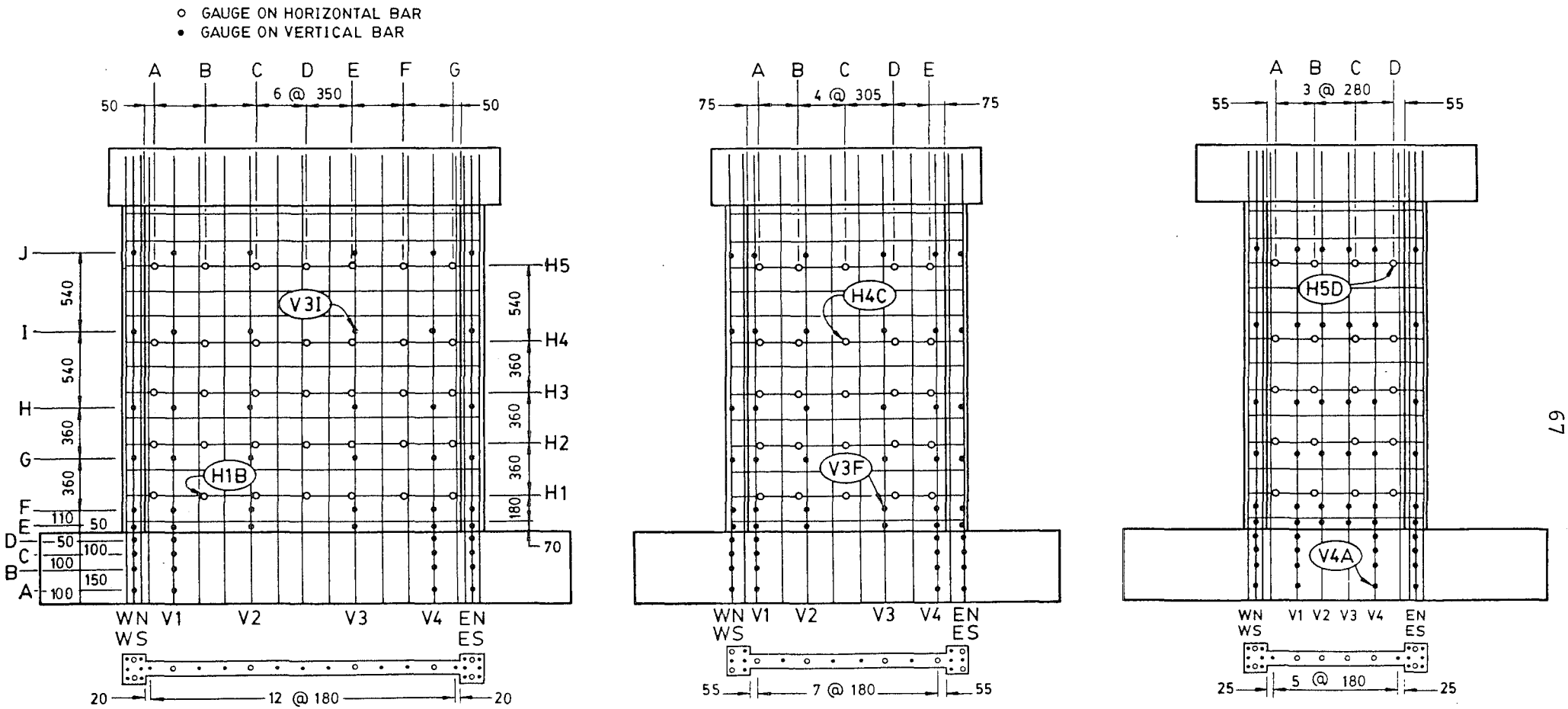

(a) Unit 1.0

(b) Unit 1.5

(c) Unit 2.0

Fig. 6.7 - Internal instrumentation

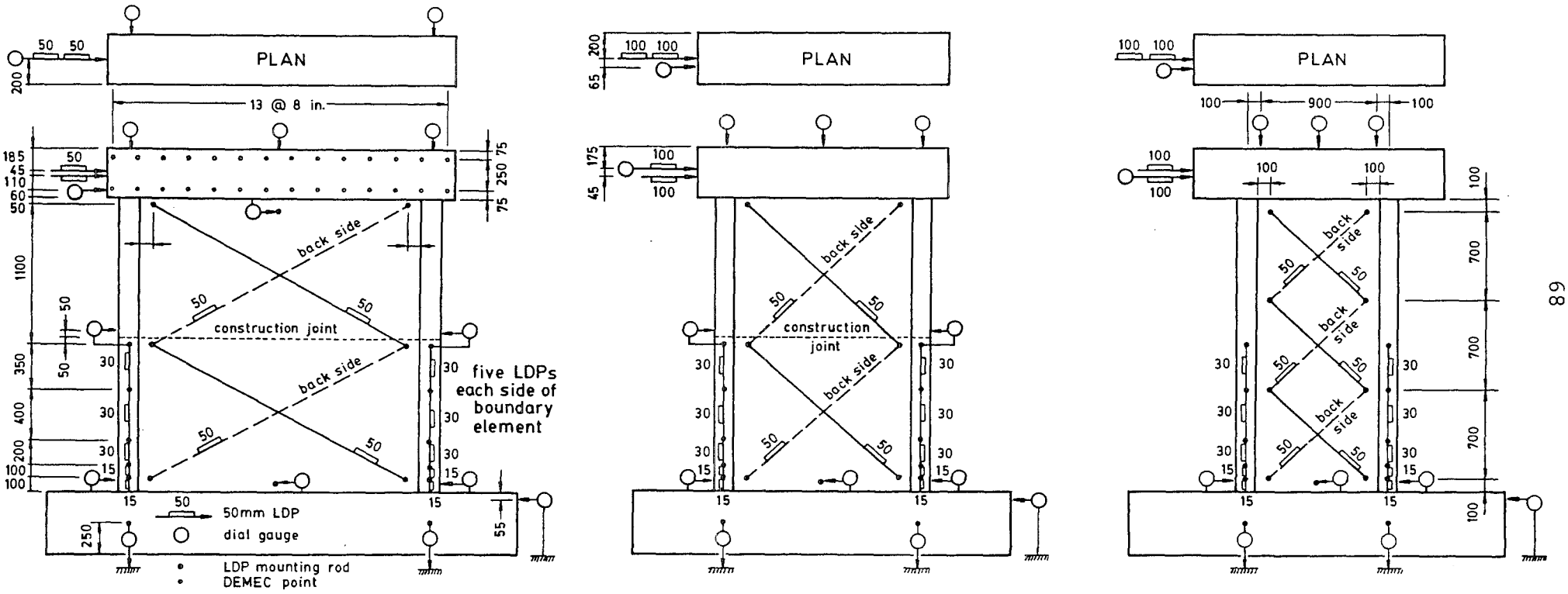

(a) Unit 1.0

(b) Unit 1.5

(c) Unit 2.0

Fig. 6.8 - External instrumentation

displacement potentiometers (LDPs) were used. Locations of the LDPs for each wall are shown in Fig. 6.8. The instantaneous voltages across the LDPs were recorded by the automatic datalogger. The various LDPs measured displacement with the precisions shown in Table 6.3. The LDPs were attached to the wall units by means of steel brackets that were mounted via single 10mm diameter bolts to potentiometer mounting rods embedded in the concrete. The embedded potentiometer mounting rods were composed of lengths of 10mm and 16mm diameter plain bar and were tied to the reinforcement cage before concreting (Figs. 6.3 and 6.5).

TABLE 6.3 - PRECISION OF LDP's

Size of LDP (max. travel in mm)	Precision (mm)
15	± 0.0002
30	± 0.0004
50	± 0.0006
100	± 0.0013

6.4.5 Automatic Datalogger

A Solartron automatic datlogger was used to record strain gauge and LDP readings at selected load/displacement increments. The datalogger contained a Solstat constant voltage power supply set at approximately 4 volts. It possessed auto-ranging capabilities through 200 channels with a resolution of 1 microvolt.

6.4.6 Dial Gauges

A number of Mitutoyo dial gauges, read manually, were used to monitor the sliding and tipping of the wall unit on the laboratory floor, sliding along construction joints, overall axial extension of the wall unit, and out-of-plane movement of the top beam (Unit 1.0 only). Each dial gauge had a range of 50mm and a least count of 0.01mm. The positions of the dial gauges are shown in Fig. 6.8.

6.4.7 DEMEC Points

For Unit 1.0, it was proposed to measure axial compression along the top beam and hogging deflection of the top beam using external demountable mechanical strain gauges (DEMEC gauges, gauge length = 8 inches, least count = 0.0001 inch). Using sealing wax, a series of DEMEC target points were attached to both sides of the top beam, as shown in Fig. 6.8(a). Readings were taken at every load peak. The top beam was so stiff and the readings so small that the errors that accumulated in the calculation of strain were of the order of 50-80 percent of the calculated strain value, rendering the calculated strain value suspect. DEMEC points were subsequently omitted for Units 1.5 and 2.0.

6.4.8 Crack Width Microscope

During the tests, the widths of selected diagonal cracks were monitored approximately using a hand-held crack width microscope with a least count of 0.001 inch. In the late stages of testing, the crack widths were often beyond the range of the microscope. In such cases, cracks widths were estimated roughly to a precision of $\pm$ 0.5mm using the naked eye and a steel rule.

6.5 TESTING PROGRAMME - GENERAL COMMENTS

6.5.1 Test Setup

The wall units were moved into position in the test rig using trolleys. An overhead crane was used to lift one end of the base beam at a time in order to place it onto a low trolley. The trolleys were dragged along the laboratory floor until the unit was nearly in position, at which time the trolleys were removed. Final positioning of the unit on the floor was achieved by jacking either end of the base beam transversely until the top beam came into line with the hydraulic jack and loading frame. Alignment was achieved using a string line. Once the base beam was clamped horizontally into postiion on the floor, each end of the base beam was lifted, and a bed of gypsum dental plaster was applied. The base beam was set down while the plaster was still fluid. Thus, uniform bearing on the floor was achieved. The test setup is shown in Fig. 6.1.

6.5.2 Initial Load Level

A loading programme for each unit was chosen based on the ideal shear strength calculated as described in Section 5.7. These ideal shear strengths, V_i, are summarized in Table 5.1. The load level for the first cycle was chosen as $0.75V_i$, according to previous University of Canterbury testing practice. Although in the testing of fully ductile units, V_i is normally taken as the ideal flexural strength, in the present tests, V_i was taken as the ideal shear strength. At this point, it must be noted that the calculation of ideal shear strength by methods currently available is much less understood and, therefore, much less precise than the calculation of flexural strength. In similar tests in the past, one initial cycle to a load level of $0.75V_i$ was imposed in order to observe the elastic characteristics of the test unit (for example, stiffness in the thoroughly cracked state) The stiffness and definition of yield deflection, Δ_y, are traditionally taken as defined in Fig. 6.9. Because of the shear-dominant nature of the present units, it was found, in Unit 1.0, that the first cycle to $0.75V_i$ produced large corner-to-corner cracks, which were evidence that the unit had been loaded beyond its elastic limit. Therefore, in order to better observe the elastic characteristics of Units 1.5 and 2.0, an initial load level of $0.25V_i$ was chosen.

6.5.3 Cyclic Loading

The elastic cyclic loading for Units 1.5 and 2.0 consisted of two cycles to $\pm 0.25V_i$ and two cycles to $\pm 0.50V_i$. Three cycles to $\pm 0.75V_i$ were imposed next, the first of which was used for the purpose of defining yield deflection, Δ_y. The deflections at $0.75V_i$ for positive and negative loading directions for the first excursion only were averaged and multiplied by 4/3 to define Δ_y. (See Fig. 6.9.) All of these initial cycles were controlled by load (based on the estimated ideal shear strength). That is, the unit was loaded to a predetermined lateral load. After cycles to $\pm 0.75V_i$, the test was controlled by deflection. That is, the unit was loaded to a predetermined top deflection.

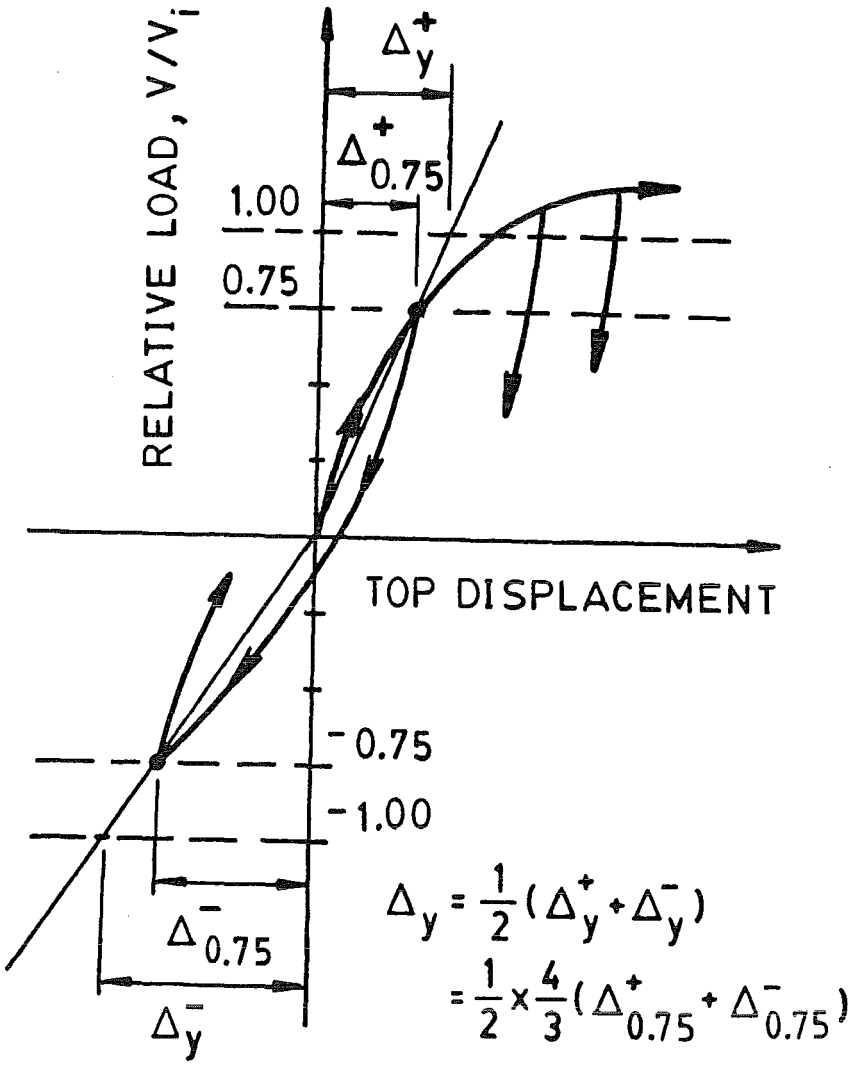

Fig. 6.9 - Definition of experimental yield displacement under cyclic loading

In previous tests of ductile members, the post-elastic portion of the testing has been deflection-controlled using displacement ductility factors ($\mu_\Delta = \Delta/\Delta_y$). Traditionally, double cycles to deflections corresponding to selected ductility factors of 2,4,6,8,etc. have been imposed. (See Fig. 2.1.) Since the present units were meant to exhibit only limited ductility, it was thought more valuable to cycle the units to deflections corresponding to selected values of drift (Δ/h_w = 1/500, 1/300, 1/200, 1/133, 1/100). Moreover, since the calculated ductility factor, $\mu_\Delta = \Delta/\Delta_y$, depends heavily upon the definition of Δ_y, and since, in the present case, Δ_y was so arbitrarily defined, by virtue of the uncertainties in estimating ideal shear strength, V_i, the drift, Δ/h_w, was established as a basis for setting levels of

inelastic cycling. This method of setting loading by means of lateral drift is also customarily used in Japanese tests. As mentioned in Section 4.1, a value of $\Delta/h_w=1/100$ is considered a practical limit on the drift to be realistically expected in low-rise structural wall buildings.

Furthermore, because walls of limited ductility frequently occur in low-rise buildings, and since such buildings vibrate at higher natural frequencies than taller buildings that contain fully ductile walls, it was deemed more useful in the present tests to investigate behaviour under a greater number of cycles at each displacement level. Therefore, instead of being subjected to just two cycles at each displacement level, these test units were subjected to three and sometimes five cycles at each displacement level. With such cyclic loading, the degree of stability in the unit's response (area of hysteretic loops, load at maximum deflection, etc.) over repeated cycling at a given displacement level could be observed.

The testing of each unit was carried out over a period of 5-7 days. For each half cycle, the loading of the units was carried out in several increments in which either load or displacement (depending on the stage in testing) was increased stepwise until the selected maximum was reached. Unloading, as well, was generally carried out in several increments. The detailed loading histories for the three units are given in Figs. 7.2, 8.1, and 9.1.

6.5.4 Recording of Data

The actual application of load for each increment lasted less than 30 seconds. When the specified load or deflection was reached, the hydraulic ram was locked at a fixed displacement. The data were then recorded. For every increment between zero and the selected maximum, the strain gauge readings, potentiometer readings, and dial gauge readings were recorded. Generally, the time that elapsed between these intermediate increments was 2-4 minutes. Because more extensive data were collected at load peaks, the time that elapsed between the maximum loading increment and the first unloading increment generally ranged from 10 to 30 minutes. Lateral load, strain gauge readings, and potentiometer readings were recorded virtually immediately

after locking of the hydraulic ram. Load was read manually from a Budd strain bridge while strain gauge and potentiometer readings were recorded automatically by the datalogger. Meanwhile, the dial gauges were read manually. This process took approximately 2-3 minutes. Next, DEMEC readings (Unit 1.0 at load peaks only) were taken manually. Next, cracks were marked with felt marking pens. Widths of selected diagonal cracks were measured with a hand-held crack width microscope. Finally, photographs were taken.

During these periods in which data were collected, some relaxation of the lateral load occurred. However, the lateral load was read immediately, before any relaxation occurred, and the relaxation of load, being small, affected readings of strains, deformation, and displacements minimally.

Since testing of a unit could not be completed in one working day, the unit was allowed to stand overnight at an increment corresponding to zero load.

SECTION 7

UNIT 1.0
LOADING HISTORY, GENERAL BEHAVIOUR, AND TEST RESULTS

7.1 CONVENTIONS IN THE PRESENTATION OF RESULTS

In this thesis, all diagrams, photographs, and test results are presented in such a way that the test unit lies in the plane of the paper and is viewed from the south. The hydraulic jack assembly is on the right-hand (east) side of the unit and lies in the plane of the paper. The positive loading direction (first half cycle) is toward the left; the negative loading direction (second half cycle) is toward the right.

7.2 LOADING HISTORY

Figure 5.2 shows the overall dimensions and reinforcement layout for the test units. Figure 7.1 shows reinforcing details for the top and base beams for Unit 1.0. The cyclic loading history for Unit 1.0 is shown in Fig. 7.2. Each dot indicates a load or displacement increment at which measurements were taken. The first three cycles were controlled by load. Beginning with the fourth cycle, the test was controlled by displacements, defined by lateral drift, Δ/h_w.

Initially, three cycles to a force of $\pm 0.75V_i = \pm 308$kN were imposed. For this wall unit, however, it was found that a lateral load of $0.75V_i$ produced large diagonal cracks and thus pushed the unit into the inelastic range. Some horizontal and vertical web bars reached yield during this first cycle. Nevertheless, an estimate of the initial stiffness has been made using the first two load increments. A total of 12 full cycles were imposed on Unit 1.0.

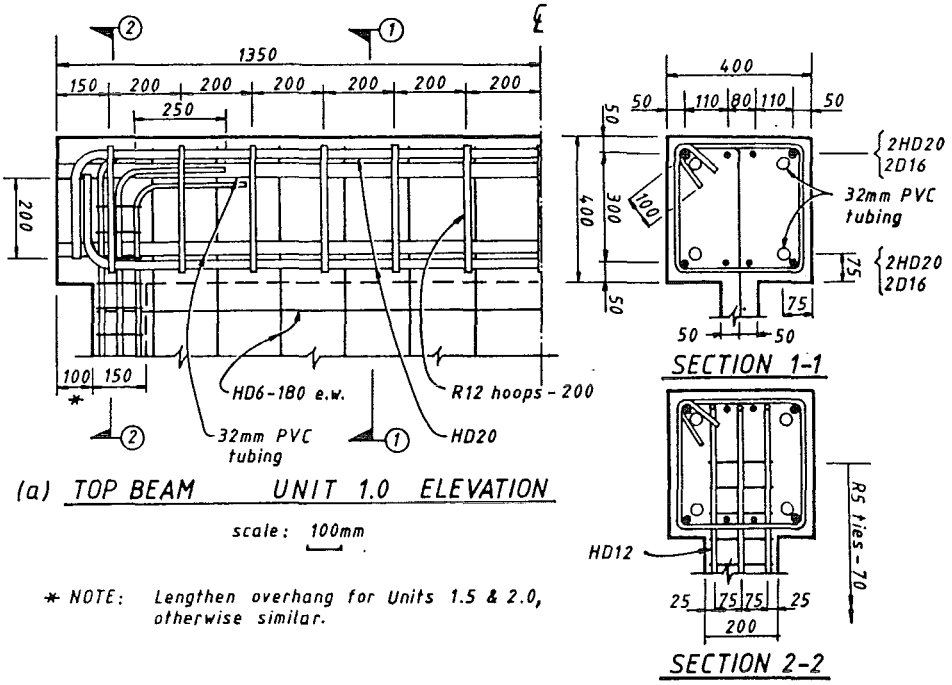

(a) TOP BEAM UNIT 1.0 ELEVATION

scale: 100mm

* NOTE: Lengthen overhang for Units 1.5 & 2.0, otherwise similar.

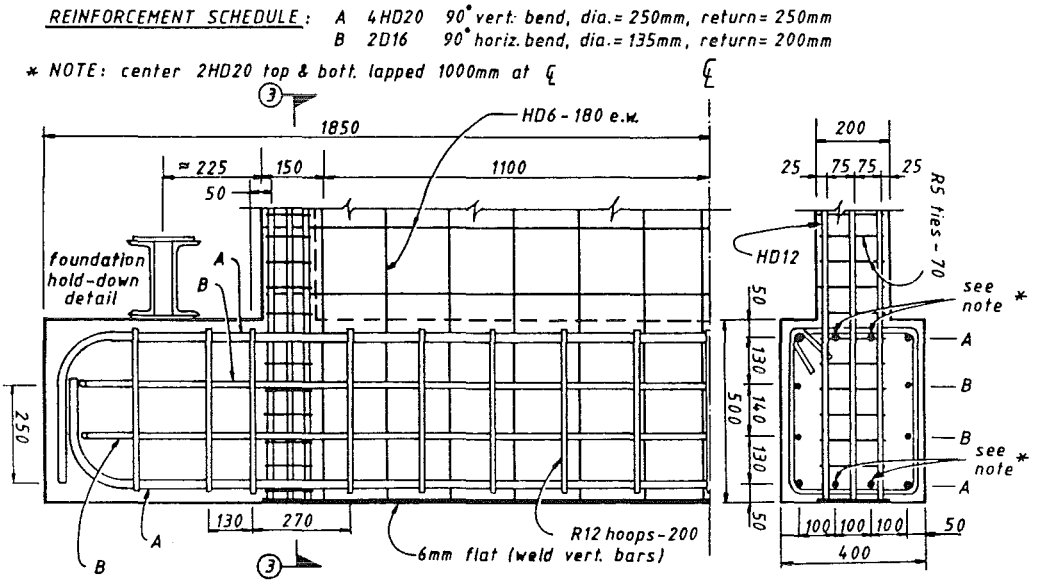

(b) BASE BEAM UNIT 1.0 ELEVATION

scale: 100mm

NOTE: similar for Units 1.5 & 2.0

SECTION 3-3

Fig. 7.1 - UNIT 1.0 - Reinforcement details for the top and base beams (Note: Details for Units 1.5 and 2.0 are similar.)

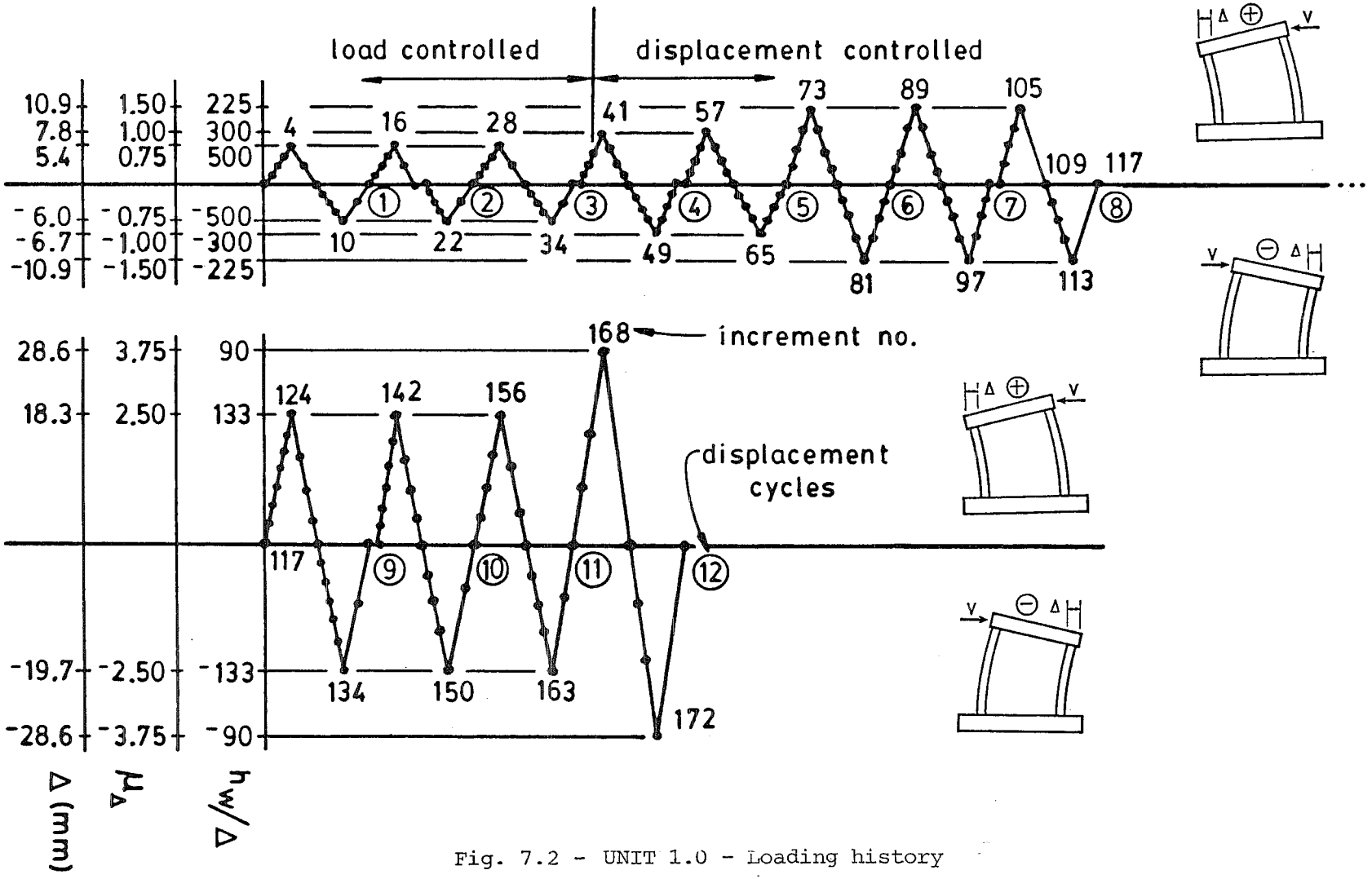

Fig. 7.2 - UNIT 1.0 - Loading history

7.3 DESCRIPTION OF OBSERVED BEHAVIOUR

Increment Number	Description
2	Positive loading. The first horizontal flexural cracks appeared in the lower part of the right-hand boundary element (RHBE). A faint crack appeared along the base construction joint to within 835mm from the compression face. No visible horizontal slippage along this joint was evident.
3	Horizontal flexural cracks appeared in the RHBE spaced at approximately 70mm (the hoop spacing, the hoops acting as crack initiators) and extending up to $0.70h_w$. Three of these flexural cracks near the bottom of the RHBE extended into the web as inclined cracks. A major diagonal crack formed suddenly and with a thudding noise at a load of V = 180kN = $0.47(V_i)_{shear}$ = $0.37(V_i)_{flex}$ = $0.35(V_{max})_{test}$. The formation of this crack, as well as most of the subequent diagonal cracks, was marked with a momentary but noticeable drop in lateral load. This crack (crack 1 in Fig. 7.7) started at a height of 1380mm in the RHBE and intersected the base beam 670mm from the compression face of the left-hand boundary element (LHBE). The crack lay at an angle of approximately 40 degrees from the horizontal. The crack along the base construction joint extended to 360mm from the compression face (not seen in Fig. 7.7).
4	Horizontal flexural cracks spaced at 70mm appeared over the entire height of the RHBE. The horizontal cracks became inclined where they entered the web. Above crack 1, some diagonal cracks formed a fan extending off crack 1. They began from the upper part of the RHBE and extended down into the web to approximately half height. These upper diagonal

cracks formed at progressively steeper angles and varied from 500 to 1000mm in length. Below crack 1, some of the horizontal flexural cracks extended approximately 300mm into the web as inclined cracks. Width of crack 1 = 1.40mm. Top deflection = 5.40mm (Fig. 7.3)

8 Negative loading. Horizontal flexural cracks spaced at 70mm appeared in the lower half of the LHBE. Some horizontal flexural cracks changed direction where they entered the web and extended diagonally downward 400-500mm into the web. The angle of these cracks was approximately 38 degrees from horizontal.

9 Further flexural cracking appeared in the LHBE up to approximately $0.70h_w$. Additional diagonal cracks appeared in the lower left-hand part of the web. These diagonal cracks were approximately equally spaced. Although the base construction joint cracked along its entire length, no significant slip was observed. V = 231kN.

10 A new diagonal crack formed suddenly and with a thudding noise at a load of V = 261kN = $0.68(V_i)_{shear}$ = $0.53(V_i)_{flex}$ = $0.57(V_{max})_{neg}$ = $0.51(V_{max})_{test}$. This crack (crack 2 in Fig. 7.7) extended from the lower right-hand corner of the web up to the LHBE at a level roughly 650mm below the level of the load application. This crack was discontinuous at mid-height of the wall and lay at an angle of approximately 39 degrees from horizontal. Width of crack 2 = 1.14mm. Horizontal flexural cracking extended up the entire height of the LHBE. Top deflection = 6.00mm. Δ_y = (4/3)x(5.40+6.00)/2 = 7.60mm. (Fig. 7.4)

16-34 During these second and third cycles to $0.75V_i$, some widening and lengthening of existing cracks was observed, but no significant changes in observed behaviour occurred.

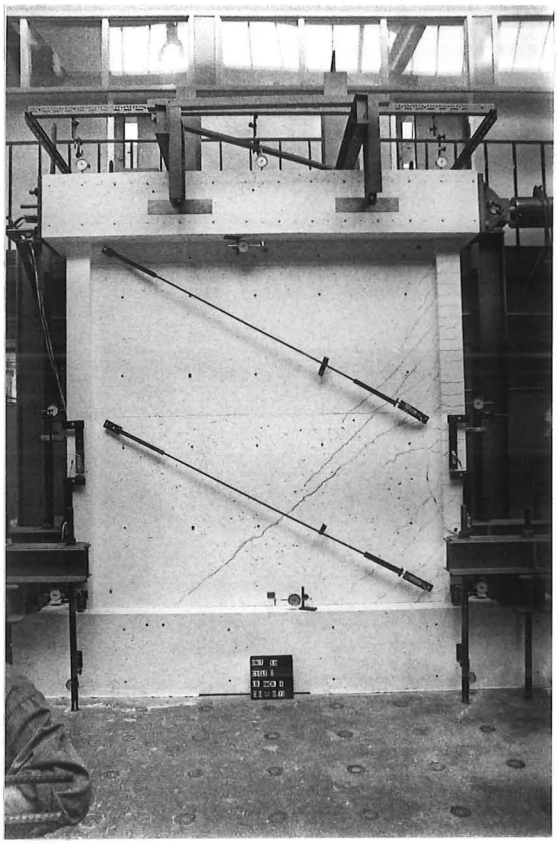

Fig. 7.3 - UNIT 1.0 - Crack pattern at increment 4

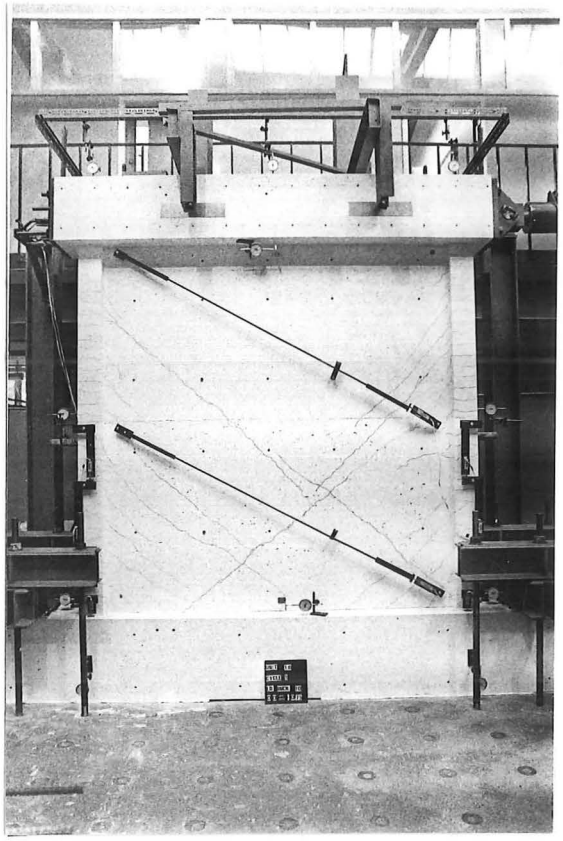

Fig. 7.4 - UNIT 1.0 - Crack pattern at increment 10

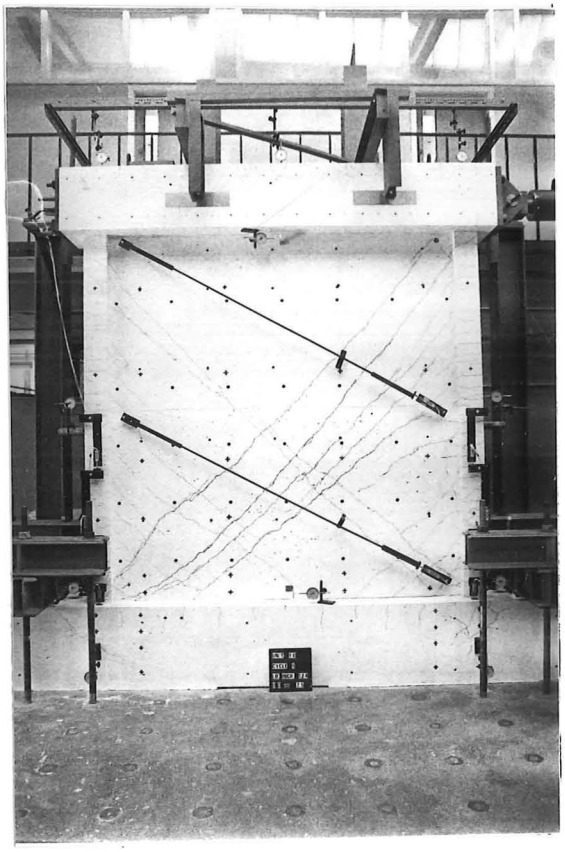

Fig. 7.5 - UNIT 1.0 - Crack pattern at increment 124

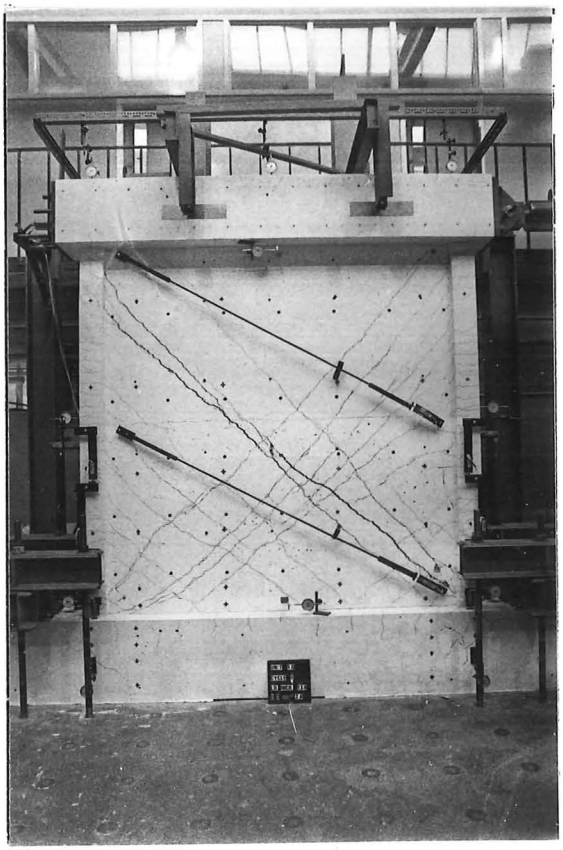

Fig. 7.6 - UNIT 1.0 - Crack pattern at increment 134

41 At this point, the test began to be controlled by displacements. Above crack 1, new diagonal cracks appeared suddenly again with a thudding noise, and existing diagonal cracks lengthened. The diagonal cracks formed a fan along the main diagonal. That is, the higher cracks formed at progressively steeper angles. The diagonal crack directily above crack 1 formed at an angle steeper than crack 1 on the right-hand side of the unit, but flattened markedly as it approached the compression face, which is characteristic of a flexural crack. Below crack 1, some of the existing diagonal cracks lengthened. Although these diagonal cracks lay approximately evenly spaced and at approximately the same angle as crack 1, they lay in the bottom right-hand corner of the web well separated from the fanning cracks on the main diagonal. Width of crack 1 = 1.45mm.

49 Although existing cracks widened, no significant additional cracking occurred. As the test had now become controlled by displacement, the applied lateral load did not exceed the previously applied maximum lateral load by the time this greater displacement was reached.

73 Below crack 1, only minor lengthening of existing cracks occurred. Above crack 1, the existing fanning diagonal cracks lengthened and flattened markedly as they extended toward the base beam, characteristic of flexural cracking.

81 Below crack 2, only minor lengthening of the existing cracks, lying in the lower left-hand corner and separated noticeably from crack 2, occurred. The two disjointed portions of crack 2 formed two full length diagonal cracks, both lying at about 38 degrees from the horizontal. The widening of cracks and lateral displacement of the wall concentrated along crack 2.

89-113 Stable behaviour was observed at these second and third cycles to Δ/h_w=1/225. Minor crack extensions were observed, however, there occurred no significant crack widening.

+ direction: width of crack 1 = 1.30mm
width of crack 3 = 1.40mm
- direction: width of crack 2 = 2.41mm

124 The maximum load was reached at this increment. $(V_{max})_{test} = (V_{max})_{pos}$ = 510kN. Below crack 1, although flexural cracking increased slightly, the significant development was the widening of the base construction joint crack (width=3mm). However, no evidence of slip was observed. Above crack 1, a new diagonal crack (crack 4, Fig. 7.7) formed suddenly and with a thudding noise. This crack lay apart from the main fan of diagonal cracks and at an angle of approximately 45 degrees. Instead of flattening as it approached the base beam, as the fanning diagonal cracks had done, it steepened as it approached the base beam. (Fig. 7.5)

128 Zero load. The base crack remained open.

134 The maximum load in the negative loading direction was reached at this increment. $(V_{max})_{neg}$ = 456kN. A new full height diagonal crack formed suddenly and with a thudding noise above crack 2 and at a steeper angle of approximately 49 degrees from horizontal. Slip along crack 2, defined as displacement parallel to the main line of crack 2 at the point of observation shown in Fig. 7.7, was detected for the first time. The width and slip along crack 2 were 5.5 and 3.5mm, respectively. No significant widening of or slip along the base construction joint crack was noticeable. The main action seemed to occur above crack 2, which lay at approximately 39 degrees from horizontal. The triangular piece below crack 2 exhibited no significant lateral displacement, while the

triangular piece above crack 2 experienced a rotation about the lower right-hand corner with a consequent opeining of crack 2. Crushing became evident in the lower right-hand corner of the web along crack 2 (Fig. 7.6).

142 Positive loading. Crack 2 (formed under negative loading) remained open at both ends (top left and bottom right) but closed in the centre, evidence that a diagonal compression strut was in effect. Additional flexural cracking occurred on the outside face of the RHBE in the lower 300mm. One horizontal crack in the LHBE, lying 500mm above the wall base remained open while all others closed.

	width (mm)
crack 4	4.5
base crack	3.0

150

crack	width (mm)	slip (mm)
2	6.0	5.5
5	1.0	-

156

crack	width (mm)
4	5.0

163

crack	width (mm)	slip (mm)
2	7.0	6.0

Additional crushing and spalling along crack 2 occurred in the lower right-hand region of the web and in the centre of the web where crack 2 intersected the diagonal cracks formed under positive loading.

168 Crack 4 opened markedly wider in the lower half of the wall compared to the upper half of the wall. The main action seemed to occur along crack 4 in the lower half of the wall and along crack 3 in the upper half of the wall. The angle formed along this line was therefore approximately 40 degrees from horizontal. Crushing and spalling occurred in the LHBE at the lower end of crack 4. Some

additional unexpected diagonal cracking occurred well above crack 4 in the upper left-hand region of the web. These cracks, however, were confined to the region below crack 2, the main diagonal crack for negative loading (Fig. 7.7).

172 Two horizontal web bars fractured along crack 2 (bar H2 and the bar between H3 and H4, Fig. 6.7(a)). The main action occurred along crack 2. A kink occurred at the base of the RHBE, resulting in a significant horizontal offset of the upper triangle with respect to the lower triangle. Concentrated bending occurred in the LHBE at the level at which crack 2 intersected it. Extensive additional horizontal flexural cracks as well as diagonal cracks formed in the LHBE at this point. As in increment 168, some additional unexpected diagonal cracks formed well above the main diagonal but below crack 4, the main diagonal crack for positive loading (Fig. 7.7). As well as displacing with respect to the lower triangle, the upper triangle also rotated about its lower right-hand corner.

7.4 FAILURE MECHANISM

The first evidence of deformation occurred in the form of horizontal flexural cracking in the lower regions of the vertical boundary elements. However, from the very early stages of the test, arch action was evident. Diagonal cracks extending across the entire web formed during the first cycle to $\pm 0.75V_i$. The shear nature of the behaviour was evident from the suddenness with which the diagonal cracks formed. Immediately upon forming, the diagonal cracks extended over nearly the entire length of the web. They also opened very widely upon first forming. As diagonal cracks formed, high strains were recorded in the nearby horizontal and vertical web bars. Horizontal strains were generally higher than vertical strains. However, strains remained low in web bars lying off the main diagonals.

Two similar diagonal strut systems developed for the

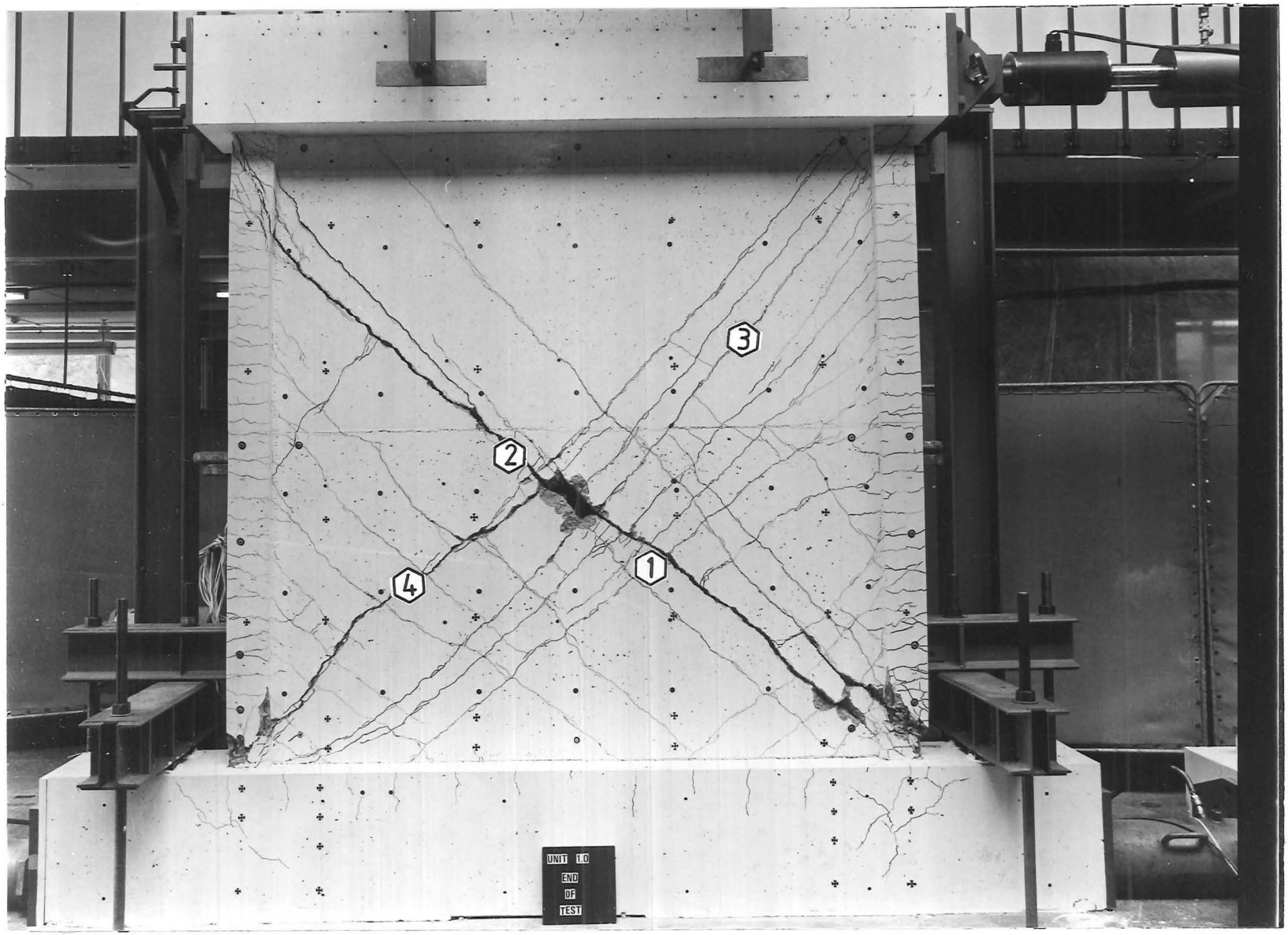

Fig. 7.7(a) - UNIT 1.0 - Crack pattern at the end of the test

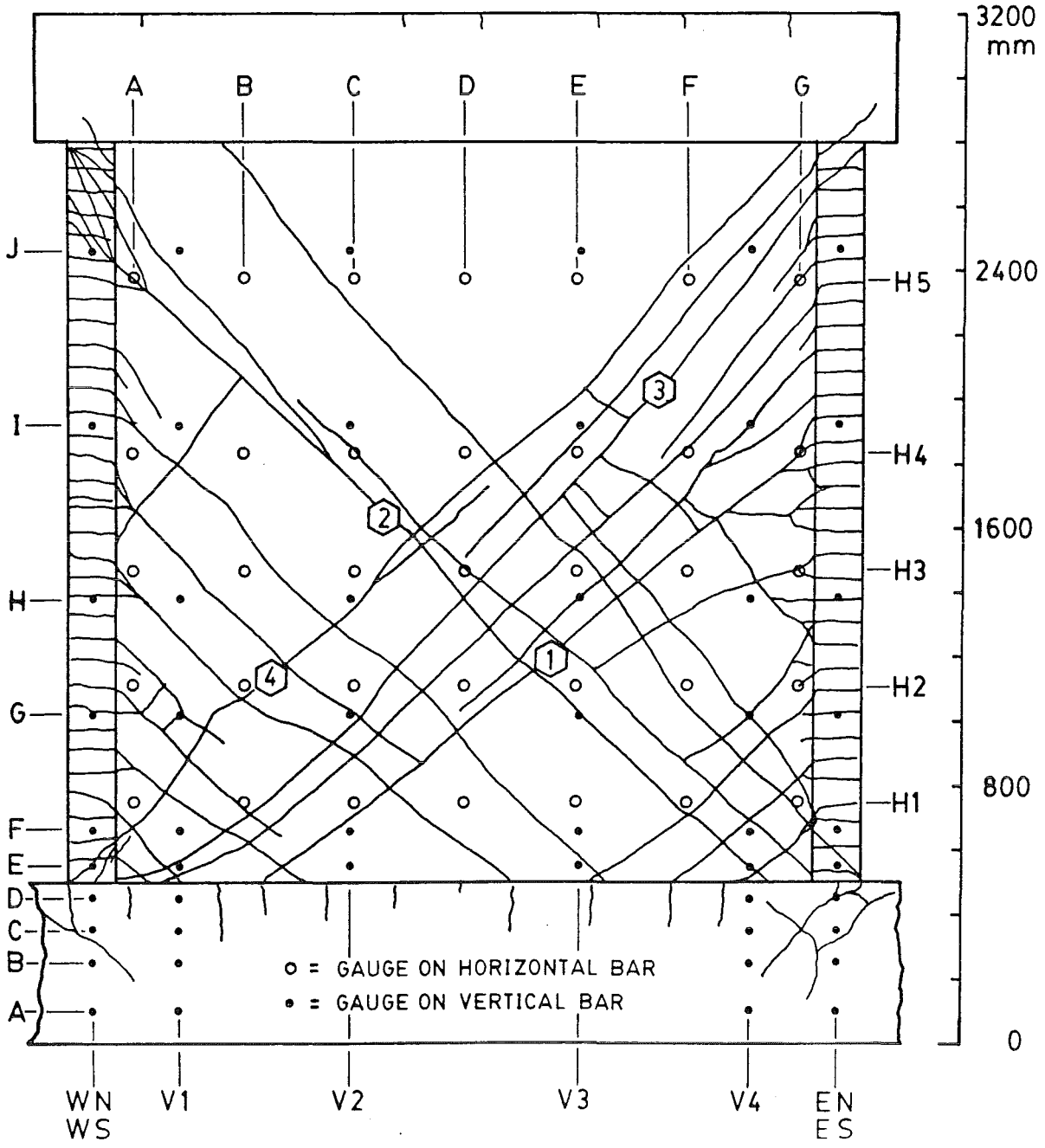

Fig. 7.7(b) - UNIT 1.0 - Crack pattern at the end of the test

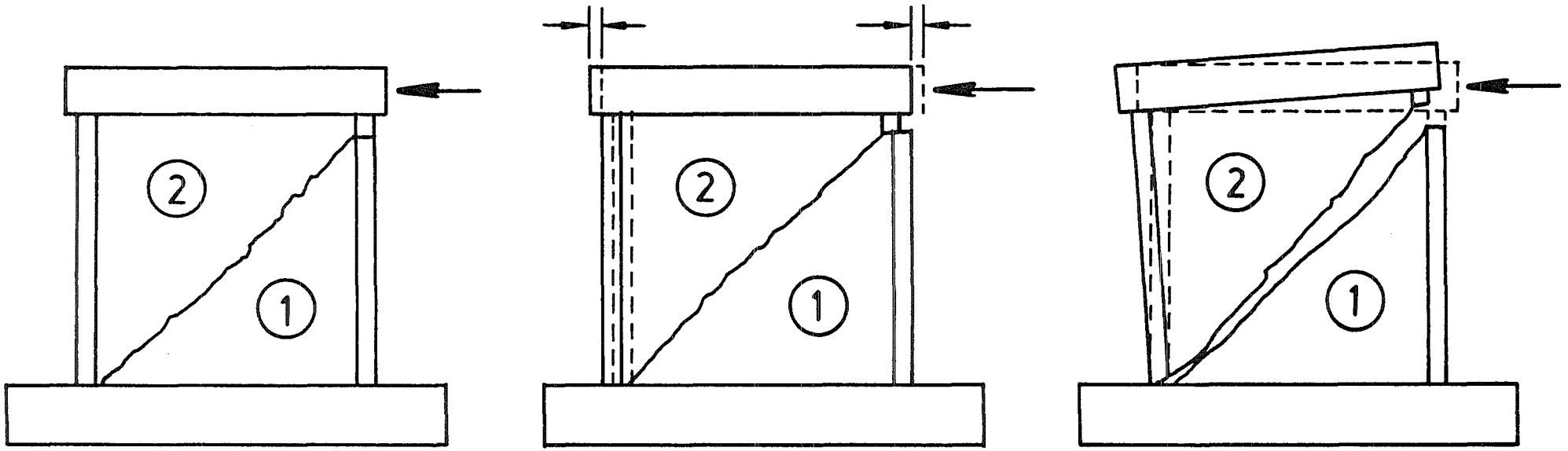

(a) Main diagonal crack (b) Horizontal displacement (c) Rotation

Fig. 7.8 - Failure mechanism

two loading directions. For the purposes of explanation, refer to Fig. 7.8. For each loading direction, the lowest, first-formed diagonal crack effectively divided the wall into two regions. As displacement levels were increased, flexural cracking extended the full height of the tensile boundary element. However, deformations in the web occurred, for the most part, in region 2. Additional diagonal cracks formed in the web at progressively steeper angles above the initial diagonal crack. Strains in web bars lying off the main diagonal were noticeably lower than strains in bars on the main diagonal. Virtually no diasplacements were recorded between region 1 and the base beam. As the test progressed, the unit attianed its theoretical ideal flexural strength as vertical bars in the tensile boundary element and nearby vertical web bars yielded throughout the entire height of the wall. Strains in horizontal bars along the main diagonals reached yield as well and were, in general, larger than strains in corresponding vertical web bars. No appreciable strain increases were recorded in web bars lying off the main diagonal. Diagonal cracking continued in region 2 until the attainment of maximum load. At this point, region 2 was displaced horizontally with respect to region 1 (Fig. 7.8(b)). Also, all of the diagonal cracks opened widely, especially near the tension face, as region 2 rotated clockwise with respect to region 1 about its lower compression corner (Fig. 7.8(c)). The horizontal displacement was marked by vertical cracking of concrete on the inside face of the compression boundary element. This cracking was followed by spalling and outward kinking of the vertical boundary element at the base. Spalling occurred also at the centre of the web, where the main diagonals for both loading directions intersected (Fig. 7.9). A final cycle to a displacement level of $\Delta/h_w = 1/90$ resulted in the fracturing of two horizontal web bars along the main diagonal crack and severe kinking of vertical bars along the main diagonal crack. Still, only negligible displacement was recorded between region 1 and the base beam. Both the wall's vertical and horizontal dimensions increased due to progressive yielding of web bars under load reversals. Details of the failed unit are shown in Fig. 7.9.

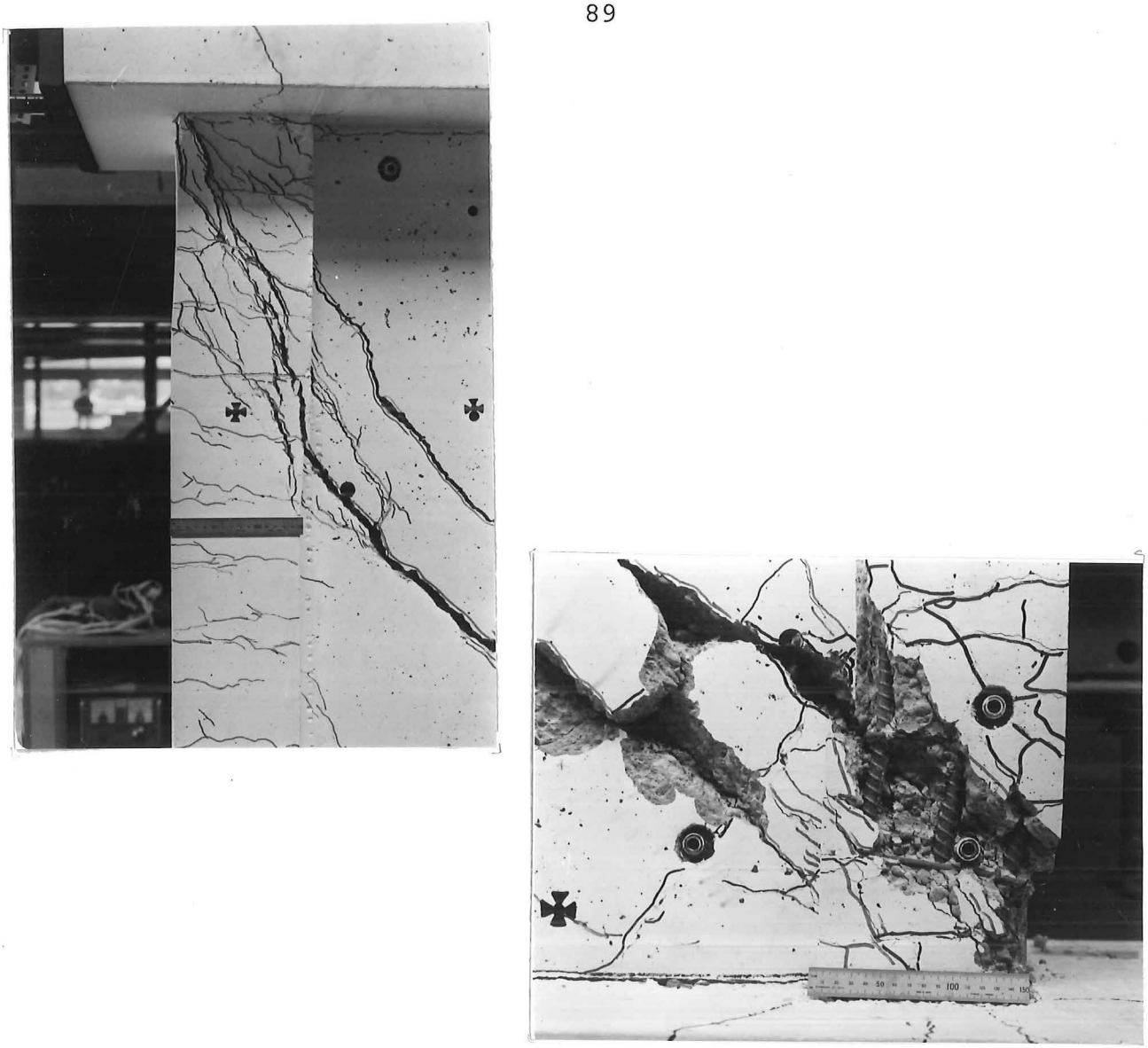

Fig. 7.9 - UNIT 1.0 - Details of the failed unit

7.5 TEST RESULTS

For the majority of test results reported here, a high degree of repeatability was observed during successive cycles to a given load/displacement level. For example, the value of a quantity, such as lateral load resistance, measured on the first cycle to a given displacement level was, in general, repeated with little change on the second and third cycles to that displacement level.

7.5.1 Elastic Cycles

The application of one full cycle to $\pm 0.75V_i$, where V_i is the estimated ideal shear strength, pushed the unit into the inelastic range. At a load of $\pm 0.75V_i$, yield strains were recorded in a number of bars. However, during the first two load increments yielding had not yet taken

place. Using these two increments, the stiffness of the wall unit was estimated to be 224.3kN/mm. At a load level of $0.75V_i$, the yield displacement (as defined in Section 6.5.3) was extrapolated to be 7.6mm (Figs. 6.9 and 7.10). The theoretical yield displacement was calculated to be 3.3mm (Appendix B). The test unit was 2.3 times as flexible as current theory predicts.

7.5.2 Lateral Load vs. Total Top Displacement

The hysteretic loops for lateral load vs. total top displacement are shown in Fig. 7.10. For load and displacement levels of $V = 0.75V_i$, $\Delta/h_w = 1/300$, and $\Delta/h_w = 1/225$, only the first cycle at each level is shown. Only the positive and negative peaks are shown for the second and third cycles. These first cycle loops are reasonably full-bodied, indicating that a moderate amount of energy was dissipated. However, they exhibit definite pinching, which is indicative of the influence of shear on the behaviour. In considering three cycles to a given displacement level, the second two loops are much more pinched than the first loop, showing that less energy is dissipated upon repeated cycling to a given displacement. For example, see increments 134, 150, and 163. (The loss of resistance is commented on below.) Energy dissipation is discussed further in Section 7.5.4.

Although the amount of energy dissipated per cycle decreased with repeated cycling to a particular displacement, the lateral load resistance, in general, remained approximately the same. For example, refer to the load peaks for increments 73, 89, 105. Particular stability in lateral load resistance is seen in the second and third cycles. (See increments 97 and 113.) This stability is substantiated later in Units 1.5 and 2.0 where up to 5 cycles were imposed at a given displacement level. This retention of lateral load resistance was observed for load levels prior to maximum load. However, after maximum load was reached, the lateral load resistance dropped sharply after the first cycle to a given displacement. (See increments 134,150,163 in Fig. 7.10.) The lateral load resistance developed on consecutive cycles is tabulated in Table 7.1 and plotted in Fig. 7.11. Prior to maximum load, the average drop in resistance was 3.2

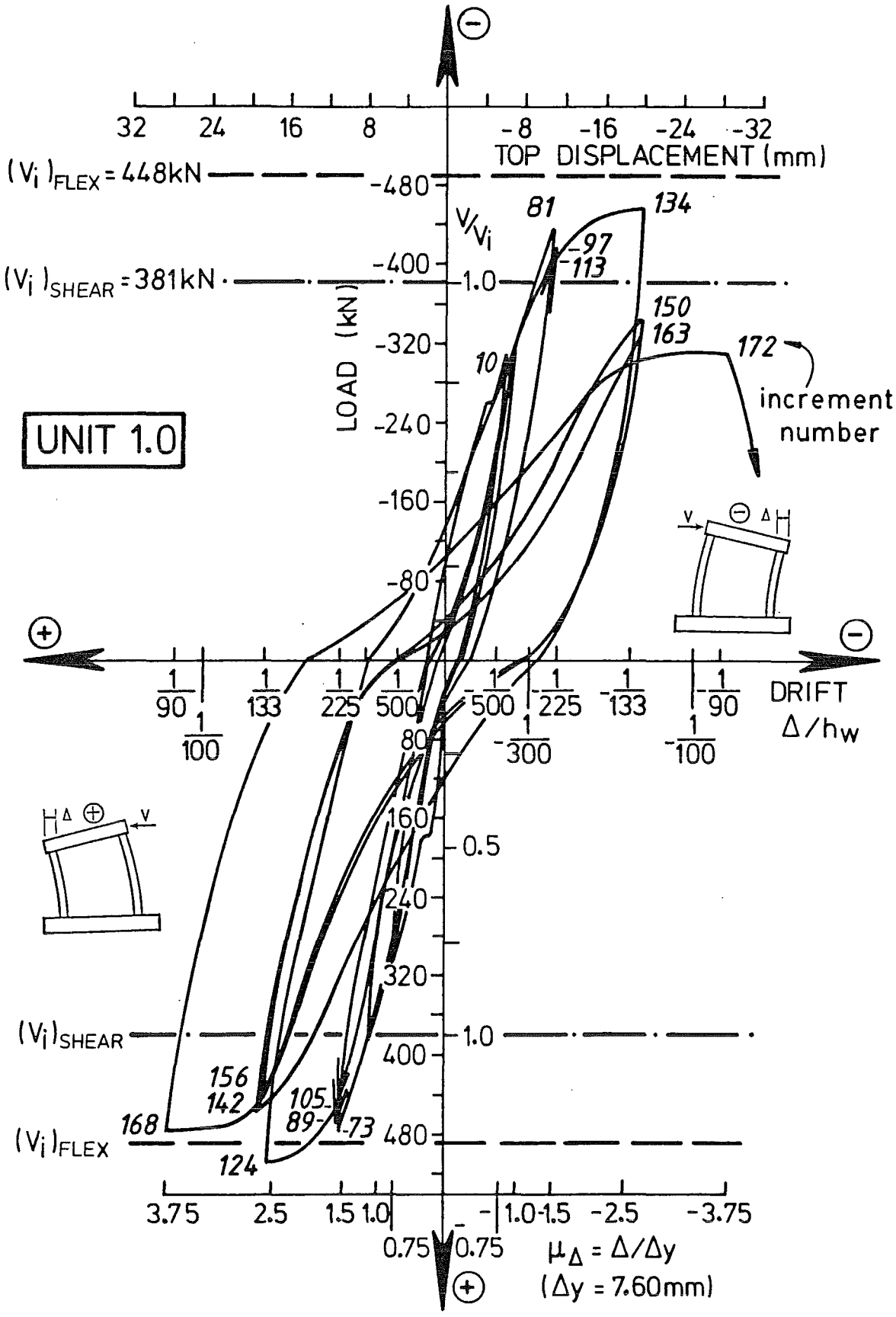

Fig. 7.10 - UNIT 1.0 - Lateral load vs. top displacement

TABLE 7.1 - UNIT 1.0 - LATERAL LOAD RESISTANCE DEVELOPED ON CONSECUTIVE CYCLES

Load/displacement level	Positive loading ←			Negative loading →		
	Increment No.	Lateral load (kN)	Reduction in lateral load (%)[1]	Increment No.	Lateral load (kN)	Reduction in lateral load (%)[1]
$V = 0.75\ V_i$	4	308	-	10	308	-
	16	308	-	22	308	-
	28	308	-	34	308	-
$\Delta/h_w = 1/300$	41	387	-	49	304	-
	57	388	-	65	297	-
$1/225$	73	478	-	81	434	-
	89	469	1.9	97	412	5.1
	105	458	4.2	113	407	6.2
$1/133$	124	510[2]	-	134	456[2]	-
	142	471	7.6	150	345	24.3
	156	445	12.7	163	324	28.9
$1/90$	168	476	-	172	310	-

(1) Reduction is given as a percentage of the lateral load developed during the first cycle to the given displacement level.

(2) Maximum load for the given loading direction.

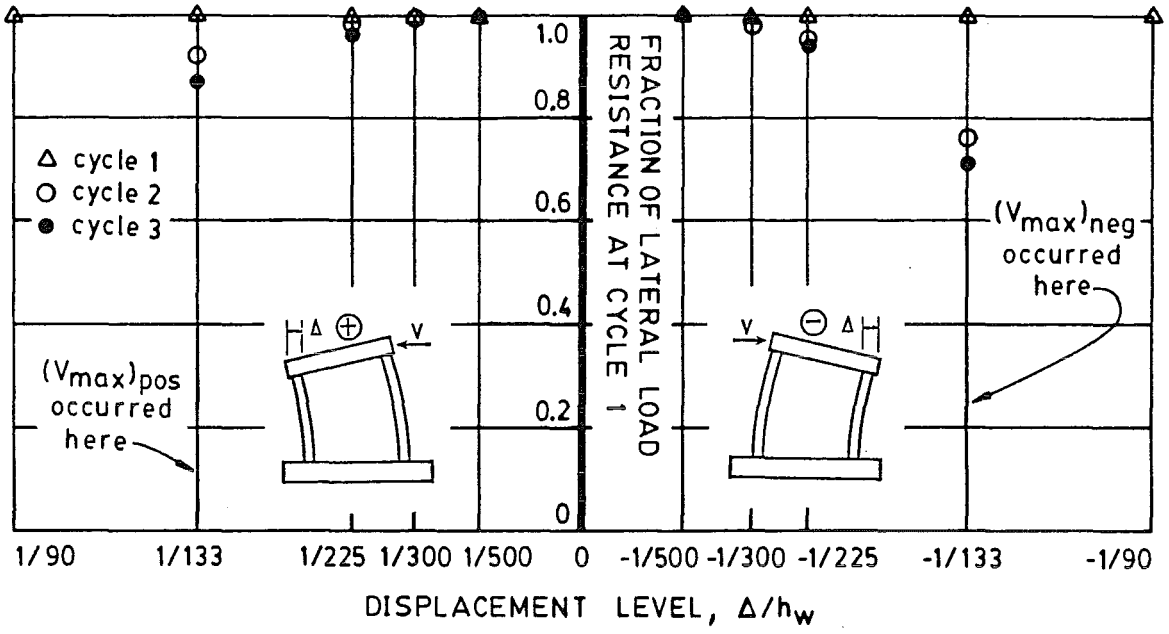

Fig. 7.11 - UNIT 1.0 - Lateral load resistance developed on consecutive cycles

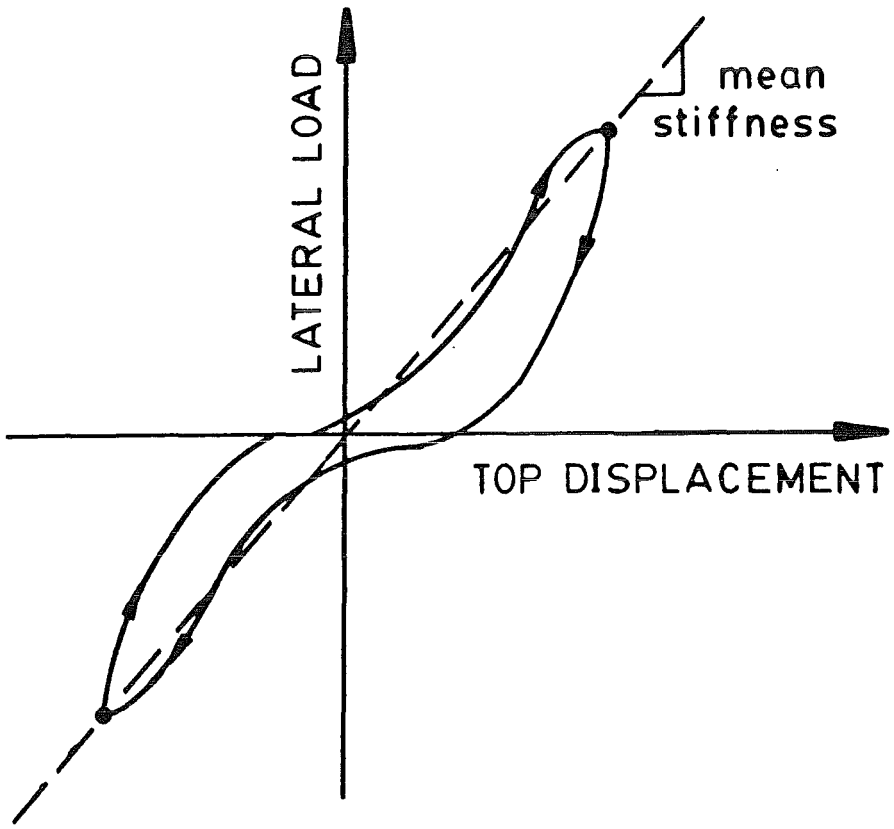

Fig. 7.12 - Estimate of mean stiffness for test units

percent. After maximum load, the average drop in resistance was 18.5 percent. As seen in Fig. 7.11, loss in lateral load resistance on consecutive cycles increased with displacement level.

A maximum load of 510kN was attained on the first half cycle to Δ/h_w=+1/133 (increment 124). The strength attained exceeded the predicted ideal shear strength by 33.9 percent and the predicted ideal flexural strength by 4.5 percent.

As seen in the progressive flattening of the angle of inclination of the hysteretic loops in Fig. 7.10, the stiffness of the unit degraded throughout the test. For the purposes of quantifying this degradation, the mean stiffness of the unit for each displacement level was estimated as follows. A line was drawn through the positive and negative load peaks for the first cycle to the given displacement level. The slope of this line was taken as an estimate of the stiffness of the unit for that displacement level (Fig. 7.12). Table 7.2 summarizes these values of mean stiffness as well as other important quantities obtained from the hysteretic loops.

7.5.3 Cumulative Displacement Ductility and Strength Reduction

As outlined in Section 2.1, the current New Zealand loadings code (1) assesses seismic resistance partly in terms of cumulative displacement ductility and strength reduction. A fully ductile structure must sustain the equivalent of four complete cycles to an overall displacement ductility of μ_Δ= 4 while retaining at least 80 percent of its original strength. (See Fig. 2.1.) In other words, the structure must sustain a cumulative displacement ductility of 32 and still retain 80 percent of its original strength. Caution must be exercised in the calculation of equivalent cumulative ductility. For example, although the cumulative ductility would still be 32, 32 cycles to a $\mu_\Delta = \pm 1$ would not be equivalent to 4 cycles to $\mu_\Delta = \pm 4$. Moreover, care must be taken in the definition of yield displacement, Δ_y. The definition of Δ_y strongly affects the ductility value that a certain displacement represents. The consistent means of defining Δ_y shown in Section 6.5.2, Fig. 6.9 helps to remedy this problem. For the present test walls, the calculation of

TABLE 7.2 - SUMMARY OF LOAD vs TOTAL TOP DISPLACEMENT HYSTERETIC BEHAVIOUR

	UNIT 1.0	UNIT 1.5	UNIT 2.0
$(V_i)_{shear}$ (kN)	381 (2)	200	160
$(V_i)_{flex}$ (kN)	488	332	256
$(V_{max})_{test}$ (kN)	510	342	274
$0.75V_i$ (kN)	308 (3)	150	120
Stiffness (kN/mm) at $V = 0.50\,V_i$	-	48.4	26.9
Stiffness (kN/mm) at $V = 0.75\,V_i$	54.0	32.2	20.2
Stiffness (kN/mm) at $\Delta/h_w = 1/300$	47.6	26.5	17.9
Stiffness (kN/mm) at $\Delta/h_w = 1/225, 1/200$	41.7	22.7	15.7
Stiffness (kN/mm) at $\Delta/h_w = 1/133$	25.4	18.1	13.1
Stiffness (kN/mm) at $\Delta/h_w = 1/90, 1/100$	13.7	9.29	10.1
Stiffness (kN/mm) (1) at $\Delta/h_w = 1/75$	-	-	7.0
$(\Delta_y)_{predicted}$ (mm)	3.3	4.0	4.9
$(\Delta_y)_{measured}$ (mm)	7.60	6.28	7.94
Cycle when $(V_{max})_{test}$ was reached	$\Delta/h_w = +1/133$	$+1/133$	$+1/100$

(1) Slope of line intersecting positive and negative peaks on lateral load vs. total top displacement hysteresis loops

(2) Calculated using actual f'_c

(3) Calculated using approximate f'_c

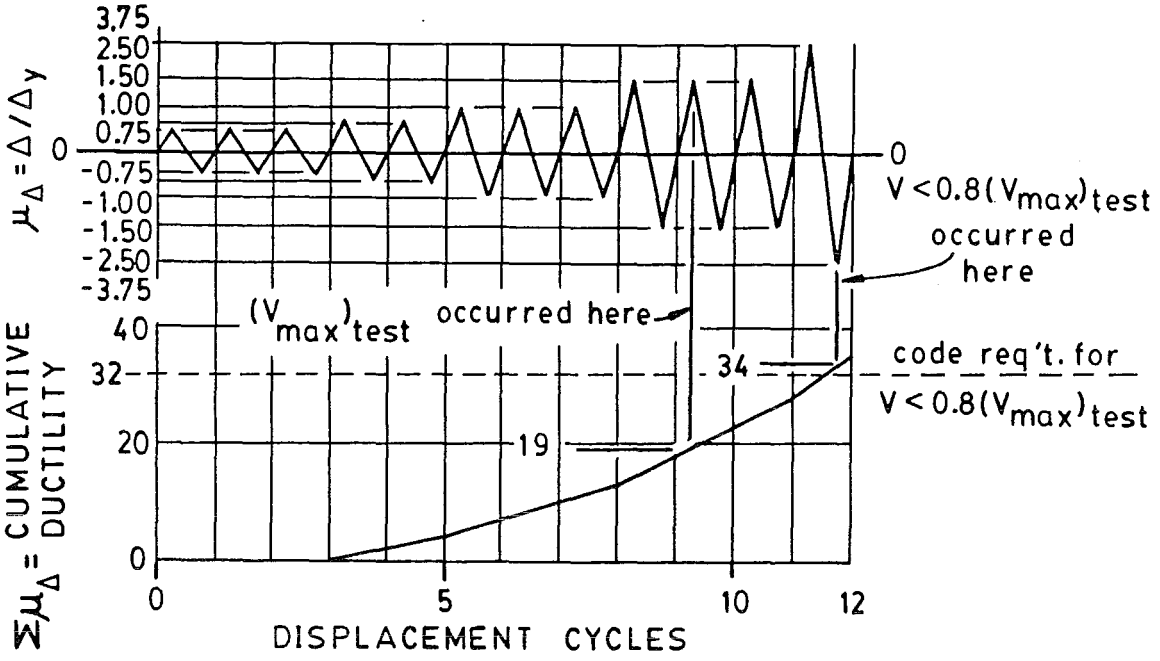

Fig. 7.13 - UNIT 1.0 - Loading history and cumulative displacement ductility

ideal shear strength, V_i, by currently available methods is somewhat imprecise. Therefore, values of cumulative ductility must be viewed with caution. Nevertheless, the loading history and cumulative displacement ductility for Unit 1.0 are shown in Fig. 7.13. The maximum load was attained at a cumulative ductility of approximately 19. By the time the load had decreased to below $0.8(V_{max})_{test}$ (increment 172), the cumulative ductility had reached approximately 34, just in excess of the code requirement for ductile structures.

7.5.4 Dissipation of Energy

In addition to cumulative displacement ductility, another important criterion for earthquake resistance is the structure's ability to dissipate seismically induced energy. For the test units, the energy dissipated during one full displacement cycle is equal to the area within the lateral load vs. total top deflection hysteretic loop (Fig. 7.10). The larger the loop area, the greater is the energy dissipated. Ideal elasto-plastic response (Fig. 2.2, curve 1) represents ideal energy dissipation. Structural steel elements demonstrate, perhaps as closely as possible, ideal energy dissipation (Fig. 2.2, curve 2). It has long been

known that carefully detailed reinforced concrete elements responding in a purely flexural mode demonstrate reasonably full-bodied loops and, thus, quite good energy dissipation characteristics. Elements failing in a non-flexural mode, such as the present wall units, exhibit various degrees of loop pinching and, thus, less than optimal dissipation of energy (Fig. 2.2, curve 3). This is one reason why a flexural failure mode is preferred. However, in the case when the non-flexural failure mode is unavoidable, it is important to quantify energy dissipation.

The energy dissipated by Unit 1.0 for each cycle of the test was obtained by measuring the areas of the lateral load vs. total top displacement hysteretic loops in Fig. 7.10. The energy dissipated for each cycle is shown in Fig. 7.14(a). As displacement level was increased, the energy dissipated per cycle increased. However, when viewing repeated cycles at a particular displacement level (Δ/h_w), it was found that the energy dissipated per cycle decreased sharply after the first cycle, particularly at displacements applied after the maximum test load was reached. This trend is shown in Fig. 7.14(b).

Although the New Zealand Standard NZS 4203 makes no specific requirements regarding energy dissipation capacity, it is instructive to compare the energy dissipated by the present wall units to the energy that would have been dissipated by an ideally elasto-plastic system subjected to the same displacement history. In Fig. 7.15 is plotted cumulative energy dissipated vs. cumulative displacement ductility for both Unit 1.0 and the ideal elasto-plastic system shown in Fig. 4.7. Again, the precautions mentioned in the previous section concerning cumulative ductility apply here. It is seen that prior to the attainment of maximum load, Unit 1.0 dissipated a high percentage of energy (greater than half that dissipated by the elasto-plastic system). After maximum load was reached, the energy dissipated by Unit 1.0 levelled off at approximately half that dissipated by the equivalent elasto-plastic system.

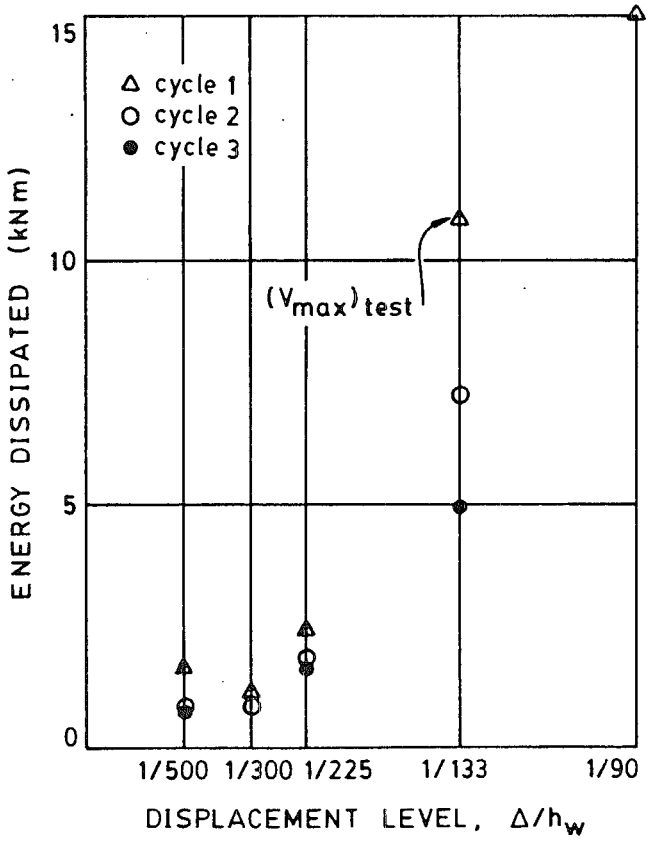

(a) Energy dissipated on each cycle

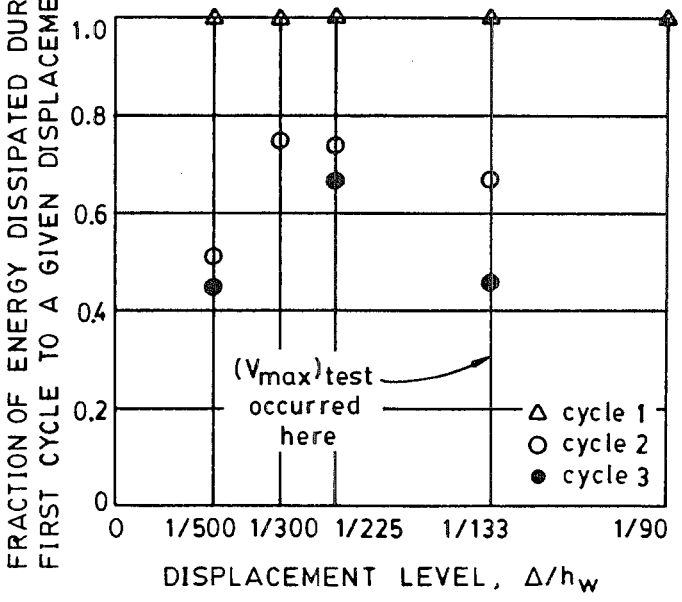

(b) Loss of energy dissipation on consecutive cycles

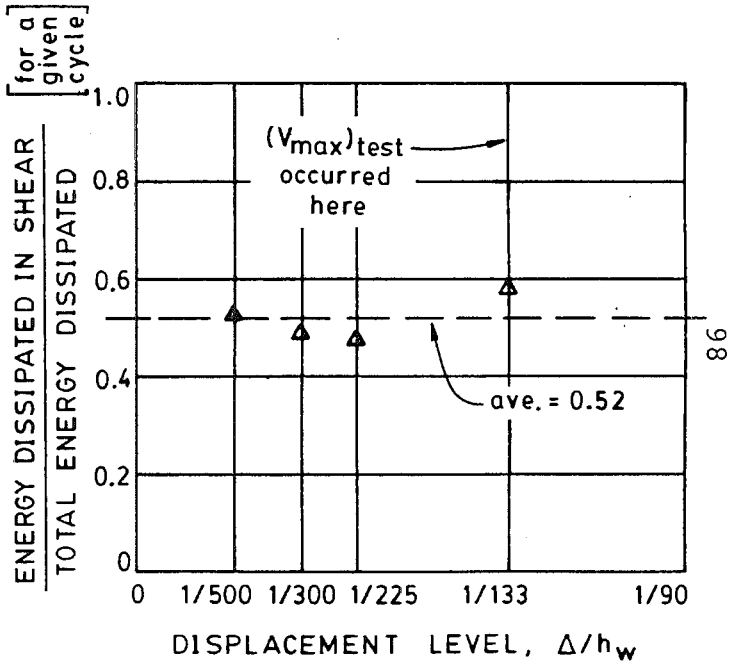

(c) Energy dissipated in shear alone

Fig. 7.14 - UNIT 1.0 - Energy dissipation characteristics

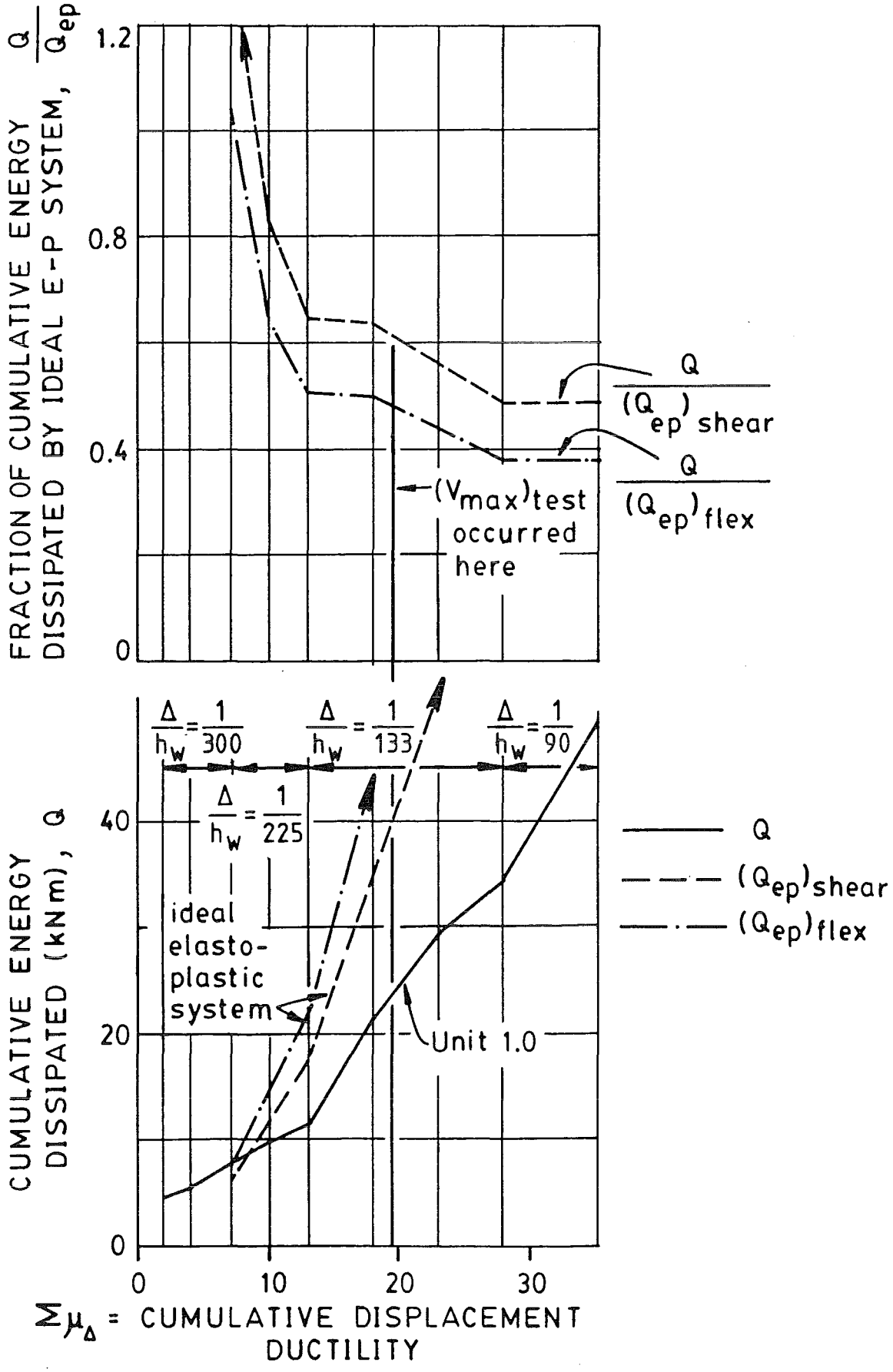

Fig. 7.15 - UNIT 1.0 - Cumulative energy dissipated vs. cumulative displacement ductility

7.5.5 Lateral Load vs. Top Displacement Due to Shear Deformations

The top deflection due to shear deformations alone, Δv, was calculated using the diagonally arranged potentiometers shown in Fig. 6.8(a). The calculation is summarized in Fig. 7.16. ℓ is the horizontal distance

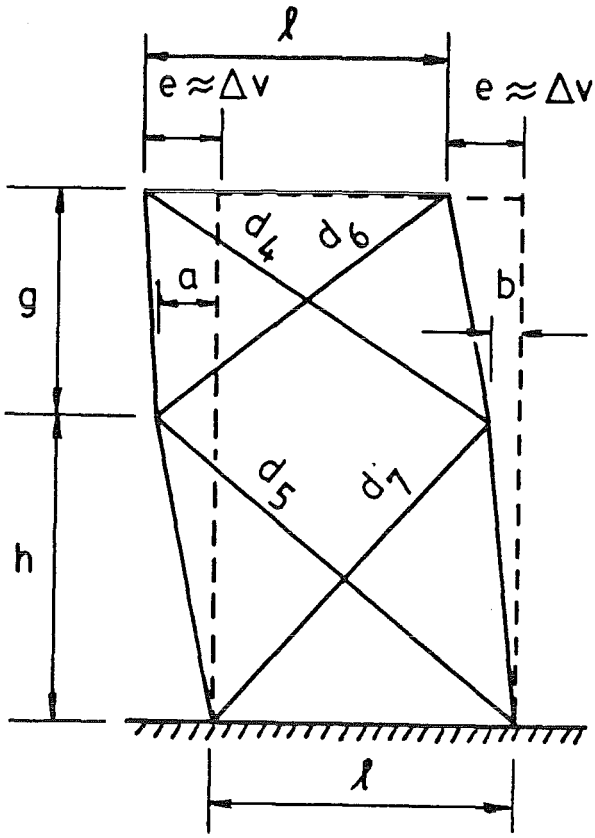

$$d_5^2 = h^2 + (\ell + a)^2 \qquad d_4^2 = g^2 + (\ell + e + b)^2$$

$$d_7^2 = h^2 + (\ell - b)^2 \qquad d_6^2 = g^2 + (\ell - e + a)^2$$

$$e \approx \Delta v$$

Fig. 7.16 - Calculation of top displacement due to shear deformations

between the ends of each diagonal potentiometer rod. h and g are the vertical distances between the ends of the potentiometer rods for the bottom and top sets, respectively. ℓ, h, and g are assumed to remain constant. d_4 to d_7 are the lengths of the diagonals in the deformed state. a is the lateral deflection a mid-height on the left-hand side of the unit, while b is the lateral deflection at mid-height on the right-hand side. e is the lateral deflection at the level of the top potentiometer mounting rods. Δv was assumed approximately equal to e.

Several approximations are inherent in the estimation of Δv. First, the potentiometers only measured deformations over a limited part of the web. (See Fig. 6.8(a).) They did not record shear deformations in the perimeter regions of the web, in the vertical boundary elements, or in the top beam. Second, the elevation at which e was calculated was approximately 300mm below the level at which Δv was taken, the level of the hydraulic jack. Third, it is recognized that measuring shear deformations only by means of the change in length of diagonals is only an approximate method that does not accurately separate out all of the flexural deformations. (See ref. 24.)

Nevertheless, this approximate method was used, and the hysteretic loops for applied lateral load vs. Δv are shown in Fig. 7.17. The shapes of these hysteretic loops are very similar to the shapes of the hysteretic loops for total top displacement (Fig. 7.10). This similarity reveals the dominance of shear in the overall response of the wall unit. This dominance is particularly noticeable in the negative (-->) loading direction. Other sources of deflection contribute significantly to the total top deflection. These are discussed further in the following section. When the areas if the hysteretic loops in Fig. 7.17 are compared with the areas of the loops in Fig. 7.10, it is found that the energy dissipated in shear alone is, on the average, 52 percent of the total energy dissipated for first excursion cycles. See Fig. 7.14(c).

7.5.6 Components of Top Deflection

The use of a series of internal strain gauges, linear differential potentiometers (LDPs), and dial gauges (Figs. 6.7(a) and 6.8(a)) allowed the measurement of several different contributions to the total top deflection. These displacement contributions are illustrated in Fig. 7.18. Δv denotes the deflection at the top of the unit resulting from shear deformations alone. The method of calculating Δv is described in the previous section. Δf denotes the deflection at the top due to flexural deformations alone. Δf was obtained by calculating the strain in each vertical boundary element, as measured by the LDPs. From these strains, the curvature at various horizontal sections were calculated.

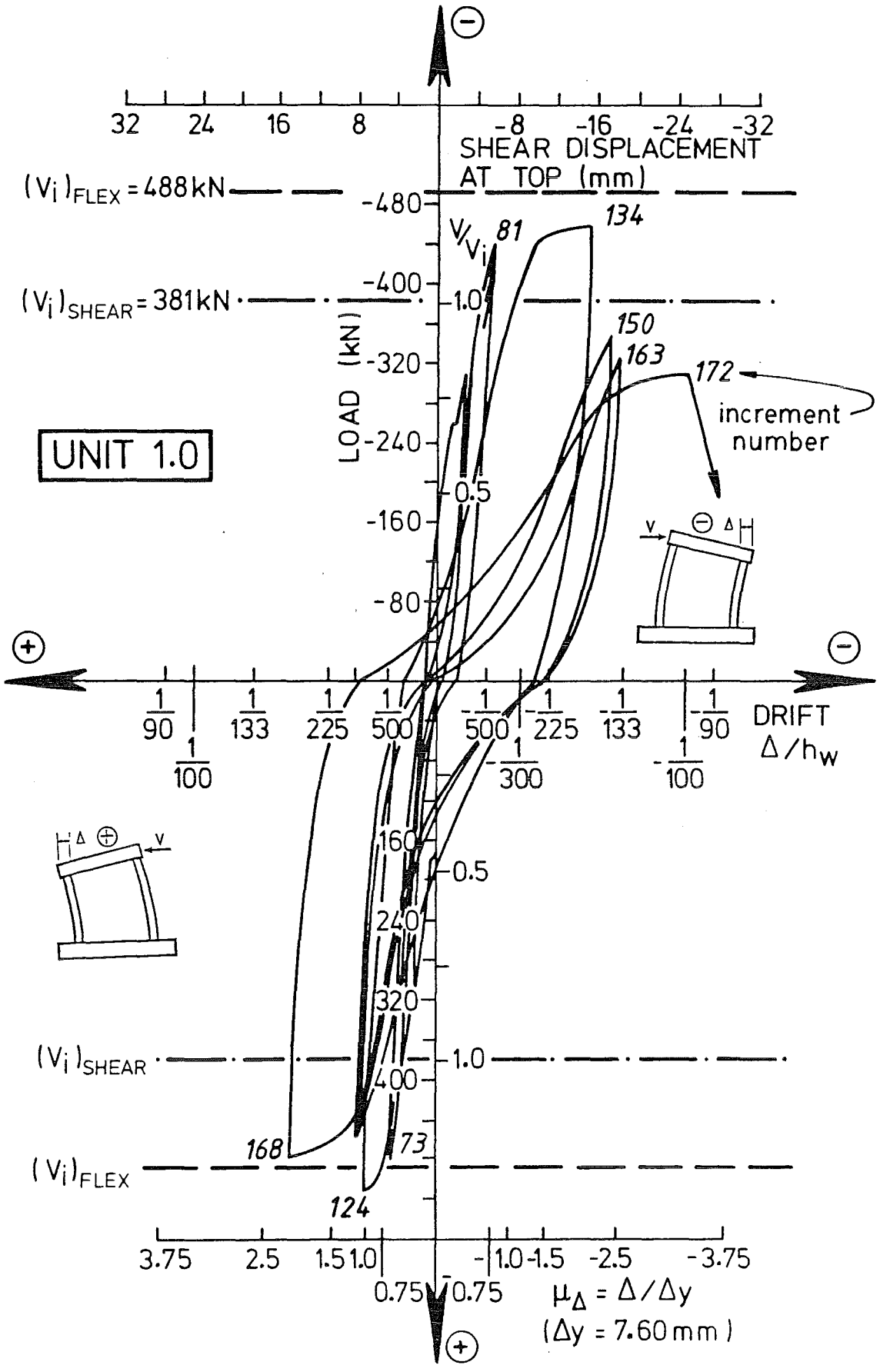

Fig. 7.17 - UNIT 1.0 - Lateral load vs. top displacement due to shear deformations alone

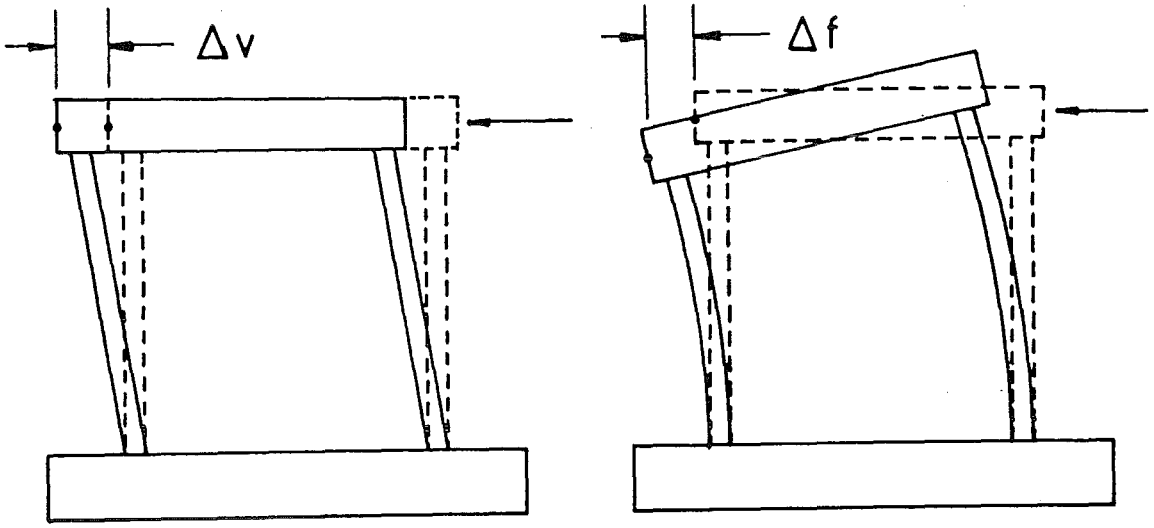

(a) Shear distortions

(b) Flexural distortions

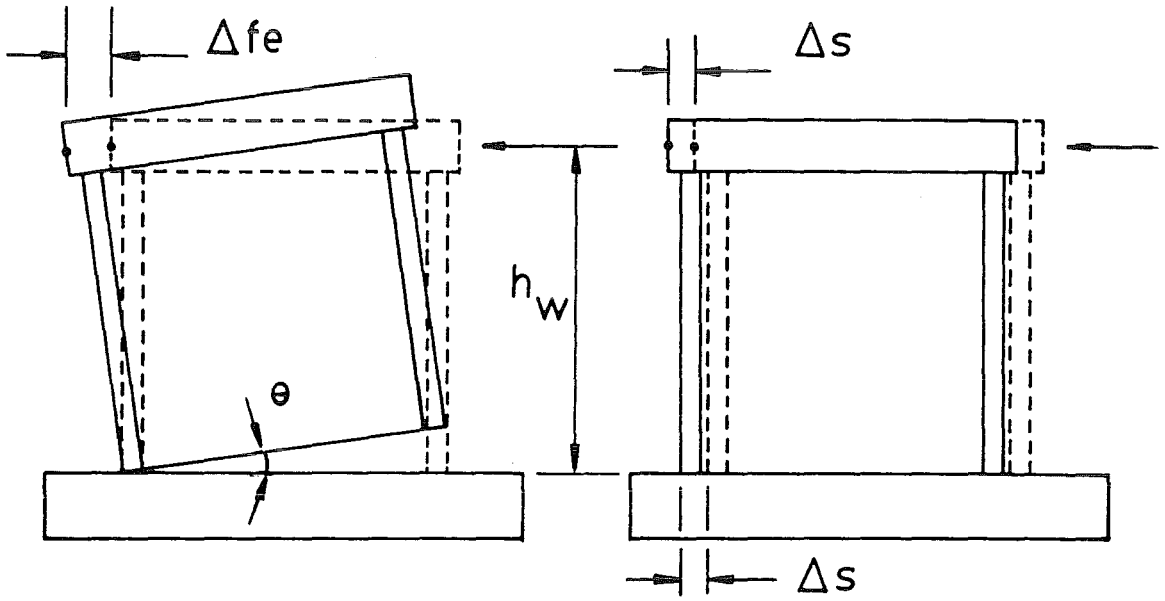

(c) Straining of bars below base level

(d) Sliding at wall base

Fig. 7.18 - Components of top deflection illustrated

These curvatures were numerically integrated twice over the height of the wall to obtain the resulting top deflection. Δfe denotes the top deflection due to a rigid body rotation of the wall resulting from the tensile straining of vertical bars below the base level. Δfe was obtained by integrating over the depth of the base beam the strains recorded in both boundary element bars to obtain the rotation of the horizontal section at the base of the wall. This rigid body rotation was multiplied by h_w to obtain top deflection. Δs denotes the top deflection resulting from sliding along the base construction joint. The contributions from these various mechanisms are plotted in Fig. 7.19. The sum of the separately calculated contributions is labelled Δc, while the top deflection actually measured during the test is plotted as Δm. The error between measured and summed deflection is most likely due to inaccuracies in measuring shear deformation or in calculating flexural deformations.

For positive (<---) loading, the sum of the indiviual displacment components is approximately equal to the actual measured deflection. Moreover, the contributions due to shear and flexure are approximately equal throughout the test. That is, flexural distortions affected the behaviour approximately as much as shear distortions. This approximate equality is shown more clearly in Fig. 7.20. The sizeable influence of flexural distortions is also evident from the crack pattern (Fig. 7.7). For positive (<---) loading, two of the main diagonal cracks flatten as they approach the compression edge, which is typical of flexural cracks.

In the negative (--->) loading direction, the crack pattern and observed behaviour were different. Figs. 7.19 and 7.20 show the dominance of shear distortions. Although there is a sizeable difference between the sum of displacement components and the and measured deflection in the early stages of loading, at displacement levels Δ/h_w=1/133 and 1/90, the discrepancy is negligible.

The difference in behaviour between positive and negative loading is quite marked. Flexural behaviour is perhaps more influencial in the positive (<---) direction because it was the first direction of loading. In both loading directions, the Δfe and Δs contributions were small.

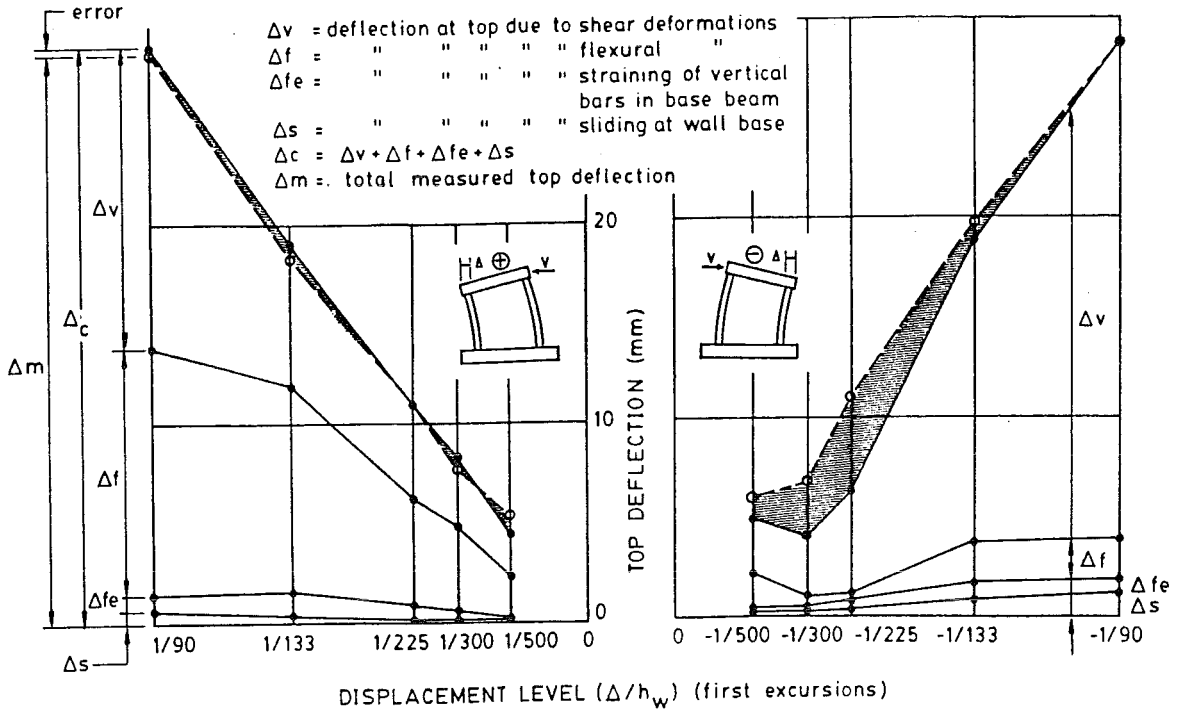

Fig. 7.19 - UNIT 1.0 - Components of top deflection

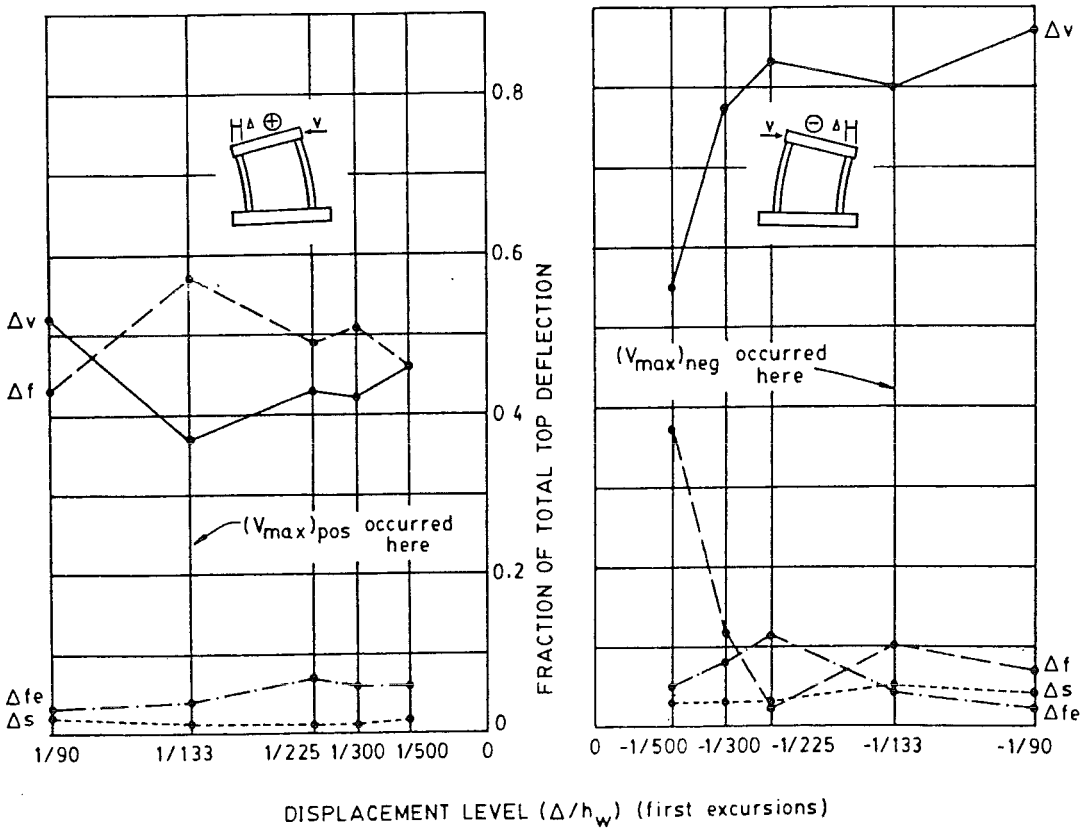

Fig. 7.20 - UNIT 1.0 - Relative proportions of top deflection

7.5.7 Strains in Horizontal Web Bars

Selected horizontal web bars were instrumented as shown in Fig. 6.7(a). The strains along each instrumented horizontal bar at the various load peaks are shown in Fig. 7.21. It was found that the strain gauge readings were affected greatly by the presence of nearby cracks. A sharp peak in the plot generally resulted from a crack having crossed the bar at the position of the strain gauge. The stress in the surrounding region of concrete is effectively transferred to the reinforcing bar at the crack. Thus, strain gauges crossed by cracks record strain concentrations and do not accurately indicate reinforcement strains within the body of the concrete. Therefore, linear interpolation of the strains between two gauges crossed by cracks is are questionable. In the plots, strain gauges crossed by cracks are marked with an asterisk.

In general, it can be seen in Fig. 7.21 that the strains were concentrated along the main diagonals. (positive (<---) direction: H1A, H1B, H1C, H2C, H2D, H3D, H3E, H4E, H4F, H5F, H5G, negative (--->) direction: H1F, H1G, H2E, H2F, H3D, H4C, H5A) It should be noted that strains in horizontal bars were, in general, larger than strains in corresponding vertical bars.

For the positive (<---) loading direction, a crack fan formed as the test progressed. Fig. 7.21 indicates an increase of strain in the crack fan region as the test progressed. Strains approached yield strain in the later stages. The only exception seems to be H4F, which is strained well beyond yield. This strain gauge appears to be located directly on a diagonal crack, which explains its unexpectedly high strain. As load was reversed, the strains either returned to zero or shifted to compression. This phenomenon is best shown by the plots for gauges H1C, H2D, H4E, H4F, H4G, H5F, and H5G. Away from the main diagonal, strains remained comparatively low.

For the negative (--->) loading direction, a similar phenomenon was observed. Inspection of the plots indicates strains near yield along the main diagonal but generally much smaller strains in regions away from the main diagonal. One exception seems to be gauge H2B, which lies off the main diagonal for negative loading yet records strains near yield

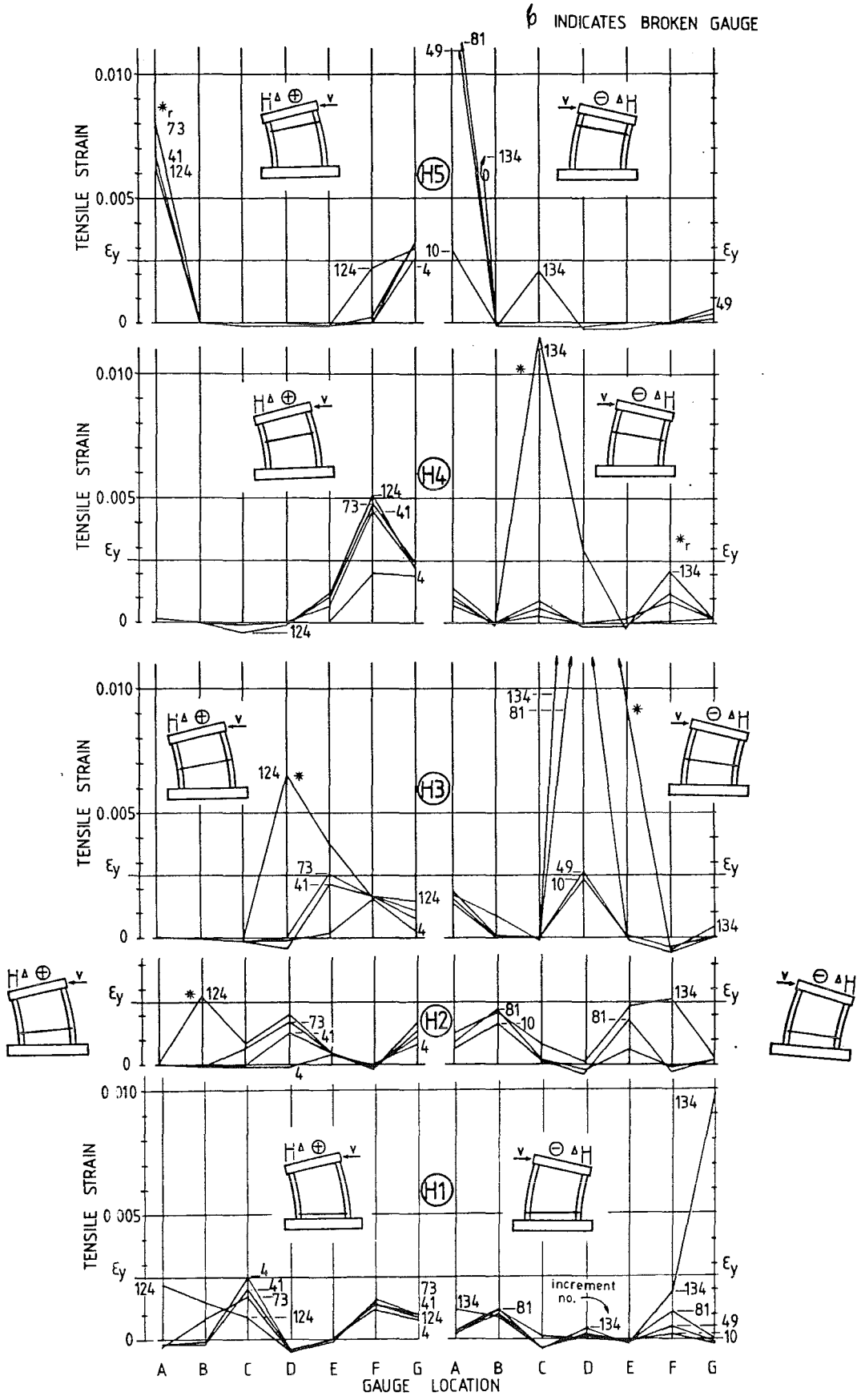

Fig. 7.21 - UNIT 1.0 - Strains in horizontal web bars

throughout the test. These unexpectedly high strains may be explained by noting that the gauge lies very near a crack that developed early in the test at increment 9. It is seen that some strain gauges (H4F ---> and H5A <---, for example) record strains greater than or equal to yield strain even though they lie well above the main wall diagonal. These gauges, however, lie along the main diagonal for loading in the opposite direction. Therefore, these high strains are most likely residual strains following excessive straining imposed by previous loading. In Fig. 7.21, these peaks are marked with an asterisk with subscript r.

The plots for bar H3 reveal that the bars in the centre of the wall (H3D) were very highly strained. These high strains are understandable since this portion of the wall was situated along the main diagonals for both loading directions. The bars were stressed in tension for both loading directions.

In general, where a crack appeared near a gauge on the first cycle to a given displacement level, the recorded strain reached a peak. During the second and third cycles to the same displacement, the strain in the vicinity of the crack tended to decrease while strains elsewhere in the bar increased. This phenomenon is most likely due to a redistribution of internal forces.

7.5.8 Strains in Vertical Boundary Element Bars

Selected longitudinal bars in the vertical boundary elements were instrumented as shown in Figs. 6.7(a). The plots of strain in these bars are shown in Fig. 7.22. In the compression boundary element, strains were small. They were slightly compressive up to a height of 500mm and slightly tensile above 500mm. In the tensile boundary element, strains were approximately uniform with height above the base level. This pattern of uniform strain is clearly indicative of arch action. (See Section 3.4.) Strains reached approximately yield strain throughout the wall height as the ideal flexural strength was attained (increments 73 and 81). Again, strain peaks occurred where a gauge was crossed by a crack. These peaks are marked with asterisks.

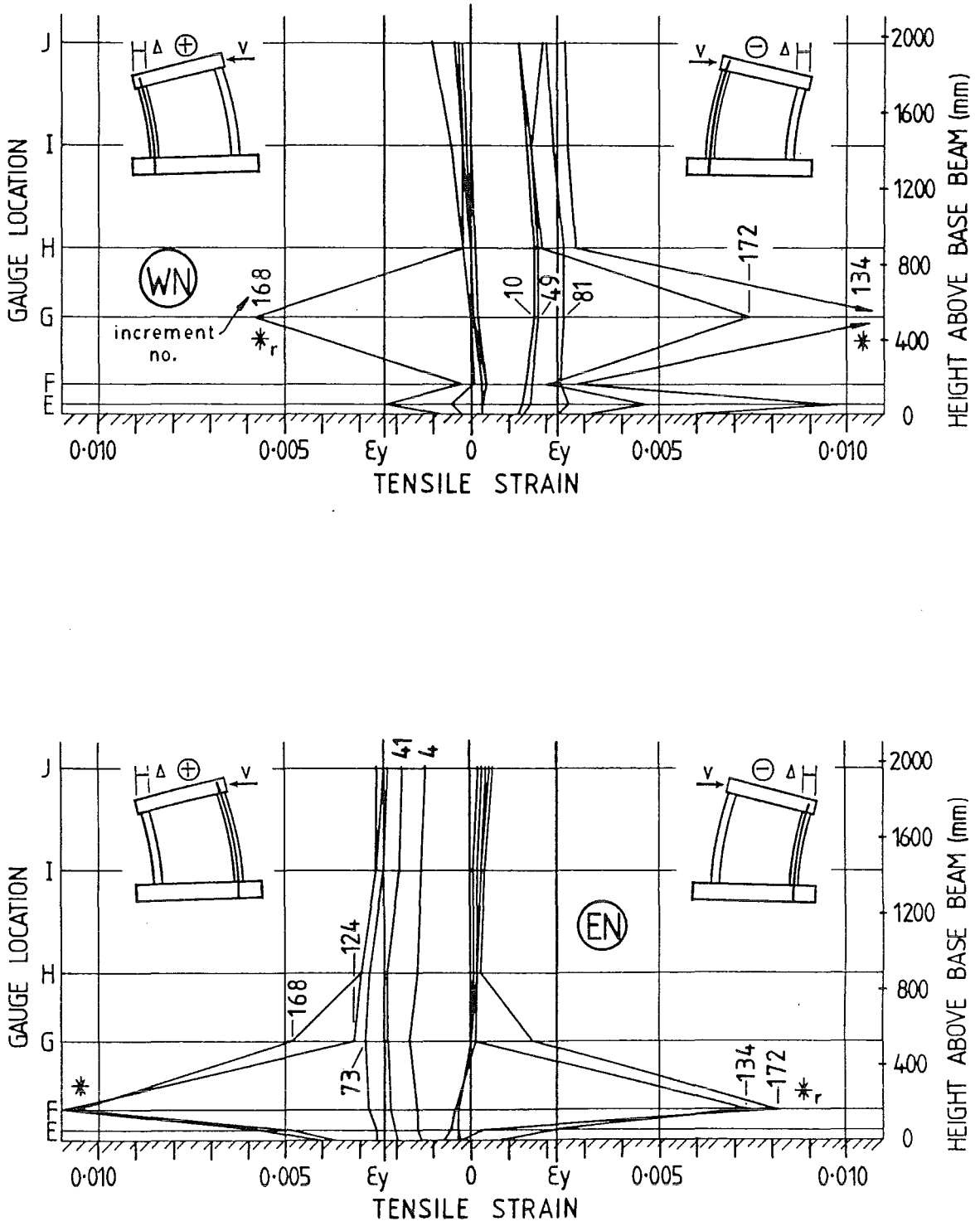

Fig. 7.22 - UNIT 1.0 - Strains in vertical boundary element bars WN & EN

7.5.9 Strains in Vertical Web Bars

Strains along the four instrumented vertical web bars (Fig. 6.8(a)) are shown in Fig. 7.23. Once again, strain readings were sensitive to the position of nearby cracks. As mentioned in Section 7.5.7, caution should be excercised in the linear interpolation of strains between two gauges crossed by cracks. Gauges crossed by cracks are marked with asterisks in the plots. A subscript r on an asterisk indicates residual strain following prior excessive straining at a crack. Also, in the later stages of the test after the attainment of maximum load, significant horizontal displacements occurred across the main diagonal cracks. These displacements resulted in the kinking of vertical web bars at the main diagonal cracks. At such a kink, the condition of uniaxial strain no longer exists. Therefore, the validity of corresponding measured strains is dubious.

For bar V1, the instrumented bar on the far left-hand side of the web, strains generally remained less than yield strain, except where a gauge was crossed by a crack. Strains reached only approximately one half yield strain in the lower region of the wall. Thus, the contribution of this bar to flexural strength was likely quite small.

For the instrumented bar V4 on the far right-hand side of the web, the strain pattern resembled that for boundary element bar EN. Strains were approximately uniform with height, reaching yield strain at the attainment of ideal flexural strength. Thus, the strain pattern for bar V4, along with the strain patterns for bars EN and WN, supports the deduction that arch action was operative. It is somewhat surprising that the strain pattern for bar V1 did not resemble more closely the strain pattern for bar WN. Perhaps the difference in behaviour between bars V1 and V4 can be accounted for when viewing the crack pattern in Fig. 7.7. For positive loading (for which bar V4 was in tension), the initial diagonal crack formed lower than the initial diagonal crack for negative loading. Also, for positive loading, many closely spaced, fanning diagonal cracks formed, while for negative loading, only one major, corner-to-corner crack formed. The diagonal compression strut for positive loading was likely much wider than the diagonal compression strut for negative loading and thus mobilized bar V4 as well as the vertical boundary element bars. The narrower diagonal

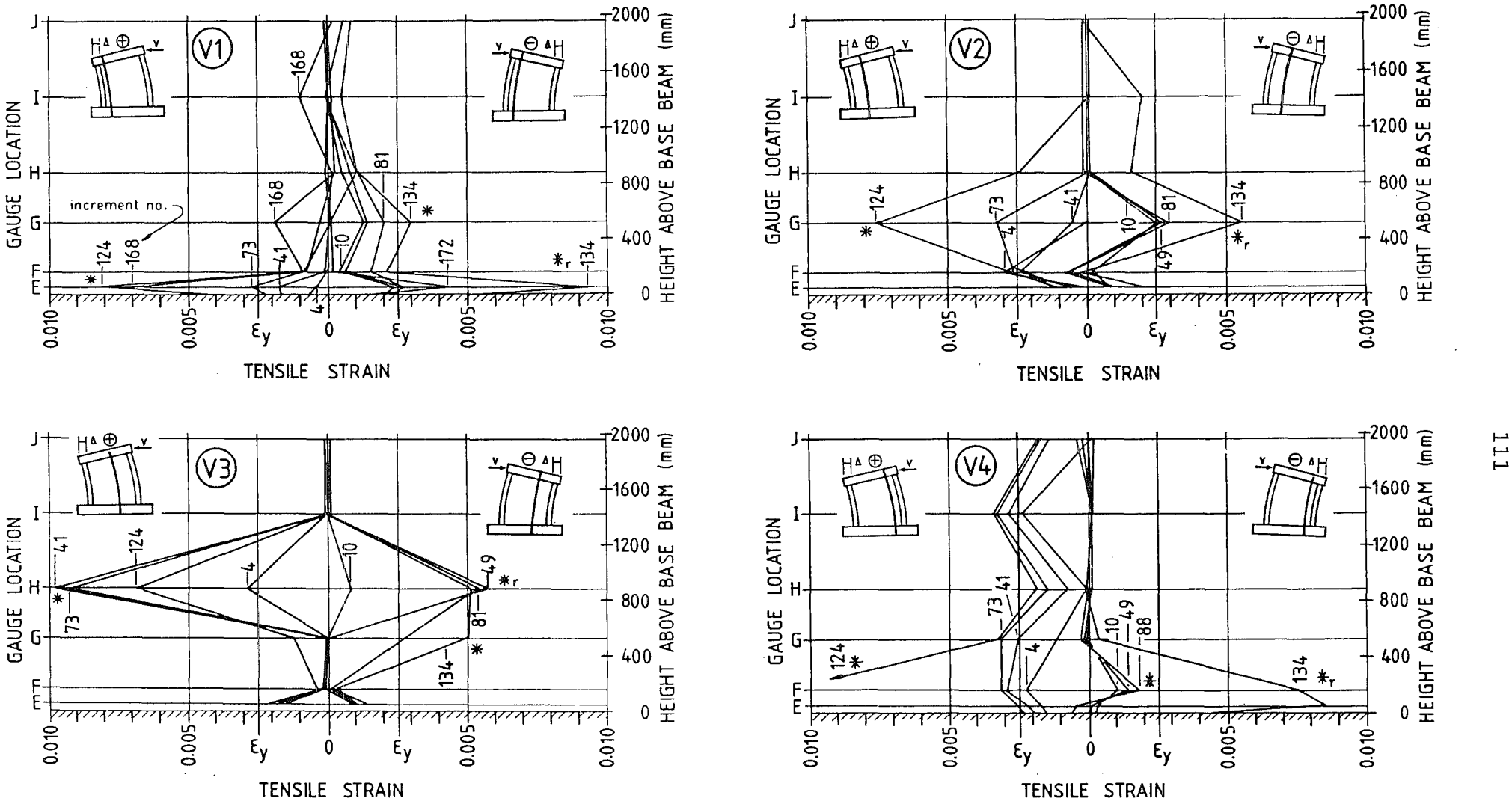

Fig. 7.23 - UNIT 1.0 - Strains in vertical web bars

compression strut for negative loading did not mobilize bar V1.

The plots of strains in bars V2 and V3, the centre-most vertical web bars, indicate that along the main wall diagonals, strains reached and exceeded yield strain, while off the main diagonals, strains remained considerably less than yield strain.

7.5.10 Location of the Vertical Compression Resultant

In Fig. 7.24 are plotted the strains in vertical bars across horizontal gauged cross sections. It is seen that in moving from horizontal section E (near the base beam) to horizontal section J (near the top beam), the neutral axis (the line of zero strain) shifts toward the tension face of the wall. For example, at section E, compressive strains were recorded only within approximately 200mm ($0.08\ell_w$) of the compression face. At section J, compressive strains were recorded to within 800mm ($0.32\ell_w$) of the tension face. The plots of Fig. 7.24 show that plane sections do not remain plane.

In an attempt to locate the actual position of the compression resultant at different elevations in the wall, the stresses at each gauged position were calculated from the strain history recorded by the gauge using a time-history computer program (30). The stress-strain model used for the reinforcement was a combination of a bilinear rule (used prior to unloading following the first yield excursion) and a Ramberg-Osgood rule with a Ramberg-Osgood factor of r=8 (used after the first yield excursion). See Fig. 7.25. For a discussion of the Ramberg-Osgood model and the choice of r=8, see Ref. 25, sections 3.4 and 3.5. Using this stress-strain model for reversed cyclic loading, a stress history was generated from the strain history recorded by each strain gauge. At this point, each horizontal gauged section was considered separately (Fig. 7.26). As an approximation, the areas of ungauged bars were considered to be lumped at the locations of the gauged bars. These equivalent bar areas were multiplied by the stresses calculated at the respective gauged positions to obtain bar forces. Finally, consideration of equilibrium of forces led to the magnitude and location of the compression resultant on each horizontal

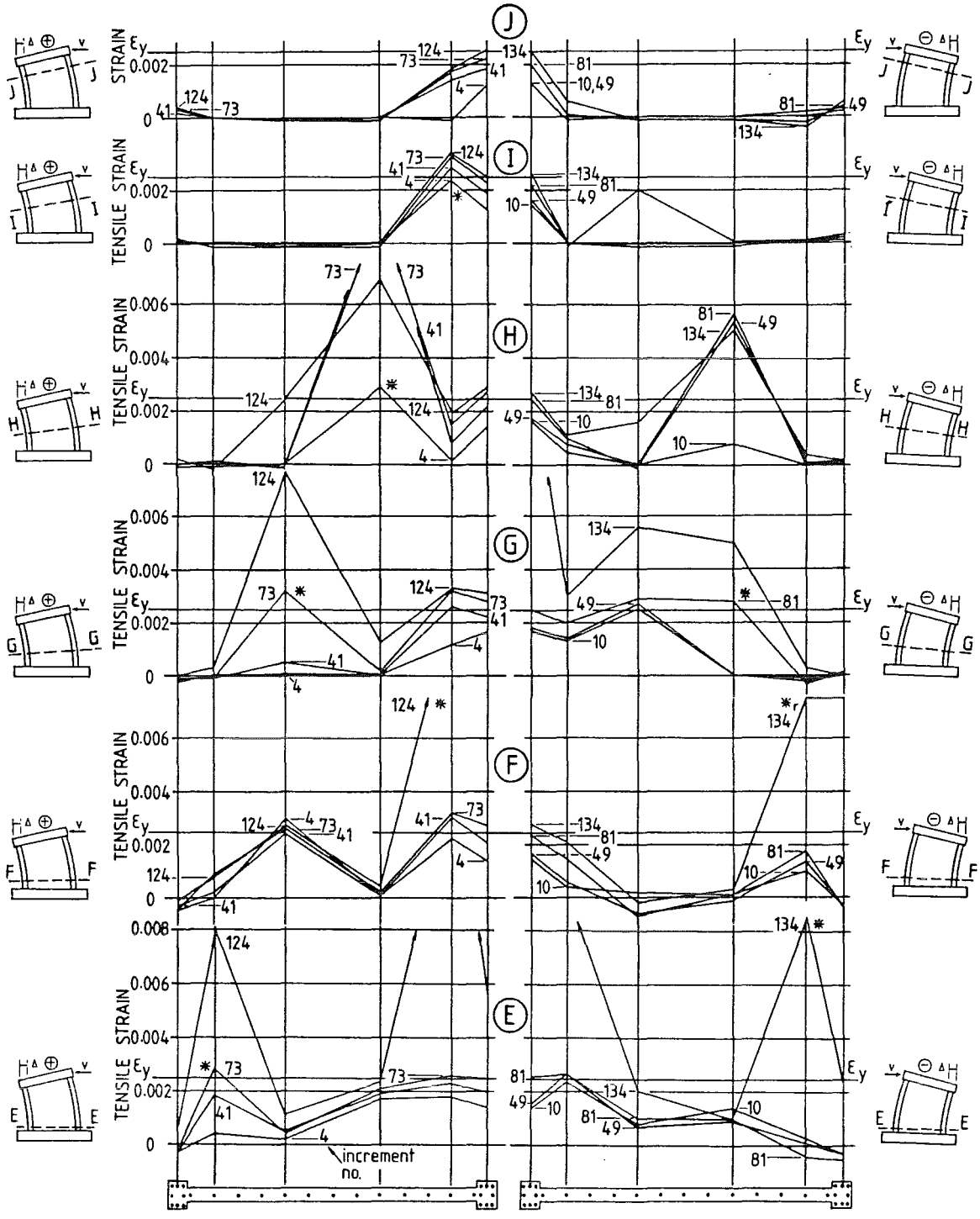

Fig. 7.24 - UNIT 1.0 - Vertical strains on horizontal gauged cross sections

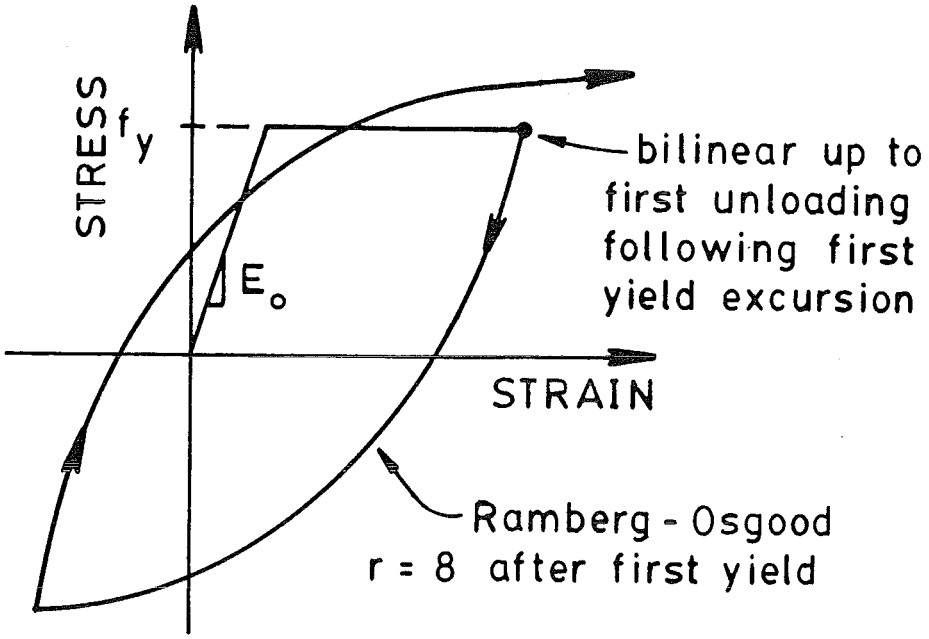

Fig. 7.25 - Hysteretic stress-strain model for reinforcing steel

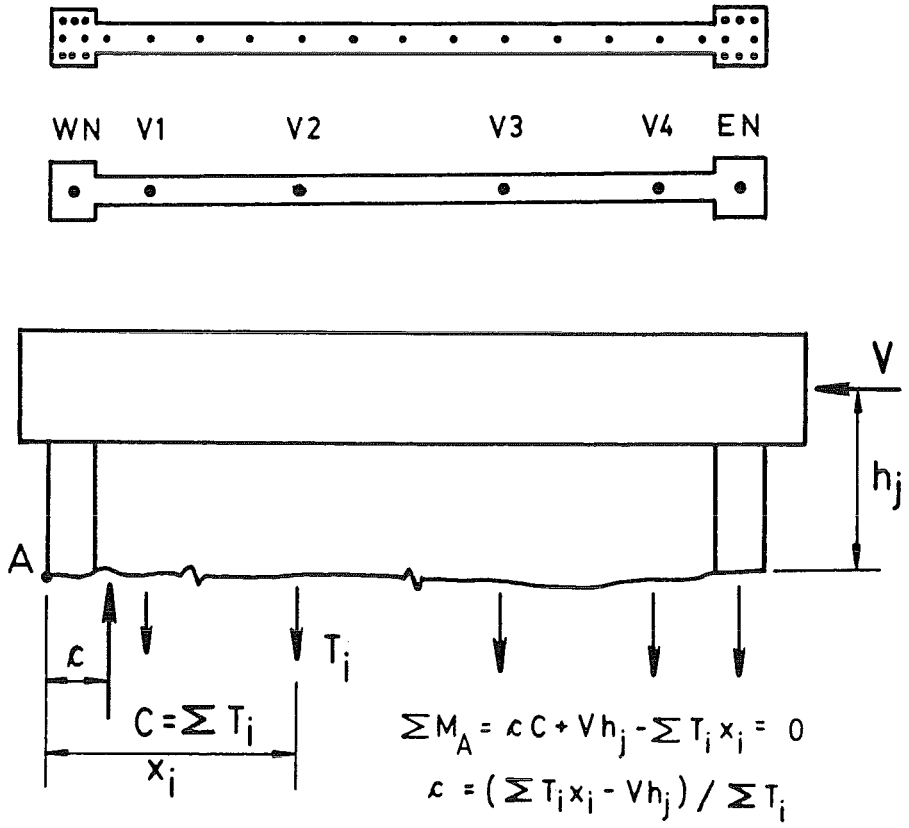

Fig. 7.26 - Calculation of location of vertical compression resultant, C

cross section (Fig. 7.26).

Fig. 7.27 shows the calculated location of the vertical compression resultant on each gauged horizontal cross section for the four displacement levels applied to Unit 1.0. It is clear that the compression resultant shifts toward the tension face of the wall as elevation of the wall sections increases. The calculated locations define the main diagonal compression strut. The shaded regions in Fig. 7.27 mark the regions within which the compression resultant would have had to lie given pure beam action.

The outer boundaries of the shaded areas in Fig. 7.27 were obtained by calculating the location of the vertical compression resultant when the applied moment was assumed equal to the ideal flexural strength of the wall, $M = (M_i)_{flex}$. The inner boundaries of the shaded areas were obtained by considering the section, above which the applied moment was less than that which would cause cracking, $0 < M < M_{cr}$. In this region, the wall section would remain uncracked. Since the axial load on the wall was zero, the neutral axis would lie at the midpoint of the web, with a triangular distribution of strain over each half of the section. Accordingly, the compression resultant would lie a distance $d = 1/3 \times (1/2 \times \ell_w)$ from the compression face. See Fig. 7.28.

It is clear from Fig. 7.27 that arch action dominated the behaviour of Unit 1.0. For a description of beam action and arch action, see Section 3.1.

7.5.11 Strains in Vertical Bars Below the Base Level

Several vertical bars were instrumented within the base beam for the purpose of observing the penetration of strain along the vertical bars into the base beam. The strains in these bars within the base beam were integrated to obtain the rigid body rotation of the wall described by Δfe in Section 7.5.6. The main difference between the layout of the 6mm diameter web bars and the layout of the 12mm diameter boundary element bars was that the 6mm diameter bars were arranged in a single curtain without any hoops or cross ties, whereas the 12mm diameter bars where enclosed within the base beam, as well as above the base beam, by rectangular hoops spaced at 70mm.

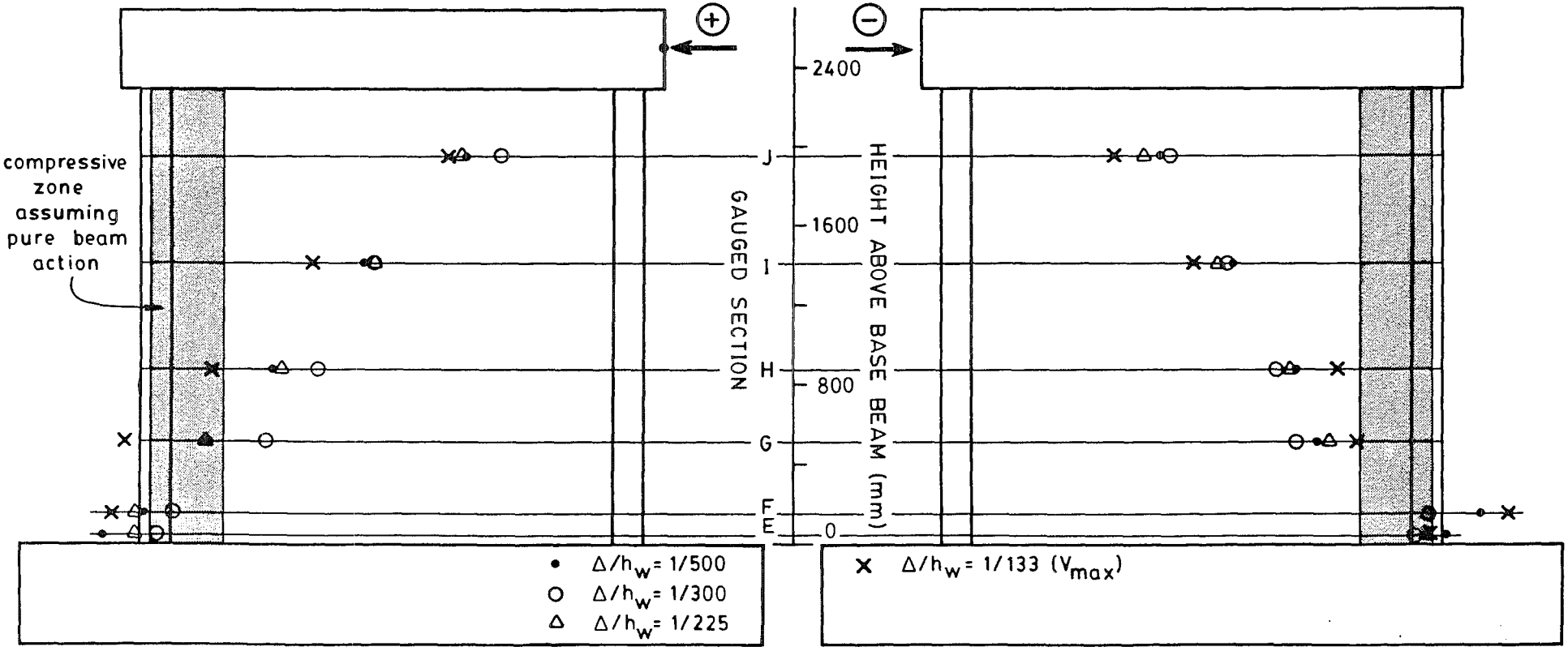

Fig. 7.27 - UNIT 1.0 - Location of vertical compression resultant

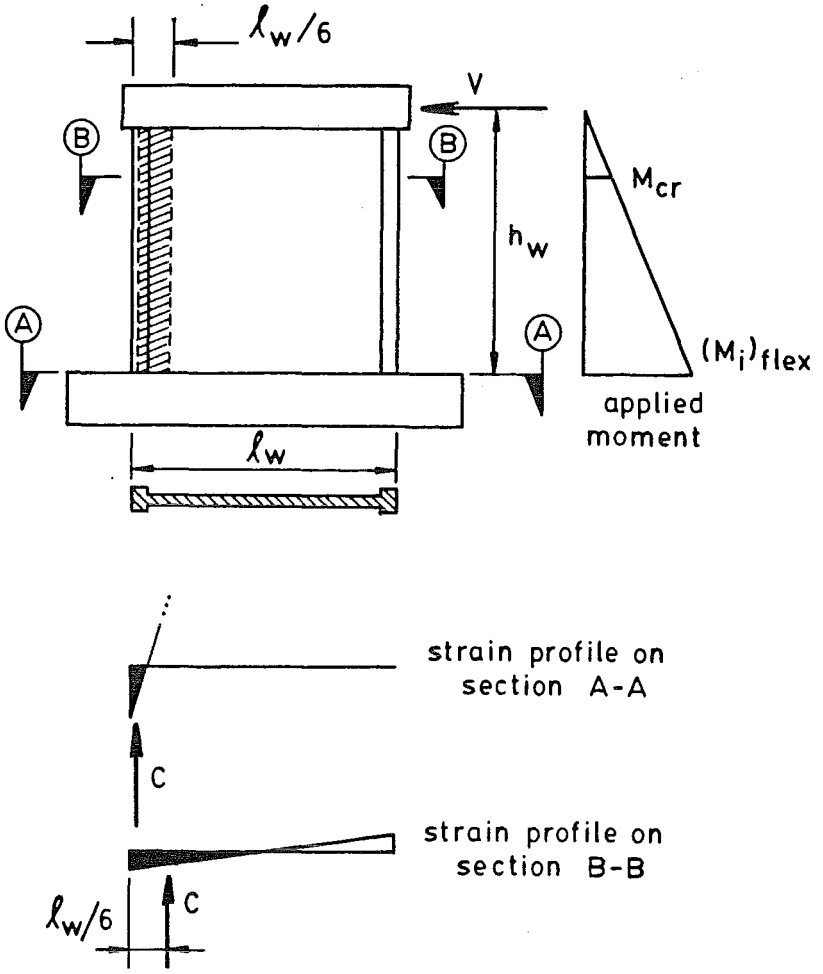

Fig. 7.28 - Location of vertical compression resultant for pure beam action

The plots of strain versus depth in the base beam are shown in Fig. 7.29. Strain penetrated more deeply along the 12mm bars than along the 6mm bars. In both cases, however, the approximately linear strain profile indicates that uniform bond stress existed along the bars. It is possible to compare these bond stresses with the allowable bond stress. However, an equivalent comparison may be achieved by comparing the actual depth of strain penetration with the required development length.

The development length of a bar is defined as the embedded length of a bar needed to develop yield force in the bar by means of concrete-to-steel bond stresses. The development length concept assumes that an average attainable bond stress exists over the embedded length. The development length requirement supplants previous ACI 318 requirements for considering nominal peak bond stress. The full developmemt length is required on either side of a section

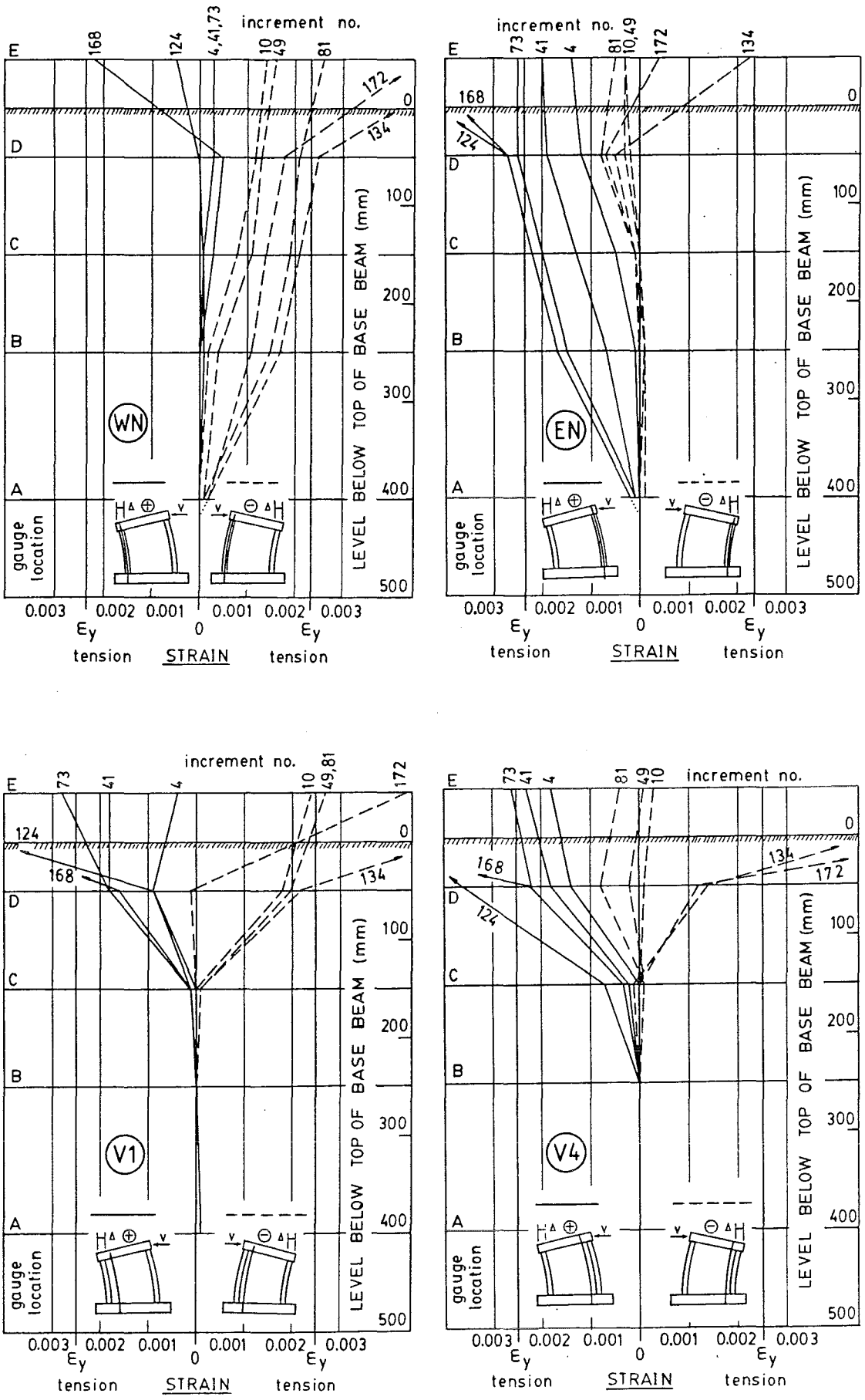

Fig. 7.29 - UNIT 1.0 - Strains in vertical bars in base beam

where the bar is stressed to yield. On one side of this critical section, the development length is needed to transfer force from the surrounding concrete to the bar. In the case of the test units, this length may be represented by the length of bar above the wall base section. On the other side of the critcal section, the development length is required to transfer force from the bar into the surrounding concrete. This length may be represented by the length of bar within the base beam. However, the intention of the code is that development length is to be measured from the point at which yield stress first occurs. In the early stages of testing, when yield stress was attained only at the wall base section, development length was required within the base beam starting from the top of the base beam. In the later stages of testing, however, yield strain penetrated into the base beam. Development length was then required extending downward from the level of yield penetration.

In Table 7.3, a comparison is made between the actual strain penetration into the base beam beyond the depth of yield penetration (column D in Table 7.3) and the development length as required by Eq. 5-6 of NZS 3101 (column A in Table 7.3). Only 12mm diameter bars were used in the boundary elements of Unit 1.0. The 16mm and 10mm diameter bars were used in Units 1.5 and 2.0, respectively. In the calculation of development length, account was taken of the fact that the actual yield strength of the bars was greater than 275MPa (parameter m_1). Although the effect of transverse hoops enclosing the vertical boundary element bars was considered (parameter m_2), it did not affect the required development length. For Unit 1.0, it is seen that the code-required development length is a good estimate of the actual length of embedment that was utilized to develop yield force in both 6mm and 12mm diameter bars.

Table 7.4 summarizes an attempt to find a correlation between bar properties (such as bar diameter, bar area, and bar yield force) and strain penetration into the base beam. In column A of the table, a description of the experimental observation or bar property is presented. Reading across the table, this parameter is given the label z_i, where i indicates the diameter of the bar under consideration. In columns B-G of the table, the bar properties and experimental

TABLE 7.3 - COMPARISON OF ACTUAL STRAIN PENETRATION INTO THE BASE BEAM AND REQUIRED DEVELOPMENT LENGTH

	Bar diameter	Bar designation	f_y (MPa)	f'_c of base beam (MPa)	Basic development length, ℓ_{db} (NZS 3101) (Eq.5-6) (mm)	(1) $m_1 = f_{y/275}$	(1) $m_2 = \frac{c}{c+k_{tr}}$	A Required development length, $\ell_d = m_1 m_2 \ell_{db}$ (mm)	B(2) Overall strain penetration (mm)	C(2) Yield strain penetration (mm)	D=B-C(2) Length of strain penetration beyond yield strain penetration (mm)	E=A/D
UNIT 1.0	6	V1	472	33.0	104	1.72	1.0	178	~ 200	45	155	1.15
		V4			104	1.72	1.0	178	250	85	165	1.08
	12	WN	451		208	1.64	1.0	341	420	90	330	1.03
		EN			208	1.64	1.0	341	420	120	300	1.14
UNIT 1.5	6	V1	472	27.7	113	1.72	1.0	195	400	75	325	0.60
		V4			113	1.72	1.0	195	400	60	340	0.57
	16	WN	465		387	1.69	0.87	570	470	150	320	1.78
		EN			387	1.69	0.87	570	450	165	285	2.00
UNIT 2.0	6	V1	472	23.9	122	1.72	1.0	210	400	80	320	0.66
		V4			122	1.72	1.0	210	400	60	340	0.62
	10	WN	443		203	1.61	1.0	328	465	210	255	1.29
		EN			203	1.61	1.0	328	480	250	230	1.43

(1) See Clause 5.3.7.3, NZS 3101.

(2) Strain penetration measured at maximum load

TABLE 7.4 - CORRELATION BETWEEN BAR PROPERTIES AND STRAIN PENETRATION IN BASE BEAM

	A	UNIT 1.0		UNIT 1.5		UNIT 2.0		Dimensionless Ratios		
		B	C	D	E	F	G	H	I	J
	Description of Parameter i = bar dia. (mm)	z_6	z_{12}	z_6	z_{16}	z_6	z_{10}	$z_{6/z_{12}}$ Unit 1.0 only	$z_{6/z_{16}}$ Unit 1.5 only	$z_{6/z_{10}}$ Unit 2.0 only
Experimental observations at maximum load	yield penetration (mm) +load	85	120	60	165	60	250	0.708	0.364	0.240
	yield penetration (mm) ave.							0.604	0.432	0.311
	yield penetration (mm) -load	45	90	75	150	80	210	0.500	0.500	0.381
	total strain penetration (mm) +load	250	420	400	450	400	480	0.595	0.889	0.833
	total strain penetration (mm) ave							0.536	0.870	0.847
	total strain penetration (mm) -load	~200	420	400	470	400	465	0.476	0.851	0.860
	strain penetration beyond yield (mm) +load	165	300	340	285	340	230	0.550	1.193	1.478
	strain penetration beyond yield (mm) ave.							0.510	1.105	1.367
	strain penetration beyond yield (mm) -load	155	330	325	320	320	255	0.470	1.016	1.255
Bar property	d_b (mm)	6	12	6	16	6	10	0.500	0.375	0.600
	$\sqrt{d_b}$	$\sqrt{6}$	$\sqrt{12}$	$\sqrt{6}$	$\sqrt{16}$	$\sqrt{6}$	$\sqrt{10}$	0.707	0.612	0.775
	A_b (mm^2) [d_b^2]	28.27	113.1	28.27	201.1	28.27	78.5	0.250	0.141	0.360
	f_y (MPa)	472	451	472	465	472	443	1.047	1.015	1.065
	$A_b f_y$ (kN)	13.34	51.01	13.34	93.51	13.34	34.78	0.262	0.143	0.384

observations of strain penetration are presented for both web bars and boundary element bars for all three test units. Only the 6mm and 12mm diameter bars of columns B, C, and H in the table are of interest for Unit 1.0. The other columns correspond to Units 1.5 and 2.0. In columns H-J of the table are presented dimensionless ratios of web bar parameter to boundary element bar parameter (for example, yield penetration along the 6mm diameter web bar divided by the yield penetration along the 12mm diameter boundary element bar or the area of the 6mm bar divided by the area of the 12mm bar). No definite correlation was discovered in Table 7.4. For design purposes, an estimation of Δfe, the top deflection due to straining of bars below the wall's base level, is made in Section 10.11.

7.5.12 Axial Extension of the Wall

Three dial gauges were placed along the top beam in order to record vertical extension of the wall along the vertical centre line. (See Fig. 6.8(a).) As reversed cyclic loading was applied, the wall experienced a permanent overall axial extension. At maximum load (increment 124), the wall had extended approximately 7.25mm. The maximum extension of 9.25mm occurred at increment 142. At the end of the test, the permanent axial extension at zero load was 6.09mm.

7.5.13 Base Beam Behaviour

Apart from minor flexural cracking in the region of the boundary elements and along the top of the beam, little action was seen to occur in the base beam. Sliding of the base beam along the laboratory floor was minimal (approximately 1 percent of the measured top displacement). Some uplift of the beam off the laboratory floor was observed under the tension boundary element, but this movement, again, was minimal (0.91mm at maximum load).

7.5.14 Top Beam Behaviour

Very little deformation was observed in the top beam. A few short flexural cracks were observed in the top of the top beam, indicating hogging deformations (Fig. 7.7). Hogging was confirmed by the three top dial gauges. Maximum

hogging deflection at the centre was 0.40mm ($0.0002x\ell_w$) at maximum load (increment 124). The two rows of external DEMEC strain gauges were meant to record compression in the top beam along its length. However, the compression strains recorded were so small, relative to the precision of the gauge itself, that the error accumulated in the calculation of average compressive strain was 50-80 percent. Thus the DEMEC readings were considered to be of little value. They were, therefore, omitted for Units 1.5 and 2.0.

7.5.15 Sliding Along Horizontal Construction Joints

The history of sliding along the base construction joint was presented in Section 7.5.6 (Δs). Sliding displacement was of the order of 0.25mm at maximum positive load and 1.00mm at maximum negative load. The maximum recorded sliding displacement was 1.35mm at increment 163 (6.8 percent of the total top deflection). No sliding displacements along the mid-height construction joint and the top construction joint were evident.

7.5.16 Displacements at Diagonal Cracks

Approximate displacements along and across a few of the major diagonal cracks were monitored using a hand-held microscope during the initial stages of testing and using simply the unaided eye and a steel rule during the later stages of testing. The locations of the observation points are shown in Fig. 7.7. The positions numbered 1, 3, and 4 mark cracks formed under positive (<---) loading. The position numbered 2 marks the main diagonal crack formed under negative (--->) loading. Displacements perpendicular and parallel to the cracks are summarized in Table 7.5.

TABLE 7.5 - MOVEMENT AT MAIN DIAGONAL CRACKS - UNIT 1.0

Crack No.	at maximum load		maximum crack displacement	
	Perpendicular displacement (mm)	Parallel displacement (mm)	Perpendicular displacement (mm)	Parallel displacement (mm)
1	1.3	-	1.3	-
2	5.5	3.5	7	6
3	1.4	-	4	2
4	4.0	-	10	6

SECTION 8

UNIT 1.5
LOADING HISTORY, GENERAL BEHAVIOUR, AND TEST RESULTS

8.1 LOADING HISTORY

The overall dimensions and reinforcement details for Unit 1.5 are shown in Fig. 5.2. The loading history for Unit 1.5 is shown in Fig. 8.1. As mentioned in Section 6.5.3, four initial cycles were added (two at $0.25V_i$ and two at $0.50V_i$) in an attempt to better observe the elastic response of the fully cracked unit. Three cycles were then imposed to $0.75V_i$, the first of which was used to calculate the yield displacement, Δ_y, as defined in Section 6.5.3. The first seven cycles were controlled by load, while the remainder of the test was controlled by displacement, in terms of lateral drift, Δ/h_w. In general, three full cycles were imposed at each successive displacement level. When three cycles to Δ/h_w=1/100 had been completed, the most useful part of the test was deemed to have been completed. However, since the unit still retained a good deal of resistance, two additional cycles to Δ/h_w=1/100 were imposed in order to investigate the stability of behaviour under excessive cyclic loading at one displacement level. Finally, the unit was loaded to failure in the positive (<--) loading direction. A total of 21.5 cycles were imposed on the unit.

8.2 DESCRIPTION OF OBSERVED BEHAVIOUR

Increment Number	Description
2-9	Two initial cycles to $\pm 0.25V_i$. No cracks were visible.
12	Positive loading to $0.50V_i$. First flexural cracks appeared. Horizontal cracks spaced at 90mm (equal to the hoop spacing) appeared in the right-hand boundary element (RHBE) up to $h_w/2$.

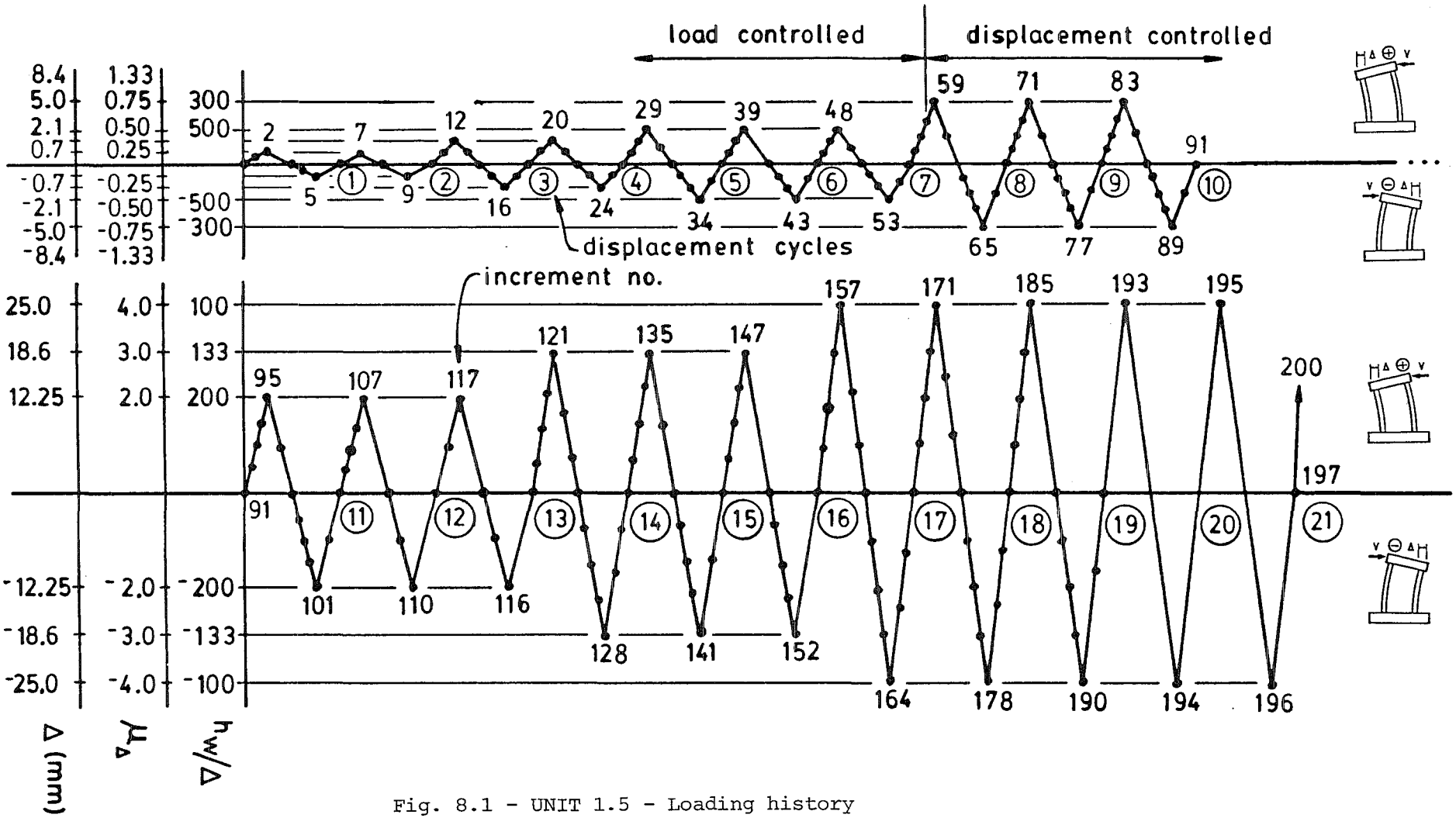

Fig. 8.1 - UNIT 1.5 - Loading history

Where they entered the web, two of these cracks sloped downward to the base level at an angle of approximately 48 degrees from the horizontal.

16 Negative loading to $0.50V_i$. Horizontal flexural cracking occurred in the lower half of the left-hand boundary element (LHBE). These cracks were spaced also at approximately 90mm. The three lowest cracks entered the web and sloped downward to the base level at an angle of approximately 45 degrees from the horizontal. The cracks flattened to approximately 35 degrees as they approached the base beam. A crack appeared along the construction joint at mid-height, but no slip was observed.

20-24 Second cycle to $0.50V_i$. No change in behaviour was observed.

29 At a load of appproximately V = 140kN = $0.7(V_i)_{shear}$ = $0.42(V_i)_{flex}$ = $0.40(V_{max})_{pos}$, a diagonal crack (crack 1 in Fig. 8.6) formed suddenly with a thudding sound at an angle of approximately 45 degrees. It extended from about $0.75h_w$ in the RHBE down to the bottom left-hand corner of the wall unit. Width of crack 1 = 1.02mm. Crack 1 flattened as it approached the compression face. Horizontal flexural cracking extended up to full height in the RHBE. Some shorter diagonal cracks fanned off from crack 1 at the top end and joined with horizontal cracks in the RHBE. Top deflection = 4.90mm. (Fig. 8.2)

34 Horizontal flexural cracks extended up to full height in the LHBE. Most of these cracks then extended diagonally downward into the web. In the web, the diagonal cracks began at an angle of approximately 50-55 degrees from horizontal and flattened to an angle of approximately 30-35 degrees as they approached the base level. At a

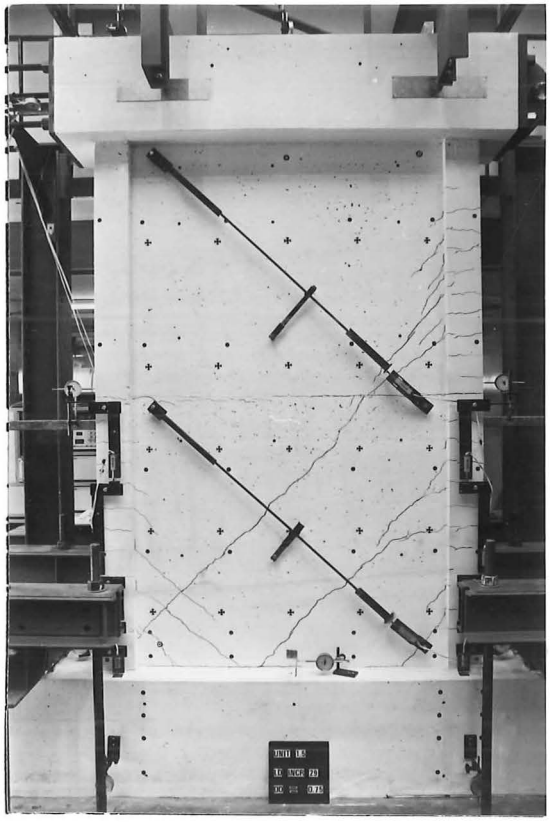

Fig. 8.2 - UNIT 1.5 - Crack pattern at increment 29

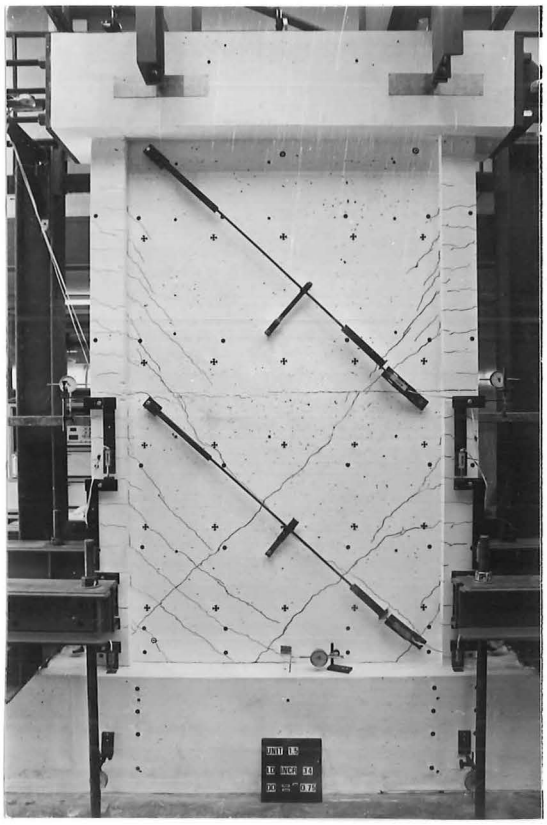

Fig. 8.3 - UNIT 1.5 - Crack pattern at increment 34

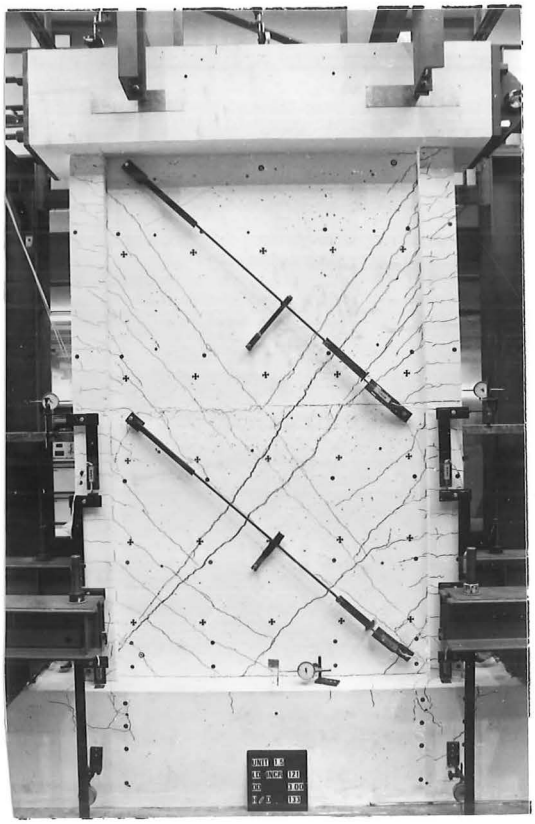

Fig. 8.4 - UNIT 1.5 - Crack pattern at increment 121

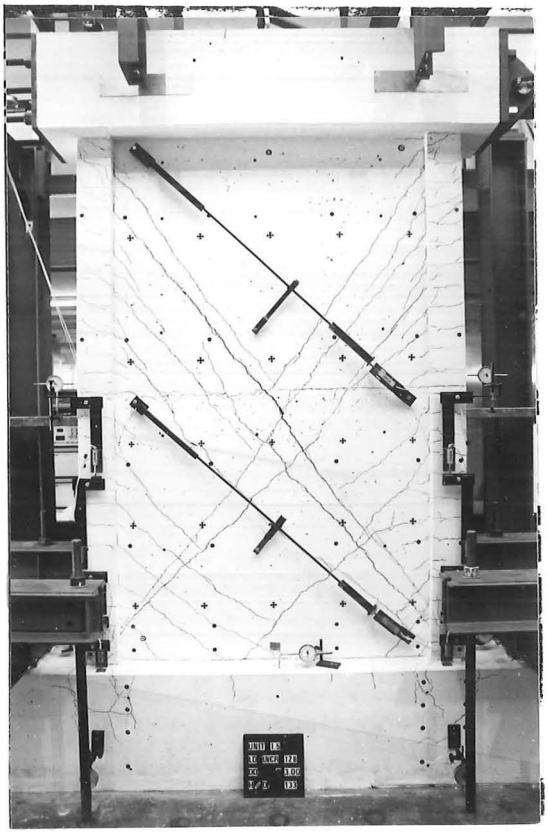

Fig. 8.5 - UNIT 1.5 - Crack pattern at increment 128

load of V = -140kN = $0.7(V_i)_{shear}$ = $0.42(V_i)_{flex}$ = $0.42(V_{max})_{neg}$, a major diagonal crack (crack 2 in Fig. 8.6) formed suddenly with a thudding noise. It extended from approximately $0.60h_w$ in the LHBE to the bottom right-hand corner of the wall unit. The angle of inclination was approximately 57 degrees at the top end and 35 degrees at the bottom end. It flattened as it approached the base level, as did the other diagonal cracks. Width of crack 2 = 0.64mm. Top deflection = 4.53mm. Δ_y = (4/3)x(4.90+4.53)/2 = 6.28mm. (Fig. 8.3)

39-53 No significant changes in behaviour were observed apart from widening and lengthening of existing cracks.

59 From this point onward, the test was controlled by displacement. An additional major diagonal crack (crack 3 in Fig. 8.6) formed above crack 1 at an angle of approximately 52 degrees from horizontal. Other cracks formed above crack 1 at progressively steeper angles, forming a fan. These new cracks did not flatten as they progressed downward. Width of crack 1 = 1.40mm.

64 Two major diagonal cracks formed suddenly with a thudding sound above crack 2 (crack 4, Fig. 8.6). Both formed at a constant angle of approximately 49 degrees from horizontal. No flattening was observed in the lower regions of these cracks. Also, no visible action was observed below crack 2.

65 No additional cracking occurred. Width of crack 2 = 0.89mm.

71-89 No significant action was observed apart from the widening and lengthening of existing cracks.

95,107,113 Some lengthening of diagonal cracks was observed above and below crack 1. The widths of both crack 1 and crack 3 were 1.65mm. Although the construction joint at mid-height was cracked, no slip was recorded.

101,110,116 No noticeable changes in the crack pattern occurred. Action along crack 4, in the upper portion of the wall, began to dominate behaviour. The width of crack 2 was 1.14mm, while the width of crack 4 was 1.52mm.

121 $V = (V_{max})_{pos} = (V_{max})_{test} = 342kN$. No significant changes in behaviour were observed below crack 1. Signs of crushing (vertical cracking) were evident at the compression face (outside of the LHBE). Diagonal cracks opened significantly, with the dominant action taking place in the upper portion of the wall. The width of crack 1 was 1.78mm. The width of crack 3 was 2.54mm. (Fig. 8.4)

128 $V = (V_{max})_{neg} = 335kN$. A lengthening of diagonal cracks occurred in the upper portion of the wall. Vertical cracking and the beginning of crushing was observed at the compression face (outside face of the RHBE). The ideal flexural strength was attained. However, action seemed to be concentrated along the diagonal cracks, particularly in the upper portion of the wall, and not at the base of the boundary elements, which would be expected in purely flexural behaviour. Displacement parallel to some of the diagonal cracks became noticeable. Here, slip along a crack is defined as displacement parallel to that crack at the point of observation.Fig. 8.5

crack	width(mm)	slip(mm)
2	1.40	-
4	3.05	1.40

135,147 Action seemed to be concentrated in the widening

and slippage along the main diagonal cracks.

crack	width(mm)	slip(mm)
1	3.18	1.52
3	2.92	1.52

141,152 The main action occurred along crack 4.

crack	width(mm)	slip(mm)
2	1.78	-
4	3.30	1.90

Some unexpected additional diagonal cracks formed well above crack 4 near the RHBE, yet still below the main diagonal crack for loading in the opposite direction.

157 Another major diagonal crack (crack 5 in Fig. 8.6) formed suddenly and with a thudding sound. It formed above all existing diagonal cracks and extended at a constant angle of approximately 52 degrees from horizontal from the top right-hand corner of the wall down to the LHBE, where it intersected it at a height of approximately 500mm above the base beam.

crack	width(mm)	slip(mm)
1	4.5	4.0
3	3.68	2.5

164 As the pre-selected displacement was approached, the load dropped noticeably. An additional major diagonal crack (crack 6 in Fig. 8.6) formed suddenly above the previously formed cracks. It lay at an angle of approximately 50 degrees from horizontal at the top left-hand side but steepened to approximately 62 degrees once it reached mid-height of the wall. It then proceeded downward to intersect the RHBE at the base level. Spalling was observed on the inside face of the LHBE (tension). Crushing occurred on the outside face of the RHBE (compression). Kinking of the RHBE at the base level was also observed. Spalling was observed at mid-height of the wall at the point of intersection of the main

diagonals. Additional flexural cracking in the LHBE and additional diagonal cracking in the web occurred mainly in the top half of the unit.

crack	width(mm)	slip(mm)
2	2.0	-
4	4.0	3.5

171 Increased cracking was observed in the upper region of the wall unit.

178

crack	width(mm)	slip(mm)	
2	3.5	1.0	
4	3.0	3.5	

185 Another major diagonal crack (crack 7 in Fig. 8.6) formed above the previously formed cracks. This crack began at the top of the wall approximately 425mm from the outside of the RHBE. It lay at an angle of approximately 52 degrees from the horizontal. The crack steepened markedly to approximately 62 degrees at a point half way across the web. Additional shorter diagonal cracks formed in the upper half of the wall near the LHBE. These cracks formed below the top diagonal crack for the opposite loading direction.

crack	width(mm)	slip(mm)
1	6.5	6.0
3	3.5	3.0

190-196 A high degree of stability was observed in hysteretic loop shape and lateral load resistance during these fourth and fifth cycles to $\Delta/h_w = 1/100$. Additional cracking generally occurred at or above the level of the main diagonals. Additional crushing and spalling occurred in both boundary elements at the base level and in the centre of the wall. Kinking of boundary element bars in an outward direction at the base level was also observed. Very little sliding of the wall upon the base beam was

observed.

200 Before the pre-selected displacement was reached, the lateral load dropped suddenly as four of the lowest horizontal web bars fractured along crack 1. Extreme outward kinking occurred in all vertical bars crossing the main diagonal cracks. A minor degree of kinking was observed in the horizontal bars crossing the main diagonal cracks (Fig. 8.7). Severe spalling occurred along the main diagonal in the lower half of the wall. Despite the seemingly poor construction joint at mid-height (see Section 6.2.5), at no point during the test were any appreciable displacements measured along the mid-height construction joint.

8.3 FAILURE MECHANISM

The overall behaviour of Unit 1.5 was similar to that of Unit 1.0, as described in Section 7.4. Strut and tie behaviour was in effect from the early stages of the test. The first diagonal cracks formed during the first cycle to $\pm$ 0.75V_i (Figs. 8.2 and 8.3). The main difference between Units 1.0 and 1.5 was that the diagonal cracks formed at steeper angles in Unit 1.5. Again, for each loading direction, the initial diagonal crack divided the wall into two regions. As the test progressed, deformations tended to occur in the upper region. Flexural cracking developed throughout the entire height of the vertical boundary elements, and diagonal cracks formed in the web at progressively steeper angles above the initial diagonal crack. The unit attained its theoretical flexural strength as the vertical boundary element bars and nearby vertical web bars yielded in tension throughout the entire height of the wall. Horizontal and vertical web bars yielded along the main diagonal, with the horizontal strains being generally larger than the vertical strains. Strains remained small in web bars lying off the main diagonals. Only minimal displacements were recorded between the lower region of the wall and the base beam. After the attainment of maximum

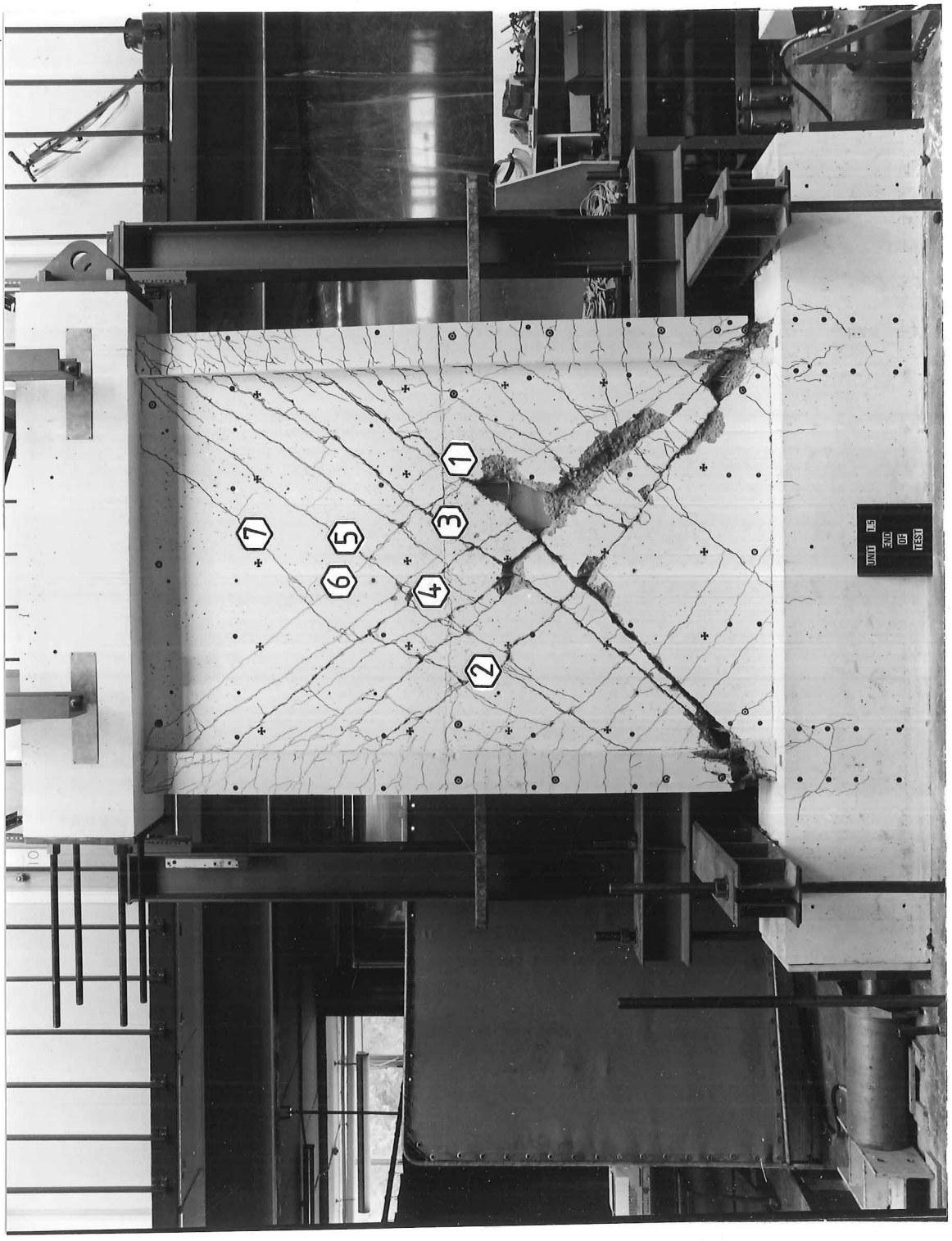

Fig. 8.6(a) - UNIT 1.5 - Crack pattern at the end of the test

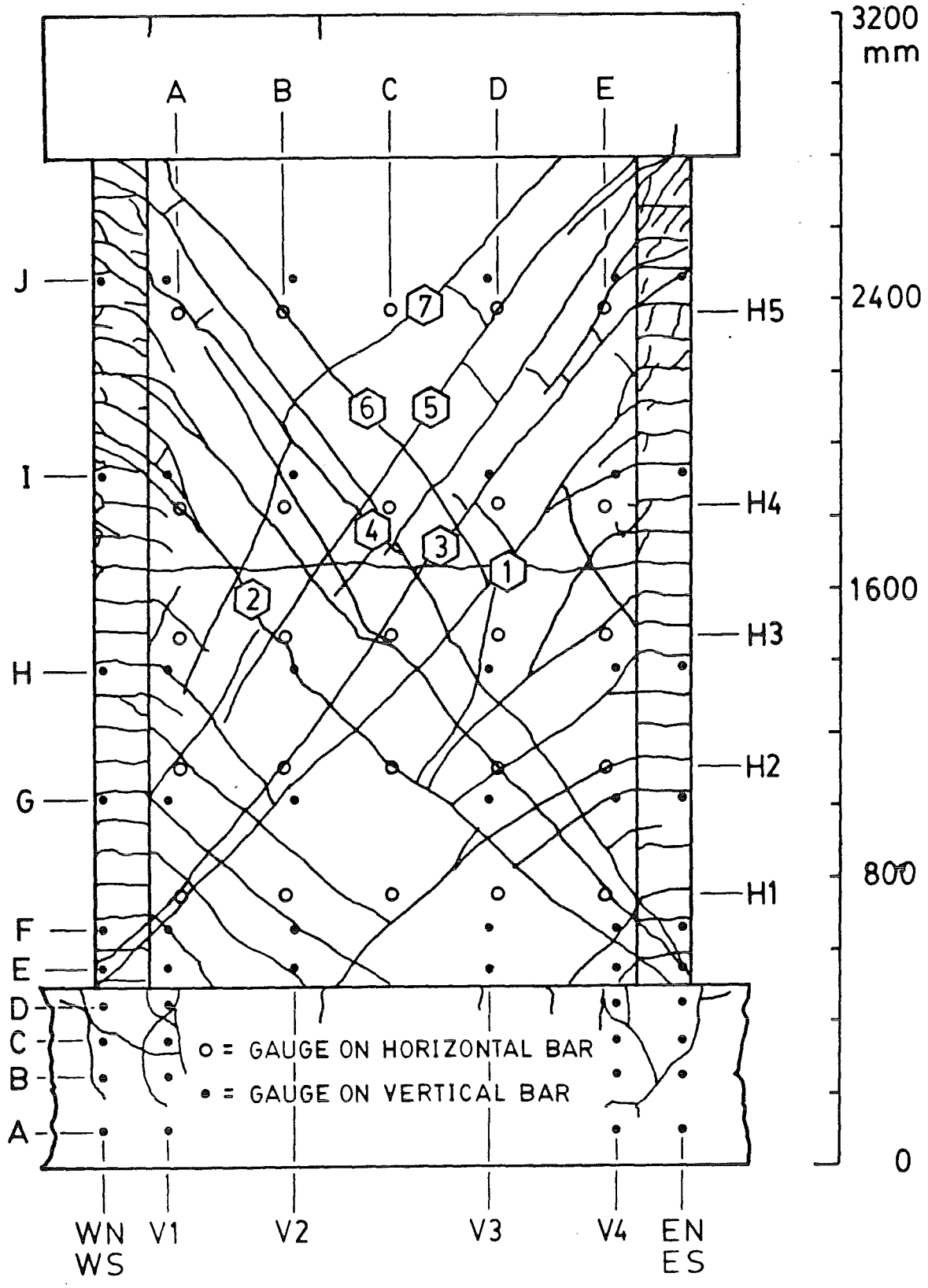

Fig. 8.6(b) - UNIT 1.5 - Crack pattern at the end of the test

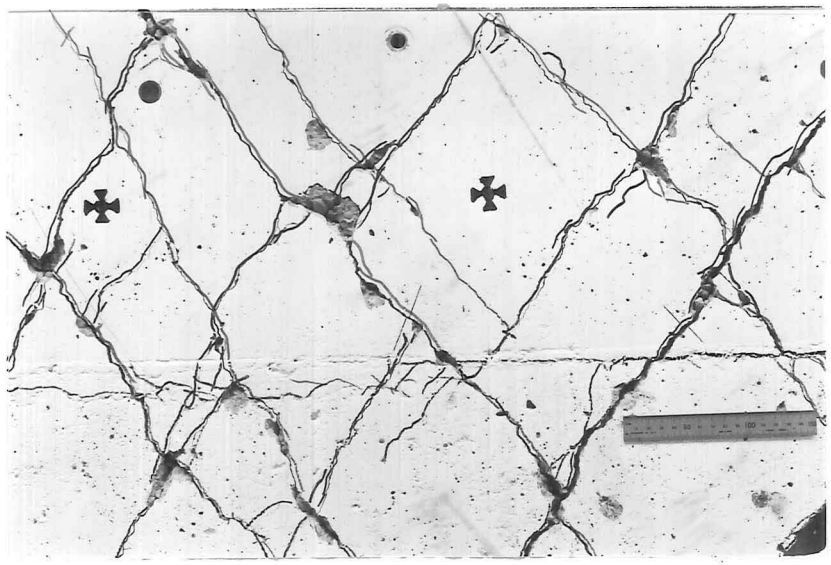

(a) Crack displacements at the centre of the web

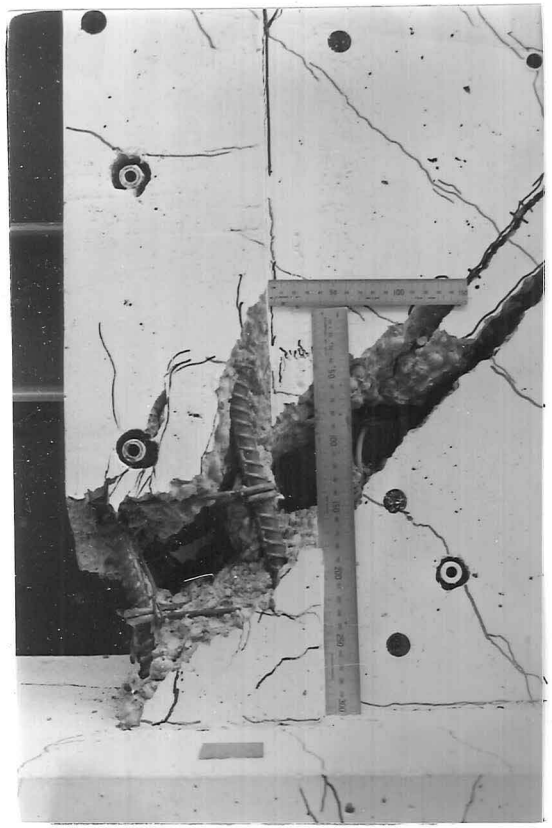

(b) Kinking in the left-hand boundary element

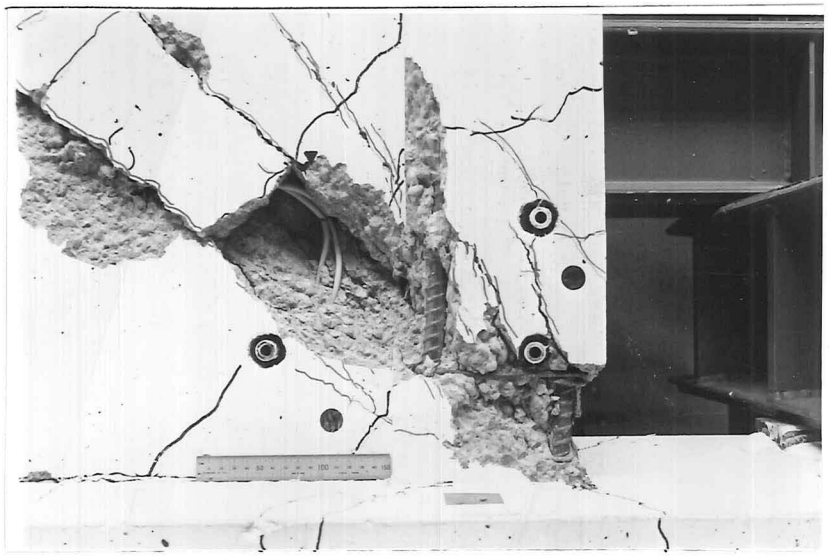

(c) Kinking in the right-hand boundary element

Fig. 8.7 - UNIT 1.5 - DETAILS OF THE FAILED UNIT

Fig. 8.7 (cont.) - UNIT 1.5
DETAILS OF THE FAILED UNIT

(d) Fractured horizontal web bars

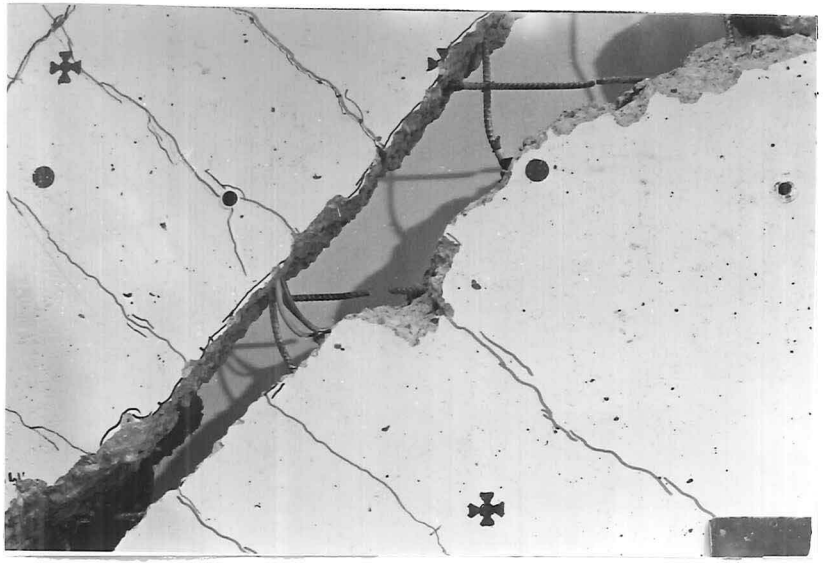

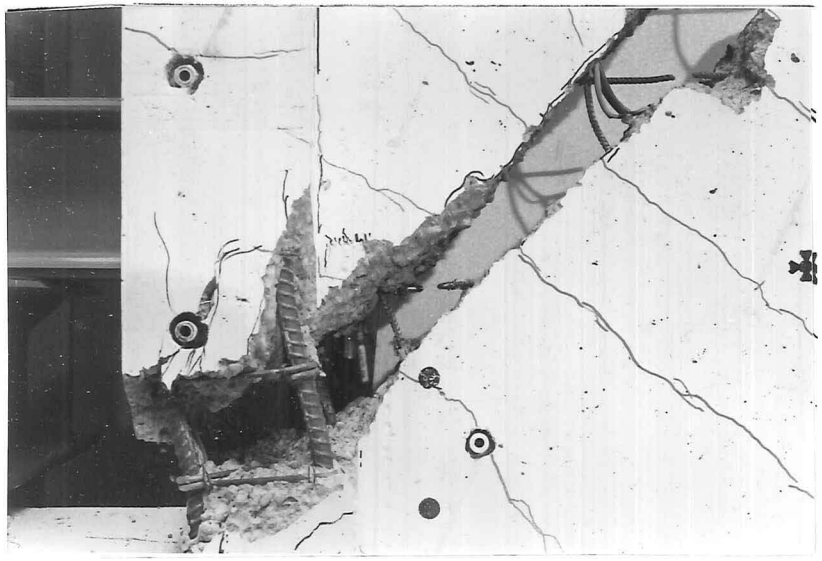

(e) Fractured horizontal web bars

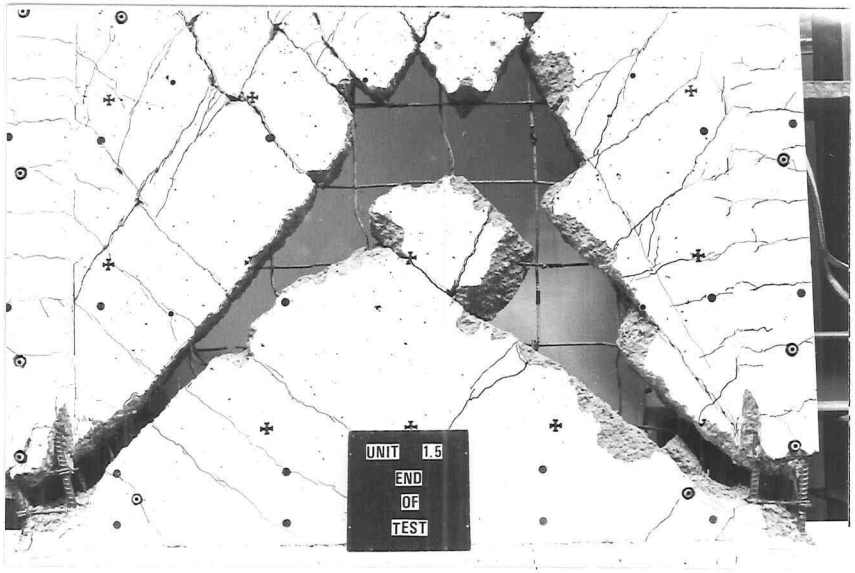

(f) Loose concrete removed from failure planes

load, the formation of additional diagonal cracks ceased as displacements concentrated along the lowest, first-formed diagonal crack. This lowest diagonal crack opened widely as the upper region of the wall was displaced horizontally with respect to the lower region (causing kinking of vertical bars). The upper region also rotated with respect to the lower region about the lower compression corner. The unit withstood reasonably well five cycles to a maximum approximate displacement of Δ/h_w=1/100. The third, fourth, and fifth cycles to this displacement, in particular, showed increasing stability in all aspects of behaviour. It is presumed, therefore, that the unit could well have managed more cycles with little further distress. A final monotonic load push in the positive (<--) direction resulted in the fracturing of four of the lowest horizontal web bars along crack 1, accompanied by severe kinking of the LHBE and severe spalling along the lower half of the main diagonal for negative (-->) loading when displacement reached approximately Δ/h_w = +1/70. Details of the failed unit are shown in Fig. 8.7.

8.4 TEST RESULTS

As for Unit 1.0, a high degree of stability was observed in most aspects of behaviour during successive cycles to a given displacement level.

8.4.1 Elastic Cycles

It was found that load cycles to $\pm 0.50V_i$ produced cracking but no yielding of reinforcement. The stiffness at $0.50V_i$ was calculated, using the convention described in Section 7.5.2 and illustrated in Fig. 7.12, to be 48.4kN/mm. At a load level of $0.75V_i$, the actual yield displacement was calculated (as in Section 6.5.3) to be 6.28mm, while the predicted yield displacement was 4.0mm (Appendix B). Actual Δ_y = 1.57 x predicted Δ_y.

8.4.2 Lateral Load vs. Total Top Displacement

The hysteretic loops for lateral load vs. total displacement at the top of the unit are shown in Fig. 8.8. For the first three load levels (increments 1 to 34), only

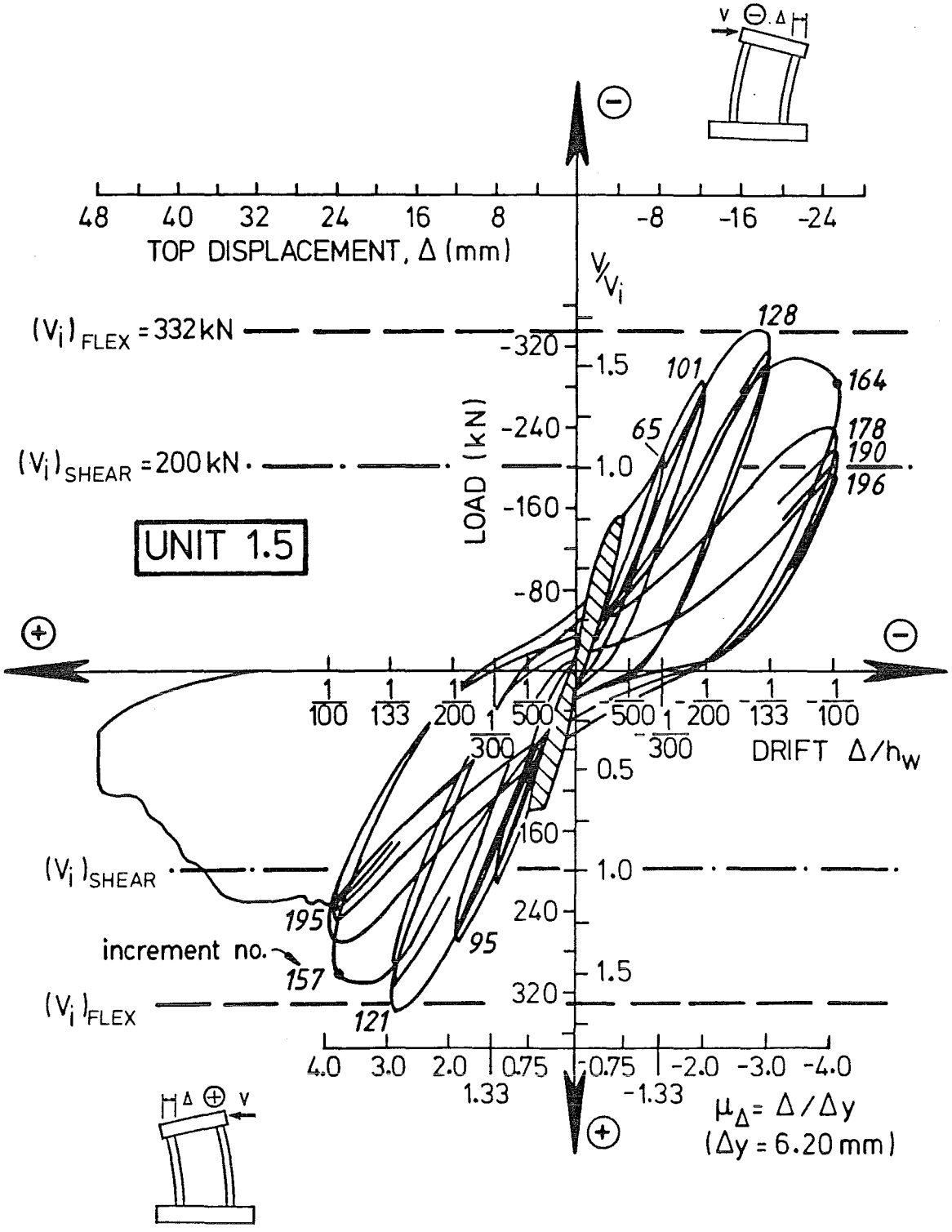

Fig. 8.8 - UNIT 1.5 - Lateral load vs. total top displacement

the envelope curve is drawn. After $0.75V_i$, all loops are drawn. The slopes of the loops are flatter than those for Unit 1.0, indicating that Unit 1.5 was more flexible. Also, the loops are noticeably pinched, which indicates the influence of shear in the response.

Two different characteristics of pinching can be observed in Fig. 8.8. First, a limited type of pinching is observed for the early stages of the test. Diagonal cracks formed at increments 29 and 34 for positive and negative loading respectively. They formed suddenly and immediately extended across the entire length of the web. Upon the formation of these cracks, the stiffness of the unit decreased slightly, as seen by the flattening in slope at increments 29 and 34. However, the lateral load resistance continued to increase because load was carried effectively in arch action by means of the diagonal compression struts that formed between the diagonal cracks. Upon unloading and loading in the opposite direction, the alternate diagonal compression strut was activated. However, before the new diagonal strut could begin to carry compressive load, the diagonal cracks previously formed must have had to close. It is postulated that this closing of the previously formed diagonal cracks is the cause of pinching at zero load in the hysteretic loops. Once these cracks had closed and the new diagonal compression strut began to carry load, the lateral load resistance increased predictably because of the integrity of the strut and tie mechanism. So, in the early stage of the test, only this pinching due to the closing of diagonal cracks at zero load was evident. (See, for example, increments 59-116.) During this part of the test, the loops for successive cycles to the same displacement are nearly identical. In other words, although this limited pinching implied less than ideal energy dissipation, the amount of energy dissipated on successive cycles remained relatively constant. This limited pinching was observed up to the attainment of maximum load (increments 121 and 128) because the lateral load carrying mechanism remained in tact and viable.

After maximum load, the strut and tie mechanisms deteriorated, and a different, more extensive type of pinching was observed. (See increments 164-196, for

example.) Here, pinching was observed not only at zero load but also throughout the entire load range. At this stage, the crack pattern was fully formed. Displacements were observed not only perpendicular to the diagonal cracks but also parallel to them. With slippage came grinding and loss of aggregate interlock. Thus, the more severe pinching observed in the later stages of the test was due to the overall deterioration of the load carrying mechanism. Significant reduction in loop area and consequent loss of energy dissipation is evident for successive cycles to a particular displacement. (Compare increments 164 and 196.) Pinching, loop area, and energy dissipation are discussed further in Section 8.4.4.

The lateral load resistance developed on consecutive cycles is summarized in Table 8.1 and plotted in Fig. 8.9. Prior to the attainment of maximum load, little resistance was lost. (See, for example, increments 101,110,116 in Fig. 8.8.) Prior to maximum load, the average loss of resistance in the second and third cycles was 4.5 percent. Also, when viewing consecutive cycles to a given displacement after the attainment of maximum load, the lateral load resistance dropped more significantly after the first cycle. (See Fig. 8.9, Δ/h_w=1/133,1/100.) However, the relative stability in response after the second cycle should be noted. Special note should be taken of level Δ/h_w=1/100, where there was a high degree of stability between the third, fourth, and fifth cycles. From this observation, it is deduced that the behaviour of the wall unit would have stabilized and not deteriorated with a number of additional cycles to the same Δ/h_w=1/100 displacement.

For Unit 1.5, a maximum load of 342kN was recorded at Δ/h_w=+1/133. The strength exceeded the predicted ideal shear strength by 71.0 percent and the predicted ideal flexural strength by 3.0 percent.

As seen in Fig. 8.8, the stiffness of the unit degraded with increased displacement level. Estimates of the stiffness as well as other important quantities are summarized in Table 7.2.

TABLE 8.1 - UNIT 1.5 - LATERAL LOAD RESISTANCE DEVELOPED ON CONSECUTIVE CYCLES

Load/displacement level	Positive loading ←			Negative Loading →		
	Increment No.	Lateral load (kN)	Reduction in[1] lateral load (%)	Increment No.	Lateral load (kN)	Reduction in[1] lateral load (%)
$V = 0.25\ V_i$	2	50	-	5	50	-
	7	50	-	9	52	-
$V = 0.50\ V_i$	12	100	-	16	100	-
	20	100	-	24	100	-
$V = 0.75\ V_i$	29	150	-	34	150	-
	39	150	-	43	150	-
	48	150	-	53	150	-
$\Delta/h_w = 1/300$	59	222	-	65	218	-
	71	214	3.6	77	208	4.6
	83	207	6.8	89	204	6.4
$1/200$	95	277	-	101	284	-
	107	268	3.2	110	278	2.1
	113	262	5.4	116	273	3.9
$1/133$	121	342[2]	-	128	335[2]	-
	135	314	8.2	141	314	6.3
	147	296	13.5	152	303	9.6
$1/100$	157	302	-	164	284	-
	171	275	8.9	178	240	15.5
	185	252	16.6	190	216	23.9
	193	242	19.9	194	204	28.2
	195	237	21.5	196	197	30.6

(1) Reduction is taken as a percentage of the lateral load developed during the first cycle to the given displacement level.

(2) Maximum load for the given loading direction.

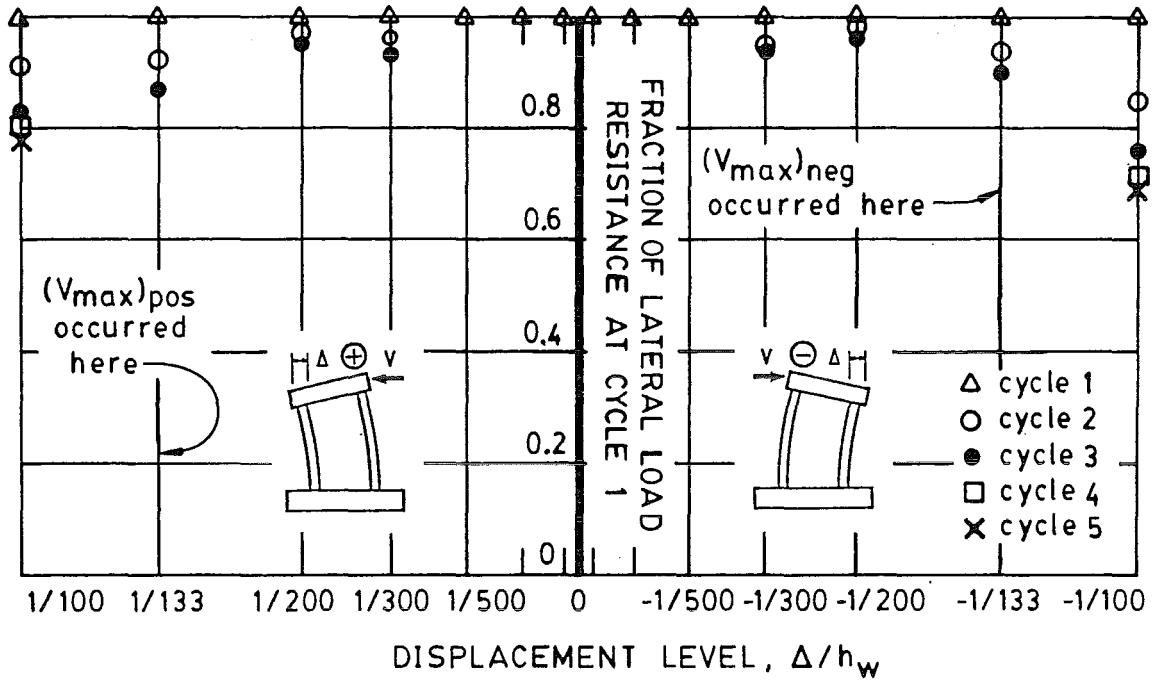

Fig. 8.9 - UNIT 1.5 - Lateral load resistance developed on consecutive cycles

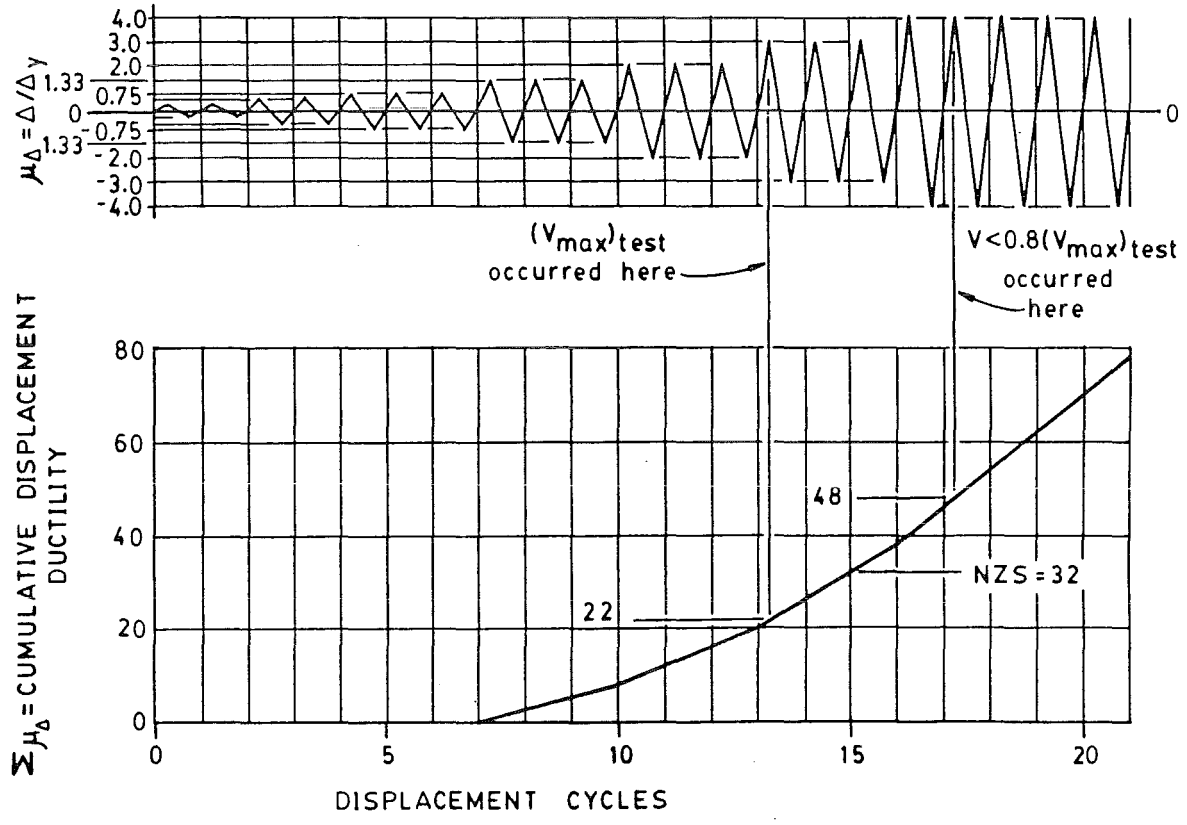

Fig. 8.10 - UNIT 1.5 - Loading history and cumulative displacement ductility

8.4.3 Cumulative Displacement Ductility and Strength Reduction

The precautions stated in Section 7.5.3 concerning the calculation of cumulative displacement ductility apply here also. Nevertheless, the loading history and cumulative displacement ductility for Unit 1.5 are shown in Fig. 8.10. At the attainment of maximum load, the cumulative displacement ductility was 22. By the time the load had fallen to approximately $0.80(V_{max})_{test}$ (increment 171), the unit had been subjected to three semi-cycles to $\mu_\Delta = 4.0$ and the cumulative displacement ductility had reached approximately 48. the code requirement. Comparison with the NZS 3101 requirement of 32 should be done cautiously, however, because the code envisages loading the structure to at least $\mu_\Delta = 1\text{-}2$ immediately. The loading increments were more gradual for the present test units.

8.4.4 Dissipation of Energy

The energy dissipated by Unit 1.5 during each cycle of the test is shown in Fig. 8.11(a). The results follow the same trend that was observed for Unit 1.0. The energy dissipated per cycle increases with displacement level. In Fig. 8.11(b) is shown the reduction in energy dissipated on consecutive cycles to a given displacement. Again, the same trend recorded for Unit 1.0 is evident here. The energy dissipated per cycle dropped off sharply after the first cycle to a given displacement level, particularly after maximum load was reached.

Fig. 8.12 compares the cumulative energy dissipated by Unit 1.5 with that dissipated by the ideal elasto-plastic system of Fig. 4.7 subjected to the same displacement history. Prior to the attainment of maximum load, the cumulative energy dissipated by Unit 1.5 was quite large relative to the energy dissipated by the ideal elasto-plastic system. After maximum load, the cumulative energy dissipated by Unit 1.5 remained at approximately 35 percent of that for the ideal elasto-plastic system.

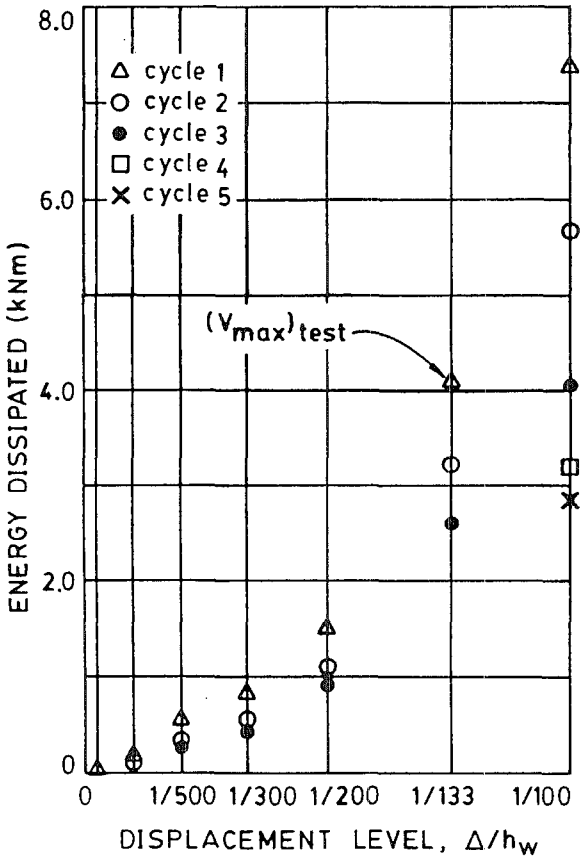

(a) Energy dissipated on each cycle

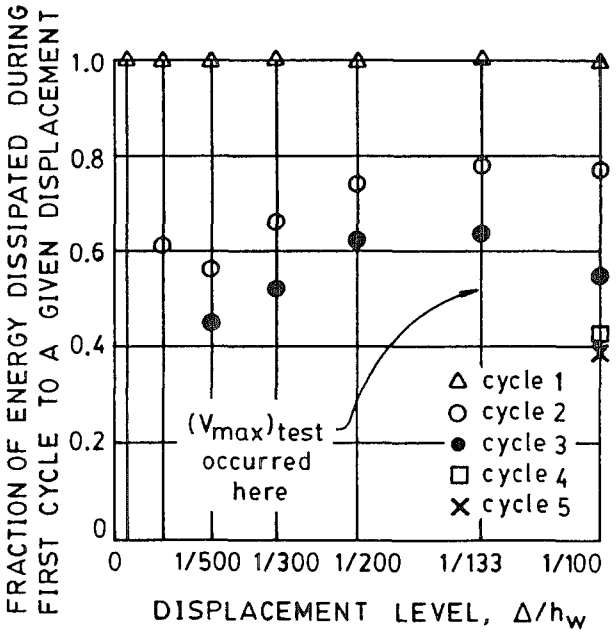

(b) Loss of energy dissipation on consecutive cycles

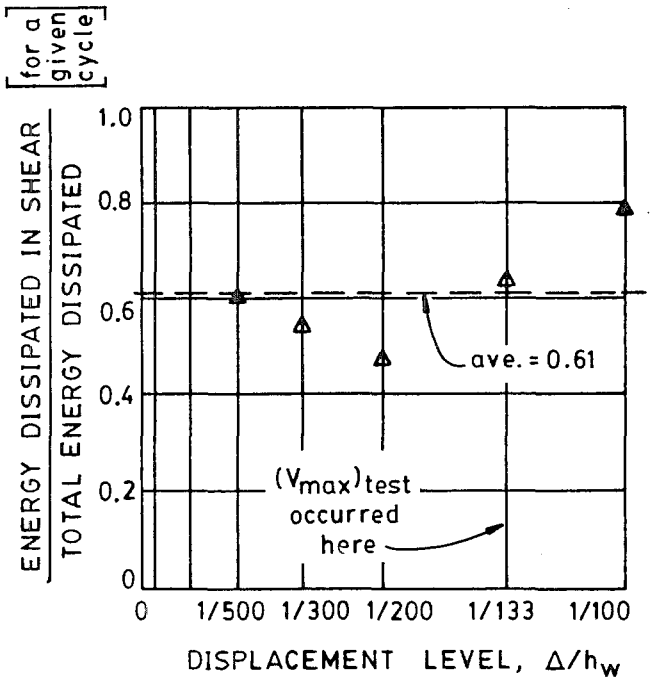

(c) Energy dissipated in shear alone

Fig. 8.11 - UNIT 1.5 - Energy dissipation characteristics

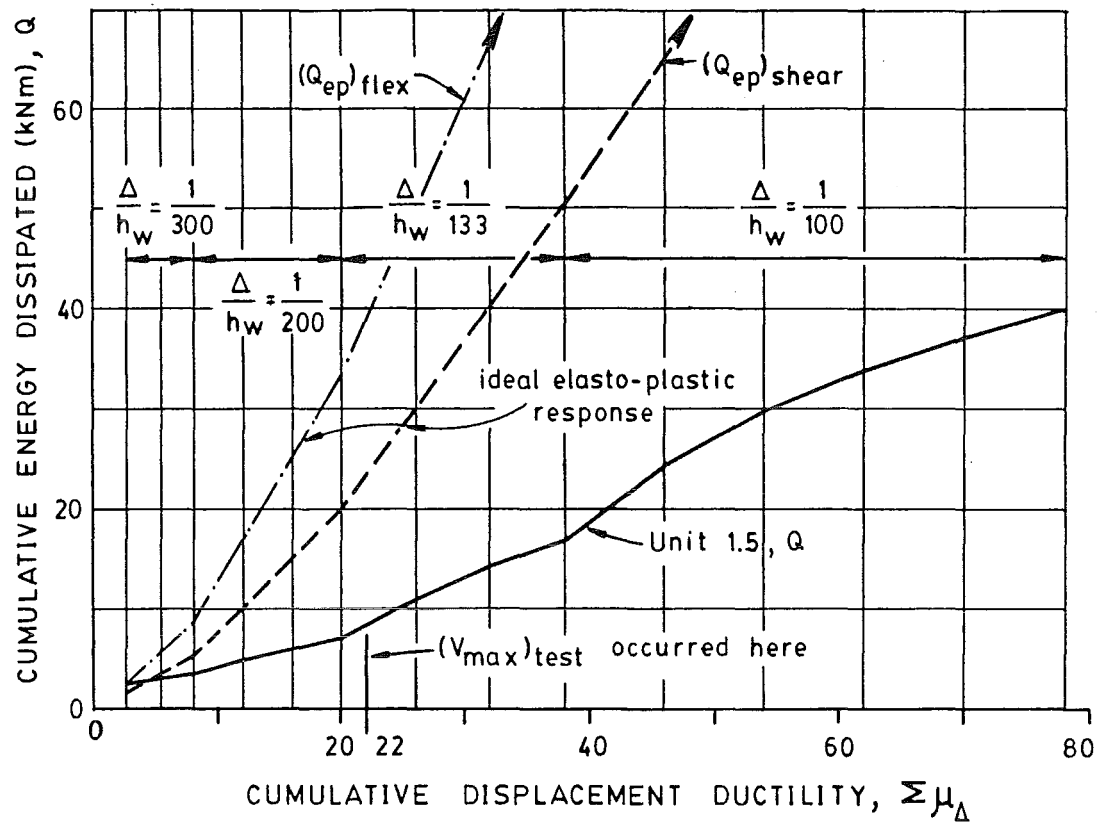

(a) Cumulative energy dissipated

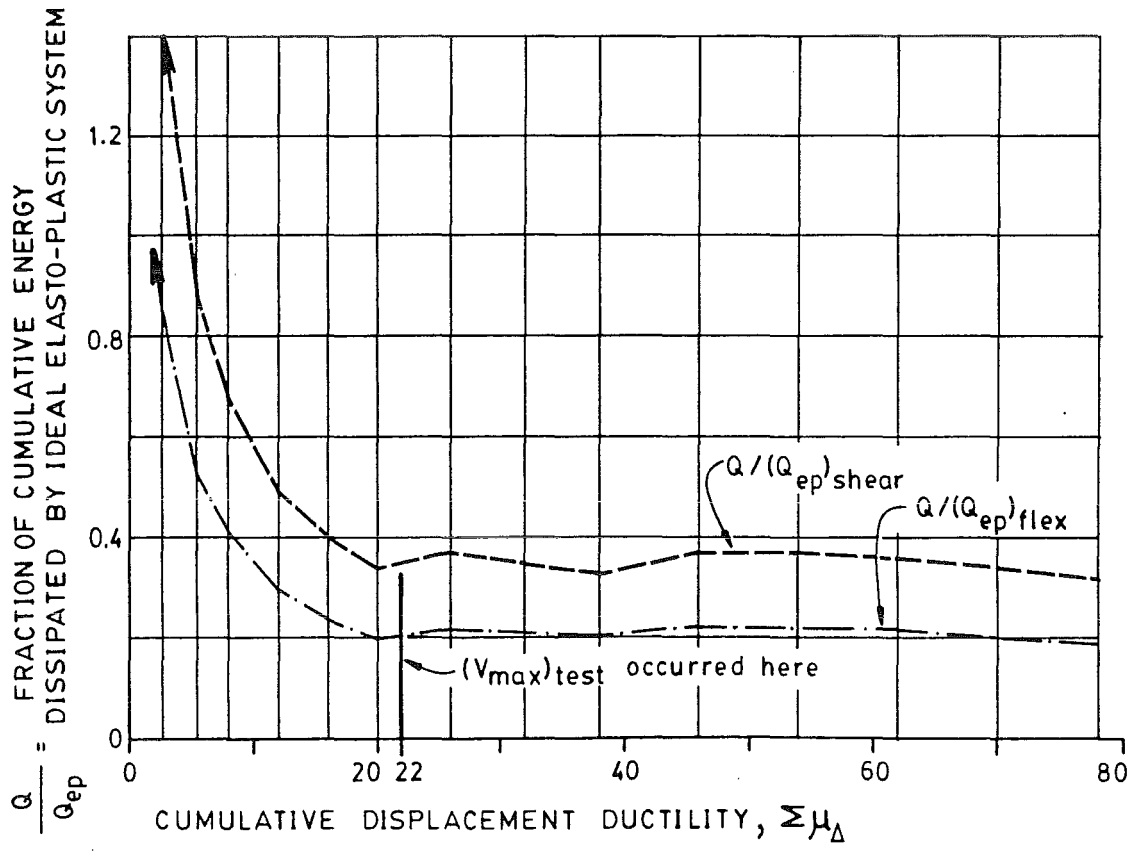

(b) Fraction of idealized response

Fig. 8.12 - UNIT 1.5 - Cumulative energy dissipated vs. cumulative displacement ductility

8.4.5 Lateral Load vs. Top Displacement Due to Shear Deformations

Fig. 8.13 shows the hysteretic loops for total lateral load vs. top displacement due to shear deformations alone. The loops are very similar to the loops for total top displacement (Fig. 8.8), especially in the late stages of the test. This similarity indicates the sizeable influence of shear on the behaviour of the unit. The influence of shear is shown also in Section 8.4.6. Fig. 8.11(c), which shows the ratio of the hysteretic area of the shear loop to the hysteretic area of the total displacement loop in the first cycles, reveals a pattern similar to that for Unit 1.0 (Fig. 7.14(c)). The fraction of the energy dissipated in shear alone decreased as the test progressed, until the maximum load was reached. Thereafter, the fraction of energy dissipated in shear alone increased. The energy dissipated in shear alone averaged approximately 61 percent of the total energy dissipated for first excursion cycles.

8.4.6 Components of Top Deflection

For Unit 1.5, the components of the top deflection, as illustrated in Fig. 7.18, are plotted in Fig. 8.14. Again, the sum of separately obtained components is plotted as Δc, while the top deflection actually measured during the test is plotted as Δm. The difference between measured and calculated deflections is small. Unlike in Unit 1.0, very similar behaviour was observed for both loading directions.

It is seen that before the maximum load was reached (at $\Delta/h_w=1/133$), each of the four components increased at a relatively constant rate. However, after the maximum load was reached, the shear deformations dominated behaviour. Another comparison of the influence of the four components during the test is seen in Fig. 8.15. Δs and Δfe were relatively small and remained approximately constant throughout the test. Δf and Δv were, by far, the most influencial components. During the elastic cycles at the beginning of the test ($\Delta/h_w=1/4000,1/1000$), flexural deformations dominated, accounting for 55-60 percent of the total deflection. This dominance of flexural deformations is confirmed by the crack pattern. No diagonal shear cracks were observed during these first cycles. However, flexural

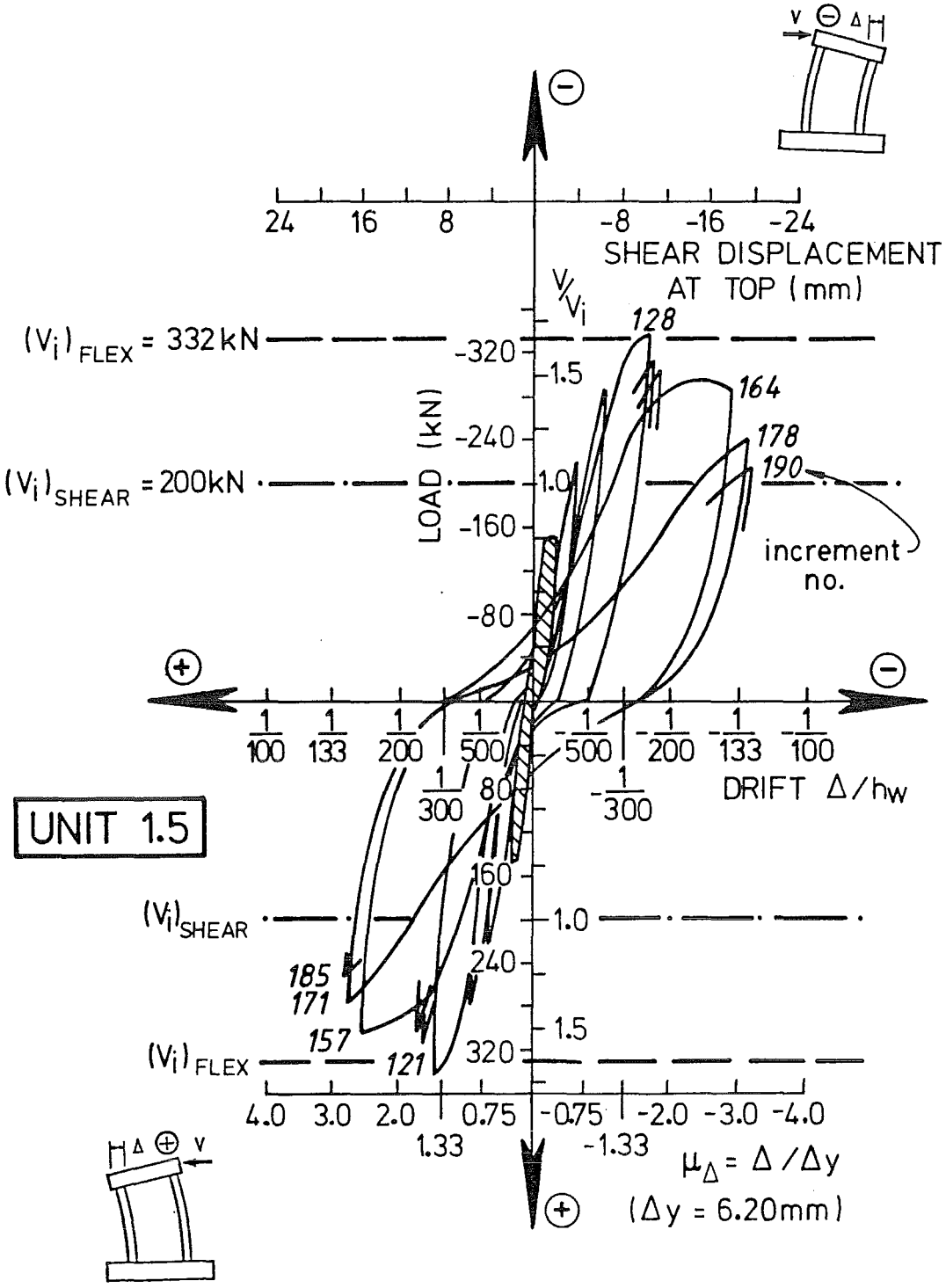

Fig. 8.13 - UNIT 1.5 - Lateral load vs. top displacement due to shear deformations alone

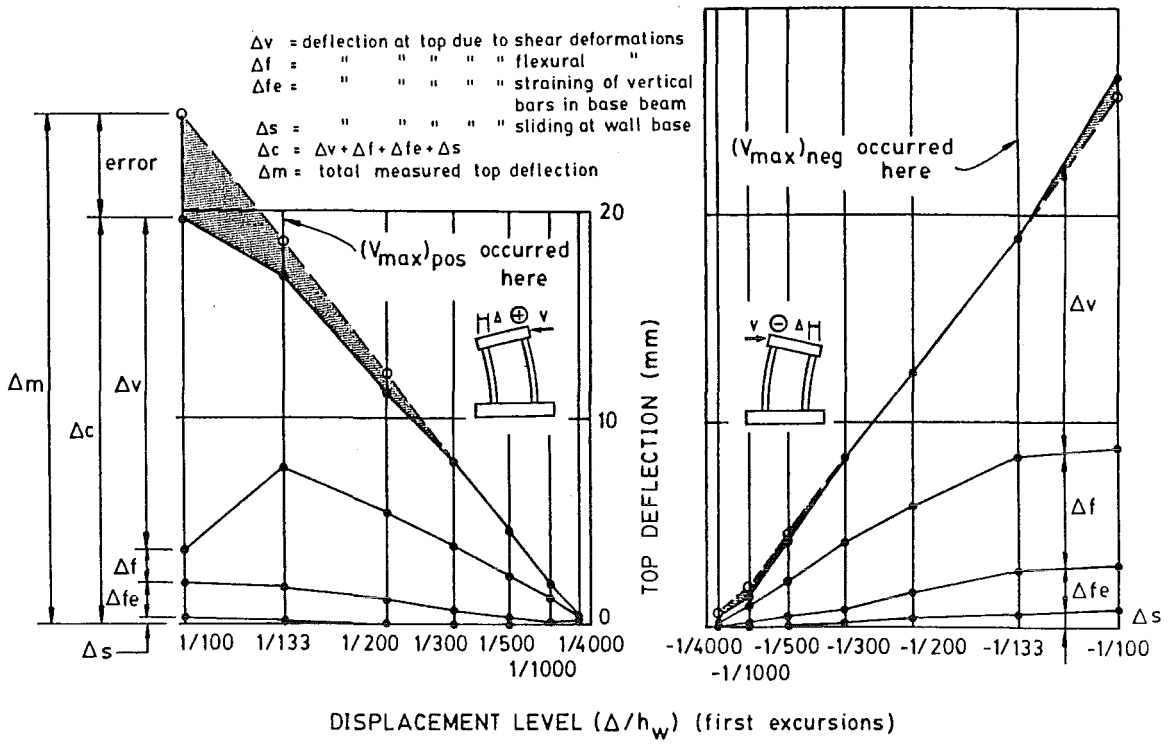

Fig. 8.14 - UNIT 1.5 - Components of top deflection

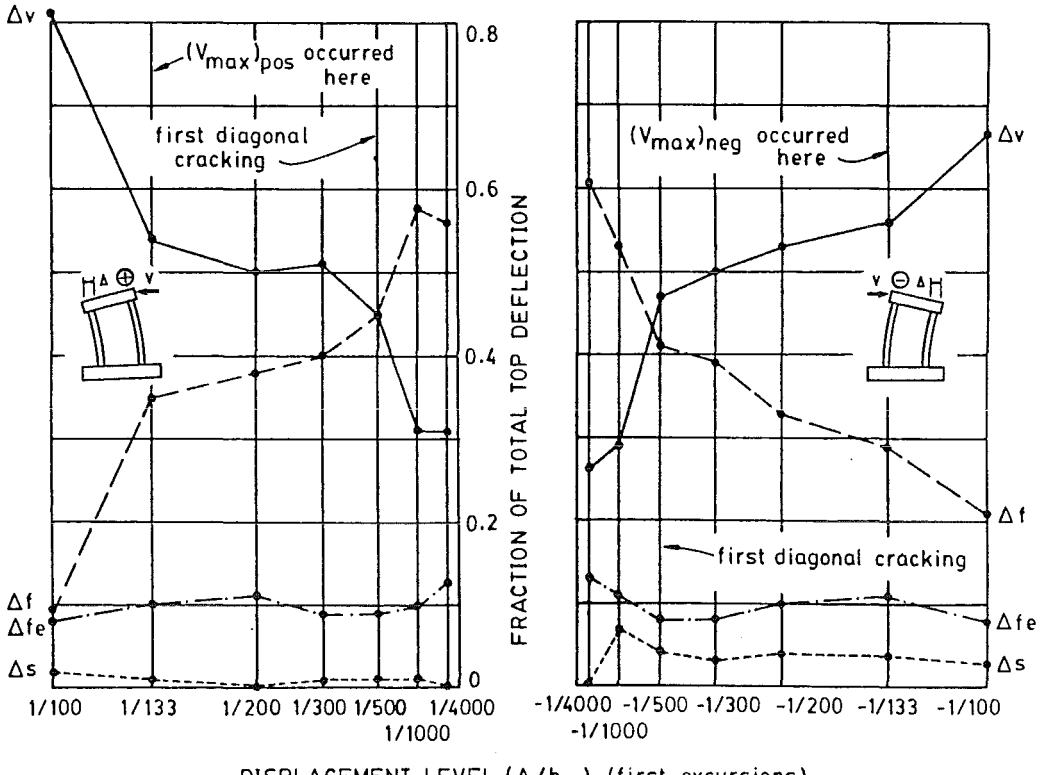

Fig. 8.15 - UNIT 1.5 - Relative proportions of top deflection

cracks did appear. At Δ/h_w=1/500 (V=0.75V_i), the first major diagonal cracks occurred (Figs. 8.2,8.3). As shown in Fig. 8.15, the shear contribution rose sharply while the flexural contribution correspondingly dropped sharply. At this point, the shear and flexural contributions were approximately equal, each comprising 45 percent of the total top deflection. Horizontal flexural cracks had, at this point, extended the entire height of the boundary elements. Between the occurrence of the first diagonal cracks (Δ/h_w=1/500) and the reaching of maximum load (Δ/h_w=+1/133), the shear contribution steadily increased while the flexural contribution steadily decreased. During this period, the two major diagonal cracks in each direction became established (Figs. 8.4,8.5). At Δ/h_w=1/133, shear deformations accounted for 50-55 percent of the total deflection while flexural deformations accounted for only 30-35 percent of the total deflection. After the maximum load was reached (Δ/h_w=+1/133), further major diagonal cracks formed in the upper regions of the wall while the shear contribution to total deflection rose sharply to 65-80 percent. The flexural contribution dropped markedly to below 20 percent. Flexural cracking was confined mainly to the boundary elements and adjacent portions of the web. At failure, shear deformations (in the form of a strut and tie mechanism) dominated behaviour.

8.4.7 Strains in Horizontal Web Bars

The positions of instrumented horizontal web bars superimposed on the crack pattern at the end of the test are shown in Fig. 8.6. Plots of the strains in these horizontal bars are shown in Fig. 8.16. As mentioned in Section 7.5.7, caution must be exercised in interpolating strains by straight lines between gauges crossed by cracks. (Note, once again, that a strain gauge crossed by a crack is marked with an asterisk in the plots. A subscript r indicates a strain peak residual following excessive straining in the opposite loading direction.)

As was found in Unit 1.0, the strains in the horizontal bars were generally less than half yield strain except along the main diagonals, where shear cracking appeared. See, for example, bars H1 and H5. In viewing

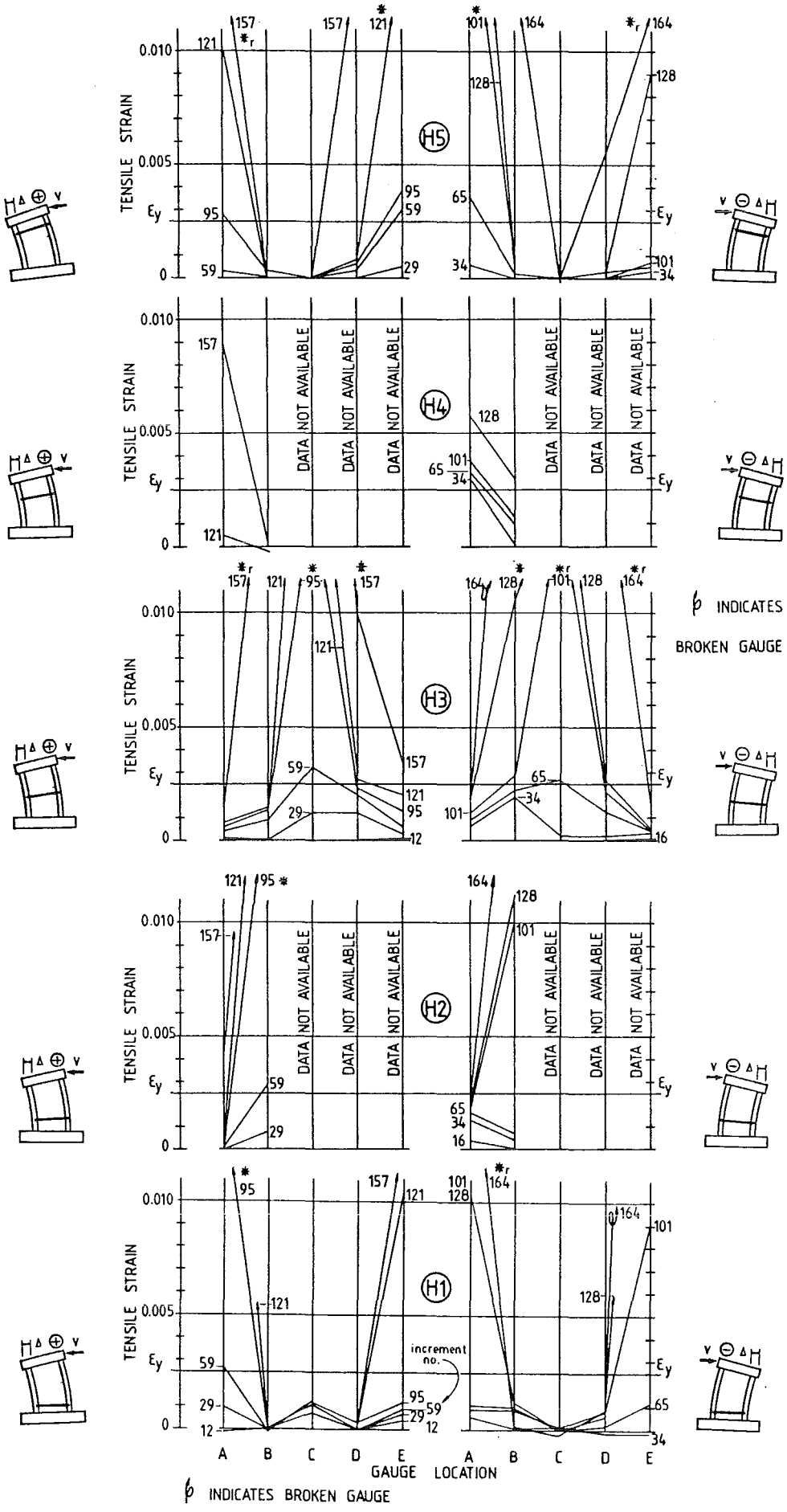

Fig. 8.16 - UNIT 1.5 - Strains in horizontal web bars

gauge positions that lay along the main diagonals, those that were not crossed directly by cracks indicate that, in general, strains along the main diagonals approached yield strain as the maximum load was reached (Δ/h_w=1/133, increments 121,128). Gauges H3B and H3D are examples of such gauges.

Once again, along the main diagonals, strains in horizontal bars were generally larger than strains in corresponding vertical bars.

8.4.8 Strains in Vertical Boundary Element Bars

Selected longintudinal bars in the vertical boundary elements were instrumented as shown in Figs. 6.7(b) and 8.6(b). The plots of strain in these bars are shown in Fig. 8.17. In the compression boundary element, strains were small. In the tensile boundary element, strains were approximately uniform with height above the base level. This pattern of uniform strain is indicative of strut and tie behaviour. (See Section 3.4.) Strains reached approximately yield strain throughout the wall height as the ideal flexural strength was attained (increments 121,128). Again, a strain peak occurred where a gauge was crossed by a crack. These peaks are marked with an asterisk in the plots.

8.4.9 Strains in Vertical Web Bars

The strains for the four instrumented vertical web bars (Fig. 6.7(b)) are shown in Fig. 8.18. As expected, the strain patterns for bars V1 and V4 resemble very closely the strain patterns for the neighbouring vertical boundary element bars. That is, strains were near zero on the compressive side of the wall and uniform with height on the tensile side. These patterns confirm strut and tie behaviour in Unit 1.5.

The plots for bars V2 and V3 are entirely different. However, most of the gauges on bar V2 were crossed by cracks and, therefore, record strain concentrations. When these observations are taken into account, the plot for bar V2 yields little useful information other than that strains remained small in areas lying off the main diagonals. The plot for V3 shows that strains remained generally less than yield strain. Along the main diagonals strains approached

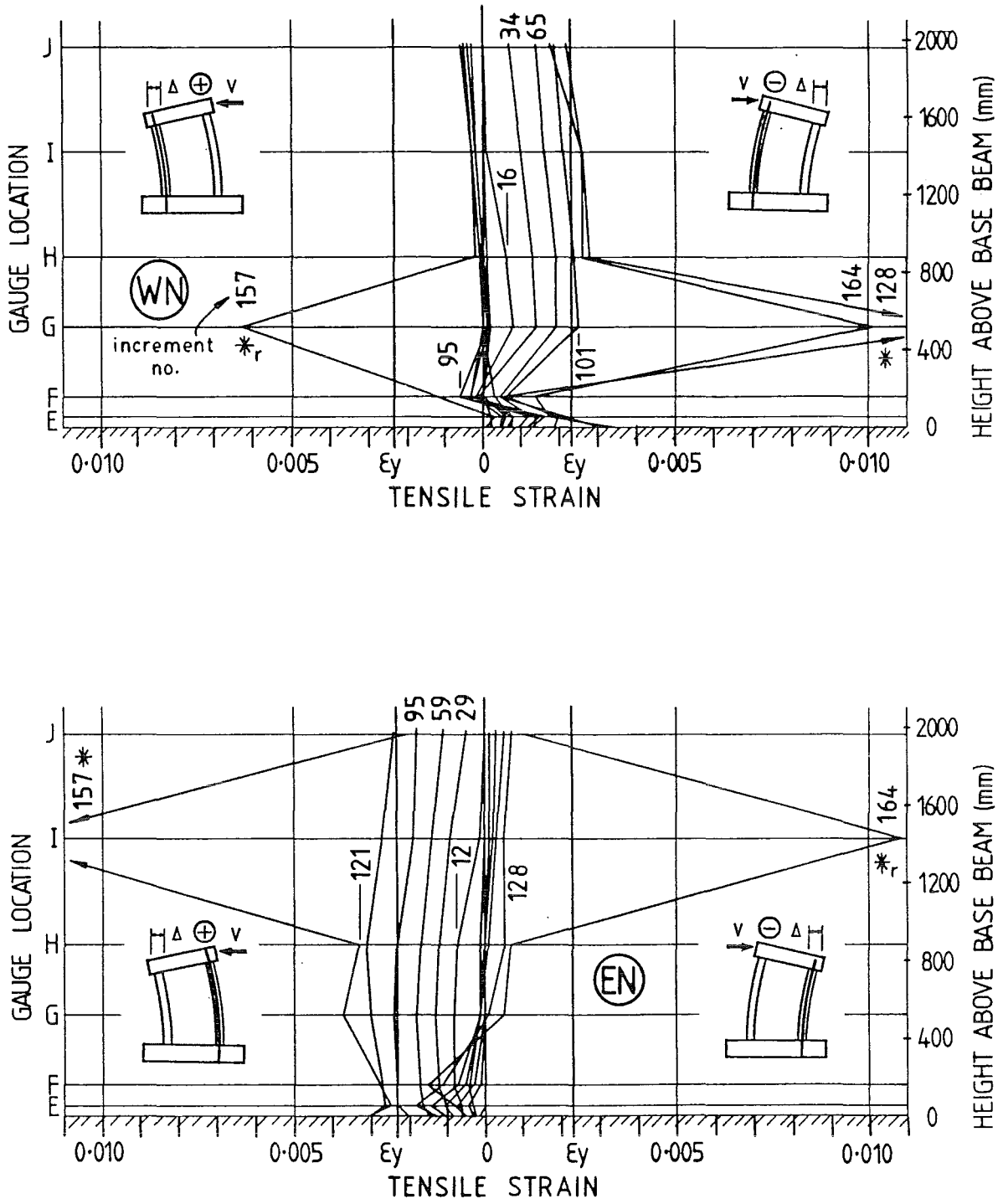

Fig. 8.17 - UNIT 1.5 - Strains in vertical boundary element bars WN & EN

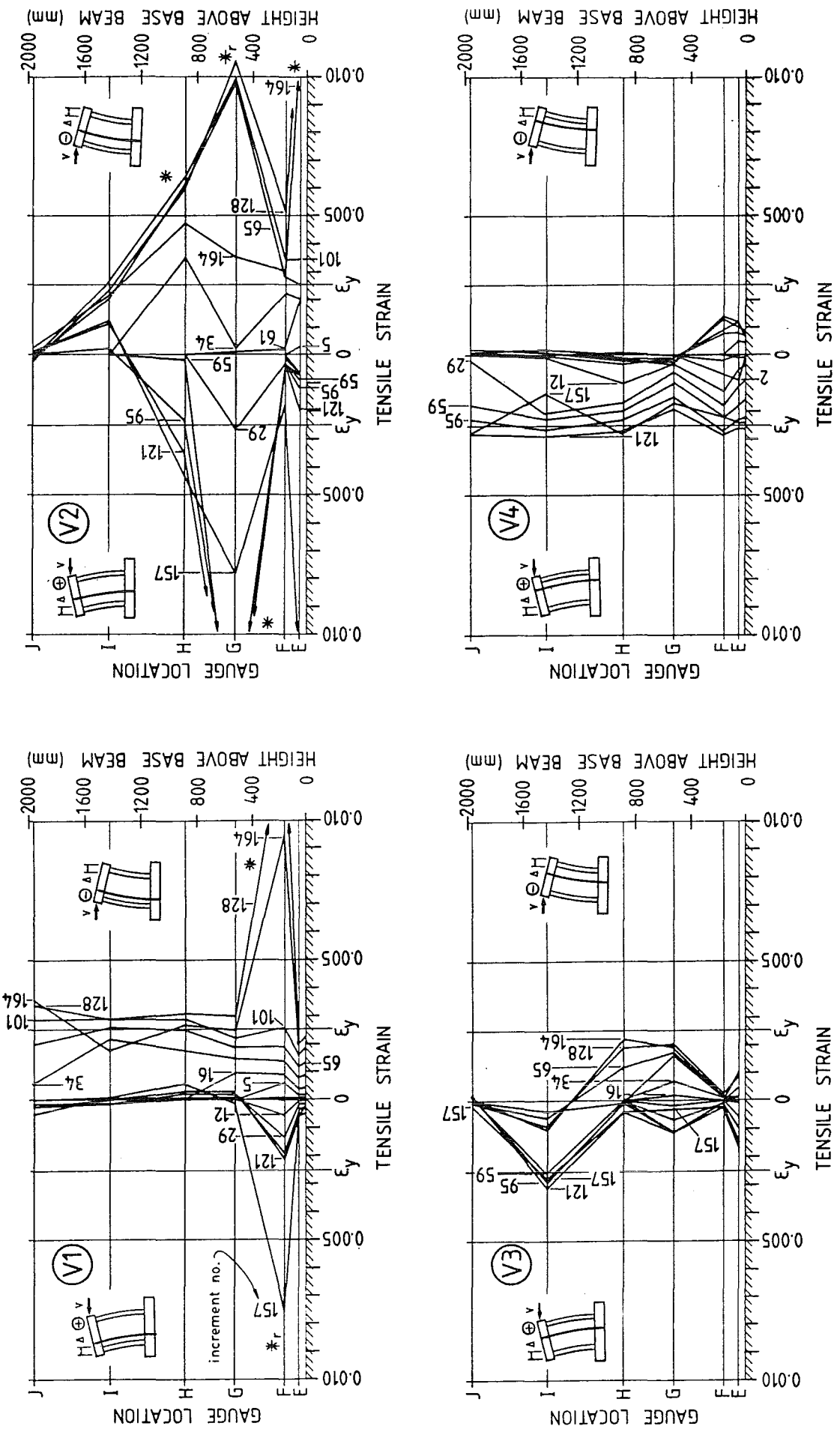

Fig. 8.18 - UNIT 1.5 - Strains in vertical web bars

yield strain. Elsewhere, they remained less than half yield strain.

Special note should be taken of gauges V2I and V3I. The development of compression in these gauges seems to indicate that the vertical compression resultant lay in the middle region of the cross section (as in strut and tie behaviour). The location of the vertical compression resultant is reported in the next section.

8.4.10 Location of the Vertical Compression Resultant

The strains in vertical bars across horizontal gauged cross sections are plotted in Fig. 8.19. As seen in Unit 1.0, the neutral axis (the line of zero strain) shifts toward the tension face as elevation in the wall increases. At section E, compressive strains are confined to within 200mm ($0.12\ell_w$) of the compression face. At section J, compressive strains extend to within 560mm ($0.34\ell_w$) of the tension face.

Stresses were calculated from strains, and bar forces were calculated from stresses, as described in Section 7.5.10. The location and magnitude of the compression resultant were then calculated from consideration of equilibrium. (Refer to Fig. 7.26.) The calculated location of the compression resultants on the horizontal gauged cross sections are shown in Fig. 8.20. Once again, the shaded region marks the region within which the compression resultant would have lain in the case of purely flexural behaviour. It is clear that arch action was in effect and that the calculated locations shown in Fig. 8.20 define the main diagonal compression strut.

8.4.11 Strains in Vertical Bars Below Base Level

Vertical bars WN, V1, V4, and EN were instrumented within the base beam in order to record strain penetration into the base. Plots of strain versus depth in the base beam are shown in Fig. 8.21. These strains were integrated to obtain the rigid body movement of the wall described by Δfe in Section 8.4.6. Although strain penetration along 6mm diameter bars was less than that along 16mm diameter bars, the difference in strain penetration was not so marked as in Unit 1.0. Again, the approximately linear strain indicates that approximately uniform bond stress existed throughout the

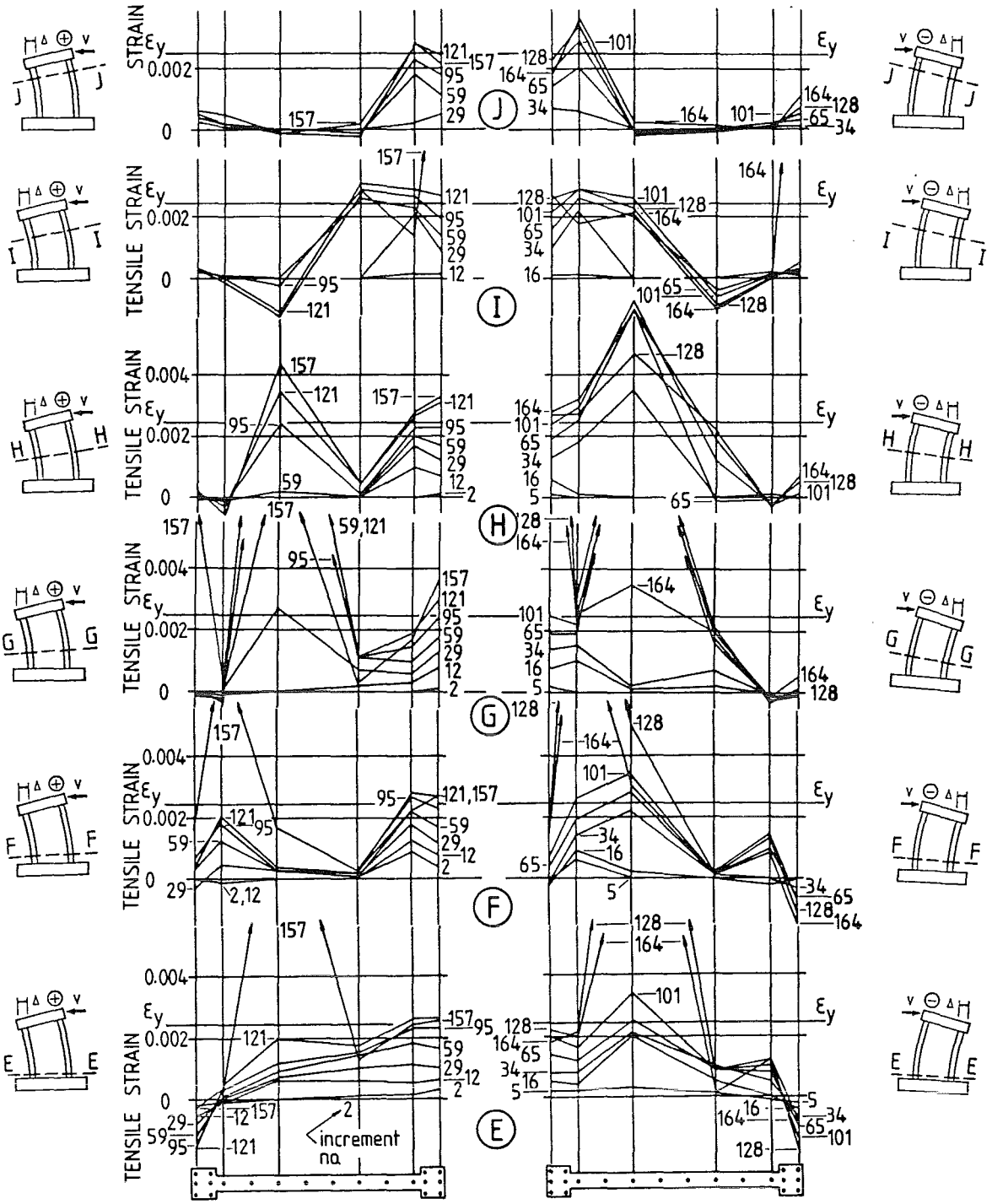

Fig. 8.19 - UNIT 1.5 - Vertical strains on horizontal gauged cross sections

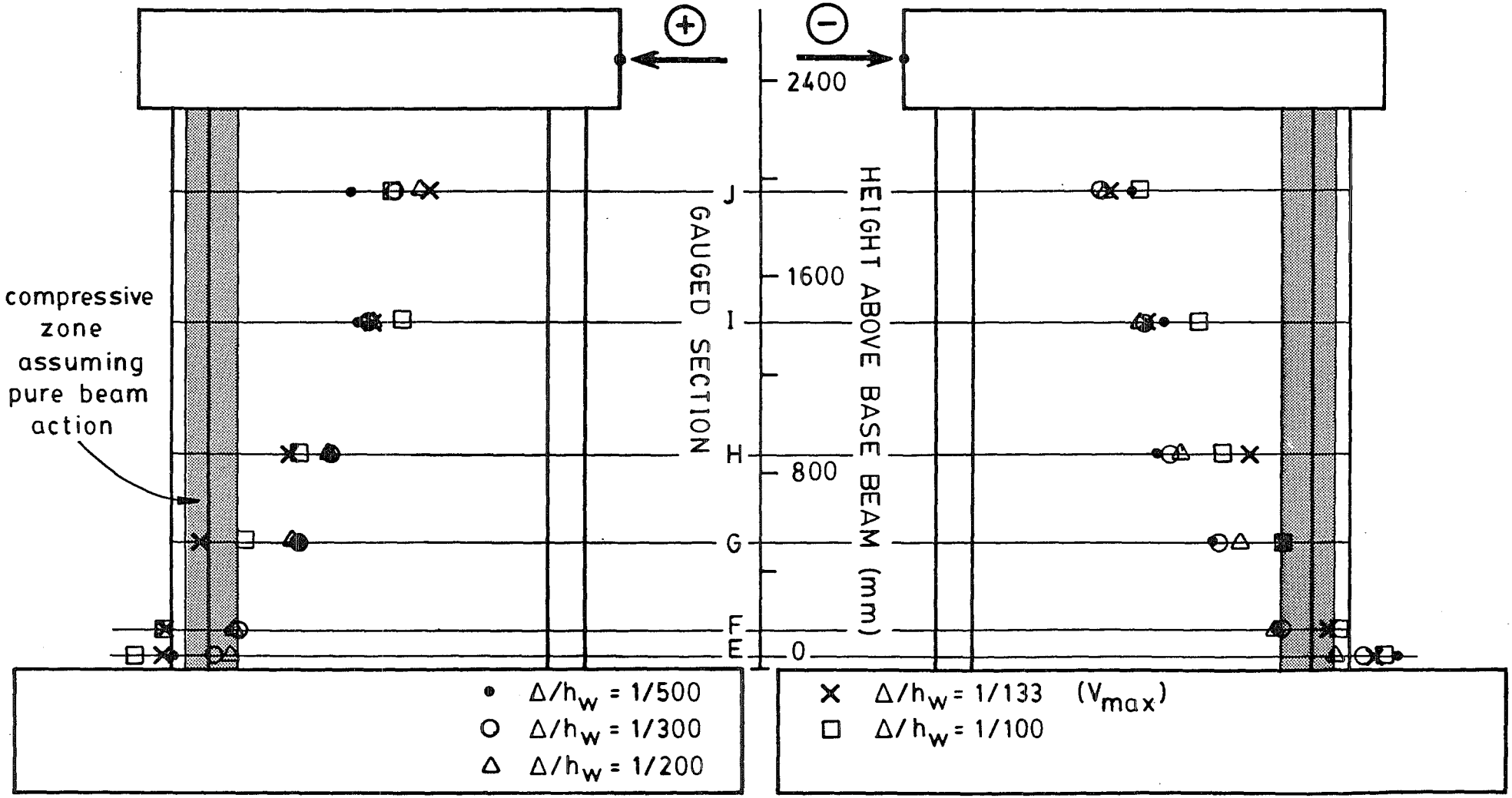

Fig. 8.20 - UNIT 1.5 - Location of vertical compression resultant

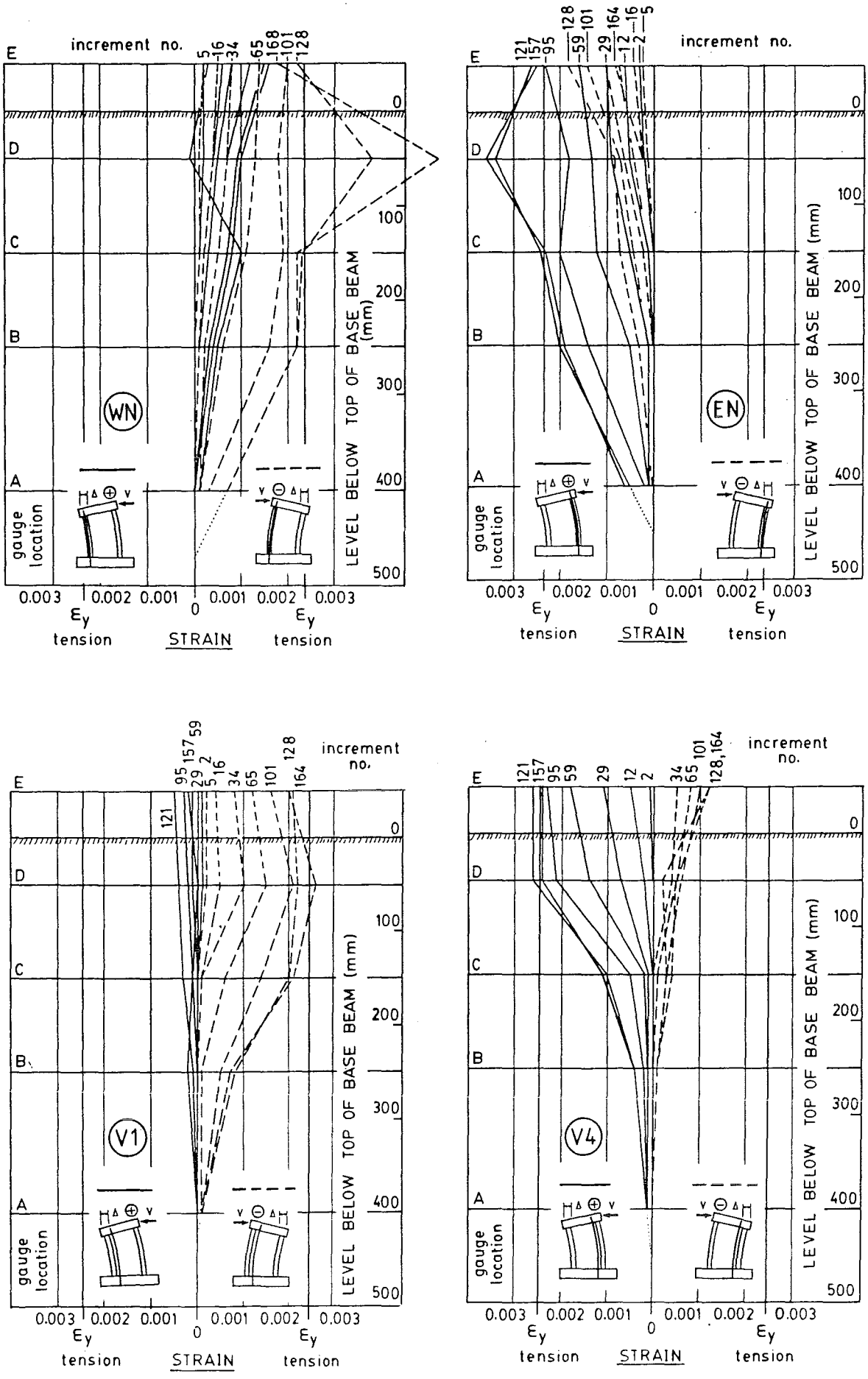

Fig. 8.21 - UNIT 1.5 - Strains in vertical bars in the base beam

depth of strain penetration.

Table 7.3 compares the development length required by NZS 3101 (column A in Table 7.3) with the actual length of penetration of strain beyond the depth of yield strain (column D in Table 7.3). Both the effect of high strength steel (m_1) and the effect of transverse hoops enclosing the boundary element bars within the base beam (m_2) were accounted for in calculating the code-required development length. For the 16mm diameter bars, the code required a value larger than the actual embedment utilized in the test. The code is conservative. However, for the 6mm diameter web bars, the code is unconservative. The actual embedment utilized during the test exceeded that required by the code by approximately 70 percent. Thus, Eq. 5-6 of NZS 3101 may be suspect for such small diameter deformed bars.

As was found for Unit 1.0, Table 7.4 reveals no definite correlation between bar properties and strain penetration.

8.4.12 Axial Extension of the Wall

As in Unit 1.0, an overall axial extension of the wall was recorded by dial gauges placed along the top beam. At maximum load (increment 121), the average axial extension was 3.76mm. A maximum average extension of 4.33mm was measured at increment 164. At the end of the test, at zero load (increment 192), the average residual axial extension was 2.22mm. Although no measurements were taken, a similar increase in the horizontal length of the wall was observed, especially in the middle region of the wall, away from the restraining effects of top and base beams.

8.4.13 Base Beam Behaviour

Some cracking occurred in the base beam below the boundary elements. Also, near the top of the base beam underneath the web, a few vertical cracks formed, which indicated that the base beam experienced a degree of hogging. However, relatively little movement of the base beam was recorded. The greatest uplift under the left-hand boundary element was 0.50mm (6.5 percent of the total rise recorded at the top of the unit). The greatest uplift under the right-hand boundary element was 0.80mm (10.8 percent of the

total rise recorded at the top of the unit). Very little slip of the base beam along the floor was recorded. The largest slip occurred at increment 89 and was 0.31mm (3.7 percent of the total top displacement).

8.4.14 Top Beam Behaviour

Very little cracking was observed in the top beam. External strain readings using DEMEC points were omitted for Unit 1.5. The flexural deformations in the top beam, as recorded by the top three dial gauges, were negligible.

8.4.15 Sliding Along Horizontal Construction Joints

The history of sliding displacements along the base construction joint was reported in Section 8.4.6 (Δs). The maximum sliding displacement was 0.93mm at increment 164. This value represents 3.6 percent of the total top displacement.

Along the mid-height construction joint, it was expected that significant sliding would take place because of the marked difference in concrete strengths. (See Table 6.1.) Moreover, when the construction joint was prepared, poor quality concrete was observed in the top of the lower lift due to excessive segregation and accumulation of water. However, despite the relatively poor quality of the construction joint, virtually no sliding displacements were recorded during the test.

No sliding along the top construction joint between the wall and top beam was observed.

8.4.16 Displacements at Diagonal Cracks

Displacements along a few of the major diagonal cracks in Unit 1.5 were measured approximately. The locations of the observation points are shown in Fig. 8.6(b), and displacements perpendicular and parallel to the cracks are summarized in Table 8.2.

TABLE 8.2 - MOVEMENT AT MAIN DIAGONAL CRACKS - UNIT 1.5

Crack No.	at maximum load		maximum crack displacement	
	Perpendicular displacement (mm)	Parallel displacement (mm)	Perpendicular displacement (mm)	Parallel displacement (mm)
1	1.78	-	6.5	6.0
2	1.40	-	3.5	1.0
3	2.54	-	3.5	3.0
4	3.05	1.40	4.0	3.5

SECTION 9

UNIT 2.0
LOADING HISTORY, GENERAL BEHAVIOUR, AND TEST RESULTS

9.1 LOADING HISTORY

The overall dimensions and reinforcement details for Unit 2.0 are shown in Fig. 5.2, and the loading history is shown in Fig. 9.1. Again, as for Unit 1.5, four initial elastic cycles were imposed before the load level $0.75V_i$ was reached. The peak positive and negative displacements reached during the first cycle to $0.75V_i$ were used to calculate the yield displacement, Δ_y, as defined in Section 6.5.3. Up to the first cycle at $0.75V_i$, the test was controlled by load. Thereafter, it was controlled by displacement. In general, the imposed displacement level (Δ/h_w) was increased gradually to a realistic maximum of Δ/h_w=1/100, with three complete cycles being imposed at each level. At the end of three cycles to Δ/h_w=1/100, the lateral load resistance had not dropped significantly. Therefore, two additional cycles to Δ/h_w=1/100 were imposed in order to better observe the degree of stability of response under repeated cyclic loading to this realistically maximum displacement level. Then, although the most useful part of the test had been deemed to be completed at this point, the wall still retained a high percentage of its original resistance. Therefore, the displacement level was stepped up to Δ/h_w=1/75, at which the lateral load resistance began to drop off. Five full cycles were imposed at this displacement level. Finally, the unit was loaded monotonically to failure in the positive (<--) loading direction. A total of 26.5 cycles were imposed on Unit 2.0.

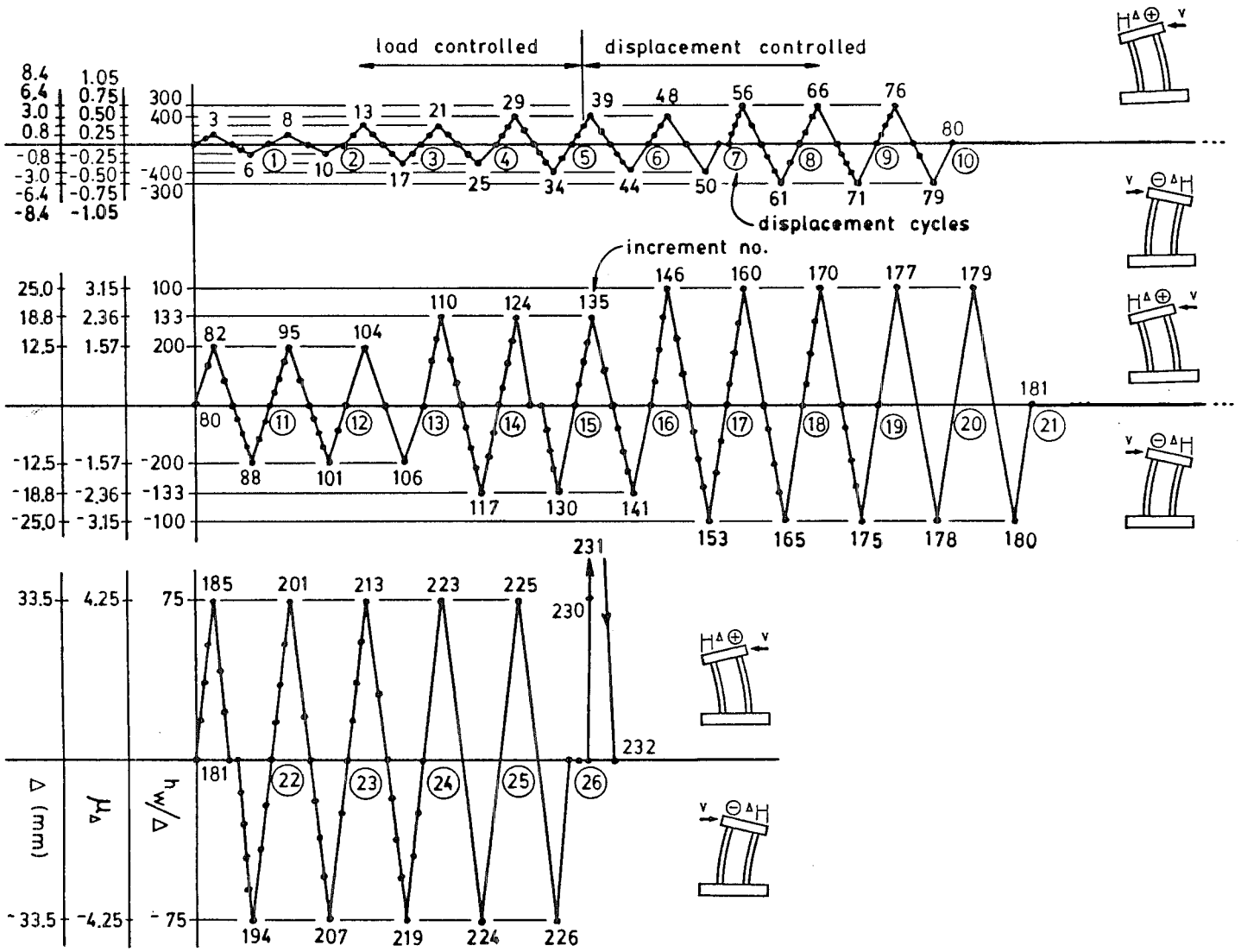

Fig. 9.1 - UNIT 2.0 - Loading history

9.2 DESCRIPTION OF OBSERVED BEHAVIOUR

Increment Number	Description
3-10	First cracking was observed: horizontal cracks in boundary elements and one inclined crack in the web within only the lowest 400mm of the wall.
13	Positive loading. Horizontal flexural cracks (spaced at approximately 90mm, the hoop spacing) formed in the right-hand boundary element (RHBE) up to a height of approximately $0.60h_w$. Two horizontal cracks extended nearly entirely across the web to the left-hand boundary element (LHBE) at the levels of horizontal bars H1 and H2, 610mm and 970mm above the base level respectively. One inclined crack formed in the web from approximately half height.
17	Negative loading. Horizontal flexural cracks (spaced at approximately 90mm, the hoop spacing) formed in the LHBE up to a height of approximately $0.78h_w$. The two horizontal cracks in the web that formed during increment 13 extended over the entire length of the web. An inclined crack (crack 1 in Fig. 9.8) formed with a thudding sound in the web at an angle of approximately 33 degrees from horizontal. It began in the LHBE at a height of 1690mm ($0.68h_w$) and extended downward to within 200mm of the RHBE at a height of approximately 970mm ($0.39h_w$). Some short vertical cracks appeared in the top of the top beam, indicating some hogging.
21-25	No noticeable changes in crack pattern were observed.
29	$V = 0.75V_i = 120kN$. Horizontal flexural cracks in

the RHBE extended up the entire height. Four major diagonal cracks formed approximately simultaneously with a thudding sound, fanning along the main diagonal of the web. (Three of the cracks are numbered 2, 4, and 6 in Fig. 9.8.) Crack 6 extended over the entire length of the web and intersected the LHBE at a height of approximately 250mm above the base level. Cracks 2, 4, and 6 formed at angles of 55, 54, and 51 degrees from the horizontal, respectively. Top deflection = 6.34mm.

34 $V = -0.75V_i = -120kN$. Horizontal flexural cracking extended up the entire height of the LHBE. No significant action seemed to occur in the lower half of the wall below diagonal crack 1. Crack 1 extended to intersect the RHBE at approximately 880mm ($0.35h_w$) above the base level. A major diagonal crack (crack 3 in Fig. 9.8) formed above crack 1. It lay at an angle of roughly 51 degrees from the horizontal and extended approximately half way across the web (Fig. 9.2). Width of crack 1 = 0.90mm. Top deflection = 5.57mm.

$\Delta_y = (4/3) \times (6.34 + 5.57)/2 = 7.94mm.$

39-50 No significant changes in the crack pattern were observed. The widths of cracks 1 and 2 were 0.89mm and 0.76mm respectively.

56 No major changes in behaviour were observed.

61 A major diagonal crack (crack 5 in Fig. 9.8) formed in the lower half of the web. The angle of inclination was approximately 45 degrees from horizontal. The widths of cracks 1 and 3 were 0.76mm and 0.89mm respectively.

66-79 No significant changes in behaviour were observed.

crack	width (mm)
1	0.64
3	1.02
5	0.89
2	1.02

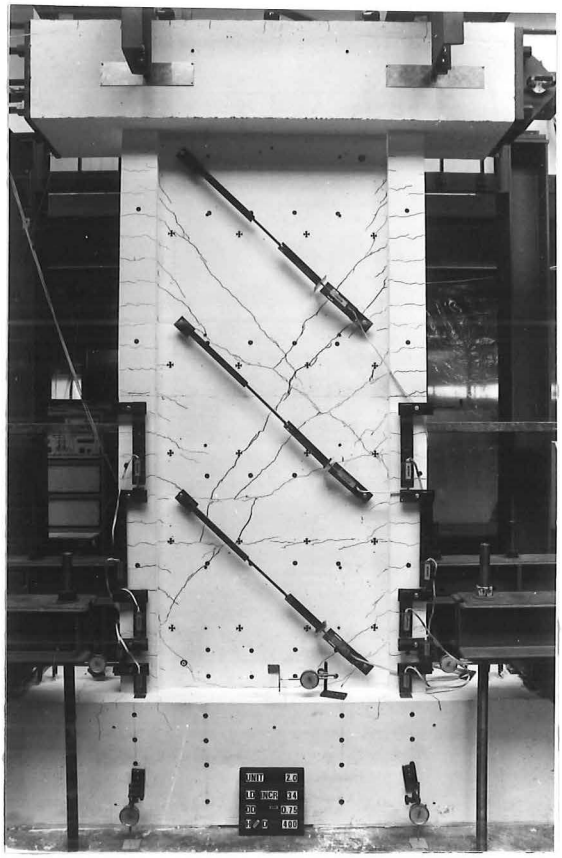

Fig. 9.2 - UNIT 2.0 - Crack pattern at increment 34

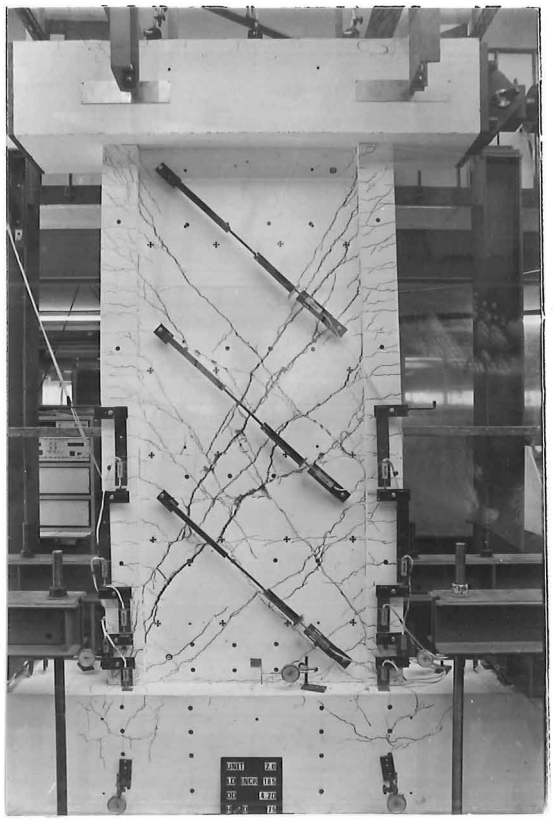

Fig. 9.3 - UNIT 2.0 - Crack pattern at increment 185

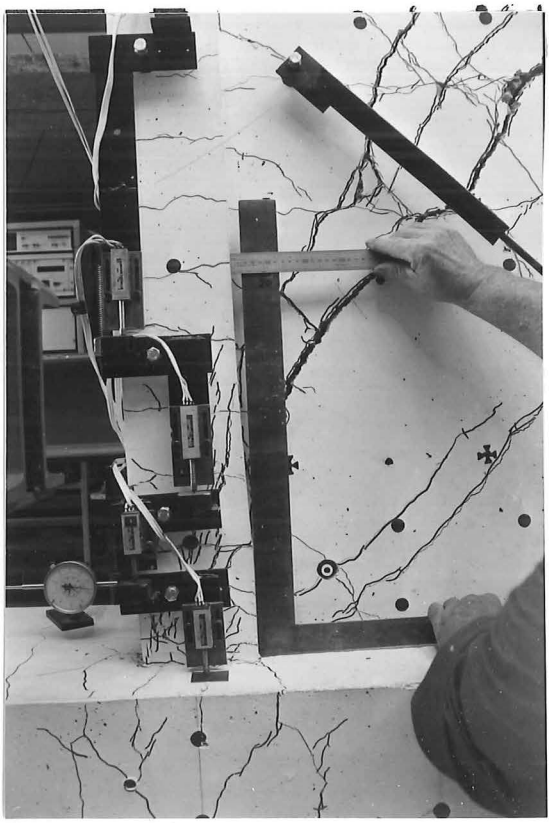

Fig. 9.4 - UNIT 2.0 - Detail of the left-hand boundary element at increment 185

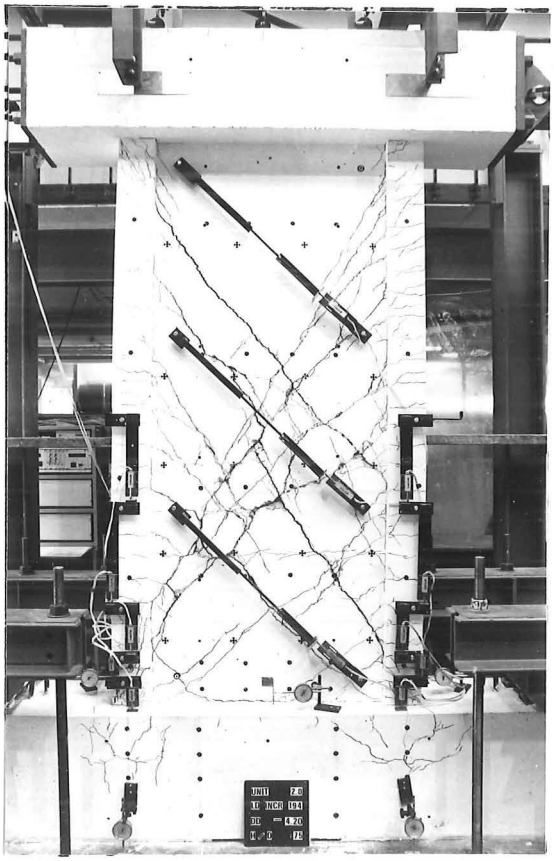

Fig. 9.5 - UNIT 2.0 - Crack pattern at increment 194

82-106 Moderate extensions of existing flexural and diagonal cracks occurred, but no new cracks appeared. At this stage, the two horizontal web cracks that formed at increment 13 were no longer open.

crack	width (mm)
1	0.13
3	1.42
5	1.65
2	2.03
4	1.32

The diagonal cracks appeared to have opened wider in the middle of the web than near the vertical boundary elements.

110 A major diagonal crack (crack 8 in Fig. 9.8) formed in the lower part of the web. It extended from the RHBE at a height of approximately $h_w/3$ down to the left-hand bottom corner of the web. It lay at an angle of approximately 43 degrees from the horizontal. The previously formed diagonal cracks lengthened. The widths of cracks 2 and 4 were 2.54mm and 2.44mm respectively.

117 A relatively steep diagonal crack (crack 7 in Fig. 9.8) formed with a popping sound and extended entirely down to the lower portion of the web, where it intersected the RHBE at a height of approximately 200mm above the base beam. The crack lay at an angle of approximately 66 degrees from the horizontal.

crack	width (mm)	slip (mm)
3	2.16	1.91
5	2.16	-
7	1.65	-

124-141 No major changes in behaviour were observed.

146 The maximum load was achieved. $(V_{max})_{test} = (V_{max})_{pos} = 274kN = 1.71(V_i)_{shear} = 1.07(V_i)_{flex}$. Only minor extensions of existing cracks were observed. The horizontal base crack opened noticeably wider than during previous increments, perhaps indicating the mobilization of the flexural strength of the unit. In the upper right-hand region of the web, crack 4 was widest. In the centre, crack 2 was widest. In the lower left-hand region, crack 6 was widest. The main action seemed to occur not along one particular diagonal crack but along an imaginary corner-to-corner diagonal line.

crack	width(mm)	slip(mm)
2	2.92	1.78
4	2.67	1.27
6	3.18	1.02

153 No major additions to the crack pattern were observed. The base crack opened to 1.5-2.0mm. The same trend in crack widths observed at increment 146 were observed here. In the upper left-hand region of the web, crack 3 was widest, whereas in the lower right-hand region, crack 7 was widest.

crack	width(mm)	slip(mm)
3	2.41	2.5
5	2.79	-
7	3.56	-
base	2.0	-

160-180 The base crack widened. Diagonal cracks that had formed under one direction of load remained open approximately 1mm under loading in the opposite direction. The large slip displacements preempted perfect closure of the cracks, and diagonal compression forces were carried as a series of point loads on the actual points of contact between the two crack surfaces. Accordingly, high local stresses and resulting local crushing of concrete occurred along the cracks.

185 The load tapered off before the specified displacement was reached. Web deformations seemed to be concentrated particularly along the lowest diagonal crack (crack 6). The portion of the wall above crack 6 seemed to have both diplaced to the left and rotated in a counterclockwise direction with respect to the lower portion. A noticeable kink was observed in the LHBE in the region beginning at a height of 150mm and ending at a height of 508mm. Above 508mm, the LHBE appeared to be relatively undeformed. The RHBE seemed to be relatively undeformed up to a height of 510mm but thereafter was observed to be deflected toward the left gradually with height (Fig. 9.3). Spalling was observed in the lower outside region of the LHBE.

crack	width(mm)	slip(mm)
2	3.0	2.5
4	2.5	1.5
6	7.5	5.5

194 $(V_{max})_{neg} = -259kN = 1.62(V_i)_{shear} = 1.01(V_i)_{flex}$ (Fig. 9.5)

crack	width(mm)	slip(mm)
3	4.0	3.5
5	4.5	-
7	5.5	0.5
base	3.0	-
2	1.0	1.5
4	1.0	1.0
6	2.5	1.0

201-226 For positive loading, displacements were concentrated along crack 6. For negative loading, displacements were concentrated along crack 3 in the upper regions of the wall and along crack 7 in the lower regions of the wall. The displacements along the base crack decreased in magnitude during these cycles. New diagonal cracking was observed in the upper regions of both boundary elements. The overall deformations observed at increments 185

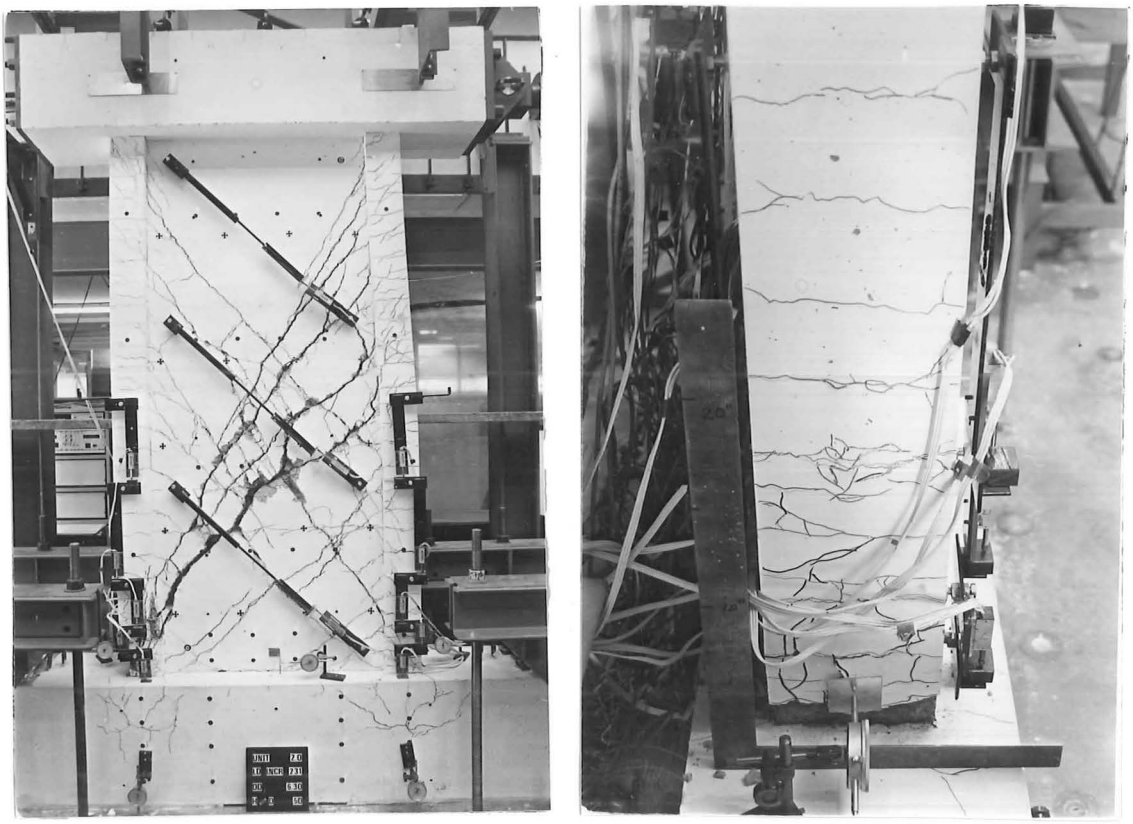

(a) Overall view (b) Left-hand boundary element

Fig. 9.6 - UNIT 2.0 - Crack pattern at increment 231

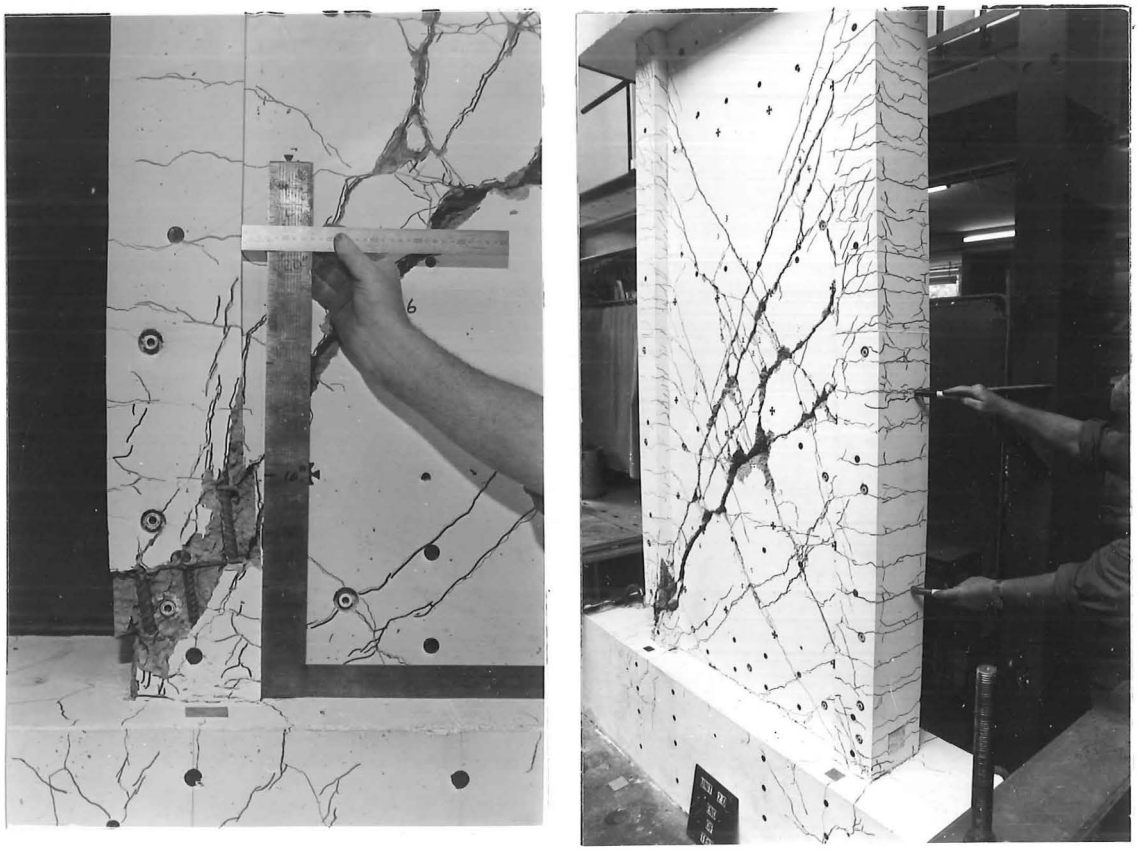

(a) Left-hand boundary element (b) Right-hand boundary element

Fig. 9.7 - UNIT 2.0 - Details of the unit at the end of the test

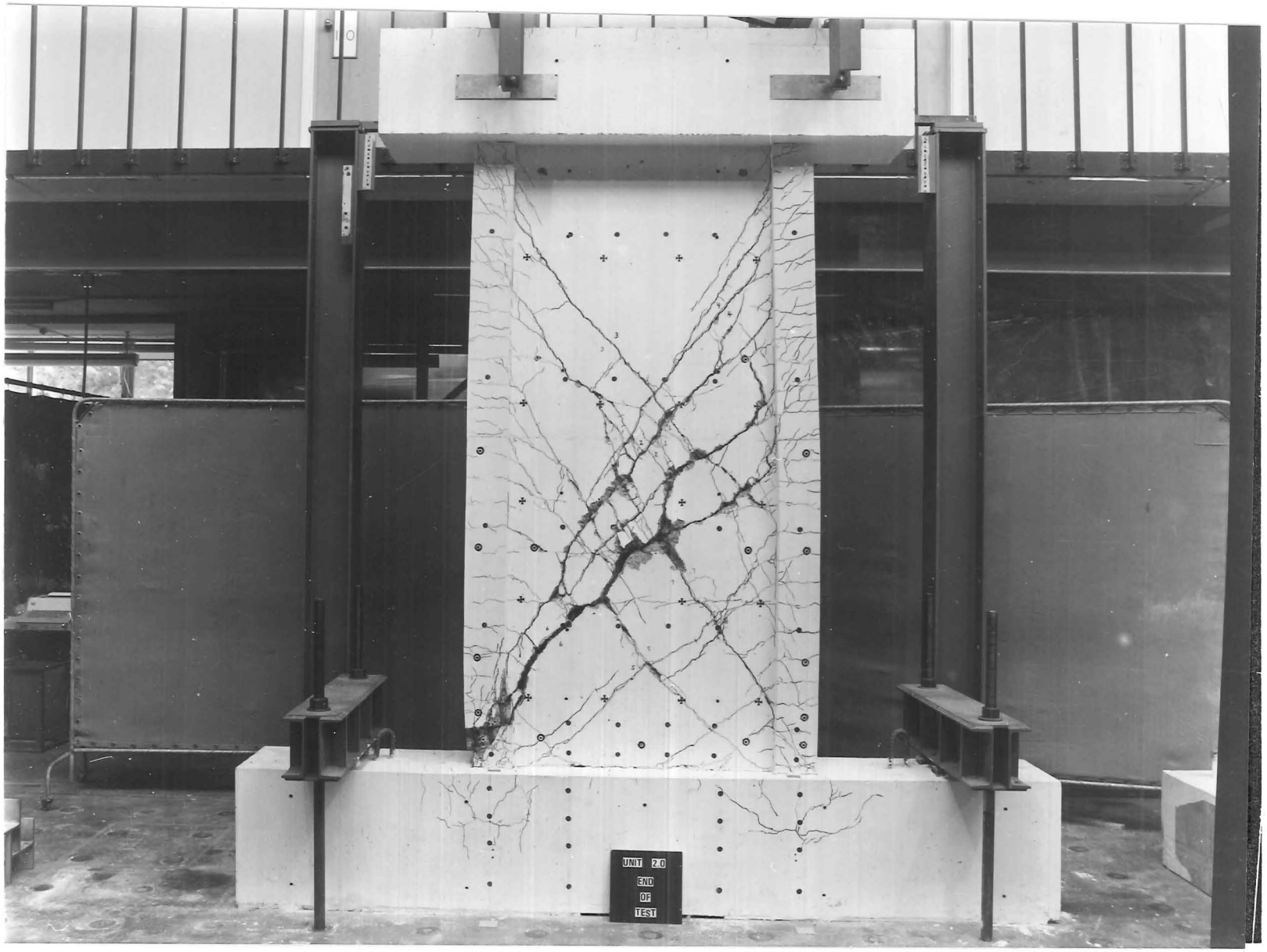

Fig. 9.8(a) - UNIT 2.0 - Crack pattern at the end of the test

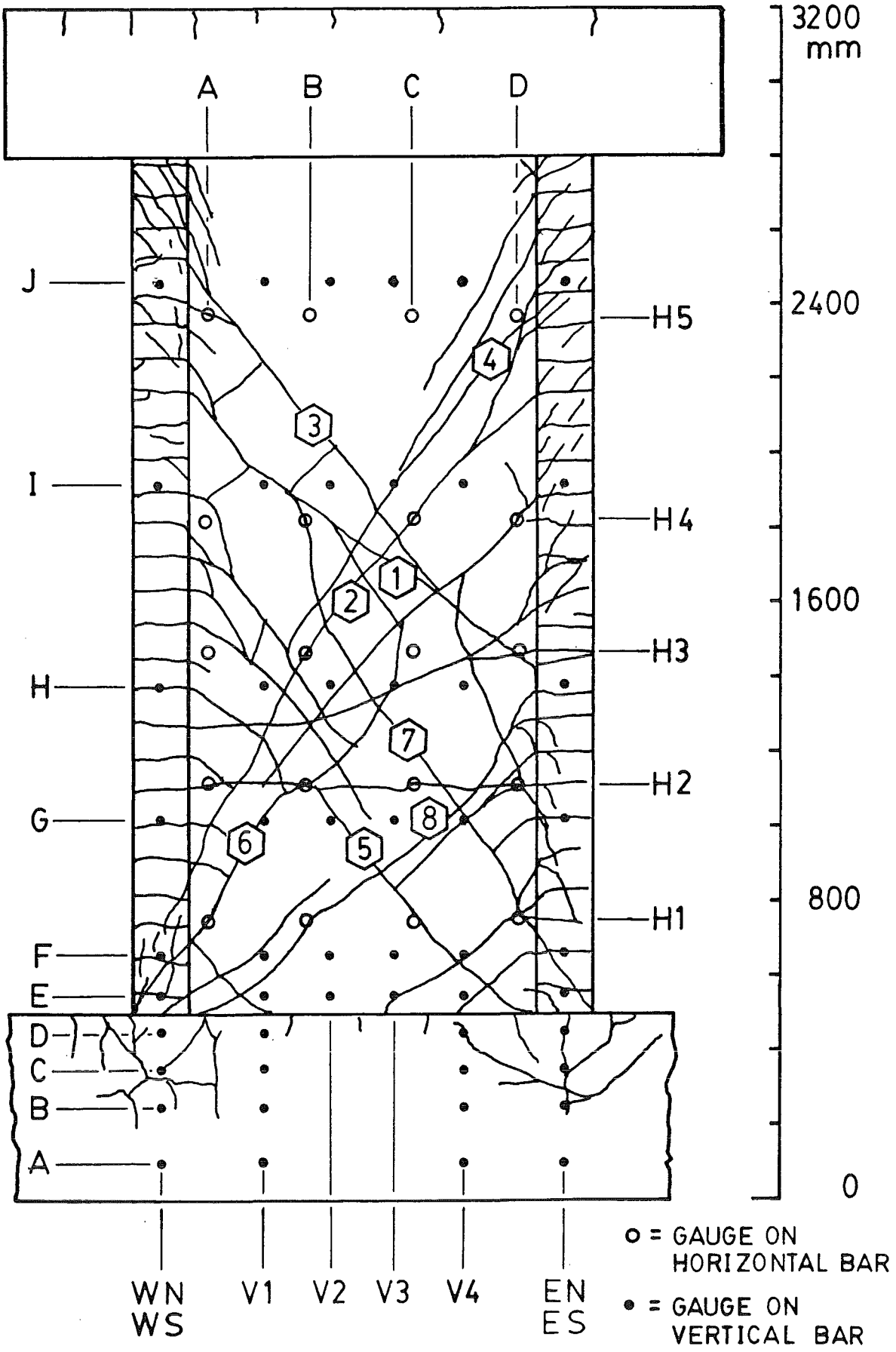

Fig. 9.8(b) - UNIT 2.0 - Crack pattern at the end of the test

and 194 were also observed at these increments.

	positive loading		negative loading	
crack	width (mm)	slip (mm)	width (mm)	slip (mm)
2	3.0	2.5	0.5	1.5
4	3.0	2.5	1.5	1.5
6	13.0	12.0	6.0	7.0
base	0.5	-	2.0	-
3	1.0	2.0	4.5	3.5
5	0.5	-	7.0	0.5
7	1.5	1.0	6.5	0.5

231 A final load push to a top deflection of 50mm (Δ/h_w=1/50) was applied. A 35mm kinking displacement was observed in the LHBE at a height of 150-508mm (Fig. 9.7(a)).Above a height of 508mm, the LHBE remained relatively straight (Fig. 9.6). The RHBE was observed to be relatively straight up to a height equivalent to the top right-hand end of crack 6. Above this level, the RHBE was gradually bent toward the left (Fig. 9.7(b)). An overall photograph of the test unit at maximum displacement in shown in Fig. 9.6.

9.3 FAILURE MECHANISM

The lateral load carrying mechanism of Unit 2.0 was somewhat different from that observed for Units 1.0 and 1.5 and is an example of the slightly more complex model truss behaviour envisioned by MacGregor (Section 3.1). In Units 1.0 and 1.5, the lateral load was carried to the base beam by means of a direct diagonal compression strut extending from the top of the wall down to the bottom compression corner. The diagonal compression strut was defined by a low 45 degree crack. As displacement was increased, further diagonal cracking defining a series of narrower compression struts developed in the upper regions of the wall above this first-formed crack. Arch action was evident both from the reinforcement strain pattern and from the location of the vertical compression resultant.

In Unit 2.0, the first diagonal crack formed in the

upper region of the wall at a slightly steeper angle of approximately 51-55 degrees from the horizontal. (See Fig. 9.9(a).) This crack indicated that the lateral load was carried from the top beam down diagonally until it encountered the compression boundary element at approximately mid-height. The vertical component of this diagonal

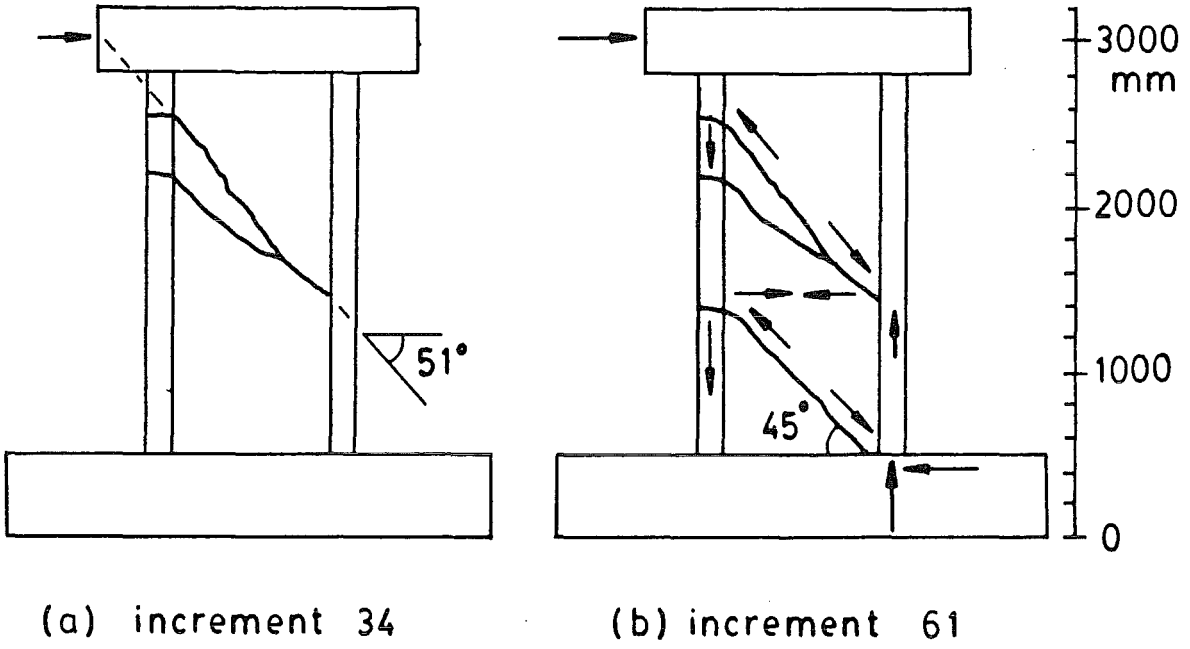

Fig. 9.9 - UNIT 2.0 - Mechanism of lateral load resistance

compression produced compression in the boundary element while the horizontal component was resisted by tension in the horizontal web bars at mid-height. The load carried by these horizontal web bars was substantiated by the strains recorded in bars H3 and H4. This horizontal component was carried back the the tension boundary element, where it entered a lower compression strut, which extended diagonally to the base of the wall. This lower diagonal compression strut was identified by a 45 degree crack that formed later during the test (Fig. 9.9(b)). Very similar behaviour was observed for both loading directions. The load-carrying mechanism is illustrated in Fig. 9.9(b).

As displacement was increased up to the attainment of maximum load, additional diagonal cracks formed between these two diagonal cracks. These additional cracks formed at steeper angles and suggest a readjustment of internal forces such that the upper compression strut steepened.

At the attainment of maximum load, the ideal flexural

strength was slightly exceeded. The formation of additional diagonal cracks ceased. Subsequent displacements occurred along the existing diagonal cracks. As diaplacements increased, crushing and grinding occurred along the diagonal cracks. Progressive yielding of web bars resulted in a noticeable increase in both the horizontal and vertical dimensions of the wall. The main displacements occurred not along one particular diagonal crack but along an imaginary line running from corner to corner of the wall. This line separated the unit into two regions. After the attainment of maximum load, the mechanism involved, first, a severe horizontal displacement of the upper portion with respect to the lower portion and, second, a rotation of the upper portion about its lower corner. (Refer Fig. 7.8.) Severe spalling and kinking of bars occurred along the diagonal cracks. A final load push in the positive (<---) direction accentuated the mechanism involved. See Fig. 9.6. The left-hand (compression) boundary element experienced a horizontal offset of 35mm between the heights of 150 and 500mm above the base beam. This boundary element was virtually undeformed above a level of 500mm. The right-hand (tension) boundary element experienced a gradual lateral deformation starting from an elevation of 1100mm above the base beam (a level equivalent to the top of crack 6). In the compression boundary element, the deformation took place over a relatively short distance of 450mm, whereas in the tension boundary element, the deformation took place over the entire upper half of the wall. For details of the unit at the end of the test, see Figs. 9.6 and 9.7.

9.4 TEST RESULTS

As for Units 1.0 and 1.5, noticeable stability was observed in most aspects of behaviour during repeated cycles to a given displacement level.

9.4.1 Elastic Cycles

Load cycles to $\pm 0.50V_i$ produced significant cracking but no yielding of reinforcement. The stiffness at $0.50V_i$ was calculated to be 26.9kN/mm. At a load level of $0.75V_i$, the experimental yield displacement was determined (as

outlined in Section 6.5.3) to be 7.94mm. The predicted yield displacement was 4.90mm (Appendix B), ie. 62 percent of that observed.

9.4.2 Lateral Load vs. Total Top Displacement

The hysteretic loops for lateral load vs. total displacement at the top of the wall unit are shown in Fig. 9.10. For the first four load/displacement levels (increments 1 to 64), only the envelope curve is drawn. Starting at Δ/h_w=1/200, all the loops are drawn. The slopes of the loops are flatter than those for both Unit 1.5 and Unit 1.0. This observation indicates, as expected, that Unit 2.0 was the most flexible of the three. As for Units 1.0 and 1.5, the loops for Unit 2.0 are pinched, with significant pinching occurring after the first cycle. Pinching of the loops and energy dissipation are discussed further in Section 9.4.4.

The reduction in lateral load resistance on repeated cycling is summarized in Table 9.1 and plotted in Fig. 9.11. As was observed in Units 1.0 amd 1.5, little lateral load was lost prior to the attainment of maximum load. The average reduction in resistance before the attainment of maximum load was 3.7 percent, which is of the order of the average reduction for Units 1.0 and 1.5 prior to maximum load. After maximum load was reached, lateral load resistance dropped significantly after the first cycle. (See increments 185 and 201 in Fig. 9.10.) However, as cyclic loading continued, some stability of lateral load resistance was reestablished. (See increments 160,170,177,179 and 213,223,225 in Fig. 9.10.) The behaviour of the unit would most likely have stabilized after a large number of cycles to a particular displacement.

A maximum load of 274kN was attained at Δ/h_w=+1/100. The strength exceeded the predicted ideal shear strength by 71.2 percent and the predicted ideal flexural strength by 7.0 percent.

As seen in Fig. 9.10, the stiffness of the unit degraded with increased displacement level. The reduction of stiffness as well as other relevant quantities is summarized in Table 7.2.

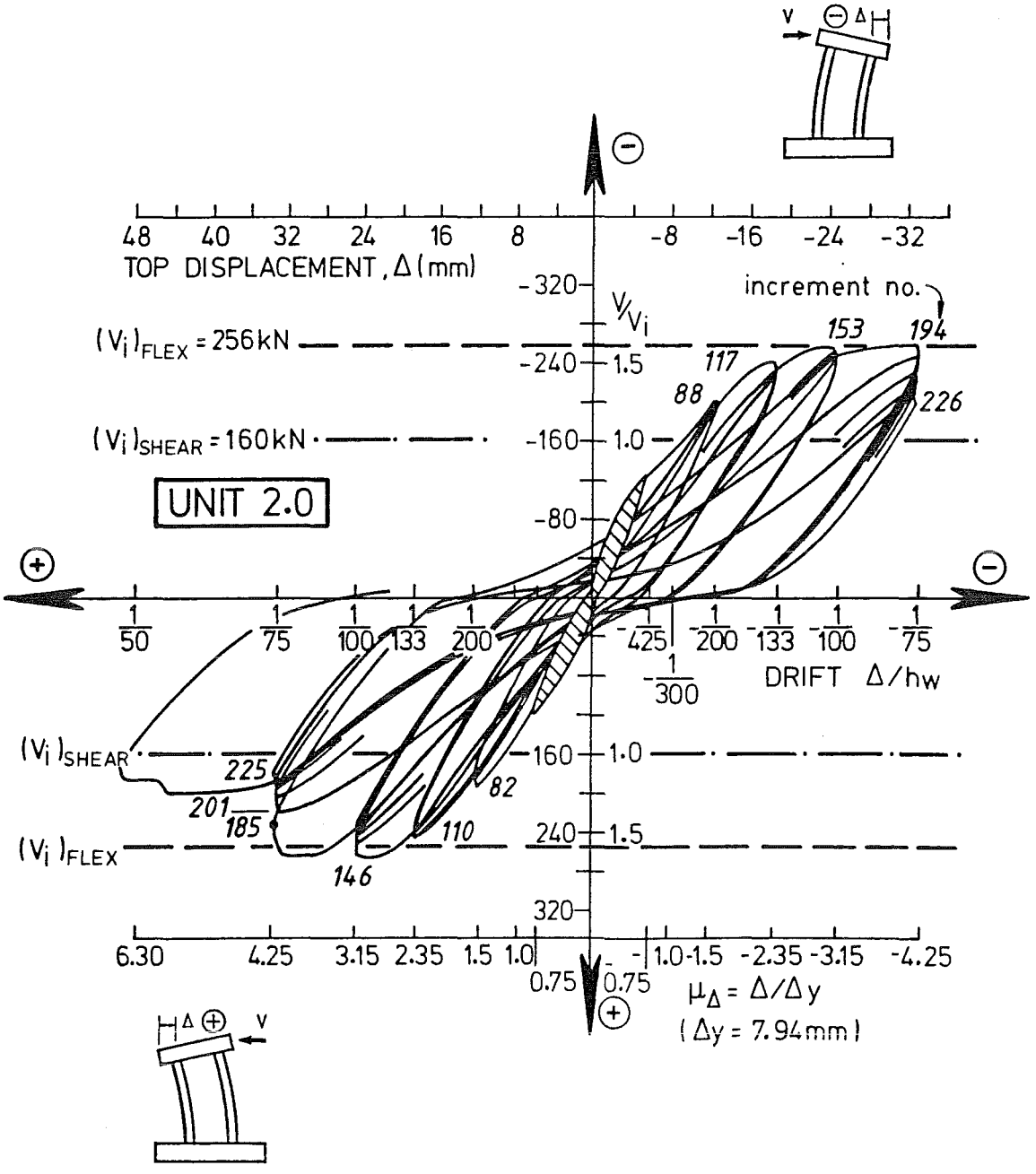

Fig. 9.10 - UNIT 2.0 - Lateral load vs. top displacement

TABLE 9.1 - UNIT 2.0 - LATERAL LOAD RESISTANCE DEVELOPED ON CONSECUTIVE CYCLES

Load/displacement level	Positive loading ←			Negative loading →		
	Increment No.	Lateral load (kN)	Reduction in lateral load (%)(1)	Increment No.	Lateral load (kN)	Reduction in lateral load (%)(1)
$V = 0.25\ V_i$	3	40	-	6	40	-
	8	40	-	10	40	-
$V = 0.50\ V_i$	13	80	-	17	80	-
	21	80	-	25	80	-
$V = 0.75\ V_i$	29	120	-	34	120	-
	39	120	-	44	117	2.5
	48	114	5.0	50	114	5.0
$\Delta/h_w = 1/300$	56	149	-	61	151	-
	66	148	0.7	71	142	6.0
	76	143	4.0	79	141	6.6
$1/200$	82	196	-	88	197	-
	95	190	3.1	101	190	3.6
	104	190	3.1	106	187	5.1
$1/133$	110	249	-	117	244	-
	124	248	0.4	130	233	4.5
	135	missing	-	141	227	7.0
$1/100$	146	274(2)	-	153	255	-
	160	253	7.7	165	251	1.6
	170	248	9.5	175	247	3.1
	177	241	12.0	178	246	3.5
	179	238	13.1	180	243	4.7
$1/75$	185	241	-	194	259(2)	-
	201	221	8.3	207	247	4.6
	213	206	14.5	219	231	10.8
	223	196	18.7	224	215	17.0
	225	193	19.9	226	206	20.5
$1/50$	230	191	-	-	-	-

(1) Reduction is taken as a percentage of the lateral load developed during the first cycle to the given displacement level.

(2) Maximum load for the given loading direction.

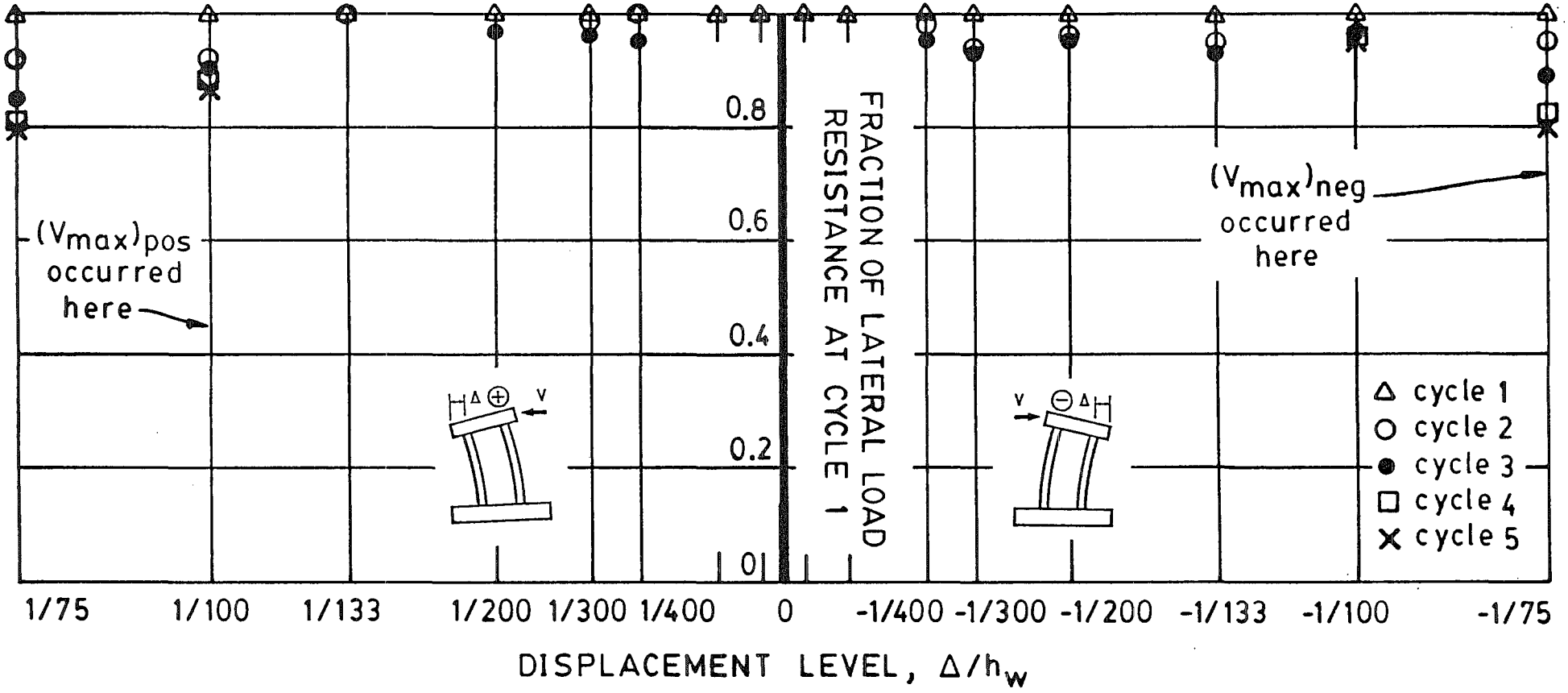

Fig. 9.11 - UNIT 2.0 - Lateral load resistance developed on consecutive cycles

9.4.3 Cumulative Displacement Ductility and Strength Reduction

The precautions stated in Section 7.5.3 concerning the calculation of cumulative displacement ductility apply here also. The loading history and cumulative displacement ductility for Unit 2.0 are shown in Fig. 9.12. Although the cumulative ductility was 31 at the atainment of maximum load and 72 after a subsequent drop in load of 20 percent, these figures cannot be directly compared with the NZS 3101 standard of 32 because the code requirement assumes that maximum load is reached at the first application of a ductility of μ_Δ=1-2. The test unit had undergone three cycles to μ_Δ=1.05, three cycles to μ_Δ=1.57, and three cycles to μ_Δ=2.36 before it reached maximum load at μ_Δ=3.15. Compare Fig. 9.12 with Fig. 2.1. The gradual buildup of cumulative ductility on the test unit was less severe than the code envisages.

9.4.4 Dissipation of Energy

The energy dissipated by Unit 2.0 during each cycle is shown in Fig. 9.13(a). The results follow the same trend that was observed for Units 1.0 and 1.5. The energy dissipated per cycle increased with displacement level. In Fig. 9.13(b) is shown the reduction in energy dissipated on consecutive cycles to a given displacement. Again, the same trend recorded for Units 1.0 and 1.5 is evident here. The energy dissipated per cycle dropped off sharply after the first cycle to a given displacement level, particularly after maximum load was reached.

Fig. 9.14 compares the observed cumulative energy dissipated by Unit 2.0 to that dissipated by the idealized elasto-plastic system of Fig. 4.7 subjected to the same displacement history. Prior to the attainment of maximum load, the cumulative energy dissipated by Unit 2.0 was a relatively high percentage of that dissipated by the idealized elasto-plastic system. After maximum load, the cumulative energy dissipated by Unit 2.0 levelled off at approximately 35 percent of that for the idealized elasto-plastic system.

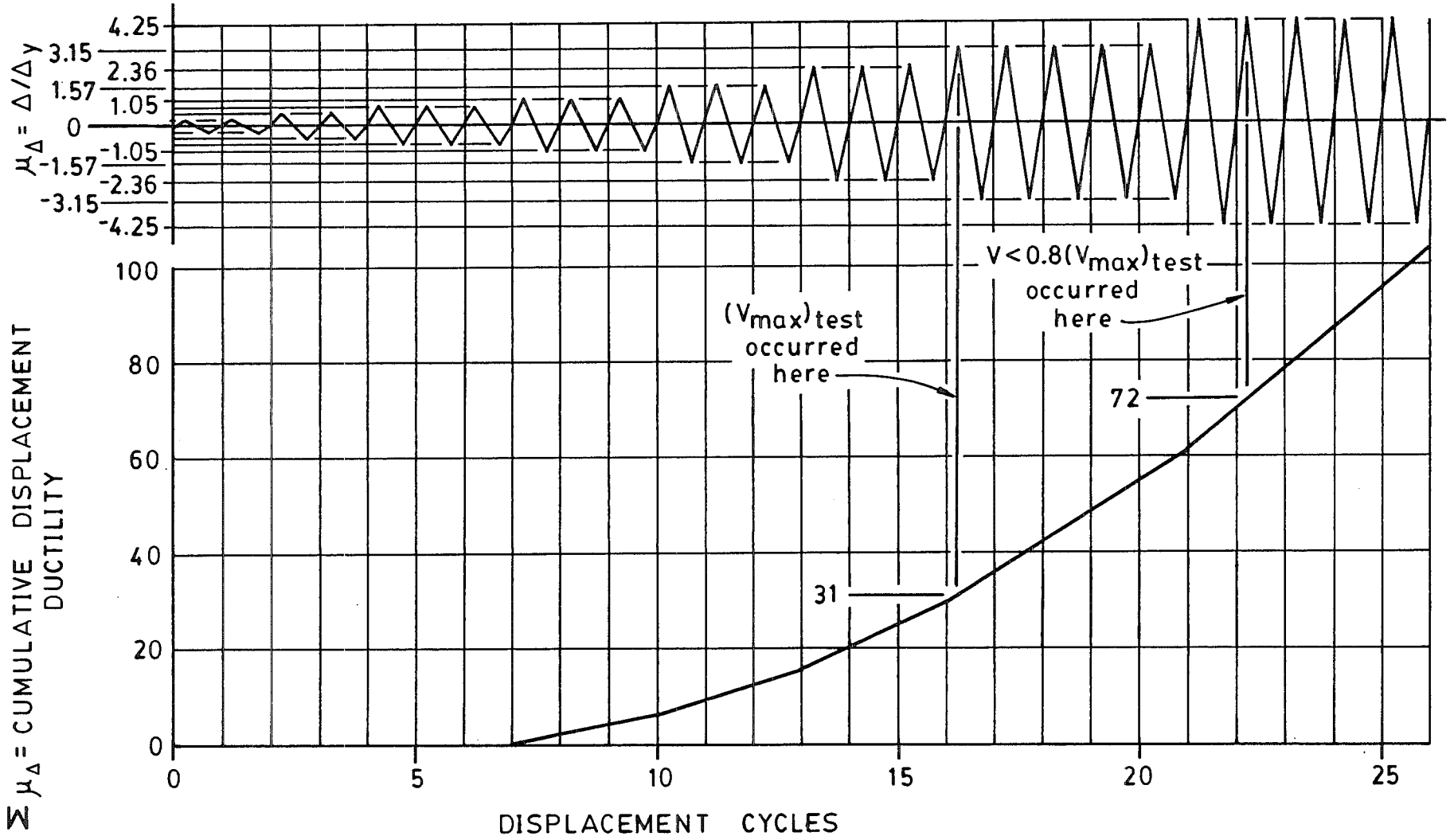

Fig. 9.12 - UNIT 2.0 - Loading history and cumulative displacement ductility

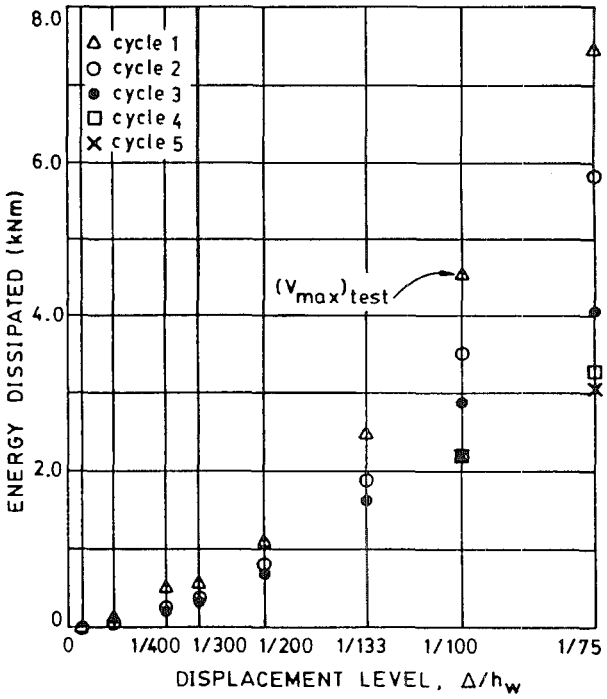

(a) Energy dissipated on each cycle

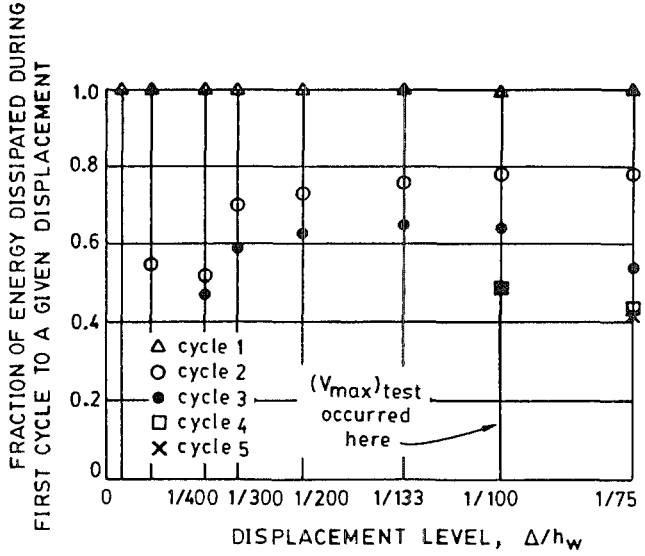

(b) Loss of energy dissipation on consecutive cycles

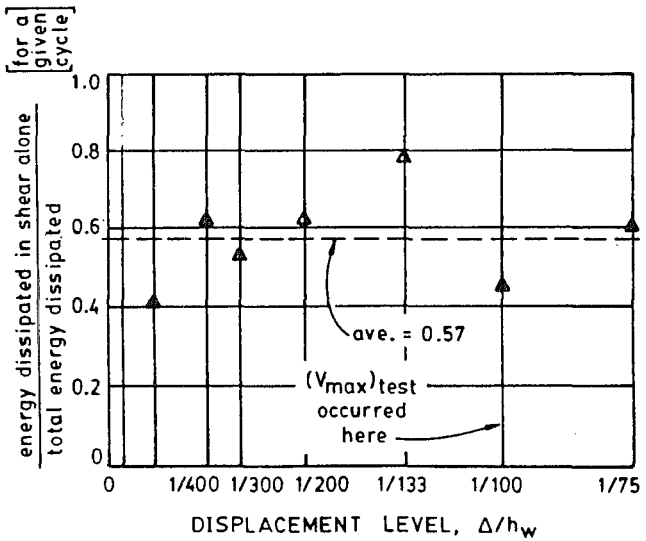

(c) Energy dissipated in shear alone

Fig. 9.13 - UNIT 2.0 - Energy dissipation characteristics

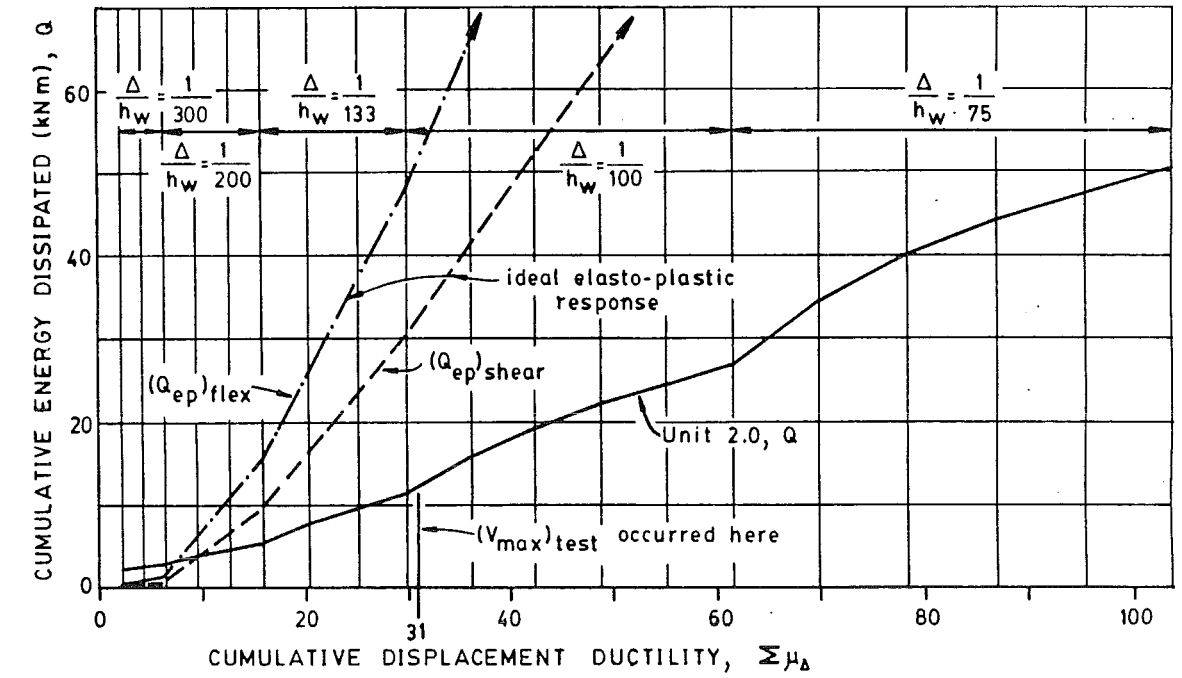

(a) Cumulative energy dissipated

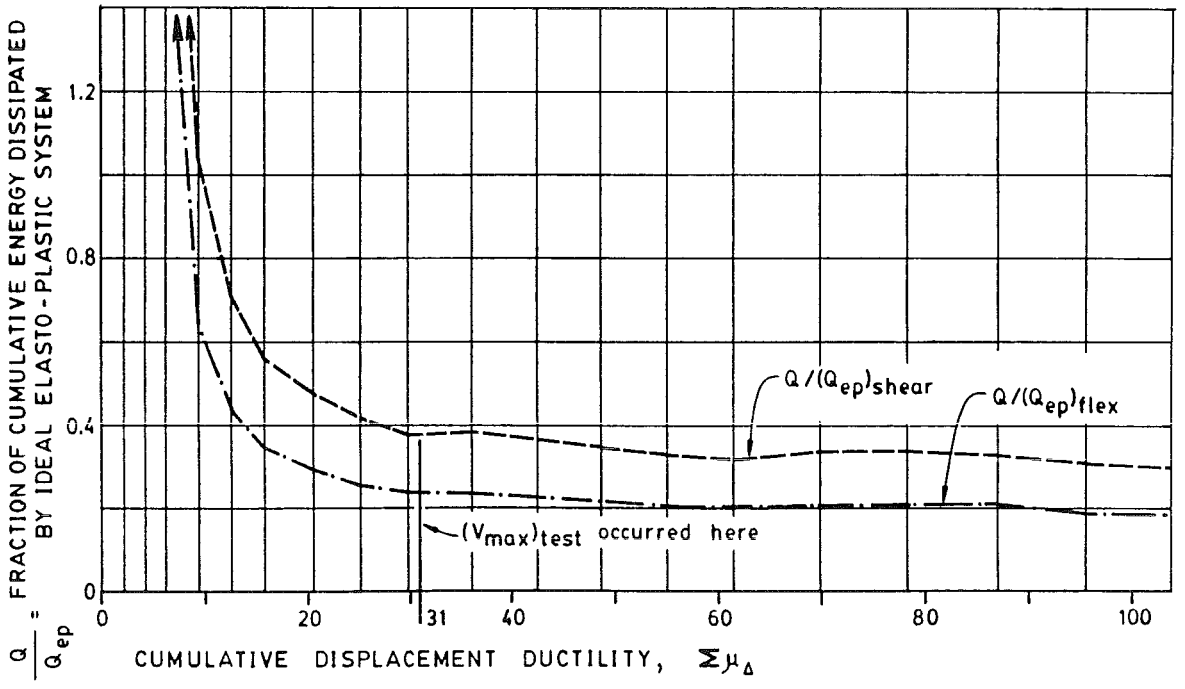

(b) Fraction of idealized response

Fig. 9.14 - UNIT 2.0 - Cumulative energy dissipated vs. cumulative displacement ductility

9.4.5 Lateral Load vs. Top Displacement Due to Shear Deformations

Fig. 9.15 shows the hysteretic loops for total lateral load vs. top displacement due to shear deformations alone. Although these loops are similar in shape to the loops for total top displacement (Fig. 9.10), the shear-induced displacements account for only just over half of the total top displacement. In Units 1.0 and 1.5, shear deformations accounted for a larger percentage of the total top displacement. More will be presented about this in the following section. Fig. 9.13(c) shows the ratio of the hysteretic area of the shear loop to the hysteretic area of the total displacement loop for each cycle. In comparing first cycle loops, a trend similar to that found for Units 1.0 and 1.5 is evident. The fraction of the energy dissipated in shear alone decreased as the test progressed, until maximum load was reached. Thereafter, the fraction of energy dissipated in shear alone increased. The energy dissipated in shear deformations alone averaged approximately 57 percent of the total energy dissipated for each first excursion cycle.

9.4.6 Components of Top Deflection

For Unit 2.0, the components of the top deflection, as illustrated in Fig. 7.18, are plotted in Fig. 9.16. Again, the value of top deflection calculated by summing the individual observed displacement components (Δc) differed very little from the measured top deflection, (Δm). The relative proportions of the observed displacement components are shown in Fig. 9.17. As was observed in Unit 1.5, relatively similar behaviour occurred for both loading directions. A slight difference in behaviour is observed in Fig. 9.17 for the elastic cycles ($V=0.25V_i$, $0.50V_i$). However, the deflection was small during these cycles, and calculation of relative proportions was, therefore, subject to greater error. After the elastic cycles, the pattern of behaviour was quite similar for both loading directions. The Δfe and Δs components amounted to less than 20 percent of the total deflection throughout the test. The shear and flexural components (Δv and Δf) accounted for the major portion of the total deflection. At the first occurrence of diagonal

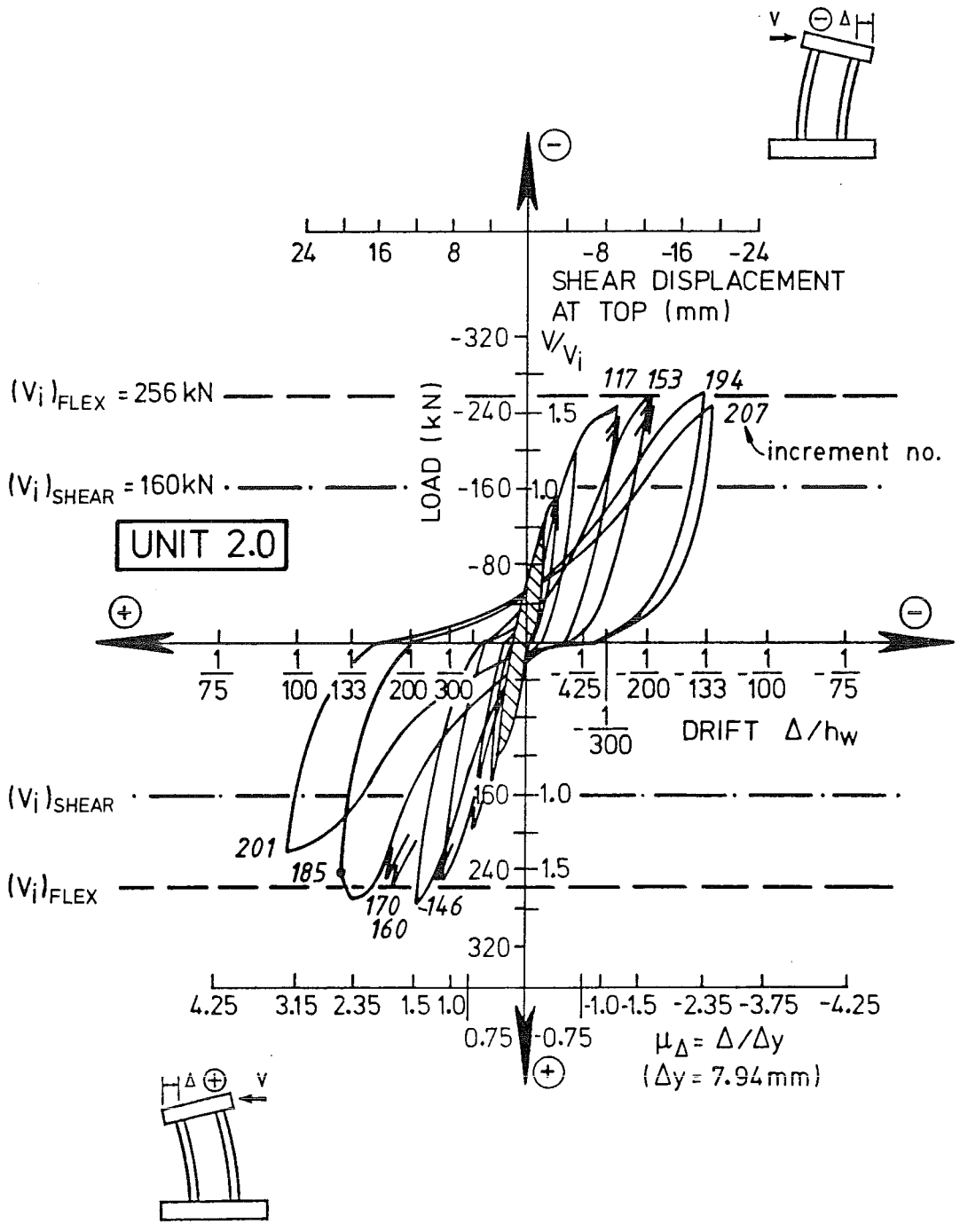

Fig. 9.15 - UNIT 2.0 - Lateral load vs. top displacement due to shear deformations alone

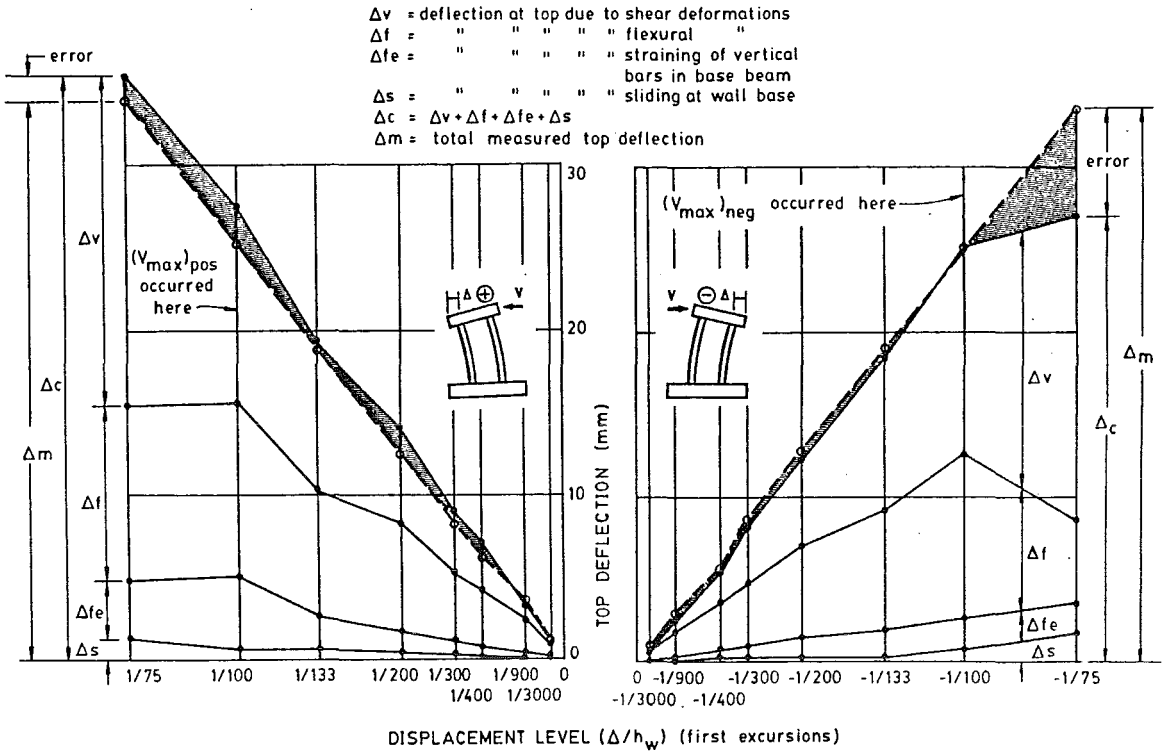

Fig. 9.16 - UNIT 2.0 - Components of top deflection

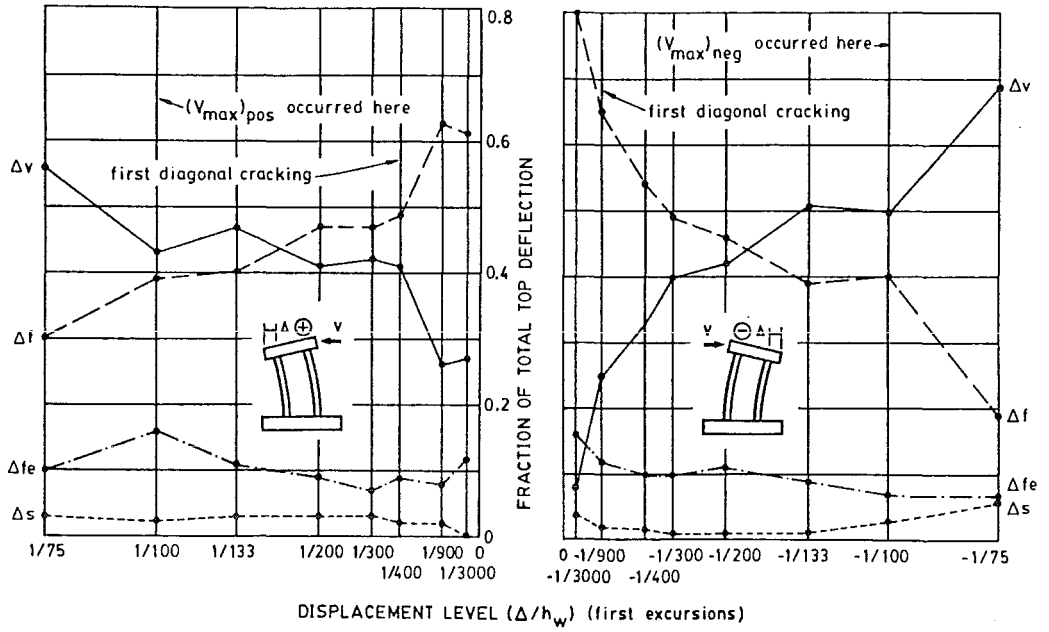

Fig. 9.17 - UNIT 2.0 - Relative proportions of top deflection

cracking, Δf composed roughly 65 percent of the total, while Δv composed roughly 25 percent. Between the occurrence of the first diagonal crack and the attainment of maximum load, diagonal cracking continued and stabilized in the upper region of the wall. These developments were marked by the gradual decrease in Δf from 65 to 40 percent and the corresponding increase on Δv from 25 to roughly 50 percent (Fig. 9.17). After the attainment of maximum load, the Δv contribution rose sharply to 55 and 70 percent for the two loading directions, while the Δf contribution dropped sharply to 30 and 20 percent. In summary, flexural behaviour dominated the initial stages of the test. As the test unit was displaced further, shear behaviour (in the form of a strut and tie mechanism) came into effect. At failure, shear deformations dominated behaviour.

9.4.7 Strains in Horizontal Web Bars

The positions of instrumented horizontal web bars for Unit 2.0 are shown superimposed on the crack pattern at the end of the test in Fig. 9.8(b). Plots of the strains in these horizontal bars are shown in Fig. 9.18. Gauges crossed by cracks are marked with an asterisk in the plots of Fig. 9.18.

As was found in Units 1.0 and 1.5, strains along the main diagonals of the wall reached yield as diagonal cracking occurred. Strains exceeded yield as the wall was displaced further. Along the main diagonals, horizontal strains were generally greater than vertical strains. Off the main diagonals, horizontal strains remained generally less than yield.

9.4.8 Strains in Vertical Boundary Element Bars

Selected longitudinal bars in the vertical boundary elements were instrumented as shown in Figs. 6.7(c) and 9.8(b). The plots of strain in these bars are shown in Fig. 9.19. In the comnpression boundary element, strains were small. In the tensile boundary element, strains were approximately uniform with height above the base level. This pattern of uniform strain is indicative of arch action. (See Section 3.4.) Strains reached approximately yield strain throughout the wall height as the ideal flexural strength was

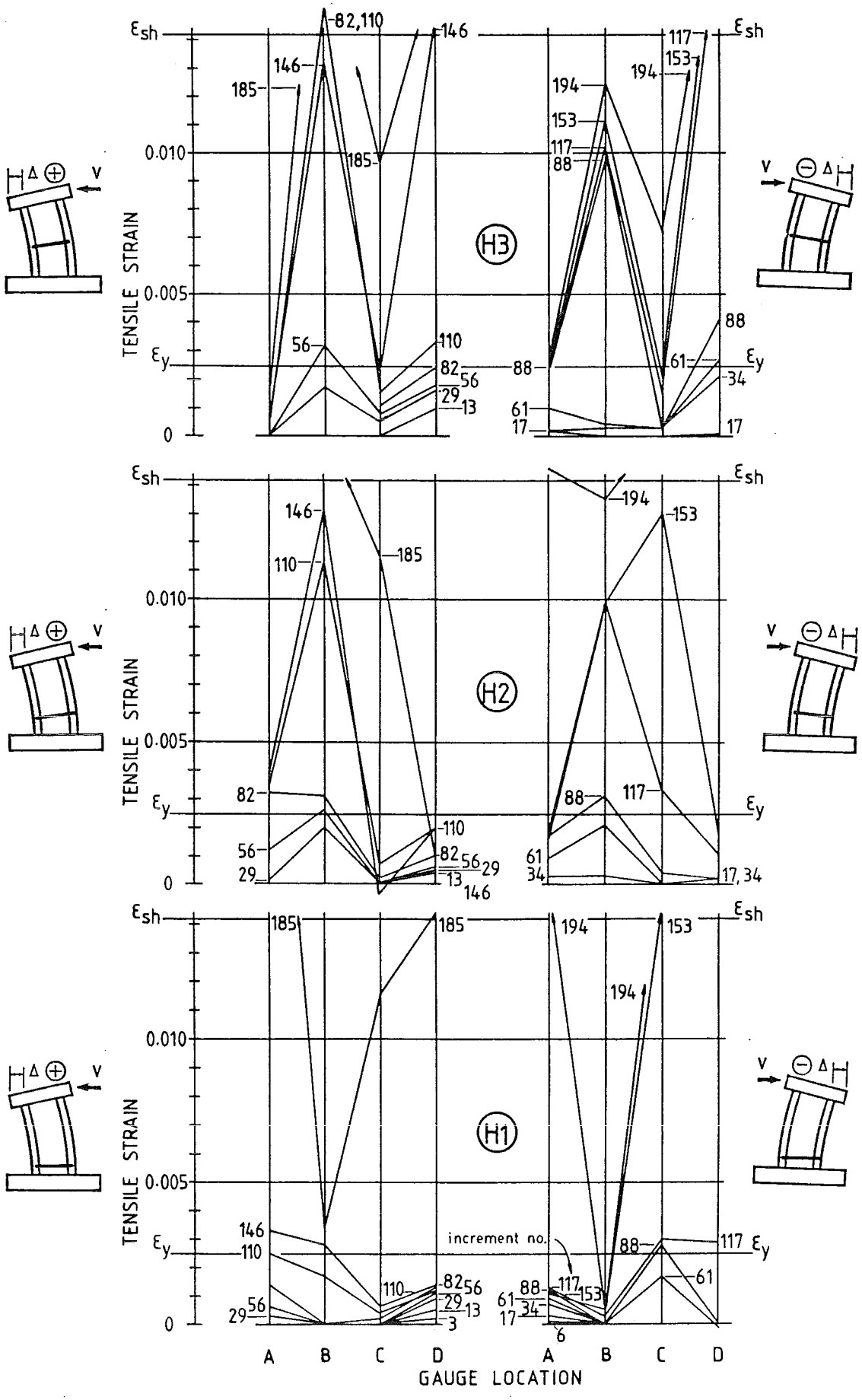

Fig. 9.18 - UNIT 2.0 - Strains in horizontal web bars H1, H2, & H3

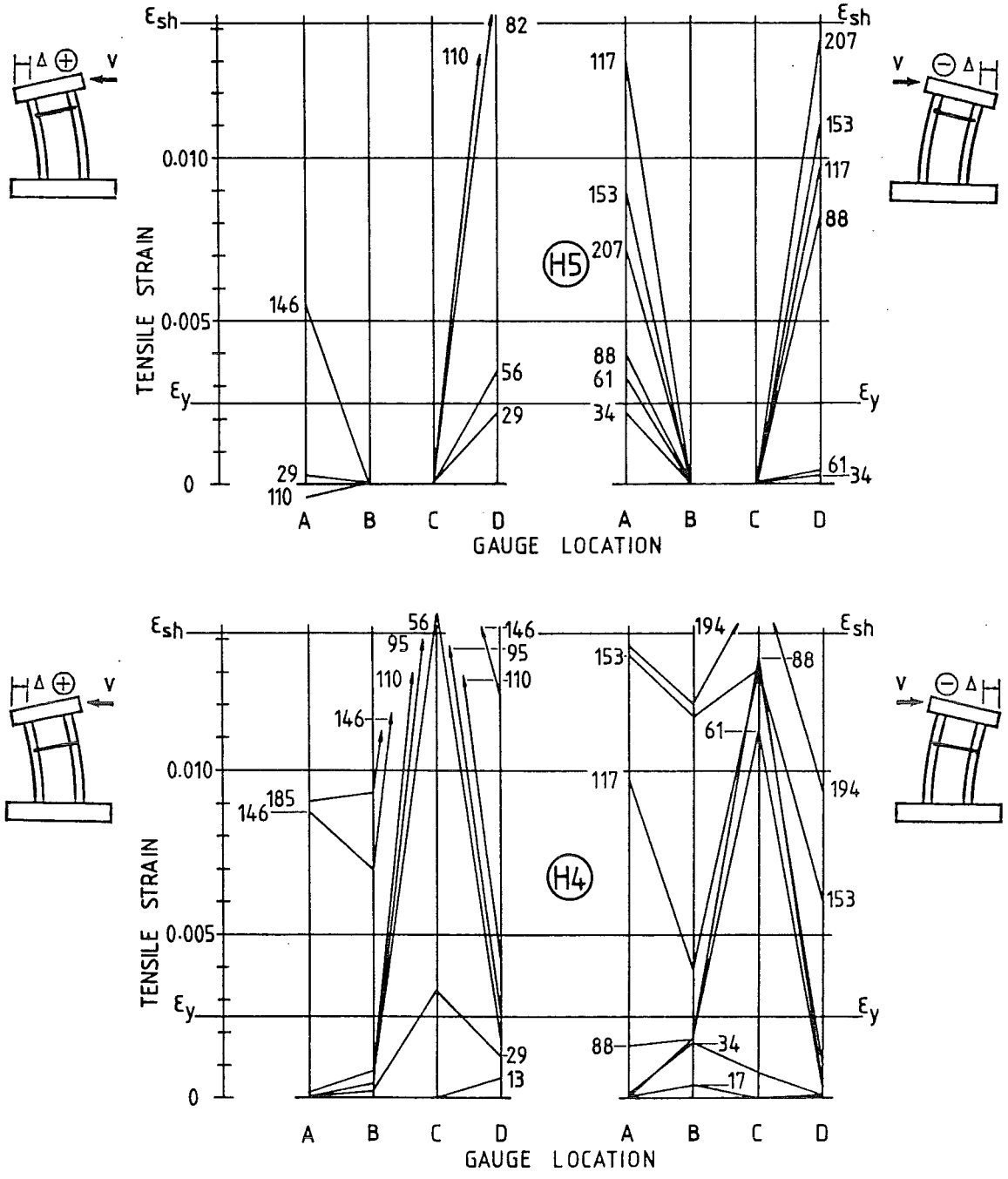

Fig. 9.18 (continued) - UNIT 2.0 - Strains in horizontal web bars H4 & H5

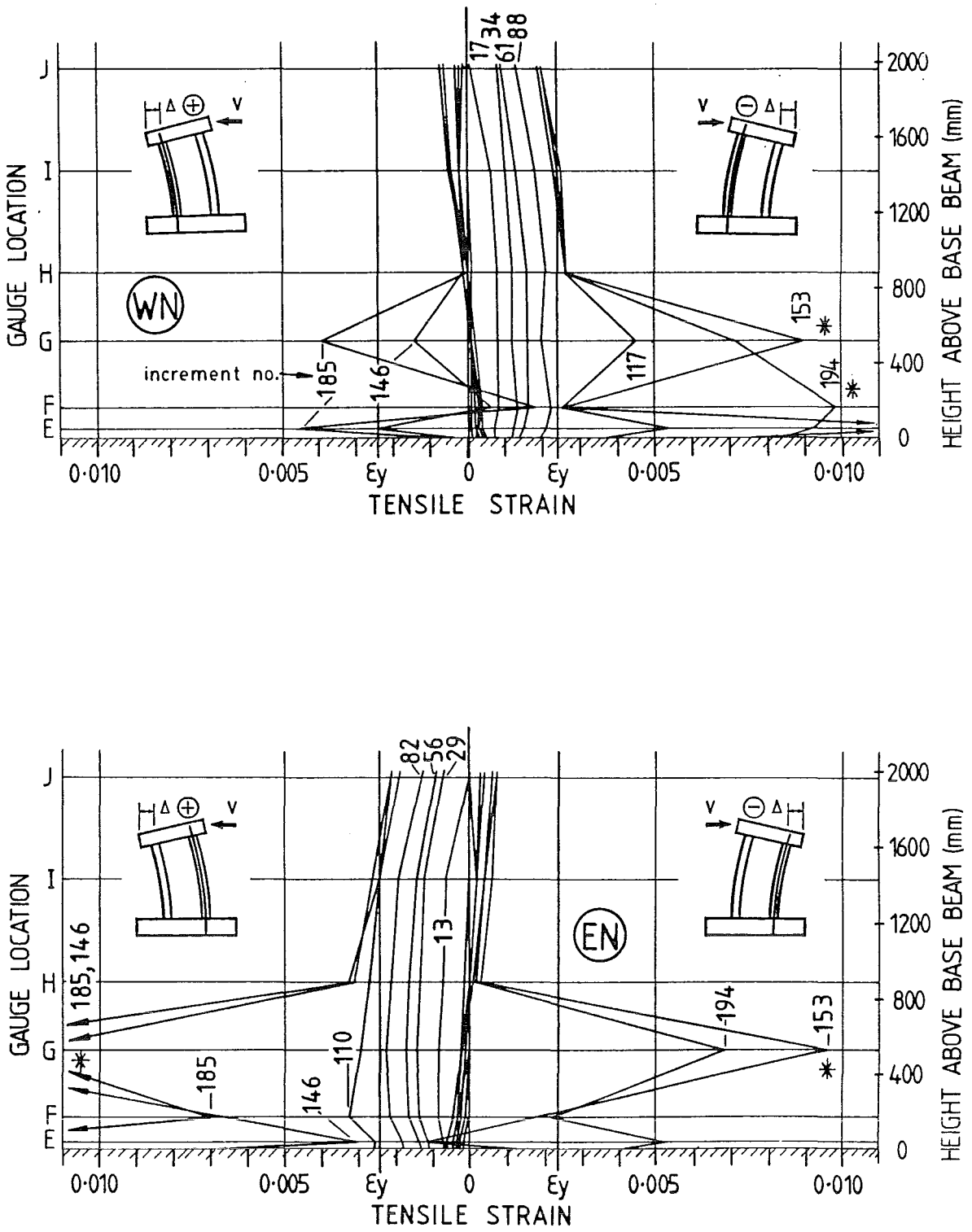

Fig. 9.19 - UNIT 2.0 - Strains in vertical boundary element bars WN & EN

attained (increments 146, 153). Again, strain peaks occurred where a gauge was crossed by a crack. These peaks are marked with asterisks.

9.4.9 Strains in Vertical Web Bars

Strains along the four instrumented vertical web bars (Figs. 6.7(c) and 9.8(b)) are shown in Fig. 9.20. When comparing the plots for Units 1.5 and 2.0, note should be taken that in Unit 2.0, bars V1 and V4 lie relatively far away from the boundary elements. They lie approximately halfway between the boundary elements and the centre of the web. Accordingly it is not expected that their strain patterns resemble greatly those of the corresponding vertical boundary element bars. In viewing the plots for all bars, it is seen that strains remained less than yield strain except where a gauge was crossed by a crack. Along the main wall diagonals, strains approached, but rarely exceeded, yield.

Again, special note should be taken of gauges V2I and V3I. The development of compression in these gauges seems to indicate that the vertical compression resultant lay in the middle region of the cross section, indicating strut and tie behaviour. The location of the vertical compression resultant is confirmed in the next section.

9.4.10 Location of the Vertical Compression Resultant

The strains in vertical bars across horizontal gauged cross sections are plotted in Fig. 9.21. As was found in Units 1.0 and 1.5, the neutral axis (the line of zero strain) shifts toward the tension face as elevation in the wall increases. At section E, compressive strains are confined to within 200mm ($0.16x\ell_w$) of the compression face. At section J, compression strains extend to within 330mm ($0.26x\ell_w$) of the tension face.

Stresses were calculated from strains, and bar forces were calculated from stresses, as described in Section 7.5.10. The location and magnitude of the compression resultant were then calculated from the consideration of equilibrium. (Refer to Fig. 7.26.) The calculated locations of the compression resultants on the horizontal gauged cross sections are shown in Fig. 9.22. Once again, the shaded region marks the region within which the

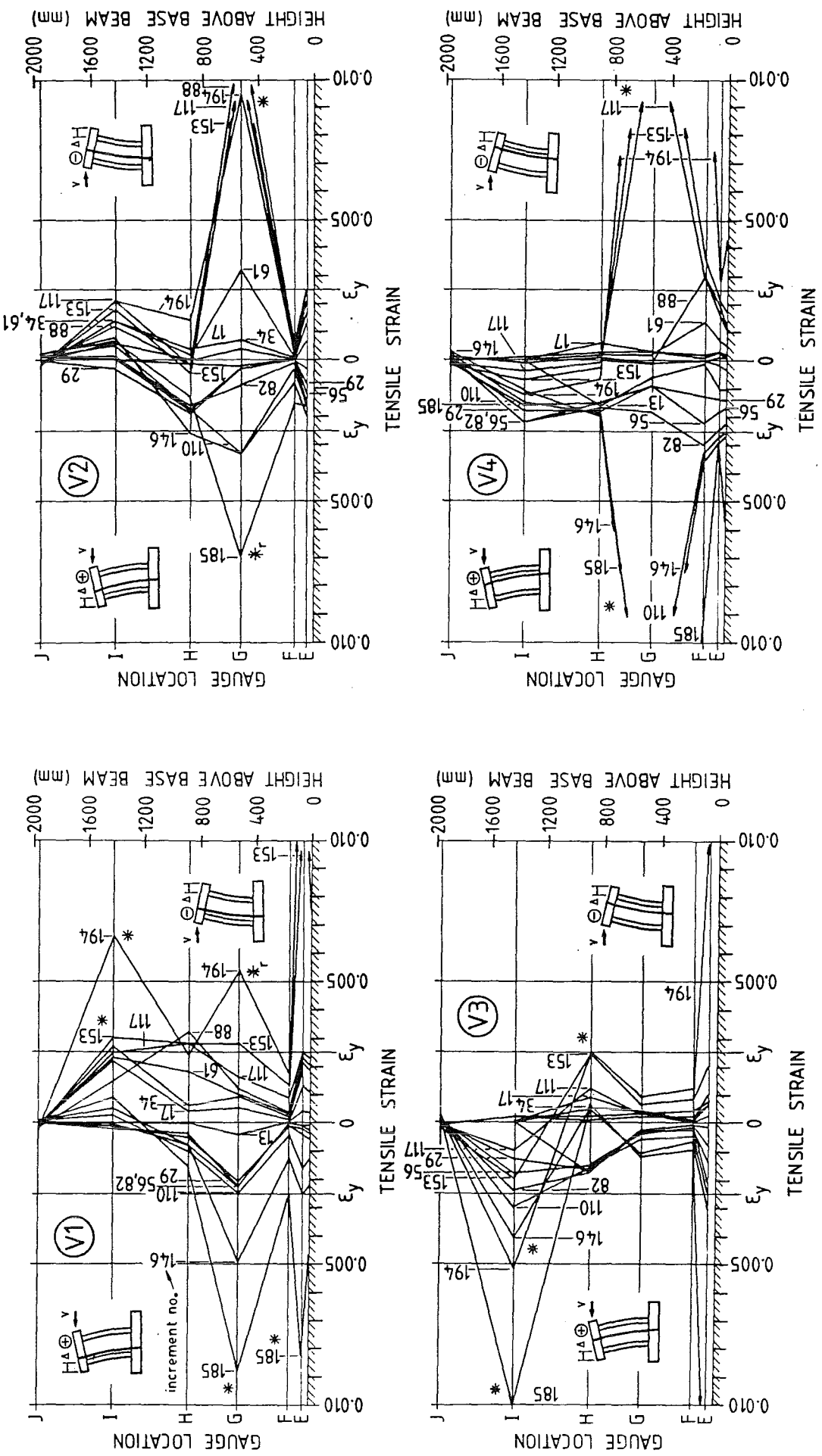

Fig. 9.20 - UNIT 2.0 - Strains in vertical web bars

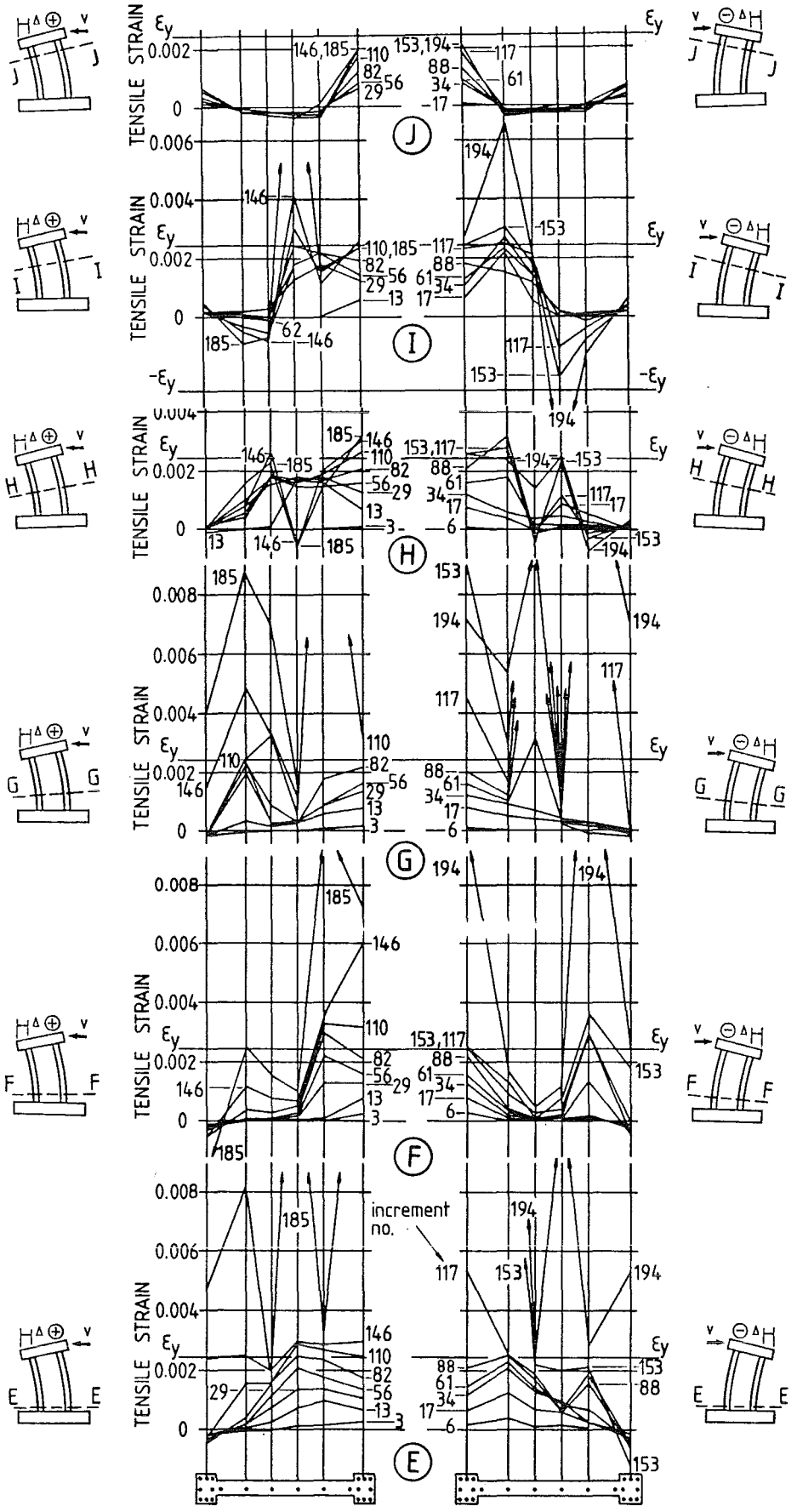

Fig. 9.21 - UNIT 2.0 - Vertical strains on horizontal gauged cross sections

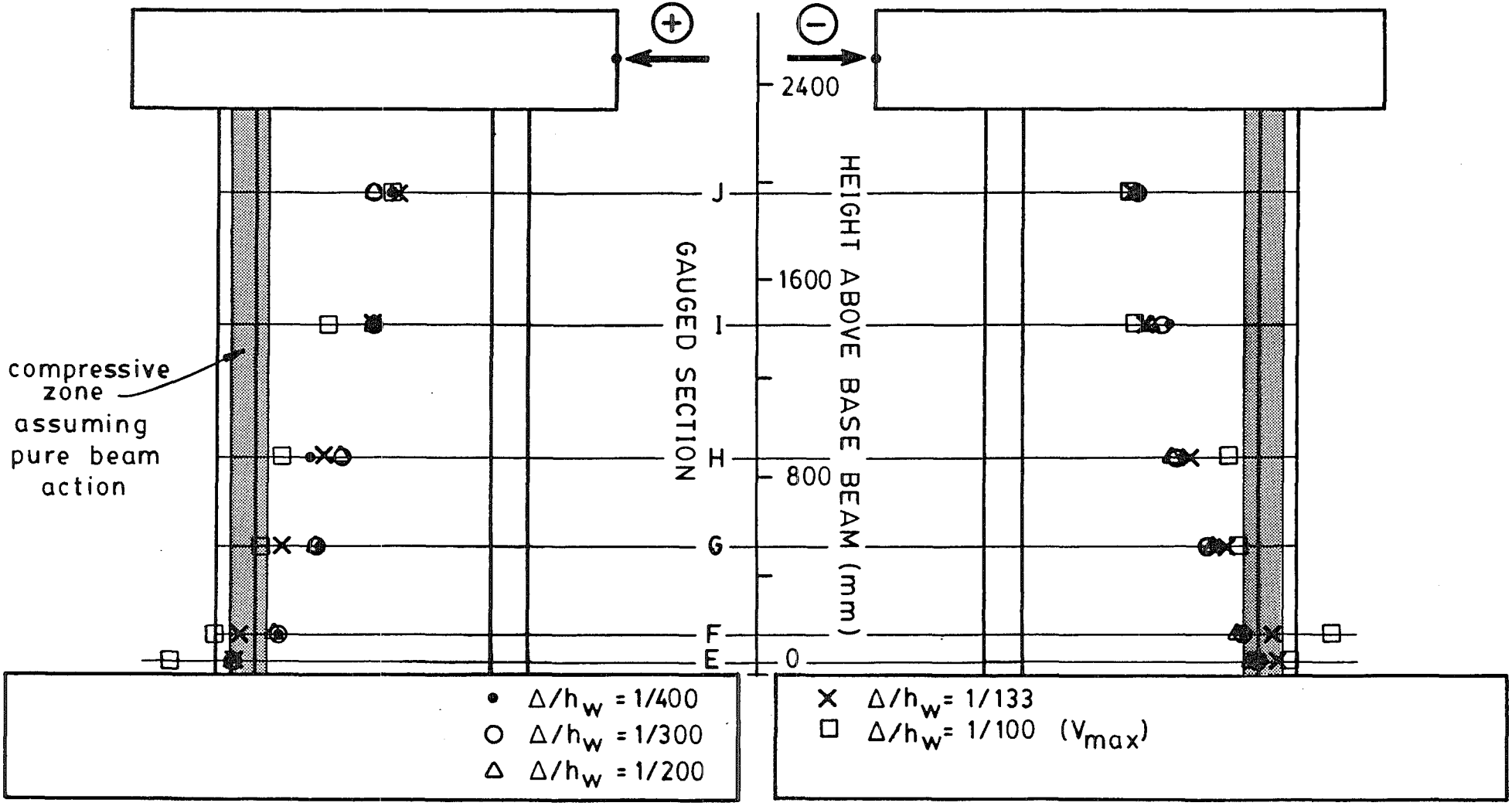

Fig. 9.22 - UNIT 2.0 - Location of vertical compression resultant

compression resultant would have lain in the case of purely flexural behaviour. It is clear that arch action was in effect and that the calculated locations shown in Fig. 9.22 define the main diagonal compression strut.

9.4.11 Strains in Vertical Bars Below Base Level

Vertical bars WN, V1, V4, and EN were instrumented within the base beam in order to record strain penetration into the base. Plots of strain versus depth in the base beam are shown in Fig. 9.23. These strains were integrated to obtain the rigid body movement of the wall described by Δfe in Section 9.4.6. Strains in Unit 2.0 resembled corresponding strains in Unit 1.5. (See Fig. 8.21.) Again, the approximately linear strain with depth indicates that approximately uniform bond stress existed along the bars.

Table 7.3 compares the development length required by NZS 3101 (column A in Table 7.3) with the actual length of penetration of strain beyond the depth of yield strain (column D in Table 7.3). The effect of high strength steel was taken into account in the calculation of development length (parameter m_1). Although the effect of transverse hoops enclosing the vertical boundary element bars within the base beam was considered (parameter m_2), it did not affect the code-required development length. Only the 10mm diameter bars were instrumented in the vertical boundary elements of Unit 2.0. The code requirement was found to be conservative for the 10mm diameter bars. It required a length of embedment slightly greater than that actually utilized during the test. For 6mm diameter bars, however, the code was found to be unconservative. The actual embedment utilized during the test exceeded that required by the code by 57 percent. Thus, Eq. 5-6 of NZS 3101 may not be applicable to such small diameter deformed bars.

As was found for Units 1.0 and 1.5, Table 7.4 reveals no definite correlation between bar properties and strain penetration. However, for the purposes of design, an estimate of Δfe, the top deflection component due to straining of bars below the base level, is made in Section 10.11.

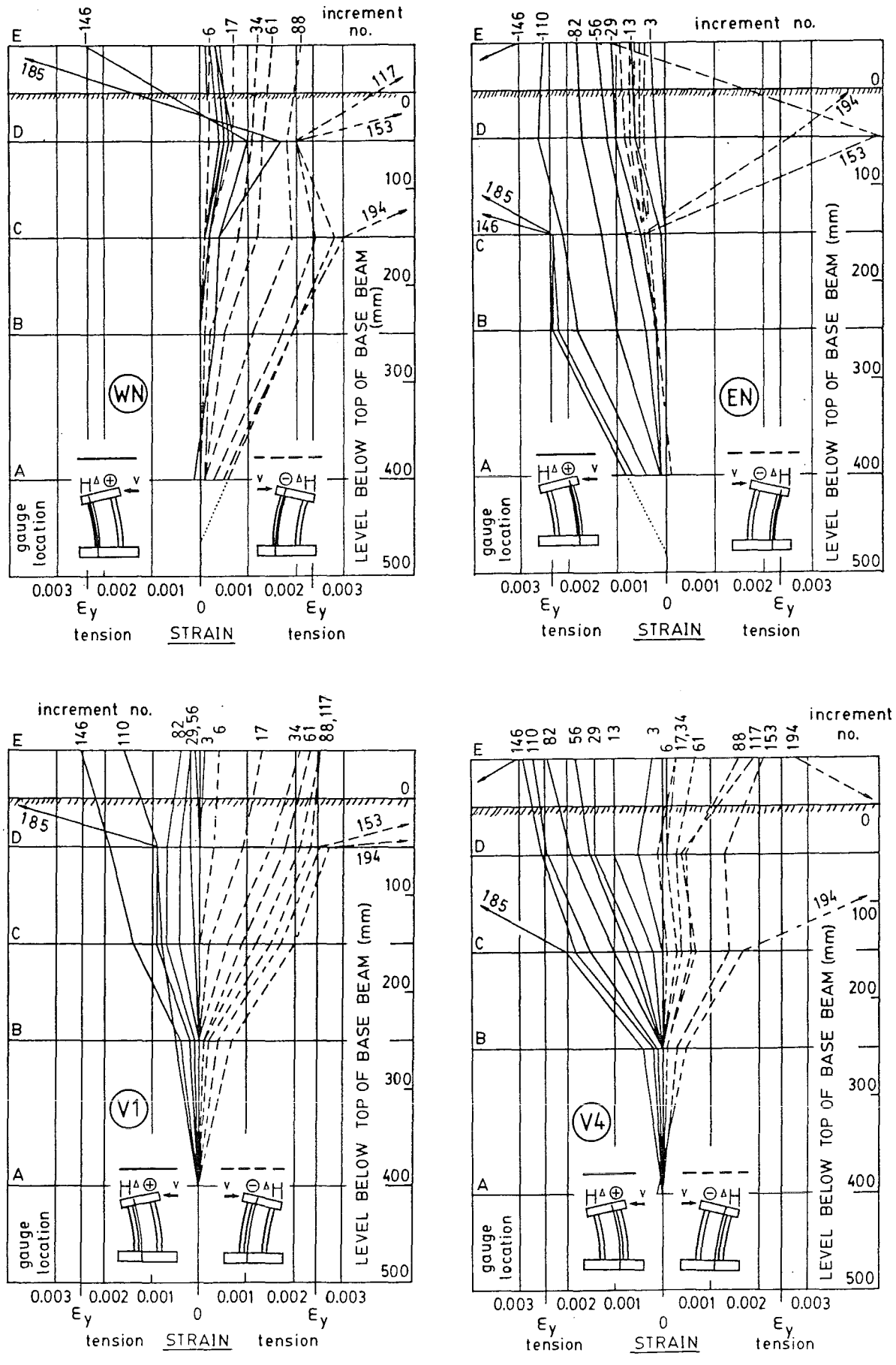

Fig. 9.23 - UNIT 2.0 - Strains in vertical bars in the base beam

9.4.12 Axial Extension of the Wall

As in Units 1.0 and 1.5, an overall axial extension was recorded for Unit 2.0. At maximum load (increment 146), the average axial extension was 4.53mm. The maximum extension was recorded to be 7.77mm at increment 194. The permanent axial extension at the end of the test, with zero load, was 4.20mm. A similar increase in the horizontal length of the wall, especially in the middle region of the wall, was observed with the naked eye. (See Fig. 9.6.)

9.4.13 Base Beam Behaviour

Only minimal action was recorded in the base beam. The maximum uplift under the left-hand boundary element was 0.79mm (6.6 percent of the total axial extension). The maximum uplift under the right-hand boundary element was 1.18mm (12.2 percent of the total axial extension). The maximum slip of the base beam along the floor was recorded to be 0.19mm (0.6 percent of the top deflection) at increment 194.

9.4.14 Top Beam Behaviour

The top dial gauges recorded negligible flexural deformations in the top beam. Some short vertical cracks were observed near the top face of the top beam (Fig. 9.8), but these cracks must have been the result of shrinkage of the concrete during curing.

9.4.15 Sliding Along Horizontal Construction Joints

The history of sliding along the base construction joint was presented in Section 9.4.6. The maximum sliding recorded was 2.13mm at increment 226. This value is approximately 6.4 percent of the total top displacement at that increment. No sliding displacements were observed along the top construction joint.

9.4.16 Displacements at Diagonal Cracks

Displacements along the main diagonal cracks in Unit 2.0 were measured. The locations of the points of observation of crack width and slip are shown in Fig. 9.8(b). A summary of these displacements is presented in Table 9.2.

TABLE 9.2 - MOVEMENT AT MAIN DIAGONAL CRACKS - UNIT 2.0

Crack No.	at maximum load		maximum crack displacement	
	Perpendicular displacement (mm)	Parallel displacement (mm)	Perpendicular displacement (mm)	Parallel displacement (mm)
1	-	-	0.89	-
2	2.92	1.78	3.0	1.78
3	4.0	3.5	4.5	3.5
4	2.67	1.27	3.0	1.5
5	4.5	-	7.0	0.5
6	3.18	1.02	13.0	7.0
7	5.5	0.5	6.5	0.5

SECTION 10

DISCUSSION OF TEST RESULTS

10.1 MAJOR FEATURES OF TEST UNIT BEHAVIOUR

The following observations of the test units reported in this thesis aid in identifying the mechanisms involved:

1) Strains in the vertical bars in the tension boundary element were roughly uniform with height, apart from strain peaks that were recorded where a gauge was crossed by a crack. These strains increased gradually to approximately yield strain at the attainment of maximum load.

2) Strains in the vertical bars in the compression boundary element remained negligible, except at the base, where they were compressive.

3) Strains in the outer-most vertical web bars nearest the boundary elements (bars V1 and V4) resembled the strains in the vertical boundary element bars (ie. uniform with height on the tension side of the unit and negligible on the compression side).

4) Strains in vertical bars at the various gauged horizontal sections indicated that the neutral axis (line of zero strain) shifted toward the tension face as the height of the section above the base of the wall increased.

5) Calculated stresses in vertical bars across the gauged horizontal sections indicated that the vertical compression resultant lay roughly along the main diagonal of the wall, regardless of aspect ratio, h_w/ℓ_w.

6) In the inner-most vertical web bars (bars V2 and

V3), tensile strains along the main diagonals rose to yield strain upon initial diagonal cracking and then to even higher strains as the test progressed further. Above and below the main diagonals, however, strains remained small.

7) In horizontal web bars, tensile strains reached yield only along the main diagonals. Off the main diagonals, strains remained less than half yield.

8) Along the main diagonals, strains in horizontal web bars were generally larger than strains in vertical web bars for a particular displacement increment. This observation was particularly true for Units 1.5 and 2.0. Units 1.0 and 1.5 both ultimately failed when horizontal web bars fractured.

Although both beam action and arch action, discussed in Section 3.1, were present in the test units, observations 1-5 indicate that arch action dominated the response of the units. Wide diagonal shear cracks extending over nearly the entire length of the web formed early in the tests. These diagonal cracks are believed to have defined the direction of the main diagonal compression struts. These diagonal compression struts, being crucial components of the mechanism, subsequently dominated the response of the units.

10.2 LATERAL LOAD RESISTANCE MECHANISMS

In Units 1.0 and 1.5, the lateral load was carried from the top beam to the base beam primarily by the horizontal component of one direct diagonal compression strut at approximately 45 degrees. In Unit 2.0, the lateral load was carried to the base beam by means of a more complex truss mechanism involving two diagonal compression struts tied together at mid-height by horizontal web bars. The upper strut developed at approximately 51 degrees from horizontal, while the lower strut developed at approximately 45 degrees from horizontal. See Fig. 10.1.

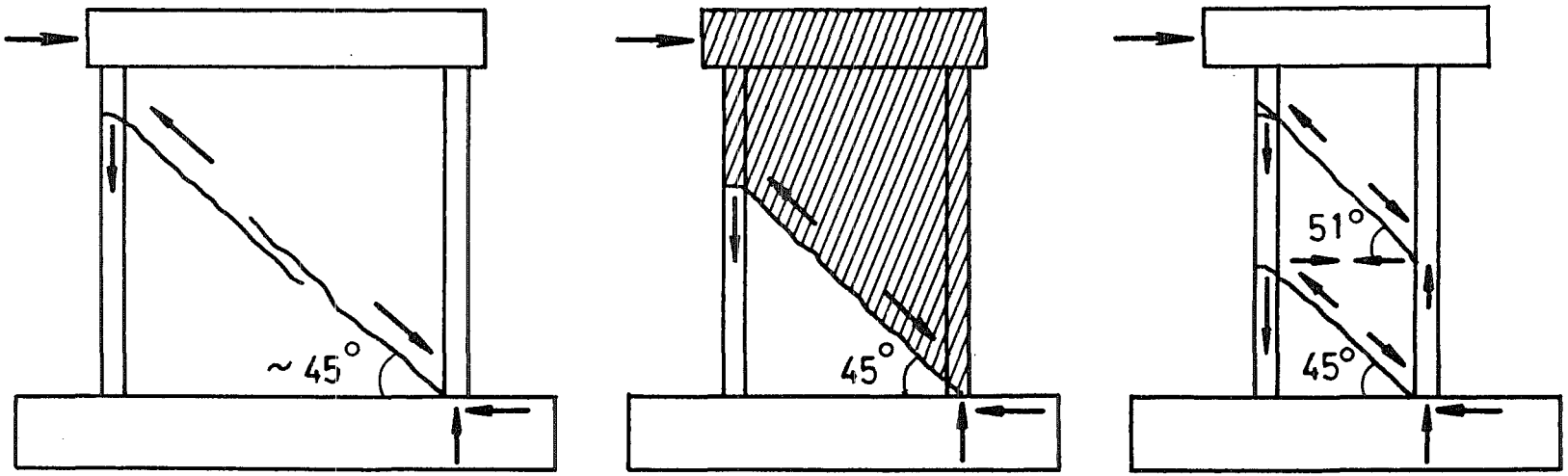

Fig. 10.1 - Mechanisms of lateral load resistance

10.3 FAILURE MECHANISMS

In Units 1.0 and 1.5, as testing progressed, additional diagonal cracks formed above the initial diagonal crack. In Unit 2.0, further diagonal cracks formed in the middle region of the wall between the two initial cracks. For all three units, the ideal flexural strength was exceeded even though the units eventually failed in a shear mode.

All three units experienced expansion in both the horizontal and the vertical directions due to the alternate yielding of reinforcement under reversed cyclic loading. This expansion was particularly noticeable in the middle regions of the wall away from the restraining effects of the top and bottom beams.

The final failure mechanism for each unit involved the horizontal displacement and rotation of the upper region of the wall (such as shown in Fig. 10.1(b)) with respect to the lower region. The horizontal displacement resulted in loss of flexural compression area and severe kinking at the base of the compression boundary element. The deformation of the compression boundary element was similar in all three units. The deformation in the tension boundary element, however, depended upon the unit's aspect ratio (h_w/ℓ_w). The more slender the unit, the more gradual were the horizontal deformations in the tension boundary element. Compare the severe kink in Unit 1.0 (Fig. 7.9) with the gradual bend in Unit 2.0 (Fig. 9.6).

In all three units, horizontal web bars were severely strained along the lowest diagonal crack. In Units 1.0 and 1.5, these bars eventually fractured. Vertical bars on the tension side of the unit were stressed to yield throughout the full height of the wall as they tied down the upper region of the wall.

As slenderness increased, the displacement capacity also increased. Unit 1.0 experienced fracture of horizontal bars at a drift of $\Delta/h_w = 1/90$. Unit 1.5 experienced fracture of horizontal bars at a drift of $\Delta/h_w = 1/70$. Unit 2.0 withstood a drift of $\Delta/h_w = 1/50$ without fracture. The increased displacement capacity is most likely due to the increased flexibility at higher aspect ratios.

10.4 STIFFNESS IN THE ELASTIC, FULLY CRACKED STATE

For the designer, it is important to estimate, for each member in a structure, the stiffness of the unit in the elastic yet fully cracked state. This stiffness is used in estimating the distribution of forces through the building and, therefore, in apportioning the earthquake-induced lateral load to the various structural elements. This was mentioned in Section 2.5.

For normal members responding in a flexural mode, the stiffness in the elastic, fully cracked state has been estimated in the past by measuring the displacement at a load of $V = 0.75(V_i)_{flex}$. This stiffness is easily obtained experimentally because of the controlled nature of flexural response. The ideal flexural strength, $(V_i)_{flex}$, can be calculated with reasonable accuracy, and flexural cracking and associated straining of bars develops gradually and predictably.

However, in the case of walls responding primarily in a shear mode, as the present test units, the estimation of this stiffness is compounded for two reasons. First, the calculation of ideal shear strength, $(V_i)_{shear}$, of such walls is very imprecise. The code (3) suggests a method for calculating shear strength. However, the equations tend to be quite conservative. Second, for walls lightly reinforced in the web, as were the present walls, it is difficult to generate a fully developed and stabilized crack pattern while the wall remains in the elastic state, ie. before significant yielding occurs. A fully developed crack pattern is one in which all major cracks have formed. In all three test units, the web reinforcement yielded upon first diagonal cracking. Therefore, it was not possible to measure the stiffness of the present wall units in the elastic, fully cracked state. The units entered the inelastic range well before the crack pattern stabilized. It was, however, possible to measure the stiffness before diagonal cracking (elastic state) and the stiffness just after the onset of diagonal cracking (inelastic state). Table 10.1 summarizes the values of top displacement predicted by current theory (Appendix B) and those measured during the tests for the conditions just before and just after the onset of diagonal

TABLE 10.1 - COMPARISON OF PREDICTED AND MEASURED DISPLACEMENTS BEFORE AND AFTER DIAGONAL CRACKING

Unit	Load at which Δ_e was measured (kN)	Increment No.	Load just after diagonal cracking (kN)	Increment No.	Δ_e = top displacement just before diagonal cracking			Δ_{dc} = top displacement just after diagonal cracking				
					Δ'_e (1) (mm)	Δ_e (3) (mm)	$\frac{\Delta'_e}{\Delta_e}$	Δ'_{dc} (1) (mm)	Δ''_{dc} (2) (mm)	Δ_{dc} (3) (mm)	$\frac{\Delta'_{dc}}{\Delta_{dc}}$	$\frac{\Delta''_{dc}}{\Delta_{dc}}$
1.0	154	2	231	3	0.86	1.10 (4)	0.78	1.59	3.48	3.27 (4)	0.48	1.06
1.5	100	12 16	150	29 34	1.70	2.07 (5)	0.82	2.93	5.21	4.65 (5)	0.63	1.12
2.0	80	13 17	120	29 34	2.10	2.98 (5)	0.70	3.64	5.62	5.96 (5)	0.61	0.94

(1) prediction using method outlined in ref. 6, Appendix I

(2) prediction using method outlined in Section 10.4

(3) actual measurement displacement

(4) for positive loading only

(5) average of values measured for positive and negative loading

cracking. It is seen that current theory overestimates the stiffness in the elastic state by approximately 23 percent and the stiffness just after the onset of diagonal cracking by approximately 43 percent.

The method used in calculating stiffness was that outlined in ref. 6, Appendix I. There, the estimation of deflection of a cracked reinforced concrete wall responding predominantly in flexure was carried out by separating the total deflection into components due to flexural deformations (Δf), shear deformations (Δv), and anchorage deformations (Δfe). Deflection due to flexural deformation was estimated assuming an effective moment of inertia of the cracked section, I_e, which is found using the well-known Branson formula adopted by both the ACI 318-77 code (27) and the current New Zealand code (3).

$$I_e = \left(\frac{M_{cr}}{M_a}\right)^3 I_g + \left[1 - \left(\frac{M_{cr}}{M_a}\right)^3\right] I_{cr} \qquad \text{(Eq. 10-1)}$$

The flexural component of deflection is obtained by using this effective moment of inertia in the formula for deflection of a homogeneous, elastic cantilever wall. In the case of the test units, this is

$$\Delta f = \frac{V h_w^3}{3 E_c I_e} \qquad \text{(Eq. 10-2)}$$

The deflection due to anchorage deformations in the foundation of the wall was estimated in ref. 6 to be approximately $0.2 \times \Delta f$. An inspection of Figs. 7.20, 8.15, and 9.17 reveals that this estimate is very nearly true for the present test units at the onset of diagonal cracking. At that stage in testing, the ratio $\Delta fe/\Delta f$ was equal to approximately 0.14, 0.20, and 0.19 for Units 1.0, 1.5, and 2.0, respectively. Therefore, the assumption of $\Delta fe = 0.20 \times \Delta f$ remains reasonable for the present walls.

The deflection due to shear deformations, on the other hand, is much less precise. The shear deflection of a homogeneous, elastic cantilever wall is given as

$$\Delta v = \frac{f V h_w}{G_c A_w} \qquad \text{(Eq. 10-3)}$$

where A_w is taken as the web area only, $b_w \ell_w$. In ref. 9, it was shown that the shear stiffness of diagonally cracked beams is only 10-30 percent of that of uncracked beams, depending on the contribution of web reinforcement. In their recommendations for fully ductile cantilever walls, Paulay and Williams suggest an effective wall area of $0.3A_w$ It may be reasoned that in the case of walls responding predominantly in shear, the effective wall area will be somewhat less, particularly in the case of low web reinforcement ratios which may result in very wide diagonal cracks. It is proposed, therefore, that an effective wall area of $0.1A_w$ be used for the present case. Thus, the shear component of deflection may be estimated by

$$\Delta v = \frac{1.2\ V\ h_w}{0.4\ E_c(0.1A_w)} \qquad \text{(Eq. 10-4)}$$

In ref. 6, the deflection due to sliding along the base, Δs, was neglected. In the present tests, it was found to be negligible at all stages of loading. Therefore it will be neglected here as well.

Summing the contributions due to flexural, anchorage, and shear deformations, the total deflection can be written as

$$\Delta = \frac{V\ h_w^3}{3\ E_c I_e} + \frac{0.2\ V\ h_w^3}{3\ E_c I_e} + \frac{30\ V\ h_w}{E_c A_w} \qquad \text{(Eq. 10-5)}$$

Following the analysis of ref. 6, it is convenient to express the total deflection in terms of the flexural deflection of a homogeneous, elastic cantilever with effective wall moment of inertia, I_w.

$$\Delta = \frac{V\ h_w^3}{3\ E_c I_w} \qquad \text{(Eq. 10-6)}$$

where I_w accounts for flexural, anchorage, and shear deformations. By equating the two above equations, I_w for cantilever walls responding primarily in shear is given by

$$I_w = \frac{I_e}{1.2 + F'} \qquad \text{(Eq. 10-7)}$$

where I_e is given by Eq. 10.1, and

$$F' = \frac{90\ I_e}{h_w^2\ b_w\ \ell_w} \qquad \text{(Eq. 10-8)}$$

Values of deflection at the onset of diagonal cracking, Δ_{dc}, calculated using the above method are compared with the measured deflections in Table 10.1. It is seen that the modified prediction agrees better with the measured values. The previous prediction resulted in errors of up to 52 percent, whereas the modified prediction results in errors of only ± 6-12 percent.

10.5 EFFECT OF REDUCED STIFFNESS IN THE ELASTIC RANGE ON DUCTILITY DEMAND IN THE INELASTIC RANGE

Errors in estimating the stiffness of a structure in the elastic state can affect the expected ductility demand imposed on the structure by the design earthquake. For the design of medium- to high-rise buildings, the equal displacement assumption is considered to apply (9). Assume that two different systems are subjected to the same ground motion. One system has high strength and responds elastically, while the other has somewhat lower strength and responds inelastically. The equal displacement principle states that both systems will experience approximately the same maximum displacement. See Fig. 10.2. However, it is recognized that for low-rise buildings vibrating at higher natural frequencies (as for the present walls), the equal displacement principle does not apply. The equal energy principle is more appropriate. This means that the energy demand on the two systems will be the same. See Fig. 10.2.

Consider the responses of two ductile structures, which are characterized by elasto-plastic bilinear responses in Fig. 10.3. The subscript i indicates the idealized or assumed response under the code-specified design earthquake. The subscript r indicates the actual response of the real structure. Although both structures are expected to develop the same lateral load resistance, the stiffness of the real structure, K_r, may be less than the ideal or assumed stiffness, K_i. Thus, the displacement at yield may be greater for the real structure ($\Delta_{yr} > \Delta_{yi}$). However, the ultimate displacement demand (Δ_{ui} and Δ_{ur}) is controlled by

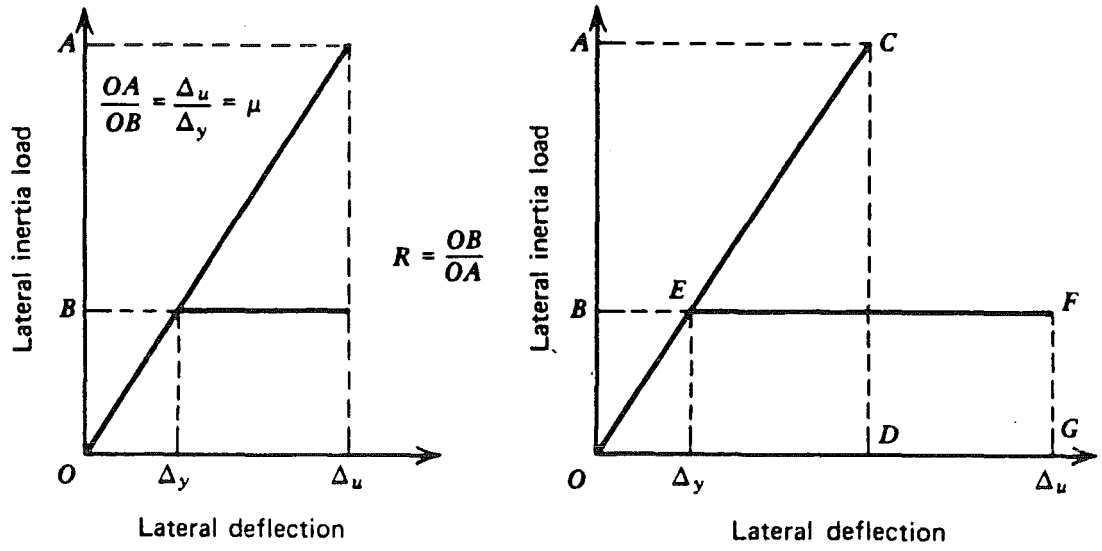

(a) Equal maximum displacement response

(b) Equal maximum potential energy response

Fig. 10.2 - Assumed responses of elastic and elasto-plastic structures (9)

the equal energy principle so that $E_i = E_r$, shown as crosshatched areas in Fig. 10.3. Thus, assuming equal energy response, the displacement ductility demand on the real structure is reduced as follows.

$$\mu_{\Delta r} = \Delta_{ur}/\Delta_{yr} = (k\mu_{\Delta i} + 1 - k) \leq \mu_{\Delta} \qquad \text{(Eq. 10-9)}$$

where $\mu_{\Delta i} = \Delta_{ui}/\Delta_{yi}$

$\mu_{\Delta r}$ = expected displacement ductility factor for the real structure subjected to the design earthquake

$\mu_{\Delta i}$ = displacement ductility factor implied by the relevant loading code

K_r = the reduced stiffness of the real structure

K_i = the theoretically calculated stiffness of the ideal structure

$k = K_r/K_i$

In reference 26, Park and Paulay show a graphical representation of the above equation. See Figs. 10.4 and 10.5. These figures are not meant to represent ductility demands imposed by a particular earthquake, but they are

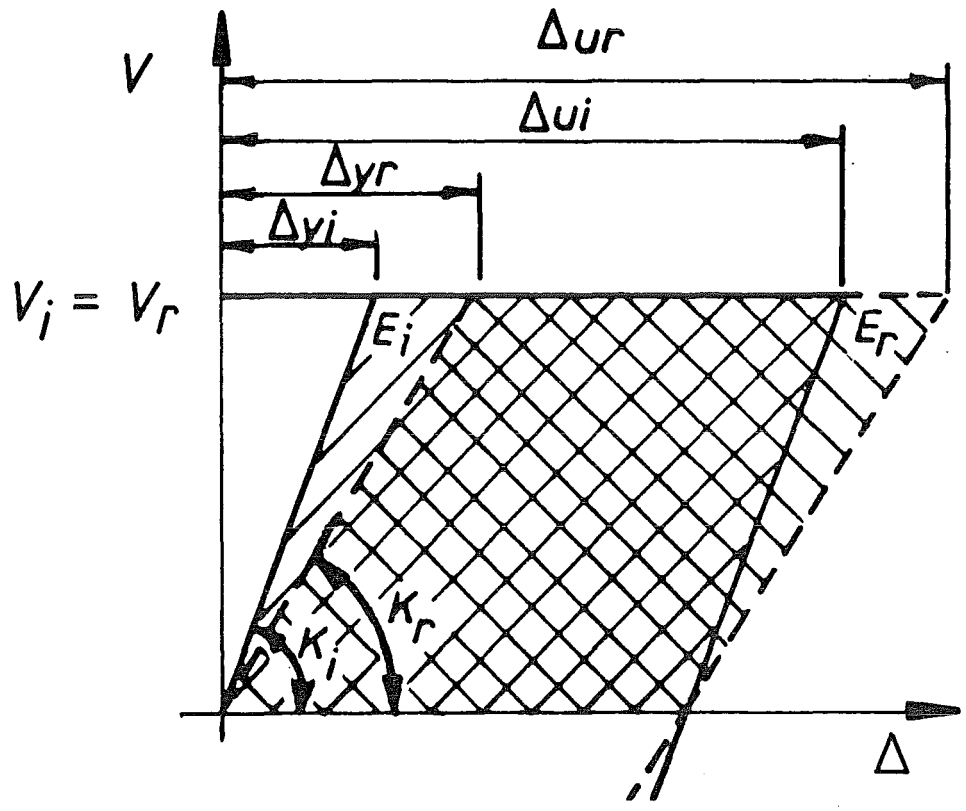

Fig. 10.3 - A comparison of energy dissipation during elasto-plastic response of structures with different stiffnesses (26)

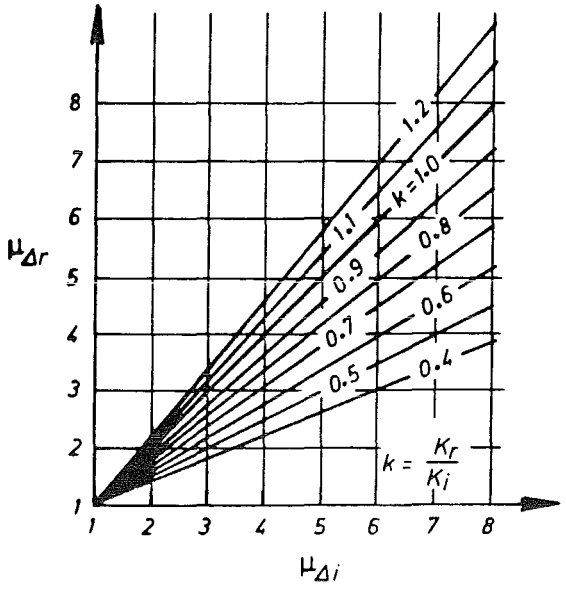

Fig. 10.4 - The relationship between displacement ductilities of real and assumed structures with different stiffnesses (26)

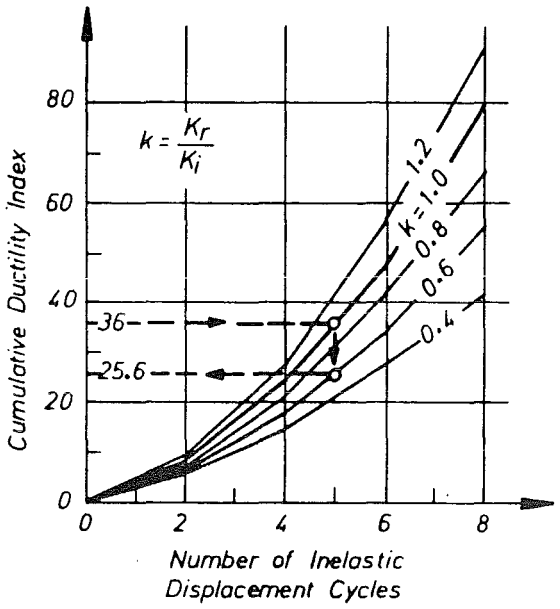

Fig. 10.5 - The dependence of the cumulative displacement ductility index on the ratio of real stiffness to assumed stiffness of specimens (26)

offered as guides to the planning of performance tests of real reinforced concrete members expected to meet the code requirements for fully ductile structures, for example, such as $\sum\mu_\Delta = 2(4x4) = 32$. As shown in Fig. 10.5, if a cumulative ductility demand of 36 is to be imposed on the ideal or assumed member, then the equivalent cumulative ductility demand on the real member may only be 25.6, if the stiffness ratio is k=0.6.

10.6 EFFECT OF LARGER NUMBER OF CYCLES AT LOWER DISPLACEMENT LEVELS ON DUCTILITY DEMAND

For the present test units, the reduced stiffness implied a reduced ductility demand. For this reason, it is not so alarming that the units failed to reach the code-required cumulative ductility of 32. However, the number of cycles imposed on a unit is also crucial. The code envisages a relatively rapid loading to a cumulative ductility of 32. Sixteen cycles to a displacement ductility of $\mu_\Delta = \pm 1$ would be much less severe than four cycles to $\mu_\Delta = \pm 4$. As mentioned earlier, the present test units were subjected to a larger number of cycles at lower displacement ductility levels. Compare Figs. 7.13, 8.10, and 9.12 for Units 1.0, 1.5, and 2.0 with the code suggestion illustrated in Fig. 2.1. So the reduction in ductility demand shown in Fig. 10.5 is not directly applicable.

The cumulative ductilities achieved by the test units appear well in excess of the code requirement for fully ductile structures. However, when the loading sequence is more lenient than that envisaged by the code (ie. a larger number of cycles to lower displacement ductilities), the equivalent cumulative ductility demand can be expected to increase. Just as equal energy response implies a reduced ductility demand for a reduced stiffness (Figs. 10.4 and 10.5), so equal energy response implies an increased cumulative ductility demand when the real loading involves a larger number of cycles at lower displacement levels than the 4 cycles to $\mu_\Delta = 4$ envisaged by the code. This relationship is illustrated in Fig. 10.6. In the figure, the cumulative dissipated energy was taken as the cumulative energy dissipated by an idealized elasto-plastic system (as in Fig.

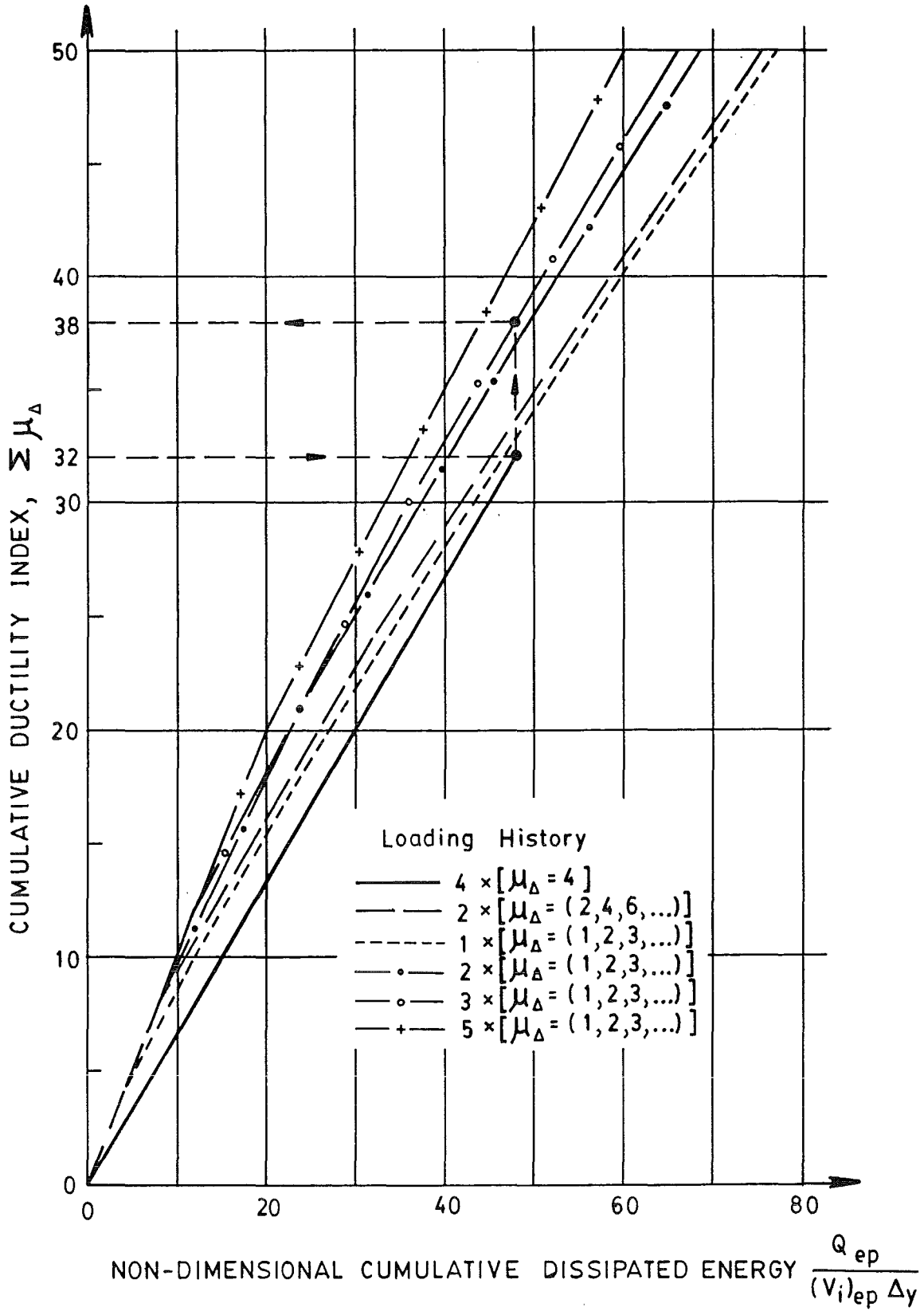

Fig. 10.6 - The dependence of the cumulative displacement ductility index on the severity of the loading history, based on equal cumulative energy dissipated

4.7) when subjected to the displacement history specified for the particular curve in Fig. 10.6. When, for example, the loading sequence involves 3 cycles to values of μ_Δ= 1,2,3,..., equal cumulative energy dissipation implies that a cumulative ductility of 38 would be the equivalent of the code-suggested $\sum\mu_\Delta$= 2(4x4) = 32.

10.7 EFFECT OF REDUCED INITIAL STIFFNESS ON DAMAGE CONTROL DURING MINOR EARTHQUAKES

As described in Section 10.5, having a real stiffness less than the ideal or assumed stiffness has the beneficial effect of reducing the ductility demand at ultimate levels. While absolute displacements may be larger, the required displacement ductility factor ($\mu_\Delta=\Delta/\Delta_y$) during an extreme earthquake will be smaller for the structure with reduced stiffness. However, a reduced stiffness may have a detrimental effect on the structural response during relatively frequent, minor earthquakes. Meeting the ultimate strength, energy dissipation, and displacement ductility requirements alone is not enough to ensure that the structure will behave adequately during minor earthquakes. A sufficiently high stiffness in the elastic, fully cracked structure must be assured in order to protect non-structural elements from damage during minor earthquakes. For example, consider a test unit which has been subjected to a maximum plausible drift of Δ/h_w=1/100 while it has shown good strength retention and good energy dissipation. If a drift of Δ/h_w=1/100 had corresponded to a displacement ductility of μ_Δ=8, then the drift at yield would have been Δ/h_w=1/800, which is well within the acceptable drift limits for damage control. If, however, the ultimate drift of Δ/h_w=1/100 had corresponded to a displacement ductility of μ_Δ=2, then the drift at yield would have been Δ/h_w=1/200, which is unacceptable for damage control. Even though this test unit may have been capable of withstanding large displacements with negligible deterioration, it must be considered too flexible at small displacements. For the present test units, displacements measured in the elastic state, just prior to diagonal cracking, and also in the early inelastic stages, just after diagonal cracking, are presented in Table 10.1.

Displacement values of Δ_{dc} = 3.3mm, 4.6mm, and 6.0mm for Units 1.0, 1.5, and 2.0, respectively, correspond to drifts of Δ/h_w = 1/765, 1/537, and 1/420. These values of drift imply adequate stiffness if the imposed loading can be considered to simulate minor earthquakes.

10.8 TOTAL DISPLACEMENT HYSTERETIC BEHAVIOUR

Loop pinching during the early cycles of loading was a consequence of low percentage of web reinforcement. The web reinforcement was set to the minimum specified for temperature and shrinkage. (Refer to Section 5.2.) Before the formation of the first diagonal crack, the tensile strength of concrete, f_t, across the potential crack surface may be approximated by $0.1f'_c$ (NZS 3101 C6.3.1.5). It may also be measured directly by a split cylinder tensile test.

The tensile strength of the web reinforcement across a wide diagonal crack inclined at an angle θ may be derived with the aid of Fig. 10.7 as follows. Both vertical and

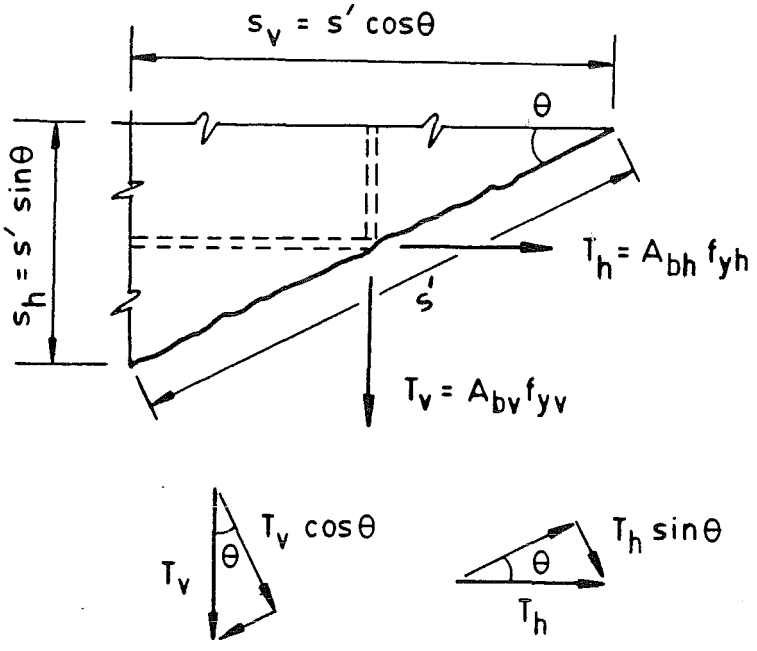

Fig. 10.7 - Forces in reinforcement crossing a potential inclined web crack

horizontal bars are assumed to yield at the crack. Let T_v be the force in the vertical bar, and let T_h be the force in the horizontal bar. The component of the vertical bar force normal to the crack is $T_v \cos\theta$. The component of the

horizontal bar force normal to the crack is $T_h \sin\theta$. The total normal force due to both vertical and horizontal reinforcement may be designated T_n Summing normal components of both vertical and horizontal reinforcement gives

$$T_n = T_v \cos\theta + T_h \sin\theta \qquad \text{(Eq. 10-10)}$$

The equivalent normal stress due to reinforcement crossing the crack plane may be designated f_{sn}.

$$f_{sn} = \frac{T_n}{b_w s'} = \frac{T_v}{b_w s'} \cos\theta + \frac{T_h}{b_w s'} \sin\theta \qquad \text{(Eq. 10-11)}$$

where s' is the spacing of reinforcement along the inclined plane. Replacing s' by its components, s_v and s_h, gives

$$f_{sn} = \frac{T_v}{b_w s_v} \cos^2\theta + \frac{T_h}{b_w s_h} \sin^2\theta \qquad \text{(Eq. 10-12)}$$

Substituting the respective values of bar area times yield stress for T_v and T_h gives

$$f_{sn} = \frac{A_{bv} f_{yv}}{b_w s_v} \cos^2\theta + \frac{A_{bh} f_{yh}}{b_w s_h} \sin^2\theta \qquad \text{(Eq. 10-13)}$$

For the case of the present test units, with identical bar area, bar spacing, and yield strength in both directions, the total tensile strength of the reinforcement across any inclined plane reduces to

$$f_{sn} = \frac{A_b f_y}{b_w s} = \frac{(28.27\text{mm}^2)(472\text{MPa})}{(100\text{mm})(180\text{mm})} = 0.74 \text{ MPa} \qquad \text{(Eq. 10-14)}$$

A comparison of the tensile strengths of concrete and reinforcement across the potential inclined crack is presented in Table 10.2. It is seen that the tensile strength of the concrete was greater than the tensile strength of web reinforcement. Because the reinforcement was incapable of resisting tensile forces in the concrete which were lost when a crack formed, immediate yielding occurred.

Upon diagonal cracking, the unit did not fail and, in

TABLE 10.2 - TENSILE STRENGTH OF CONCRETE AND REINFORCEMENT ACROSS A POTENTIAL INCLINED WEB CRACK

Unit	Concrete			Reinforcement
	f'_c (MPa)	$0.1f'_c$ (MPa)	f_t (MPa)	f_{sn} (MPa)
1.0	27.0	2.7	3.2	0.74
1.5	17.0	1.7	2.4	0.74
2.0	26.5	2.6	3.3	0.74

fact, experienced only negligible reduction in resistance. The reason for this was that a redistribution of internal forces occurred, and a second lateral load resisting mechanism was activated. The initial mechanism was one of pure shear in the uncracked concrete. The subsequent mechanism was a truss mechanism involving strut and tie action (refer Section 3.1). The loss in the vertical component of the web force when the concrete cracked was compensated for by a mobilization of tension in the vertical boundary element tying down the diagonal strut. The loss in the horizontal component of the web force was compensated for by an increase in direct shear transferred in the flexural compression zone at the base of the wall.

The displacements of the two lateral load resisting mechanisms were incompatible. The truss mechanism involved tensile straining of reinforcement and was therefore considerably more flexible than the initial mechanism, which involved direct shear in the uncracked concrete. Moreover, the truss mechanism was only mobilized after large crack displacements. Therefore, of necessity, the transfer of load from one mechanism to the other upon diagonal cracking was very sudden and dramatic. The suddenness of the load transfer was evident in the tests from both the loud popping noise and the immediate large crack. However, as mentioned

above, loss of resistance and collapse was not a danger in the transfer of mechanisms. Only a momentary and minor loss of resistance was observed. Once mobilized, the truss mechanism continued to carry additional lateral load. However, this occurred at the expense of very wide diagonal cracks.

The closing of these large diagonal cracks upon the reversal of load produced pinching of the loops around the zero load level. If the web reinforcement ratio had been larger, such that the strength of reinforcement was greater than the cracking strength of the web concrete, then the widths of the diagonal cracks would have been controlled, and pinching in the hysteretic loops would have been less pronounced. Thus, energy dissipation characteristics would have been better. The lower the percentages of web reinforcement, the worse will be the expected energy dissipation. The code-specified minimum percentage of web reinforcement used in the present test units represents poor energy dissipation.

After the attainment of maximum load, additional deterioration in the web concrete developed, which gave rise to more severe loop pinching. The yielding of web bars under both directions of load resulted also in large tangential crack displacements. Upon the reversal of load, these displacements resulted in the two crack surfaces meeting only at the high points. High local bearing stresses and subsequent crushing of concrete along the diagonal cracks resulted. This crushing was particularly evident in the centre of the web where the main diagonal cracks for both loading directions intersected. (See Figs. 7.9, 8.6, and 9.8.) Such deterioration of the web concrete resulted in the reduction of stiffness and significant loss of energy dissipation.

During the early stages of testing before the attainment of maximum load, the shapes of the loops up to the same displacement level were almost identical. There was negligible drop in lateral load resistance and negligible loss of energy dissipation on consecutive cycles to a given displacement.

After the attainment of maximum load, significant reductions in both lateral load resistance and energy

dissipation were observed on subsequent cycles. However, after the second cycle to the given displacement, a stabilization of both quantities was observed. This repeatability implies that the units would probably not have deteriorated greatly if they had been subjected to a larger number of cycles to the given displacement. This stability under a large number of cycles may be particularly relevant to low-rise walls, which vibrate with higher natural frequencies and thus will be subjected to a larger number of reversals than high-rise walls during similar ground motions.

However, during a real earthquake, there is no assurance that all of the displacements imposed during this larger number of cycles will be less than or equal to that at the first excursion, as was the case for the displacement-controlled testing. Some of the subsequent displacements may be larger. However, the important factor affecting stability of the hysteretic response is the maximum displacement previously encountered. The hysteretic quantities (lateral load resistance and energy dissipation) developed at the largest displacement previously encountered should be used as the basis for evaluating the stability during subsequent reversals.

10.9 STRENGTH

In each test unit, the maximum observed lateral load resistance greatly exceeded the ideal shear strength predicted by current methods. For Units 1.0, 1.5, and 2.0, the ideal shear strength was exceeded by 33.9, 71.0, and 71.2 percent, respectively.

The NZS 3101 Section 7.3 equations for shear strength of concrete are taken largely from previous ACI 318 provisions and were formulated without regard for capacity design procedures or reversed cyclic loading imposed by earthquakes. They tend to be relatively conservative for design purposes. That is, they tend to underestimate the available shear strength of concrete. Nevertheless, Table 10.3 compares the various code predictions for V_c with the diagonal cracking loads measured in the tests. It is seen that NZS 3101 Eq. 7-31, given here as Eq. 5-6, estimates the diagonal cracking load reasonably well.

TABLE 10.3 - COMPARISON OF NZS 3101 EQUATIONS AND BARDA'S PROPOSAL FOR IDEAL SHEAR STRENGTH WITH MEASURED VALUES OF LOAD

Unit	diagonal cracking load (kN)	V_c (kN)					$\frac{(V_{max})test}{1.25}$ (kN)	$V_i = V_c + V_s$ (kN)					V_u Eq.4-2 (Barda) (kN)
		Eq.5-3	Eq.5-4	Eq.5-5	Eq.5-6	Eq.5-7		Eq.5-3	Eq.5-4	Eq.5-5	Eq.5-6	Eq.5-7	
1.0	231	89	142	208	285	267	408	262	315	381	458	440	671
1.5	150	47	51	112	154	86	274	170	174	235	277	209	376
2.0	120	44	35	103	142	61	219	136	127	195	234	153	333

$$v_c = 0.2 \left(\sqrt{f'_c} + \frac{P_u}{A_g}\right) \quad \text{(MPa)} \qquad \text{(Eq. 5-6)}$$

Furthermore, the ideal shear strengths, V_i, obtained using the various NZS 3101 Section 7.3 equations for V_c and the contribution of the web reinforcement, V_s, assuming yielding of all horizontal web bars crossing a 45 degree crack, can be compared with an equivalent "ideal" strength measured in the tests. This experimental "ideal" strength was obtained by reducing the maximum test load by a factor of 1.25 in order to account for the overstrength developed by the test units due to strain hardening of the steel. The comparison of code-estimated ideal strengths with experimental "ideal" strengths appears in Table 10.3. Again, NZS 3101 Eq. 7-31 (Eq. 5-6 above) represents a reasonably simple, yet not unduly conservative estimate of the ideal strength of the test units.

The validity of Barda's proposed equation for the ideal shear strength for walls with aspect ratio $h_w/\ell_w \geq 1.0$ (Section 4.1) may be checked using data from the present tests. Barda's proposal is:

$$v_u = 0.5\sqrt{f'_c} + \rho_n f_y \quad \text{(MPa)} \qquad \text{(Eq. 4-2)}$$

$$V_u = b_w(0.8\ell_w) \times (0.5\sqrt{f'_c} + \rho_n f_y)/1000 \quad \text{(kN)}$$

In Table 10.3, the predicted values of shear strength are presented along with the measured strengths of the test units. It is seen that Barda's proposal overestimates the shear strength and is therefore unconservative for design purposes. However, Barda's proposal may not be so unconservative in the case of monotonic testing.

Finally, even though response of the test units was primarily a shear response, in the form of large corner-to-corner cracks and the predominance of arch action rather than beam action, in each of the test units, the ideal flexural strength was exceeded. In Unit 1.0, the ideal flexural strength was exceeded only once in the positive loading direction by 4.5 percent. In Unit 1.5, the ideal flexural strength was exceeded once in the positive loading direction by 3.0 percent and once in the negative loading

direction by 1.0 percent. In Unit 2.0, the ideal flexural strength was exceeded once in the positive direction by 7.0 percent and once in the negative direction by 1.2 percent. In general, the ideal flexural strength, $(V_i)_{flex}$, was attained only once. On subsequent cycles, the influence of shear deformations increased. With large shear deformations, the capacity of the shear mechanism decreased, which resulted in a noticeable reduction in lateral load resistance. The units eventually failed in shear.

10.10 ENERGY DISSIPATION

In Sections 7.5.4, 8.4.4, and 9.4.4, results of energy dissipation were reported for the three test units. In an attempt to quantify the energy dissipation characteristics of each unit, the energy dissipated by the test unit was compared with the energy that would have been dissipated by an idealized elasto-plastic system having the same ideal strength and yield displacement and subjected to an identical displacement history. The idealized system was given a strength equal to the theoretical ideal shear strength of the unit, $(V_i)_{shear}$. As mentioned earlier, this ideal shear strength was greatly exceeded during the tests. Had the idealized system been given a strength equal to the flexural strength, $(V_i)_{flex}$, then the energy dissipated by the test unit would not have appeared so favourable compared with the idealized elasto-plastic system. The ratio of the cumulative energy dissipated by the test unit to the cumulative energy dissipated by the idealized system governed by flexural rather than shear strength would have been much less.

For example, let $(Q_{ep})_{shear}$ represent the cumulative energy dissipated by the idealized elasto-plastic system when it is given a strength equal to the ideal shear strength of the test unit. Let $(Q_{ep})_{flex}$ represent the cumulative energy dissipated by the idealized elasto-plastic system when it is given a strength equal to the ideal flexural strength of the test unit. Let Q represent the cumulative energy dissipated by the test unit. For Unit 1.0, the ratio of the cumulative energy dissipated by the test unit (Q) to the cumulative energy dissipated by the idealized elasto-plastic system (Q_{ep}) levelled off at a cumulative displacement ductility of

approximately $\sum\mu_\Delta$=28. See Fig. 7.15(b). At this value of $\sum\mu_\Delta$, it was found that $Q/(Q_{ep})_{shear}$ = 0.50, while $Q/(Q_{ep})_{flex}$ = 0.38. For Unit 1.5, Q/Q_{ep} levelled off at a cumulative displacement ductility of approximately $\sum\mu_\Delta$=20 (Fig. 8.12(b)). At this value of $\sum\mu_\Delta$, $Q/(Q_{ep})_{shear}$ was 0.35, while $Q/(Q_{ep})_{flex}$ was 0.21. For Unit 2.0, Q/Q_{ep} levelled off at a cumulative ductility of approximately $\sum\mu_\Delta$=30 (Fig. 9.14(b)). At this value of $\sum\mu_\Delta$, $Q/(Q_{ep})_{shear}$ was 0.35, whereas $Q/(Q_{ep})_{flex}$ was 0.22.

In terms of response to the extreme earthquake, walls similar to the present test units can be expected to dissipate at least 20 percent of the energy dissipated by an equivalent elasto-plastic system by the time they reach the maximum feasible displacement of Δ/h_w=1/100. For smaller displacements, especially prior to the attainment of flexural strength, energy dissipation will be markedly better. It may be as much as 50 percent of that dissipated by the equivalent elasto-plastic system. Also, as mentioned in Section 10.8, the use of code-specified minimum web reinforcement used in the present test units in both horizontal and vertical directions resulted in poor energy dissipation. Larger percentages of web reinforcement are likely to result in greater energy dissipation.

Barda (17) systematically varied the percentages of web reinforcement in some of his test units. For those particular units he neither reported the amount of energy dissipated nor presented the load-displacement hysteretic loops, so that the energy dissipation characteristics could later be extracted. However, he did report results of energy absorbed. As described in Section 4.1, he reports absorbed energy as the area under the envelope of the load-displacement curves. Barda found that the energy absorbed by units with the higher percentages of both horizontal and vertical web reinforcement was greater than the energy absorbed by units with lower web reinforcement percentages. This was due, in part, to the better control of cracking. If, at least qualitatively, the same trends apply for energy dissipation, then Barda's results would support the above proposal. That is, larger percentages of both horizontal and vertical web reinforcement are likely to produce greater energy dissipation.

10.11 COMPONENTS OF WALL DEFLECTIONS

In general, the influence of flexural deformation increased with aspect ratio. (See Figs. 7.20, 8.15, and 9.17.) Flexural deformations were particularly influencial at small displacements. However, once diagonal cracking occurred, shear deformations began to dominate behaviour. In the later stages of testing, after the attainment of maximum load, shear deformations accounted for 50-70 percent of the total top displacement, while flexural deformations accounted for only 20-40 percent of the total top displacement. For all three test units, the horizontal sliding displacement at the base of the wall was negligible at all stages of testing. For each test unit, anchorage deformations, Δfe, were observed to remain relatively constant throughout the test. For Units 1.0, 1.5, and 2.0, Δfe averaged respectivley 5.6, 9.2, and 9.7 percent of the total top deflection. Thus, for walls in which shear deformations dominate behaviour, Δfe can be expected to account for approximately 10 percent of the total top deflection. If, however, flexural deformations were more influencial in the response, then the contribution of anchorage deformation could be expected to increase. Increased flexural deformations would be associated with higher strains in vertical bars, perhaps as high as strain hardening. These higher strains penetrating into the foundation would result in a larger Δfe component of the deflection. Even in the case of the present test units, the relationship between anchorage deformations, Δfe , and flexural deformations, Δf, can be seen in the average values of Δfe reported above. As aspect ratio increased, flexural deformations increased, and, in turn, anchorage deformations increased.

10.12 STRAINS IN VERTICAL BARS BELOW THE BASE LEVEL

The development length required by the code (3) was found to be a slightly conservative estimate of the actual embedment length utilized for 10mm, 12mm, and 16mm diameter bars. (See Table 7.3.) For the 6mm diameter bars in Unit 1.0, the code estimated nearly exactly the utilized embedment

length. However, for the 6mm diameter bars in Units 1.5 and 2.0, the code underestimated the utilized embedment length by approximately 40 percent. Although linear strains indicated that approximately uniform bond stresses existed along the vertical bars in the base beam, no conclusive relationship was found relating strain penetration to bar diameter (Table 7.4). However, as discussed above, since shear deformations, rather than flexural deformations, dominated behaviour, strains in the vertical bars remained relatively low (just above yield strain at the attainment of maximum load). Anchorage deformations, being related to flexural deformations via strain level in the vertical bars, were also small for the test units. Had flexural deformations, and consequently anchorage deformations, been more influencial, then a clearer relationship between bar diameter and strain penetration into the base beam may have emerged.

10.13 HYSTERETIC DAMPING AND SHIFT IN STRUCTURAL PERIOD

Although it has long been acknowledged that good energy dissipation characteristics, in the form of full-bodied hysteretic loops, are influencial in reducing the effects of earthquake excitations, it is also felt that, for certain structures, the shift in structural period during inelastic response may play a major role in altering earthquake-induced forces. When displaced beyond its elastic limit, the assemblage is essentially transformed into a different structure with longer fundamental period of vibration. Increased hysteretic damping, in the form of larger loop areas, will certainly decrease seismic forces on a structure with a given period (see Fig. 10.8). However, a shift in structural period, may, as well, alter the earthquake-induced forces imposed on the structure.

For structures with a fundamental period of approximately T = 0.5 sec. or larger, an increase in structural period due to cracking will most likely reduce the seismic forces (Fig. 10.8, path A-A'). However, for squat buildings, which may have fundamental periods as low as T = 0.1 sec., an increase in fundamental period due to cracking may increase seismic forces (Fig. 10.8, path B-B'). Therefore, in design, it may be important to estimate the

magnitude and effect of the shift in period that may occur once inelastic behaviour sets in.

For the present test units, an estimate of the shift in structural period may be obtained from the shift in values of mean stiffness extracted from the test units and presented in Table 7.2. The fundamental period of vibration may be estimated as $T = 2\pi\sqrt{M/K}$, where M = reactive mass and K = structural stiffness. Assuming that the reactive mass is held constant, the fundamental period becomes proportional to $\sqrt{1/K}$. If T_e and K_e represent the fundamental period and stiffness of the wall in the elastic state just prior to diagonal cracking, then an estimate of the shift in period is given by

$$T/T_e = \sqrt{K_e/K} \qquad \text{(Eq. 10-15)}$$

This index was calculated for each of the test units for three displacement levels: just after diagonal cracking, at the attainment of maximum load, and at a maximum feasible drift of $\Delta/h_w = 1/100$. The results are presented in Table 10.4. The shift in structural period is significant for Unit 1.0 even as early as the onset of diagonal cracking. Therefore, period shift may be influencial in determining seismic forces in walls with aspect ratios of $h_w/\ell_w \leq 1.0$. As slenderness increases, period shift becomes less noticeable at the onset of diagonal cracking and thus exerts less influence on the determination of seismic forces at these lower displacement levels. However, at the attainment of maximum load and beyond, the period shift is significant for all the aspect ratios presented. Thus, period shift can be expected to significantly alter the expected seismic forces if the strength of the structure, as built, is attained. For long period structures, seismic forces will most likely be reduced. For very short period structures, which may include many structures of limited ductility, seismic forces may be increased. Thus, the period shift may represent a worse case for design purposes. Therefore, for short period structures, it may be important to account for period shift in the design process.

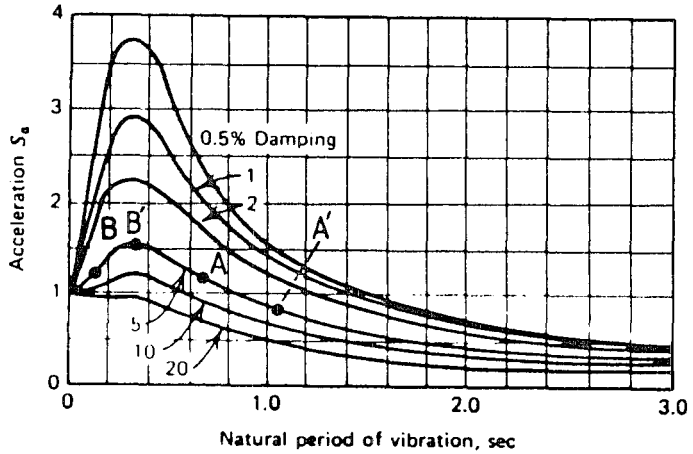

Fig. 10.8 - Design response spectrum giving acceleration vs. period of vibration for a single degree of freedom oscillator - The effect of increase in damping and increase in structural period on expected acceleration (9)

TABLE 10.4 - ESTIMATED SHIFT IN STRUCTURAL PERIOD AT VARIOUS STAGES OF TESTING

Unit	Elastic state just prior to diagonal cracking	Just after diagonal cracking			At maximum load			At maximum feasible drift, Δ/h_w = 1/100		
	K_e (kN/mm)	K (kN/mm)	K_e/K	$\frac{T}{T_e}=\sqrt{\frac{K_e}{K}}$	K (kN/mm)	$\frac{K_e}{K}$	$\frac{T}{T_e}=\sqrt{\frac{K_e}{K}}$	K (kN/mm)	$\frac{K_e}{K}$	$\frac{T}{T_e}=\sqrt{\frac{K_e}{K}}$
1.0	140.0	54.0	2.59	1.61	25.4	5.51	2.35	13.7	10.22	3.20
1.5	48.4	32.2	1.50	1.23	18.1	2.67	1.64	9.3	5.21	2.28
2.0	26.9	20.2	1.33	1.15	10.1	2.66	1.63	10.1	2.66	1.63

SECTION 11

SUMMARY OF PERFORMANCE AND RECOMMENDATIONS

11.1 SUMMARY OF PERFORMANCE OF TEST UNITS

The evaluation of the performance of the test units must centre on the four characteristics discussed in Section 2: 1) strength, 2) energy dissipation, 3) displacement ductility capacity, and 4) damageability. In the following sections, the performance of only the present test units will be discussed regarding these four characteristics. In Section 11.2, these four concepts will be drawn together in recommendations for walls of limited ductility in general.

11.1.1 Strength

The ultimate strength of the units can be considered good. At the attainment of maximum load, the ideal shear strengths and ideal flexural strengths were exceeded by 33.9, 71.0, 71.3 and 4.5, 3.0, 7.0 percent for Units 1.0, 1.5, and 2.0, respectively. However, one drawback in the behaviour was the significant drop in strength upon repeated cycles to a given displacement level after the attainment of maximum load. The maximum loss in strength recorded was approximately 30 percent for Unit 1.5 on its fifth cycle to a drift of Δ/h_w = 1/100. A 30 percent loss in resistance is greater than that envisaged by the code for fully ductile structures. However, such a loss in resistance may not be so critical in a structure of limited ductility that has a high initial strength to begin with because it will have been designed with a higher structural type factor (S = 2.5, for example). After the loss, the resistance may still be greater than that required for a fully ductile structure. Furthermore, having been designed for limited ductility, the structure will not be expected to develop such high displacement ductilities. For example, the maximum expected displacement ductility may be only μ_Δ = 2.50 instead of μ_Δ = 4 or 6.

11.1.2 Energy Dissipation

Due to the nature of the shear response, there existed significant pinching of the hysteretic loops and associated lack of energy dissipation. When compared with idealized elasto-plastic response, the units dissipated a relatively low amount of seismic energy, 38, 21, and 22 percent of the cumulative energy dissipated by the idealized system at cumulative ductilities greater than approximately $\sum\mu_\Delta$=30. However, the idealized elasto-plastic response may not necessarily be attainable even for a well-behaved wall with a good flexural plastic hinge. For example, Goodsir's fully ductile cantilever wall units achieved values of cumulative dissipated energy only 40-50 percent of those for the equivalent idealized bilinear response at equivalent cumulative ductilities. (See ref. 29, Section 7.6.2.) When seen in this light, the energy dissipation performance of the present test units was reasonably good.

Another feature of response was the significant drop in energy dissipation observed on repeated cycles to a given displacement after the attainment of maximum load. However, for smaller displacements, particularly before the attainment of maximum load, the cumulative energy dissipated was much larger (up to 50 percent of the cumulative energy dissipated by the idealized system). Also, the case of code-specified minimum web reinforcement used in the test units represents poor energy dissipation. A higher percentage of web reinforcement would most likely result in better energy dissipation because it would better control crack widths. (See ref. 17.)

11.1.3 Displacement Ductility Capacity

The test units demonstrated significantly less displacement ductility capacity than envisaged by the code for fully ductile structures. At the attainment of maximum load, Units 1.0, 1.5, and 2.0 achieved displacement ductilities of $\mu_\Delta = \pm 2.50$, ± 3.00, and ± 3.15, respectively. However, being walls of limited ductility, the test units were not expected to achieve code-specified full ductility levels. As mentioned in Section 2.6, a trade-off between strength and ductility is allowable. This will be discussed in Section 11.2. Nevertheless, before the attainment of

maximum load, at the above-mentioned displacement ductility factors, good strength retention and consistent energy dissipation were observed on consecutive cycles to given displacement levels.

Regarding the loading sequences adopted for the present test units, several points not considered by the code are worth mentioning. Although the units were subjected to smaller initial displacement ductilities than normal, they were subjected to relatively high final displacement ductilities of $\mu_\Delta = \pm 3.75$, $\mu_\Delta = \pm 4.00$, and $\mu_\Delta = \pm 4.25$. These ductilities corresponded to drifts of $\Delta/h_w = 1/100$, $\Delta/h_w = 1/100$, and $\Delta/h_w = 1/75$, where $\Delta/h_w = 1/100$ is considered the maximum plausible drift expected for low-rise wall structures. In addition, the units were subjected typically to more cycles at each displacement level. Units 1.5 and 2.0 were subjected to 5 cycles at $\Delta/hw = 1/100$ and 1/75, respectively. Although significant losses in strength and energy dissipation were recorded upon the second cycle to these displacements, a reasonable amount of stability regarding these two quantities was observed on susequent cycles. In terms of earthquake response, this observation suggests that such a wall, when displaced to its maximum expected displacement ($\Delta/h_w = 1/100$), may experience a certain drop in strength and energy dissipation. However, upon further excitation, its properties will not be expected to deteriorate significantly or catastrophically.

11.1.4 Damageability

As mentioned in Section 10.7, the test units showed large stiffness in the elastic state, just prior to diagonal cracking, and sufficient stiffness in the inelastic state, just after diagonal cracking, to ensure adequate control of damage during minor earthquakes. The measured values of drift just after diagonal cracking were $\Delta/h_w = 1/765$, 1/537, and 1/420 for Units 1.0, 1.5, and 2.0, respectively.

11.1.5 Main Finding of the Tests

The main finding of the tests was that even though the shear strength of the wall was less than the flexural strength, the strength retention and energy dissipation characteristics upon repeated cycles could be considered

reasonably good up to the attainment of maximum load. This was true even for as many as five cycles to a given displacement. When, however, the maximum load was exceeded, a significant reduction in lateral load resistance and energy dissipation was observed such that the maximum load was never again achieved. Nevertheless, upon further cycling, a stabilization of both lateral load resistance and energy dissipation was observed with respect to those values observed at the maximum displacement previously encountered.

11.2 DESIGN RECOMMENDATIONS FOR CANTILEVER WALLS OF LIMITED DUCTILITY

11.2.1 New Walls

For reasons outlined in Section 2, some structural walls may be unavoidably overreinforced for flexure and thus may be weaker in shear than in flexure. While responding in a non-flexural mode, these walls may exhibit only limited ductility. However, even though they exhibit ductility less than the code-required full ductility, they can still be considered adequate during earthquakes if they have a strength higher than the code-required strength for fully ductile structures and if they have good energy dissipation characteristics and a sufficiently high stiffness in the elastic state to limit damage during minor earthquakes. Granted that a trade-off between strength and ductility is acceptable, as illustrated in Fig. 2.5, one of the vital questions posed in Section 2.6 was: For a wall with strength between that assigned to fully ductile walls (R_{fd}, Fig. 2.5) and that required for elastically responding walls (R_{max}, Fig. 2.5), what specific combinations of strength and ductility are acceptable?

The equal energy principle can be expressed by the following equation (9):

$$\frac{R}{R_{max}} = \frac{1}{\sqrt{2\mu_{\Delta} - 1}} \qquad \text{(Eq. 11-1)}$$

Furthermore, in the design process, the lateral load resistance is set equal to the static lateral load implied by

the code (1).

$$R = V = CRSM\ W_t \qquad \text{(Eq. 11-2)}$$

The risk factor, R, the material factor, M, and the reactive weight, W_t, may be assumed constant for the purpose of this study. Assuming that C in held constant by virtue of the structural period of low-rise buildings being less than or equal to approximately T = 0.4 sec. (see ref. 1, Fig. 3), then the lateral load resistance, R, becomes directly proportional to the structural type factor, S.

$$R = R_{fd}\ S \qquad \text{(Eq. 11-3)}$$

For fully ductile cantilever wall connected by rigid floor diaphragms, the code specifies S = 1.0. Therefore, $R = R_{fd}$. Substituting Eq. 11-3 into Eq. 11-1 gives

$$\frac{R_{fd}S}{R_{max}} = \frac{1}{\sqrt{2\mu_\Delta - 1}} \qquad \text{(Eq. 11-4)}$$

For an elastically responding wall, the code specifies S = 5.0. Therefore, $R_{max}/R_{fd} = 5.0$. This relationship gives

$$\frac{1}{5} S = \frac{1}{\sqrt{2\mu_\Delta - 1}} \qquad \text{(Eq. 11-5)}$$

A rearrangement of this equation gives the relationship between μ_Δ and S. Thus, assuming that the equal energy principle applies, the expected displacement ductility demand as a function of structural type factor is given as

$$\mu_\Delta = 12.5 \frac{1}{S^2} + 0.5 \qquad \text{(Eq. 11-6)}$$

This relationship is summarized in Fig. 11.1.

It was observed in the present tests that energy dissipation and strength retention on repeated cycling to a given displacement were consistent and repeatable, particularly at displacement levels prior to the attainment of maximum load. After the attainment of maximum load,

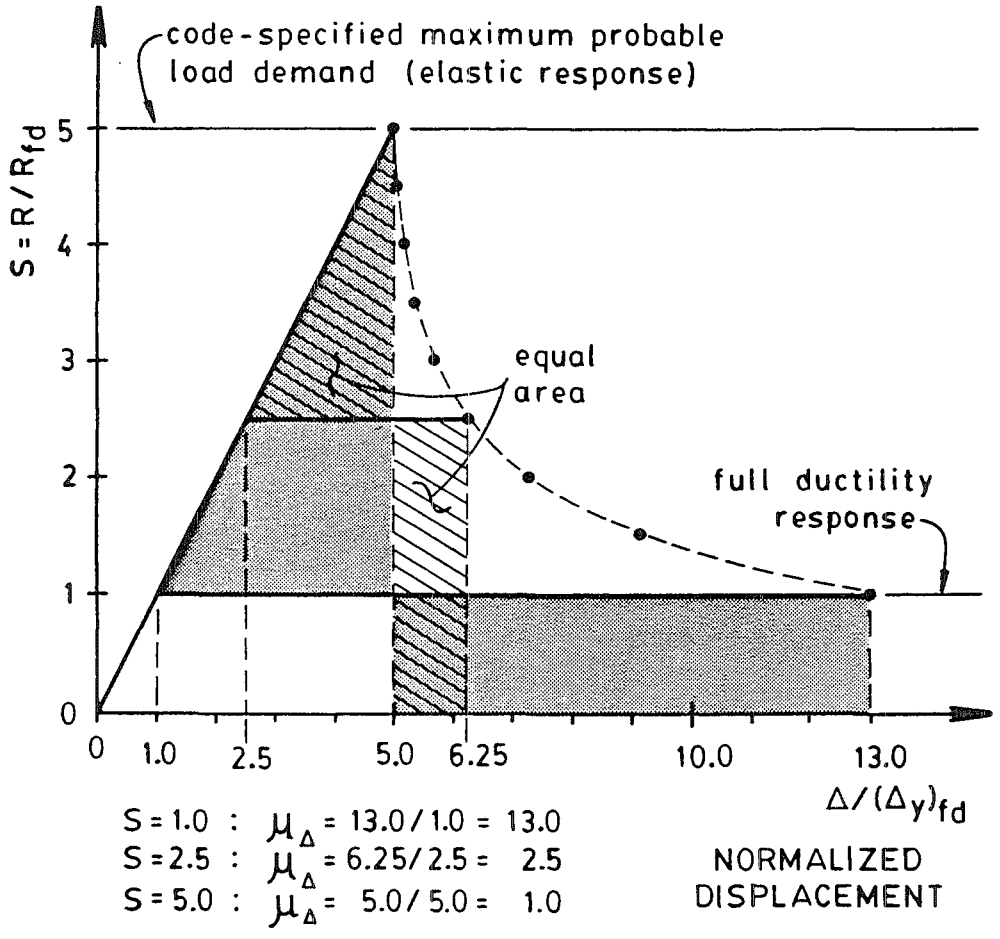

(a) Structural type factor vs. displacement

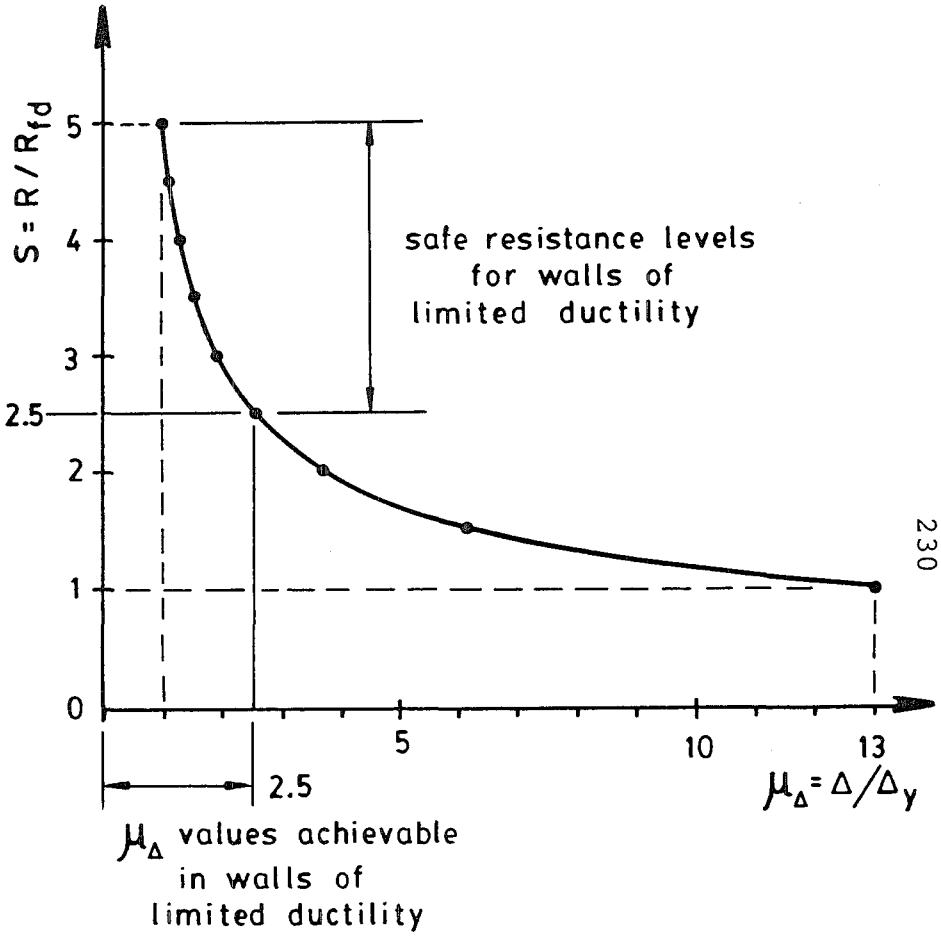

(b) Structural type factor vs. expected displacement ductility

Fig. 11.1 - The relationship between structural type factor, S, and the expected displacement response, based on the equal energy principle

significant deterioration of strength and energy dissipation occurred. Furthermore, in all three test units, the ideal flexural strength was exceeded, even though shear deformations dominated behaviour. For walls of limited ductility, therefore, it is proposed that, as long as the maximum strength of the wall is not exceeded, energy dissipation and strength retention characteristics will be good under repeated displacement reversals. For design purposes, the maximum strength of the wall may be taken as the ideal flexural strength. Since the present test units developed ductilities of $\mu_\Delta = \pm 2.50$, ± 3.00, and ± 3.15 at the attainment of maximum load, it is proposed that prototype walls will be able to safely develop ductilities up to $\mu_\Delta = \pm 2.50$. Assuming that the equal energy principle applies, this displacement ductility corresponds to a structural type factor of approximately S = 2.5 (Fig. 11.1(b)). This means that if a cantilever wall has a resistance equal to or greater than that corresponding to S = 2.5, then it will most likely be able to meet the corresponding ductility demands. Therefore, it is proposed that cantilever walls of limited ductility be designed using a structural type factor of $S \leq 2.5$. If flexural strength is provided to meet this load demand, then the imposed displacement ductility demands will most likely be achievable, and strength retention and energy dissipation characteristics will most likely be good. However, if strengths lower than that corresponding to S = 2.5 are allowed, then the wall may not be capable of developing the required displacement ductility.

It is suggested that the ideal flexural strength be calculated using standard flexural strength calculations for walls and that the ideal shear strength of concrete be conservatively calculated using Eq. 5-6:

$$v_c = 0.2 \left(\sqrt{f'_c} + \frac{P_u}{A_g}\right) \quad \text{(MPa)} \qquad \text{(Eq. 5-6)}$$

If the wall happens to be displaced beyond the point at which the maximum strength is attained, then it may experience a significant reduction in resistance and energy dissipation. However, on subsequent displacement reversals, it can be expected to retain approximately 65 percent of its maximum strength with consistent repeatability up to a

maximum feasible drift level of $\Delta/h_w = 1/100$.

For the purposes of apportioning code-specified lateral loads to various structural members and ensuring damage control during minor earthquakes, the deflection (or, conversely, the stiffness) in the elastic, fully cracked state of cantilever walls subjected to a single force at the top and responding predominantly in shear may be estimated using the formulae found in ref. 6 modified as in Section 10.4. The deflection at the onset of diagonal cracking, Δ_{dc}, may be estimated by

$$\Delta_{dc} = \frac{V\, h_w^3}{3\, E_c I_c} \qquad \text{(Eq. 10-6)}$$

where $$I_w = \frac{I_e}{1.2 + F'} \qquad \text{(Eq. 10-7)}$$

and $$F' = \frac{90\, I_e}{h_w^2\, b_w\, \ell_w} \qquad \text{(Eq. 10-8)}$$

It is suggested that the associated value of stiffness at the onset of diagonal cracking, $K_{dc} = 3E_c I_w / h_w^3$, also be used for the estimation of fundamental period of vibration, T, in order to obtain the basic seismic coefficient, C, in ref. 1, Fig. 3. These formulae are very approximate. However, they may provide improved accuracy for design purposes until further investigations can provide improved estimates.

One alarming feature of response that concerns damageability during minor and moderate earthquakes was the width of diagonal cracks at relatively small displacements. Immediately upon the formation of a diagonal crack the web reinforcement crossing the crack yielded, resulting in a very wide crack. (See Section 10.8.) However, the widths of the diagonal cracks did not appear to significantly affect the lateral load resistance of the units.

If large cracks cannot be tolerated, then the designer may wish to increase the percentage of web reinforcement so that the tensile strength of reinforcement across the potential diagonal crack, f_{sn}, is greater than the tensile strength of concrete. From Eq. 10-13,

$$f_{sn} = \rho_n f_{yv} \cos^2\theta + \rho_h f_{yh} \sin^2\theta > f_t = 0.1 f'_c \quad \text{(Eq. 11-7)}$$

Assuming a 45 degree crack,

$$\rho_n f_{yv} + \rho_h f_{yh} > 0.2\ f'_c \quad \text{(Eq. 11-8)}$$

Although the effects of increasing the web reinforcement were not specifically studied in the tests, it is suspected that the widths of diagonal cracks would be less. The web bars would not be expected to yield upon crack formation, as they did in the tests. However, this increased web reinforcement may also significantly increase the shear strength of the wall and the stiffness of the strut and tie mechanism, perhaps even to the point that flexural deformations dominate response. Such an increase in web reinforcement may even result in a shear strength in excess of the flexural strength. In such a case, it may be more rational to abandon the limited ductility design approach and simply use capacity design.

Shift in structural period may significantly alter the expected seismic forces once the wall enters the inelastic range. Furthermore, for the more squat walls with aspect ratios $h_w/\ell_w \leq 1.0$, this shift in period may cause an increase in the expected seismic forces. This may be true even for the low levels of displacement suggested above (ie. prior to the attainment of maximum load). This possible increase in seismic force for very short period structures is not presently provided for in the design response spectra of the current loadings code (ref. 1, Fig. 3). Nevertheless, it was found in the present test units that the structural period at the attainment of maximum load was of the order of 50 percent higher than the structural period at the onset of diagonal cracking. (See Table 10.4.) For very short period structures, this period shift may represent a significantly worse case for design.

11.2.2 Existing Walls

Existing low-rise cantilever walls may have been designed using any of a number of different design codes, depending on the age of the wall. Walls built before the current capacity design procedures were introduced may well

have a flexural strength in excess of its shear strength. It is proposed that the evaluation of the likely seismic performance of such walls be carried out as follows.

First, given the dimensions and reinforcement details of the wall as built, the flexural strength may be calculated using standard flexural strength calculation procedures. (See Appendix A, for example.) The shear strength may be calculated using a value of V_c given by Eq. 5-6 (NZS 3101 Eq. 7-31) and a value of V_s assuming yielding of web bars across a 45 degree crack. If the shear strength turns out to be less than the flexural strength, then, during an extreme earthquake, fully ductile response cannot be expected. It is suggested, then, that the structural type factor, S, be back-calculated according to 1986 standards (ref. 1) in order to evaluate the wall's likely performance. The reactive weight, W_t, the material factor, M, and the risk factor, R, should be assessed. The basic seismic coefficient, C, may be assessed using a structural period based on the wall stiffness calculated using Eqs. 10-6, 10-7, and 10-8. The structural type factor may therefore be calculated as follows:

$$S = \frac{(V_i)_{flex}}{CRM\ W_t} \qquad \text{(Eq. 11-9)}$$

It is proposed that if S is greater than a value of 2.50 then the expected displacement ductility demand will be less than approximately md = 2.50 (Fig 11.1). The present tests showed that this level of displacement ductility was attainable even though shear deformations dominated the response. Also, at this level of displacement ductility, strength retention and energy dissipation characteristics were reasonably good even during a large number of reversals. Therefore, it is proposed that if the back-calculated value of S is greater than 2.50, then reasonably good seismic response can be expected. One drawback of the response may be the formation of very wide diagonal cracks associated with shear behaviour and an associated reduction if stiffness. These cracks may require major structural repair after the earthquake. However, during the earthquake, the strength, ductility, and energy dissipation characteristics can be

expected to be reasonably good.

On the other hand, if the back-calculated structural type factor has value of S less than approximately 2.50, then the wall may be incapable of sustaining the higher ductility demands that can be expected during a major earthquake. Also, significant loss in lateral load resistance and energy dissipation may occur.

11.3 RECOMMENDATIONS FOR FURTHER RESEARCH

Estimates of the values of displacement ductility that are safely achievable in cantilever walls of limited ductility were obtained from the laboratory test units. Theoretical strength and displacement ductility demands were estimated assuming that the equal energy principle applied to low-rise, short period structures. Even though this assumption is thought to hold true for many instances involving low-rise walls, it may not be universally applicable or always correct. It would be useful to obtain a more accurate estimate of the actual ductility demands imposed on limited ductility walls in dynamic situations by different earthquakes. To do this, it is envisaged that analytical assemblages of low-rise walls be constructed with varying levels of strength above the reduced strength allowed for fully ductile walls and below the strength corresponding to elastic response. These assemblages could be subjected to actual earthquake records using computer time-history analyses. The resulting improved estimates of displacement ductility demands under dynamic conditions could then be compared with the available displacement ductilities observed in the laboratory.

The method suggested for estimating deflections of limited ductility walls at the onset of diagonal cracking is very approximate. An improved estimate of the component of deflection resulting from shear deformations, Δ_v, is desirable. It may be appropriate to study the effect of varying web reinforcement percentages since this will most likely strongly influence the width of diagonal cracks. It should be remembered that the present test units contained only minimum amounts of web reinforcement envisaged by current codes.

Although estimates of shift in structural period during inelastic response were obtained from the tests, more work is required in investigating the magnitudes and effects of period shift to be expected for low-rise walls responding predominantly in shear. A clearer understanding of the relationship between period shift and a change in seismic forces for low period structures is desirable.

REFERENCES

1. STANDARDS ASSOCIATION OF NEW ZEALZND. NZS 4203:1976 (Incorporating Amendment No. 1 and No. 2), Code of Practice for General Structural Design and Design Loadings for Buildings. Wellington, New Zealand: Standards Association of New Zealand, February 1976, 104 pp.
2. STANDARDS ASSOCIATION OF NEW ZEALAND. DZ 4203/A3, Draft Amendment No. 3 to Code of Practice for General Structural Design and Design Loadings for Buildings. Wellington, New Zealand: Standards Association of New Zealand, 1983, 12 pp.
3. STANDARDS ASSOCIATION OF NEW ZEALAND. NZS 3101:Part 1:1982, Code of Practice for the Design of Concrete Structures. Wellington, New Zealand: Standards Association of New Zealand, July 1982, 127 pp.
4. STANDARDS ASSOCIATION OF NEW ZEALAND. NZS 3101:Part 2:1982, Commentary on the Code of Practice for the Design of Concrete Structures. Wellington, New Zealand: Standards Association of New Zealand, July 1982, 156 pp.
5. PAULAY, T. The Design of Reinforced Concrete Ductile Shear Walls for Earthquake Resistance. Research Report No. 81-1, Department of Civil Engineering, University of Canterbury, Christchurch, New Zealand, February 1981, 133 pp.
6. PAULAY, T. and WILLIAMS, R.L. "The Analysis and Design of and the Evaluation of Design Actions for Reinforced Concrete Ductile Shear Wall Structures." Bulletin of the New Zealand National Society for Earthquake Engineering, Vol. 13, No. 2, June 1980, pp. 108-143.
7. SYNGE, A.J. Ductility of Squat Shear Walls. Research Report No. 80-8, Department of Civil Engineering, University of Canterbury, Christchurch, New Zealand, February 1980, 142 pp.
8. PAULAY, T., PRIESTLEY, M.J.N. and SYNGE, A.J. "Ductility in Earthquake Resisting Squat Shearwalls." Journal of the American Concrete Institute, Proceedings V. 79, No. 4, July 1982, pp. 257-269.
9. PARK, R. and PAULAY, T. Reinforced Concrete

Structures. New York: John Wiley and Sons, 1975.

10. ROGOWSKY, D.M., MACGREGOR, J.G., AND ONG, S.Y. Tests of Reinforced Concrete Deep Beams. Structural Engineering Report No. 109, Department of Civil Engineering, University of Alberta, Edmonton, Alberta, Canada, September 1983, 167 pp.
11. ROGOWSKY, D.M. and MACGREGOR, J.G. Shear Strength of Deep Reinforced Concrete Continuous Beams. Structural Engineering Report No. 110, Department of Civil Engineering, University of Alberta, Edmonton, Alberta, Canada, November 1983, 178 pp.
12. MACGREGOR, J.G. "Design of Deep Beams." Background notes for a series of seminars given in Australia and New Zealand, May-June 1984.
13. MARTI, P. "Basic Tools of Reinforced Concrete Beam Design." Journal of the American Concrete Institute, Proceedings V. 82, No. 1, January 1985, pp. 46-56.
14. SCHLAICH, J. and WEISCHEDE, D. Ein Praktisches Verfahren zum Methodischen Bemessen und Konstruieren im Stahlbetonbau (A Practical Method for the Methodical Dimensioning and Construction of Reinforced Concrete), Bulletin D'Information No. 150, Comite Euro-International Du Beton, Paris, March 1982, 163 pp.
15. COLLINS, M.P. Prestressed Concrete Structures. Lecture notes for a postgraduate course at the University of Canterbury, Christchurch, New Zealand, May-August, 1983.
16. GROB, J. and THÜRLIMANN, B. "Ulitmate Strength and Design of Reinforced Concrete Beams Under Bending and Shear." Memoires, International Association for Bridge and Structural Engineering, Vol.36-II, Zurich, 1976, pp. 105-120.
17. BARDA, F. Shear Strength of Low-rise Walls with Boundary Elements. Phd. Dissertation, Dept. of Civil Engineering, Lehigh University, Bethlehem, Pennsylvania, 1972.
18. BARDA, F., HANSON, J.M. and CORLEY, W.G. "Shear Strength of Low-rise Walls with Boundary Elements." Reinforced Concrete Structures in Seismic Zones, sp-53. Detroit: American Concrete Institute, 1977, pp. 149-202.
19. ROBINSON, L.M. "Shear Walls of Limited Ductility."

Bulletin of the New Zealand National Society for Earthquake Engineering, Vol. 13, No. 2, June 1980, pp. 144-161.

20. GLOGAU, O.A. "Low Rise Reinforced Concrete Buildings of Limited Ductility - Some Lessons from Recent Earthquake Damage." Bulletin of the New Zealand National Society for Earthquake Engineering, Vol. 13, No. 2, June 1980.
21. HUTCHISON, D.L. and VAN GELDERMALSEN, T.J. "Optimum Design of Reinforced Concrete Shear Walls." Bulletin of the New Zealand National Society for Earthquake Engineering, Vol. 17, No. 3, September 1984, pp. 185-197.
22. STANDARDS ASSOCIATION OF NEW ZEALAND. NZS 3112 Part 1:1980, Specification for Methods of Test for Concrete, Part 1, Tests Relating to Fresh Concrete. Wellington, New Zealand: Standards Association of New Zealand, December 1980, 22 pp.
23. STANDARDS ASSOCIATION OF NEW ZEALAND. NZS 3112 Part 2:1980, Specification for Methods of Test for Concrete, Part 2, Tests Relating to the Determination of Strength of Concrete. Wellington, New Zealand: Standards Association of New Zealand, December 1980, 21 pp.
24. HIRAISHI, H. "Evaluation of Shear and Flexural Deformations of Flexural Type Shear Walls." Bulletin of the New Zealand National Society for Earthquake Engineering, Vol. 17, No. 2, June 1984, pp. 135-144.
25. SPURR, D.D. Post-Elastic Behaviour of Reinforced Concrete Frame-Wall Comnponents and Assemblages Subjected to Simulated Seismic Loading. Phd. Thesis, Department of Civil Engineering, University of Canterbury, Christchurch, New Zealand, 1984.
26. PAULAY, T. and PARK, R. Joints in Reinforced Concrete Frames Designed for Earthquake Resistance. Research Report No. 84-9, Department of Civil Engineering, University of Canterbury, Christchurch, New Zealand, June 1984, 71 pp.
27. AMERICAN CONCRETE INSTITUTE COMMITTEE 318. Building Code Requirements for Reinforced Concrete (ACI 318-77). Third printing. Detroit, Michigan: American Concrete Institute, August 1978, 103 pp.

28. AMERICAN CONCRETE INSTITUTE COMMITTEE 318. Commentary on Building Code Requirements for Reinforced Concrete (ACI 318-77). Third printing. Detroit, Michigan: American Concrete Institute, May 1979, 132 pp.

29. GOODSIR, W.J. The Design of Coupled Frame-Wall Structures for Seismic Actions. Research Report No. 85-8, Department of Civil Engineering, University of Canterbury, Christchurch, New Zealand, August 1985, 359 pp.

30. CARR, A.J. "Hysteresis," Computer Program Library, Department of Civil Engineering, University of Canterbury, 1985.

APPENDIX A

STRENGTH CALCULATIONS

Typical strength calculations are presented here for Unit 2.0.

Material Properties

boundary element bars: 4HD16 $f_y = 465$ MPa, $f_y = 443$ MPa } say $f_y = 455$ MPa

$(E_s)_{16} = 198\,000$ MPa, $(E_s)_{10} = 190\,000$ MPa } say $E_s = 194000$ MPa

web bars: HD6-180 $f_y = 470$ MPa

$(E_s)_6 = 190\,000$ MPa

concrete: $f'_c = 26.5$ MPa

Ideal Shear Strength of Concrete

ACI 318-71, clause 11.4.1

$$v_c = 0.17\sqrt{f'_c} = 0.17\sqrt{26.5} = 0.8751 \text{ MPa}$$

$$\underline{V_c} = v_c b_w \times 0.8\ell_w = 0.8751(100)(0.8)(1250) = \underline{87.5 \text{ kN}}$$

ACI 318-71, Eq. 11-4

$$v_c = 0.16\sqrt{f'_c} + 17.2\rho_w \frac{V_u d}{M_u} \leq 0.29\sqrt{f'_c}$$

$$\rho_w = \frac{A_b}{b_w s} = \frac{28.27 \text{ mm}^2}{100 \text{ mm}(180 \text{ mm})} = 0.00157$$

$$\frac{V_u d}{M_u} = \frac{V_u(0.8\ell_w)}{V_u h_w} = \frac{0.8\ell_w}{h_w} = \frac{0.8(1250)}{2500} = 0.40 < 1.0$$

$$v_c = 0.16\sqrt{26.5} + 17.2(0.00157)(0.40) = 0.8345 \text{ MPa} < 0.29\sqrt{26.5} = 1.49 \text{ MPa}$$

$$\underline{V_c} = 0.8345 \text{ (100 x 0.8 x 1250)} = \underline{83.4 \text{ kN}}$$

ACI 318-71, Eq. 11-6

$$v_c = 2(1 + 0.0005 \frac{P_u}{A_g})\sqrt{f'_c} \approx 0.17\sqrt{f'_c} \quad \text{(above)}$$

since $P_u \approx 0$

NZS 3101, Eq. 7-3

$$0.8\sqrt{f'_c} \leq \{v_c = v_b = (0.07 + 10\rho_w)\sqrt{f'_c}\} \leq 0.2\sqrt{f'_c}$$

$$\{v_c = [0.07 + 10(0.00157)]\sqrt{f'_c}\}$$

$$0.08 f'_c < \{v_c = 0.0857\sqrt{f'_c} \quad\} < 0.2\sqrt{f'_c}$$

$$v_c = 0.4412 \text{ MPa}$$

$$\underline{\underline{V_c}} = 0.4412 (100 \times 0.8 \times 1250) = \underline{\underline{44.1 \text{ kN}}}$$

NZS 3101, Eq. 7-24

$$v_c = (2\frac{d}{a}) v_b \qquad d = 0.8\ell_w$$

$$= 2(0.4)v_c \text{ (above)} \qquad a = h_w$$

$$\frac{d}{a} = \frac{0.8\ell_w}{h_w} = \frac{0.8(1250)}{2500} = 0.4$$

$$\underline{\underline{V_c}} = 0.8V_c \text{ (above)} = \underline{\underline{35.3 \text{ kN}}}$$

NZS 3101, Eq. 7-31

$$v_c = 0.2\sqrt{f'_c} \text{ (compression)}$$

$$v_c = 0.2\sqrt{26.5} = 1.0296 \text{ MPa}$$

$$\underline{\underline{V_c}} = 1.0296 (100 \times 0.8 \times 1250) = \underline{\underline{103.0 \text{ kN}}}$$

NZS 3101, Eq. 7-32

$$v_c = 0.27\sqrt{f'_c} + \frac{1}{4}\frac{P_u}{A_g}$$

$$P_u = (0.4\,\text{m})(0.4\,\text{m})(1.940\,\text{m})(24\,\text{kN/m}^3) \quad \text{top beam}$$

$$+ (0.950\,\text{m})(0.1\,\text{m})(2.3\,\text{m})(24\,\text{kN/m}^3) \quad \text{web}$$

$$+ 2(0.2\,\text{m})(0.15\,\text{m})(2.3\,\text{m})(24\,\text{kN/m}^3) \quad \text{boundary elements}$$

$$P_u = 16.00 \text{ kN}$$

$$A_g = 100\,\text{mm}(950\,\text{mm}) + 2(150\,\text{mm})(200\,\text{mm}) = 155000\ \text{mm}^2$$

$$v_c = 0.27\sqrt{26.5} + \frac{1}{4}\frac{16000}{155000} = 1.4157 \text{ MPa}$$

$$\underline{\underline{V_c}} = 1.4157 (100 \times 0.8 \times 1250) = \underline{\underline{141.6 \text{ kN}}}$$

NZS 3101, Eq. 7-33

$$v_c = 0.05\sqrt{f'_c} + \frac{\ell_w(0.1\sqrt{f'_c} + 0.2\frac{P_u}{A_g})}{\frac{M_u}{V_u} - \frac{\ell_w}{2}}$$

$$\frac{M_u}{V_u} = \frac{V_u h_w}{V_u} = h_w$$

$$\frac{M_u}{V_u} - \frac{\ell_w}{2} = h_w - \frac{\ell_w}{2}$$

$$= 2500 - \frac{1250}{2}$$

$$= 1875 \text{ mm}$$

$$v_c = 0.05\sqrt{26.5} + \frac{1250(0.1\sqrt{26.5} + 0.2(0.1032)}{1875} = 0.6143 \text{ MPa}$$

$$\underline{\underline{V_c}} = 0.6143 \text{ (100 x 0.8 x 1250)} = \underline{\underline{61.4 \text{ kN}}}$$

NZS 3101, Eq. 7-43

$$v_c = 0.6\sqrt{\frac{P_e}{A_g}} = 0.6\sqrt{\frac{16\,000 \text{ N}}{155\,000 \text{ mm}^2}} = 0.1928 \text{ MPa}$$

$$\underline{\underline{V_c}} = 0.1928 \text{ (100 x 0.8 x 1250)} = \underline{\underline{19.3 \text{ kN}}}$$

Ideal Shear Strength of Reinforcement

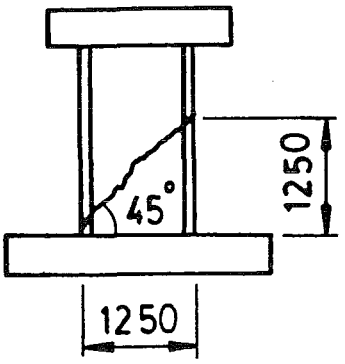

$$A_s = \frac{1250 \text{ mm}}{180 \text{ mm}} \text{ x } 28.27 \text{ mm}^2 = 196.3 \text{ mm}^2$$

$$V_s = f_y A_s = \frac{0.470 \text{ kN}}{\text{mm}^2} \text{ x } 196.3 \text{ mm}^2$$

$$V_s = 92.3 \text{ kN}$$

Fig. A.1 - Yielding of horizontal bars crossing an assumed 45° web crack

Ideal Shear Strength of Wall

$$(V_i)_{shear} = V_c + V_s$$

For the purpose of setting the loading, assume $(V_i)_{shear} = 160$ kN

Ideal Flexural Strength of Wall

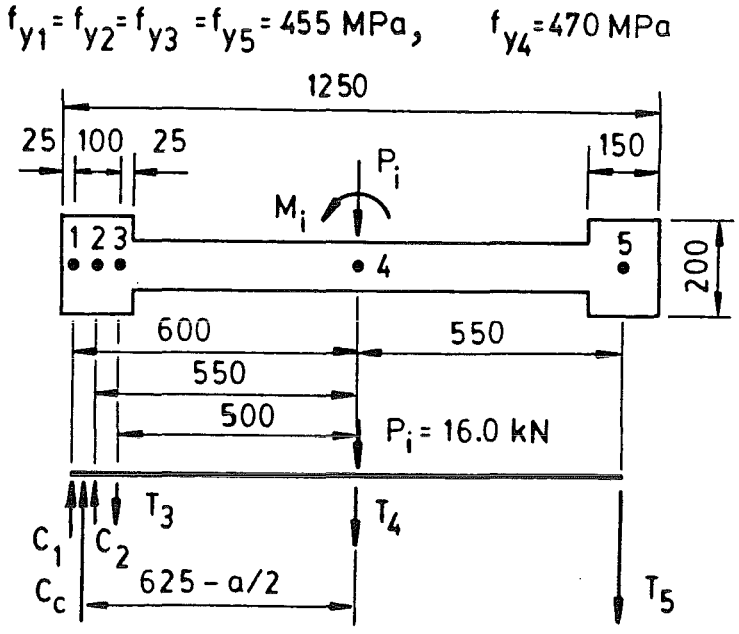

Fig. A.2 - Internal forces present at the attainment of ideal flexural strength

Component	A_s (mm^2)	Force $= A_s f_y$ (kN)	Lever arm (m)	M_{CG} (kNm)
C_1	480.5	218.6	0.600	131.2
C_2	157.1	71.5	0.550	39.3
T_3	480.5	109.3 (1)	0.500	- 54.6
T_4	170.0	79.9	0	0
T_5	1118.4	508.9	0.550	279.9
C_c	$0.85f'_c$ ab =	4.50a	0.578	245
P_i	-	16.0	0	0

$\sum F = 0 \Rightarrow a = 94$ mm

$c = \frac{a}{0.85} = 111$ mm

$(M_i)_{flex} = \sum M_{CG} = 640.8$ kNm

$\underline{(V_i)_{flex}} = \frac{(M_i)_{flex}}{h_w} = \frac{640.8}{2.5\ m}$ kNm = $\underline{256.3\ kN}$

(1) $(\frac{1}{2} f_y) \times A_s$

APPENDIX B

STIFFNESS CALCULATIONS

Typical stiffness calculations using the methods outlined in reference 6, Appendix I are presented here for Unit 2.0.

Predicted displacement at the application of $V = 0.75(V_i)_{shear} = 0.75(160\ kN)$

$E_s = 194\ 000$ MPa

$E_c = 4700\sqrt{f'_c} = 4700\sqrt{26.5} = 24195$ MPa NZS 3101 3.3.4.1

$n = E_s/E_c = 8.02$

$f_r = 0.6\sqrt{f'_c} = 0.6\sqrt{26.5} = 3.09$ MPa NZS 3101 Eq. 4-6

Flexural stiffness, I_e :

$$I_g = \frac{1}{12}(0.1m)(0.950m)^3 + 2\left[\frac{1}{12}(0.2m)(0.15m)^3 + (0.2m)(0.15m)(0.55m)^2\right]$$

$$= 0.0254\ m^4$$

$$M_{cr} = \frac{f_r I_g}{y_t} = \frac{3.09(0.0254)}{0.625} \times 10^6 = 125.5\ kNm$$ NZS 3101 Eq. 4-5

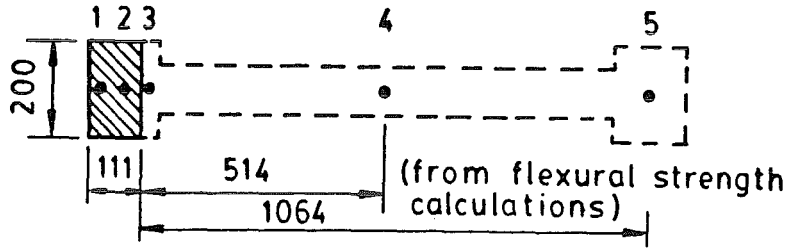

Fig. B.1 - Cracked transformed section at the attainment of ideal flexural strength for the calculation of deflections

$$n A_4 = 8.02\ (170.00\ mm^2) = 1363\ mm^2$$

$$n A_5 = 8.02\ (1118.4\ mm^2) = 8970\ mm^2$$

$$I_{cr} \approx \frac{1}{12}(200mm)(111mm)^3 + 200\ mm\ (111mm)(111\ mm/2)^2$$
$$+ 1363\ mm^2\ (514\ mm)^2$$
$$+ 8970\ mm^2\ (1064\ mm)^2$$

$$I_{cr} \approx 0.0106\ m^4$$

$$M_a = 0.75V_i \times h_w = 0.75(160\ kN)(2.5\ m) = 300\ kNm$$

$$I_e = \left(\frac{M_{cr}}{M_a}\right)^3 I_g + \left[1 - \left(\frac{M_{cr}}{M_a}\right)^3\right] I_{cr}$$ NZS 3101, Eq. 4-4

$$= \left(\frac{125.5}{300}\right)^3 (0.0254\ m^4) + \left[1 - \left(\frac{125.5}{300}\right)^3\right](0.0106\ m^4)$$

$$\underline{\underline{I_e = 0.0117\ m^4}}$$

Stiffness including shear and anchorage deformations:

$$F = \frac{30\ I_e}{h_w^2\ b_w\ \ell_w} = \frac{30(0.0117)}{(2.5)^2(0.1)(1.250)} = 0.4486$$

$$\underline{\underline{I_w}} = \frac{1}{1.2+F}\ I_e = \frac{1}{1.2+0.4486}\ (0.0117) = \underline{\underline{0.0071\ m^4}}$$

$$K = \frac{3\ E_c\ I_w}{h_w^3} = \frac{3(24\ 195000\ kN/m^2)(0.0071\ m^4)}{(2.5\ m)^3} = 32.9\ kN/mm$$

Prediction of yield deflection (Fig. 2.4)

$$\underline{\underline{\Delta_y}} = \frac{V_i}{K} = \frac{160\ kN}{32.9\ kN/mm} = \underline{\underline{4.9\ mm}} \quad \text{(Table 7.2)}$$

Predicted displacement immediately prior to diagonal cracking (increments 13 and 17)

$$V_{13} = V_{17} = 80\ kN$$

$$M_a = Vh_w = 80\ (2.5) = 200\ kNm$$

$$\frac{M_{cr}}{M_a} = \frac{125.5}{200} = 0.6275$$

$$I_g = 0.0254\ m^4$$

$$I_g = 0.0106\ m^4$$

$$I_e = (0.6275)^3(0.0254) + [1 - (0.6275)^3](0.0106) = 0.0143\ m^4$$

$$F = \frac{30\ I_e}{h_w^2\ b_w\ \ell_w} = \frac{30(0.0143)}{(2.5)^2(0.1)(1.250)} = 0.5475$$

$$I_w = \frac{1}{1.2+F} = 0.0082\ m^4$$

$$K = \frac{3\ E_c\ I_w}{h_w^3} = \frac{3(24\ 195\ 000)(0.0082)}{(2.5)^3} = 38.0\ kN/mm$$

$$\underline{\underline{\Delta'_e}} = \frac{V_{13}}{K} = \frac{80}{38.0} = \underline{\underline{2.10\ mm}} \quad \text{(Table 10.1)}$$

Predicted displacement immediately after the onset of diagonal cracking (increments 29 and 34)

$$V_{29} = V_{34} = 120\ kN$$

$$M_a = Vh_w = 120(2.5) = 300 \text{ kNm}$$

$$\frac{M_{cr}}{M_a} = \frac{125.5}{300} = 0.4183$$

$$I_g = 0.0254 \text{ m}^4$$

$$I_g = 0.0106 \text{ m}^4$$

$$I_e = (0.4183)^3(0.0254) + [1 - (0.4183)^3](0.0106) = 0.0117 \text{ m}^4$$

$$F = \frac{30\ I_e}{h_w^2\ b_w\ \ell_w} = \frac{30(0.0117)}{(2.5)^2(0.1)(1.250)} = 0.4486$$

$$I_w = \frac{1}{1.2+F}\ I_e = 0.0071 \text{ m}^4$$

$$K = \frac{3\ E_c\ I_w}{h_w^3} = \frac{3(24\ 195\ 000)(0.0071)}{(2.5)^3} = 33.0 \text{ kN/mm}$$

$$\underline{\Delta'_{dc}} = \frac{V_{29}}{K} = \frac{120}{33.0} = \underline{3.64 \text{ mm}} \qquad \text{(Table 10.1)}$$

Predicted displacement immediately after the onset of diagonal cracking (modified as per Section 10.4)

$$F = \frac{90\ I_e}{h_w^2\ b_w\ \ell_w} = \frac{90(0.0117)}{(2.5)^2(0.1)(1.250)} = 1.3458 \qquad \text{(Eq. 10-8)}$$

$$I_w = \frac{1}{1.2+F}\ I_e = \frac{1}{1.2+1.34}\ (0.0117) = 0.0046$$

$$K = \frac{3\ E_c\ I_w}{h_w^3} = \frac{3(24\ 195\ 000)(0.0046)}{(2.5)^3} = 21.4 \text{ kN/mm}$$

$$\underline{\Delta''_{dc}} = \frac{V_{29}}{K} = \frac{120}{21.4} = \underline{5.62 \text{ mm}} \qquad \text{(Table 10.1)}$$

APPENDIX C

POTENTIAL FOR CONSTRUCTION JOINT FAILURE

In Unit 1.5, the potential for construction joint failure at mid-height was envisaged because of low quality concrete, the segregation of aggregate, and the accumulation of excess water in the lower half of the wall. (See Section 6.2.5.) Extra care was taken in preparing the construction joint by roughening the lower concrete surface with a hammer and chisel. During the test, a full length crack was observed along the construction joint, but no horizontal slip was recorded. In the later stages of testing, displacements occurred, instead, along the diagonal cracks. Therefore, even in the case of poor quality concrete on one side of the joint, the potential for construction joint failure can be eliminated by careful preparation of the joint.